TUM School of Life Sciences
Technische Universität München

Identification of the human cathelicidin LL-37 as inhibitor of amyloid self-assembly of islet amyloid polypeptide (IAPP) and study of the IAPP/LL-37 cross-interaction

Valentina Armiento

Vollständiger Abdruck der von der TUM School of Life Sciences der Technischen Universität München zur Erlangung einer

Doktorin der Naturwissenschaften (Dr.rer.nat.)

genehmigten Dissertation.

Vorsitzende: Prof. Dr. Caroline Gutjahr

Prüfende/r der Dissertation: 1. Prof. Dr. Aphrodite Kapurniotu
2. Prof. Dr. Johannes Buchner

Die Dissertation wurde am 22.09.2021 bei der Technischen Universität München eingereicht und durch die TUM School of Life Sciences am 02.02.2022 angenommen.

Parts of this thesis were previously published in:

1. Angewandte Chemie International Edition, V. Armiento, K. Hille, D. Naltsas, J. S. Lin, A. E. Barron, A. Kapurniotu, Angew. Chem. Int. Ed. 2020, 59, 12837.

2. Angewandte Chemie International Edition, V. Armiento, A. Spanopoulou, A. Kapurniotu, Angew. Chem. Int. Ed. 2020, 59, 3372.

Abstract

The pathogenesis of many cell-degenerative diseases is linked to protein misfolding and amyloid fibril formation. Protein misfolding is related to several amyloidoses, including type 2 diabetes (T2D) and Alzheimer's disease (AD). Pathological features of these two diseases are linked to the aggregation into amyloid fibrils of islet amyloid polypeptide (IAPP) (in the case of T2D) and amyloid beta (Aβ) (in the case of AD). In fact, in AD aggregates of the 40(42)-residue Aβ cause neuronal loss and affect brain function, whereas in T2D aggregation of IAPP, a 37-residue neuropeptide regulator of glucose homeostasis, leads to pancreatic inflammation and β-cell degeneration. Molecules that may intervene with protein aggregation and block its devastating effects could become promising drug candidates. However, the molecular mechanisms underlying amyloid self-assembly and its links to disease have not been yet fully understood. Antimicrobial peptides including cathelicidins have a fundamental role in the innate immune system. Their role is to recognize pathogens, prevent infections, and modulate inflammatory processes. The 37-residue polypeptide LL-37 is the only human cathelicidin; it is known for its antimicrobial, antiviral, and immunoregulatory effects. It is expressed by a large number of non-immune and immune cells, including pancreatic β-cells. Additionally, the secretion of the cathelicidin-related antimicrobial peptide (CRAMP), which is the mouse LL-37 orthologue, in prediabetic NOD mice was found to have a protective role in T1D, converting inflammatory cells into regulatory ones. In addition to the above, recent in vitro studies have shown that LL-37 is able to interact with Aβ42 and block its amyloid self-assembly. The overarching aim of my thesis was to address the question as to whether LL-37 may also interact with IAPP and interfere with IAPP amyloid self-assembly in vitro and if yes, what are the molecular determinants of its inhibitory function. In fact, LL-37 and IAPP, which share a 42% of sequence similarity, were found to interact with high affinity. Interestingly, LL-37 interacted both with IAPP monomers and with IAPP fibrils. Furthermore, LL-37 was found to efficiently block IAPP amyloidogenesis and cytotoxicity by sequestering pre-fibrillar IAPP species into non-toxic/non-fibrillar hetero-assemblies. Mechanistic studies suggested that IAPP and LL-37 form hetero-complexes, in particular hetero-tetramers, which appeared to be required to have an inhibitory effect. Two-photon microscopy studies suggested that LL-37 clusters IAPP thus preventing amyloid fibrils formation. Also, when IAPP fibrils were treated with LL-37 prior to use, their seeding capability was completely lost. Fluorescence spectroscopic titrations identified IAPP(8-28) as a key IAPP segment of its interaction with LL-37 while studies with peptide arrays identified LL-37(6-10) and LL-37(25-27) as LL-37 core regions for the interaction with IAPP. In addition, the LL-37 sequence was dissected into segments LL-37(1-14) and LL-37(15-37). These two segments exhibited no inhibitory potency, but the central/C-terminal segment LL-37(15-37) was found to bind IAPP with high affinity. Furthermore, the question was addressed which is the shortest LL-37 segment that retains the inhibitory potency of the full-length LL-37. To this end, several N- or C-terminal shortened LL-37 segments were synthesized and studied. Segments LL-37(1-34) and LL-37(3-37) were found to be nanomolar inhibitors of IAPP self-assembly similar to LL-37. When both C- and N-termini were absent, leading to LL-37(3-34), the inhibitory potency was significantly weakened. Importantly, studies using circular dichroism (CD) spectroscopy identified a specific structure-activity relationship (SAR) feature in LL-37 which appeared to be required for its amyloid inhibitor function. In addition, detailed biophysical and biochemical studies led to the identification of Phe5 and Phe6 as key residues for the LL-37 inhibitory properties. Taken together, the studies of my PhD thesis identified LL-37 as a potent inhibitor of IAPP amyloid formation and important molecular requirements of the IAPP/LL-37 interaction and its function. These results might find application in the design of a new class of molecules as leads for drugs that combine anti-amyloid, antimicrobial and immunoregulatory functionalities.

Zusammenfassung

Die Pathogenese vieler zelldegenerativer Erkrankungen wird mit Proteinmissfaltung und der Bildung von Amyloidfibrillen in Verbindung gebracht. Proteinmissfaltung spielt eine Rolle bei mehreren Amyloidosen, einschließlich Typ 2-Diabetes (T2D) und der Alzheimer-Erkrankung (AD). Pathologische Merkmale dieser Erkrankungen hängen mit der Bildung von Amyloidfibrillen, die aus dem Inselamyloid-Polypeptid (IAPP) (bei T2D) oder dem Amyloid-β-Peptid (Aβ) (bei AD) bestehen, zusammen. So führt die amyloide Aggregation des aus 40(42) Aminosäuren bestehenden Aβ zum Verlust von Neuronen und beeinträchtigt die Gehirnfunktion von AD-Patienten. Unter Bedingungen des T2D führt die amyloide Aggregation des IAPP, eines 37-Aminosäuren-langen Neuropeptids mit regulatorischer Funktion in der Glukosehomöostase, zur pankreatischen Entzündung und β-Zelldegeneration. Daher könnten Moleküle, die mit der Proteinaggregation interferieren und ihre pathogenen Auswirkungen verhindern, vielversprechende Kandidaten für die Entwicklung von Medikamenten darstellen. Allerdings sind die molekularen Mechanismen, die der Amyloidbildung und deren Zusammenhang mit den entsprechenden Erkrankungen zugrunde liegen, noch nicht vollständig verstanden. Antimikrobielle Peptide, einschließlich der Cathelicidine, spielen eine fundamentale Rolle im angeborenen Immunsystem. Ihre Aufgabe ist es, Pathogene zu erkennen, Infektionen vorzubeugen und Entzündungsprozesse zu modulieren. Das 37-Aminosäuren-lange Polypeptid LL-37 ist das einzige menschliche Cathelicidin. Es ist bekannt für seine antimikrobiellen, antiviralen und immunregulatorischen Funktionen und wird von einer großen Anzahl an Immun- und nicht-Immunzellen, einschließlich der pankreatischen β-Zellen, exprimiert. Außerdem wurde berichtet, dass die Sekretion des Maus-Orthologs von LL-37 *Cathelicidin-related antimicrobial peptide* (CRAMP) in prädiabetischen NOD-Mäusen eine protektive Rolle bei Typ 1-Diabetes spielt, indem es die Konvertierung von inflammatorischen in regulatorische Zellen fördert. Darüber hinaus wurde kürzlich gezeigt, dass LL-37 in der Lage ist, mit Aβ42 zu interagieren und seine Amyloidbildung *in vitro* zu unterdrücken. Das übergeordnete Ziel meiner Doktorarbeit war die Frage anzugehen, ob LL-37 auch mit IAPP interagieren und dessen Amyloidbildung *in vitro* verhindern kann und, falls ja, welche die molekularen Determinanten seiner inhibitorischen Funktion sind. Tatsächlich stellte sich heraus, dass LL-37 und IAPP, die eine 42% Sequenzähnlichkeit aufzeigen, mit hoher Affinität interagieren. Interessanterweise bindet LL-37 sowohl IAPP-Monomere als auch IAPP-Amyloidfibrillen. Weiterhin wurde gezeigt, dass LL-37 die IAPP-Amyloidogenese und Zelltoxizität effektiv unterdrücken kann, und dass dies durch seine Bindung an präfibrilläre IAPP-Spezies und ihre Sequestrierung in nicht-toxische/nicht-fibrilläre Heteroaggregate vermittelt wird. Mechanistische Untersuchungen deuteten darauf hin, dass IAPP und LL-37 Heterokomplexe, insbesondere Heterotetramere, bilden. Die Bildung von Heterotetrameren schien für die LL-37-Amyloid-inhibitorische Funktion notwendig zu sein. Untersuchungen mittels Zwei-Photonen-Mikroskopie wiesen darauf hin, dass sich LL-37 um IAPP anlagert, wodurch die Bildung von Amyloidfibrillen verhindert wird. Außerdem verloren mit LL-37 vorbehandelte IAPP-Fibrillen vollständig ihre Eigenschaft die IAPP-Fibrillierung zu beschleunigen. Fluoreszenzspektroskopische Titrationen identifizierten IAPP(8-28) als Schlüsselsegment für die IAPP-Wechselwirkung mit LL-37, während Untersuchungen mittels Peptidarrays LL-37(6-10) und LL-37(25-27) als Kernregionen der LL-37-Wechselwirkung mit IAPP identifizierten. Zudem wurde die LL-37-Sequenz in LL-37(1-14) und LL-37(15-37) aufgeteilt. Diese zwei Segmente wiesen keine inhibitorische Funktion auf. Dennoch wurde gezeigt, dass das zentrale/C-terminale Segment LL-37(15-37) IAPP mit hoher Affinität bindet. Weiterhin wurde die Frage untersucht, welches das kürzeste LL-37-Segment ist, das die Amyloid-inhibitorische Wirkung des Volllängen-LL-37 beibehält. Zu diesem Zweck wurden mehrere N- oder C-terminal gekürzte LL-37-Segmente synthetisiert und untersucht. Unter diesen wurden LL-37(1-34) und LL-37(3-37) identifiziert, die ähnlich zu LL-37 nanomolare Inhibitoren der IAPP-Amyloidbildung waren. Das Weglassen der beiden N- und C-terminalen Di- bzw. Tripeptid-Segmente, das zum Segment LL-37(3-34) führte, ging dann mit einer deutlich schwächeren inhibitorischen Wirkung einher. Interessanterweise wurde durch Circulardichroismus(CD)-Spektroskopie ein Struktur-Aktivitätsbeziehungs-Merkmal in LL-37 identifiziert, welches für seine Amyloidinhibitorfunktion notwendig zu sein scheint. Weiterhin haben detaillierte biophysikalische und biochemische Untersuchungen zur Identifikation von Phe5

und Phe6 als „Schlüsselreste“ für die inhibitorischen Eigenschaften von LL-37 geführt. Zusammenfassend haben die Untersuchungen im Rahmen meiner Doktorarbeit LL-37 als hochwirksamen Inhibitor der amyloiden Selbstassemblierung von IAPP identifiziert und wichtige molekulare Erfordernisse für die IAPP/LL-37-Wechselwirkung und ihre Funktion aufgedeckt. Diese Ergebnisse könnten Anwendung in der Entwicklung von neuen Molekülen finden, die als Leitstrukturen für Wirkstoffe, die antimikrobielle, immunregulatorische und T2D-assoziierte Anti-Amyloid-Funktionen kombinieren, dienen könnten.

Abbreviations

α	Alpha
α-syn	α-synuclein
A	Absorbance
Å	Angstrom
AA	Aminoacid
Aβ	β-amyloid peptide
Aβ40	β-amyloid peptide (sequence [1-40])
Aβ42	β-amyloid peptide (sequence [1-42])
ACN	Acetonitrile
Ac_2O	Acetic anhydride
AD	Alzheimer's disease
AMP	Antimicrobial peptide
APP	Amyloid precursor protein
ATP	Adenosine triphosphate
β	Beta
BBdp	Biobreeding (rat)
BCA	Bicinchoninic acid
BMP	Bone morphogenetic protein
BSA	Bovine serum albumin
C	Concentration
CD	Circular dichroism
CL	Cross-linking
CPE	Carboxypeptidase E
CR	Congo red
CRAMP	Cathelicidin-Related Anti-Microbial Peptide
CSF	Cerebrospinal fluid
Da	Dalton
Dac	7-Diethylaminocoumarine-3-carboxylic acid
ddH_2O	Double distilled water
DIEA	Diisopropylethylamine
DMF	Dimethylformamid
DPC	Dodecylphosphocholine
EM	Electron microscopy
ER	Endoplasmic reticulum
FAM	Carboxyfluorescein
FCS	Fetal calf serum
fIAPP	IAPP fibrils
Fluos	5(6)-Carboxyfluorescein
Fmoc	9-Fluorenylmethoxycarbonyl
GSIS	Glucose-stimulated insulin secretion
h	Hour
hAM	Human pancreatic amylin
HATU	2-(7-Aza-1H-benzotriazole-1-yl)-1,1,3,3-tetramethyluroniumhexafluorophosphate

H-CAP18	Human Cationic Antimicrobial Protein
HCCA	α-Cyano-4-hydroxycinnamic acid
HCl	Hydrochloric acid
HD	Huntington's disease
HFIP	1,1,1,3,3,3-Hexafluoro-2-propanol
HOBt	1-Hydroxybenzotriazole
H_2O_2	Hydrogen peroxide
IAPP	Islet amyloid polypeptide (human)
IAPP-GI	[(N-Me)G24, (N-Me)I26]-IAPP
IC_{50}	Half maximal inhibitory concentration
IDE	Insulin-degrading enzyme
IgG	Immunoglobulin G
ISMs	Interaction surface mimics (peptides)
k	Kilo
LPS	Lipopolysaccharides
M	Molar
MALDI	Matrix-assisted laser desorption ionization mass spectrometry
MCIPs	Macro-cyclic inhibitory peptides
µg	Microgram
mg	Milligram
min	Minutes
µl	Microliter
ml	Milliliter
µM	Micromolar
mM	Millimolar
MSCs	Mesenchymal strom/stem cells
MTT	3-(4,5-dimethylthiazol-2-yl)-2,5-diphenyltetrazolium bromide
MW	Molecular weight
NAD	Nicotinamide adenine dinucleotide
NaOH	Sodium hydroxide
NIDDM	Non-insulin-dependent diabetes
nm	Nanometer
nM	Nanomolar
NMR	Nuclear magnetic resonance
NOD	Non-obese diabetic (mice)
2-PM	2-Photon microscopy
PBS	Phosphate-buffered saline
PC 1/3	Prohormone convertase 1/3
PC2	Prohormone convertase 2
POD	Peroxidase
prg.	HPLC Program
Prp	Prion protein
PSEN1	Presenilin 1
PSEN2	Presenilin 2
RP-HPLC	Reverse-phase high performance liquid chromatography

RXR	Retinoid X receptor
Scr	Scrambled
SD	Standard deviation
SDS	Sodium dodecyl sulfate
SEC	Size-exclusion chromatography
SPPS	Solid phase peptide synthesis
SS-NMR	Solid state nuclear magnetic resonance
$\mathbf{t_{1/2}}$	Half life time
T1D	Type 1 diabetes
T2D	Type 2 diabetes
TBS	Tris buffered saline
TBSn	Tris-buffered saline with Tween20
TBTU	N,N,N′,N′-Tetramethyl-O-(benzotriazol-1-yl)uronium tetrafluoroborate
tBu	Tert-butyl
TEM	Transmission electron microscopy
TFA	Trifluoroacetic acid
ThT	Thioflavin T
TIS	Triisopropylsilan
TLRs	Toll-like receptors
$\mathbf{T_M}$	Transition point
$\mathbf{t_R}$	Retention time
Tris-HCl	2-Amino-2-(hydroxymethyl)-1,3-propanediol hydrochloride
Trt	Trityl
UV	Ultraviolet
WB	Western blot

Contents

1 Introduction

1.1 Protein folding

1.1.1 Protein misfolding

Pathogenesis of many neurodegenerative and cell devastating diseases is linked to misfolding of proteins and their consequential aggregation into amyloid fibrils (1). This results in a reduction of the protein in the amount that is available for its normal role and into the conversion of these peptides or proteins in highly structured fibrillary aggregates. The term amyloid was coined by Rudolph Virchow in 1854 to describe a macroscopic tissue abnormality of the nervous system, which was first considered as starch. Nowadays, the term is used to indicate a large group of disorders of protein folding (2). In fact, the terms amyloid fibrils or plaques are generally referred to the extracellular accumulation of these structures, while the expression “intracellular occlusion” is used to indicate fibrils related to extracellular plaques that form inside the cell (3). The misfolding of proteins is related to many amyloidoses such as Alzheimer's disease (AD), Parkinson’s disease (PD), type 2 diabetes (T2D), Huntington’s disease (HD), and prion protein (PrP)-related encephalopathies. The common feature of all these diseases is the misfolding of a soluble, non-toxic protein or a polypeptide into a cytotoxic, fibrillary, β-sheet rich amyloid aggregate (1, 4).

1.1.2 The structure of amyloid fibrils

Amyloid fibrils derived from different pathologies exhibit similar morphology. They consist of several protofilaments, twisted in thread-like structures that have diameters in the nanometer and length in the micrometer range (3). When examined with X-ray, amyloid fibrils display a cross β-sheet diffraction pattern (4). The β-sheet motif was described for the first time in 1935 by the biophysicist William Astbury, who exposed his poached eggs white to X-rays (4, 5). The repeating substructure consists of two layers of intermolecular β-sheets that run in the direction of the fiber axis. This motif is made of intermolecular interacting β-sheets, of which each one comprises thousands of identical replicas of the same strand that stack through hydrogen bonds. The backbone amide hydrogen bond has a spacing of 4.8 Å in the fibril direction. Of these β-sheets, two or more lie in parallel, 6 to 12 Å apart (Figure 1). The X-ray structures show that the cross-β-sheet structure is made of two β-sheet filaments with a steric zipper side-chain interface lacking in water. The protein strands forming the β-sheets can run in the same direction (parallel β-sheets) or alternate in opposite directions (antiparallel β-sheets) (5). Binding dyes such as Thioflavin-T (ThT) and Congo red (CR) are used to monitor the presence of amyloids since they form ordered arrays along the fibril length giving a rise in the spectral signal (3). When ThT is bound to amyloid fibrils an enhancement of its fluorescence intensity at 482 nm and a shift of the emission maximum of ThT from 430 nm to 482 nm occur, while CR shows gold-green birefringence under polarized light (6-8).

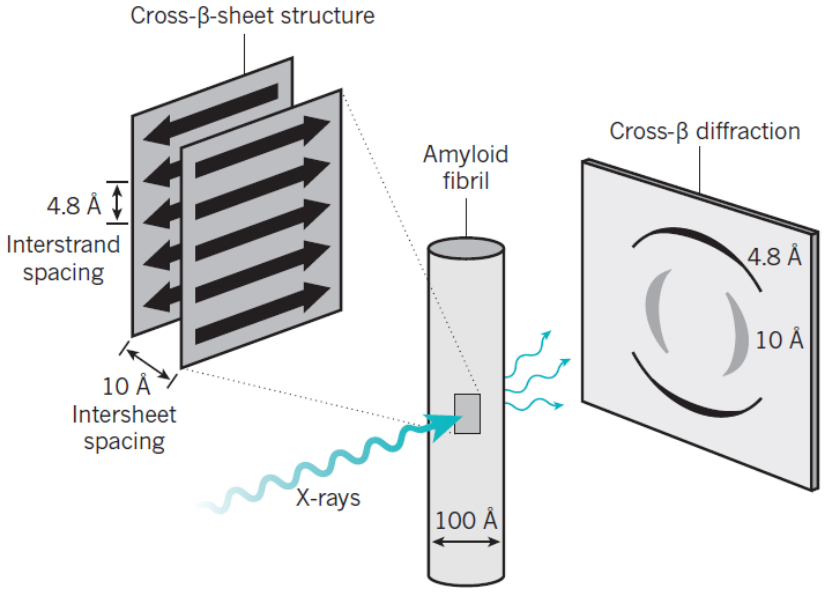

Figure 1. Representation of X-ray fiber diffraction pattern in amyloids. The fiber diffraction pattern is characterized by a meridional reflection at about 4.8 Å, corresponding to the interstrand spacing, and a protein-dependent equatorial reflection at 6–12 Å, corresponding to the intersheet distance. The figure is taken from ref. (5).

1.1.3 The process of amyloid formation

To understand the mechanism and the kinetics of amyloidogenesis, several experimental and mathematics approaches were applied. When the fibril formation is monitored using the fluorescence of the ThT dye, a sigmoidal trend of the kinetics is observed, generally characterized by three phases: a lag phase, an exponential phase, and an equilibrium phase. In a simplified mechanism of a nucleation-dependent process of aggregation, unordered monomers convert into nuclei through an unfavorable thermodynamic process (lag phase). Fibrils are then generated by the further addition of monomers on the nuclei. Nuclei are considered the smallest species able to initiate fibril elongation (1). Alongside the primary nucleation mechanism, an important number of other processes can occur in the process of amyloid fibril formation (Figure 2). Monomer-dependent secondary nucleation events can take place. In this process, the nucleus formation from monomers is catalyzed by existing aggregates composed of the same type of monomeric building blocks (9). Through the application of several analytical approaches to determine the kinetics of amyloidogenesis, it has been shown that the lag and the exponential phases do not only correspond to nucleus formation and fibril elongation respectively. Each phase is a combination of several molecular events like primary nucleation, fibril elongation, secondary nucleation, and fibril fragmentation (1). The monomer-dependent secondary nucleation is the mechanism taking place in the aggregation of several proteins, such as Islet Amyloid Polypeptide (IAPP), insulin, amyloid beta (Aβ), and α-synuclein (α-syn), involved in diseases like diabetes, Alzheimer's, and Parkinson's diseases. The autocatalytic proliferation of the aggregates due to secondary nucleation is a reason why the intervention to cure these diseases is very difficult (9).

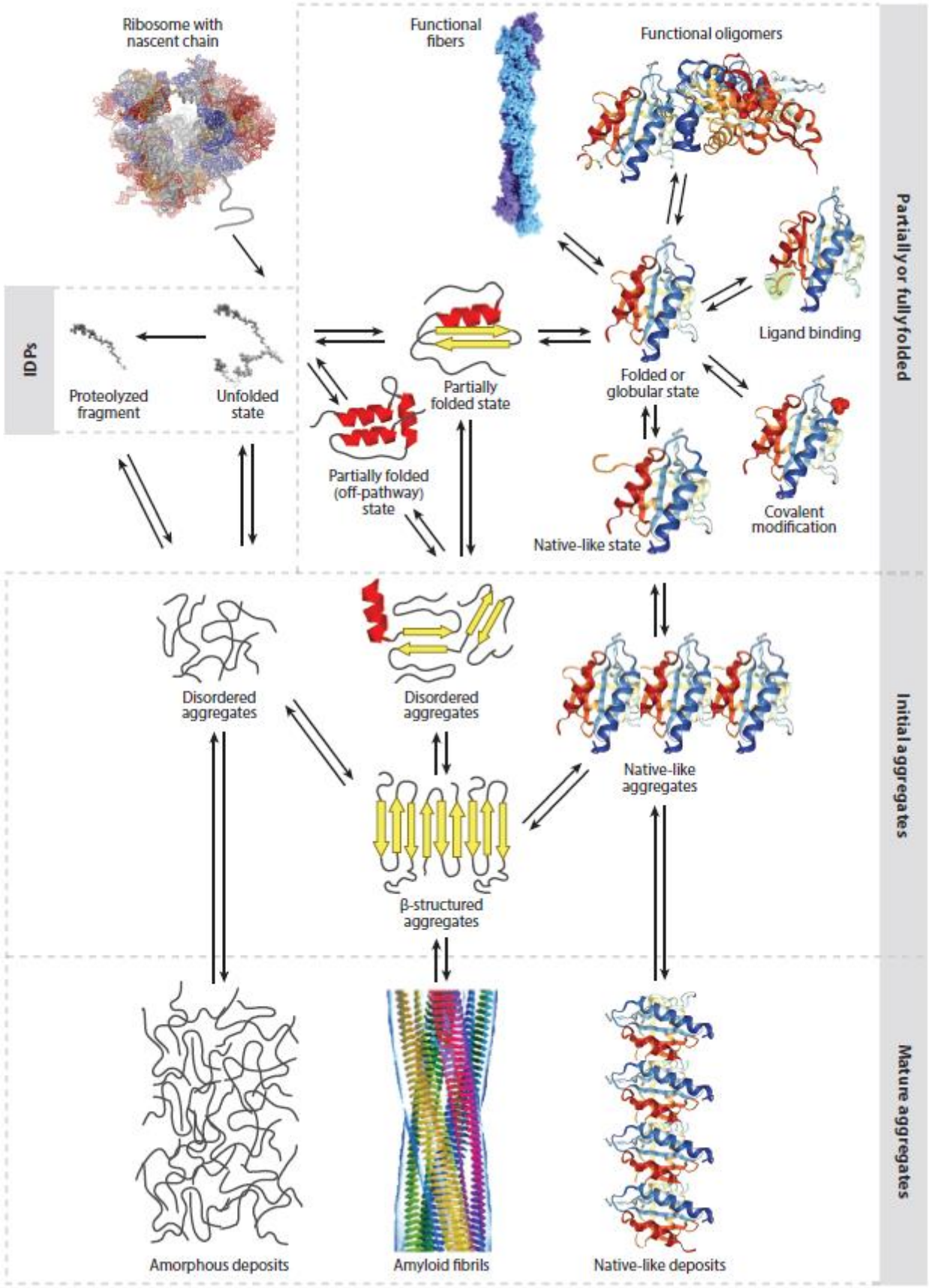

Figure 2. Illustration scheme of the conformational states that a protein presents and of the possible transitions between different states Protein misfolding and aggregation can lead to amorphous deposits, amyloid fibrils, or native-like deposits and it is involved in multiple pathological states of diverse diseases. The figure is taken from ref. (1).

1.2 Type II diabetes

Diabetes type II, also known as non-insulin-dependent diabetes (NIDDM) is a widespread metabolic disease affecting more than 285 million and is predicted to reach 438 million people by 2030. T2D is characterized by chronic insulin resistance and loss of β-cell function in time, leading to diminished insulin release and hyperglycemia. Insulin is secreted in the pancreatic islets of β-cells and has the function to maintain the blood sugar level in healthy individuals. When insulin resistance occurs and the blood sugar level is not maintained, β-cells increase insulin production. Nevertheless, under chronic insulin resistance, pancreatic β-cell failure may occur (10). All these aspects contribute, together with the reduction of the cell mass and cell function, to T2D pathogenesis (11). Genetic and environmental factors are believed to contribute to β-cell failure during insulin resistance. This dysfunction is related to glucolipotoxicity, islet cholesterol accumulation, and islet inflammation and in particular to the formation of toxic IAPP (amylin) aggregates (10). The Islet Amyloid Polypeptide (IAPP) is a neuropancreatic hormone that forms pancreatic islet amyloid in T2D and contributes to β-cell dysfunction and death (12). The physiological role is still the object of studies, but in rodent models, IAPP is involved in the suppression of satiety and adiposity, as well as the regulation of glucose homeostasis via inhibition of glucose-stimulated insulin secretion (GSIS), gastric emptying, suppression of glucagon release, vasodilatation, and the excretion of calcium, potassium, and sodium (12). Furthermore, it has been shown that the accumulation of IAPP into aggregates is linked to β-cells dysfunction, loss of cell mass, and apoptosis (10).

1.2.1 IAPP

The 37-aa long IAPP is expressed initially as a part of an 89-aa preprotein, containing a 22-aa signal peptide and two short flanking peptides (11, 13). The preproIAPP gene contains three exons of which the last two encode the full prepromolecule. In the endoplasmic reticulum (ER) the signal peptide is cleaved off, and the conversion of the ProIAPP to IAPP occurs in the secretory vesicles. The two endoproteases, prohormone convertase 2 (PC2) and prohormone convertase 1/3 (PC1/3), and carboxypeptidase E (CPE) are responsible for processing the ProIAPP in the late Golgi and secretory granules (11, 14). PC2 cleaves proIAPP at position Lys10 Arg11, and PC1/3 cleaves at position Lys50 Arg51 (14). PC2 can still process proIAPP at the C-terminus in absence of PC1/3. Essential for the full biological function is the amidation of the C-terminal glycine and the disulfide bond between the two cysteines 2 and 7, as shown in Figure 3. The two flanking peptides from proIAPP stay in the secretory granule. Exocytosis occurs, as equimolar concentrations of the removed peptides and their respective final hormonal product are released (11).

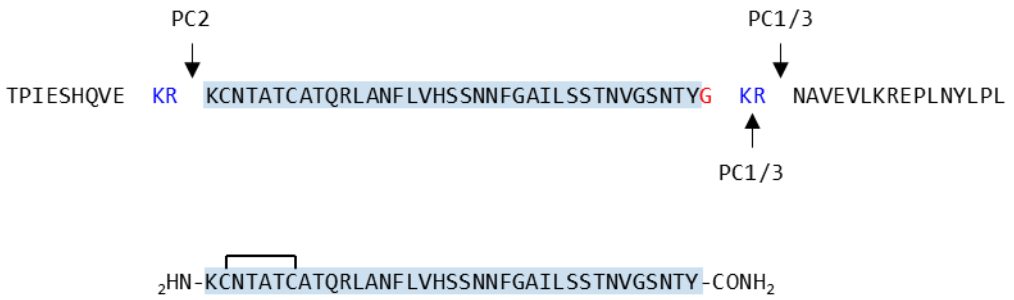

Figure 3. Processing of the human pro-islet amyloid polypeptide (proIAPP). ProIAPP PC2 is responsible for its cleavage at the -NH_2 terminus and PC1/3 for the cleavage at the -COOH terminus. After the PC1/3 processing, the KR residues (blue) are bound to the -COOH terminus and are subsequently cleaved by the carboxypeptidase E (CPE). The exposed glycine residue results then amidated (red). Below is shown a cartoon representation of IAPP (blue) with amidated -COOH terminus and intramolecular disulfide bond between cysteines 2-7. Figure adapted from ref (11).

In T2D, almost all diabetics show the presence of amyloid plaques mainly composed of IAPP in the pancreas (15). The determination of the IAPP structure in its still soluble state has been a challenging task throughout the years, due to its ability to form fibrils at low concentrations and in physiological conditions (16). It has been shown that in solution IAPP is natively disordered, but mouse IAPP also is α-helical in a transient state during the fibrillation process (17). Based on these findings, Eisenberg et al. determined the IAPP structure in its non-fibrillar state (15). The crystal structure of IAPP fused to maltose-binding protein (IAPP-MBP) reveals that IAPP adopts an α-helical conformation, in particular in segments 8-18 and 22-28. The obtained structure also indicates that IAPP can form dimers with two IAPP molecules that interact at a helical interface centered at the aromatic stack of two Phe15 residues (15). IAPP fibrils have been extensively studied to identify the amyloidogenic regions of the sequence. X-ray fiber diffraction, electron diffraction, and cryo-EM were used by Sumner Makin and Serpell to examine fibrils of IAPP, concluding that the fibrils are made of extended strands running perpendicular to the fibril axis, 4.7 Å apart, as is found in the cross-β structure (18). Structures of two amyloidogenic segments of IAPP are reported in the literature, NNFGAIL (residues 21-27) and SSTNVG (residues 28-33) (16) (Figure 4a). The SSTNVG segment has a fibril-like structure. Each SSTNVG segment forms hydrogen bonds with identical segments 4.8 Å above and below it, in an extended parallel β-sheet, and assembles into class I steric zippers, typically associated with amyloidogenic protein segments. In contrast, although the NNFGAIL segment is not a typical steric zipper, it still forms amyloid-like fibrils and assembles into close-packed β-sheets (16). In 2020, three different IAPP cryo-EM structures were published by the Schröder (19) (Figure 4d), the Radford and Ranson (20) (Figure 4c), and the Eisenberg (21) (Figure 4b) groups. Schröder determined the structure of three different polymorphs of IAPP fibrils. They are made of two helical intertwined protofilaments, although they exhibit remarkable differences in their folding. PM1, which is the most abundant polymorph (90% of the fibrils), consists of an S-shaped structure, PM2 is made of a fibril core extending the entire IAPP segment, and PM3 containing a minimal interface, consisting of three residues. The atomic model of the main polymorph PM1 exhibits two monomeric S-shaped filaments with approximately 2_1 symmetry, comprising residues Ala13–Tyr37 and stabilized by both hydrophilic and hydrophobic contacts. This polymorph is made of three short β-strands, 14–20, 26–32, and 35–37 and a fibril core interface from residue 22 to 29 (NFGAILS) together with tyrosine 37 and the amidated C-terminus (19). Ranson et al. found a similar structure of IAPP fibrils. It is consisting of two symmetric protofilaments with 2_1 screw axis symmetry. Each monomer folds into an S-shape and it is forming three β-strands 14-19, 26-31, and 35-36, as found by the Schöder research group and separated by the loops 20-25 and 32-34. The interface of the protofilaments is made of a hydrophobic steric zipper consisting of residue F23 with A25 and L27, and with Y37 of the opposing monomer (20). By contrast, Eisenberg et al. found an I-shaped structure for IAPP fibrils (22). Their cryo-EM structure shows that the fibril core is made of residues 14-37, while residues 1-13 were found to be flexible and not participating in the core structure. The stability of the interface between two monomers consists of side chains from Phe23, Ala25, Ile26, Leu27, and Val32, together with Gly24 and Gly33. This extended 14-residue hydrophobic core confers great stability to IAPP fibril, which makes them irreversible and consistent with the pathogenicity in T2D (21).

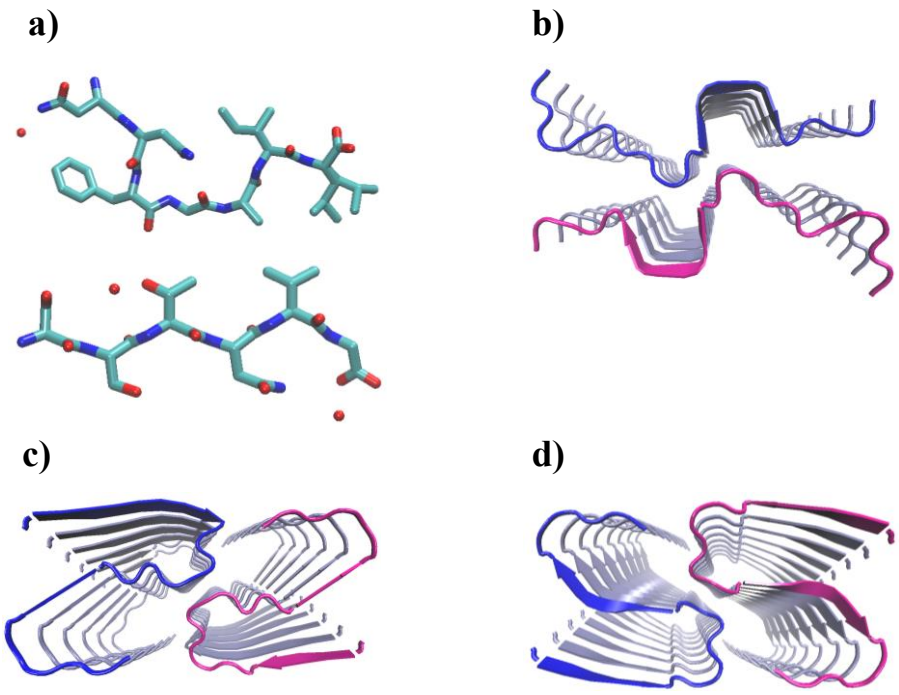

Figure 4. Overview structures of IAPP amyloid-like segments and IAPP fibrils. a) X-ray diffraction structures of the NNFGAIL (top, PDB: 3DGJ) and SSTNVG (bottom, PBD: 3DG1) amyloid-like segments of IAPP (16). Cryo-EM structures of IAPP fibrils: b) PDB: 6VW2 (21), c) PDB: 6ZRF (20), and d) PDB: 6Y1A (19).

1.2.2 Peptide-based inhibitors that target IAPP self-assembly

As T2D is a worldwide spread disease, the design of inhibitors to interfere with amyloid fibril formation has been a challenge that is nowadays still the object of numerous studies. Antibodies and proteins, small organic molecules, and peptides or peptidomimetics are the three main classes, to which these inhibitors belong to. Inhibitors are designed to interfere and block the process of amyloid formation. As shown in Figure 5, several stages of the amyloidogenesis can be blocked: the production of the amyloidogenic protein can be blocked or it is possible to intervene in the primary or secondary nucleation processes, in the first case by sequestering monomers, in the latter through the binding to oligomeric/protofibrillar species. Finally, inhibitors can block fibril growth or disassemble fibrils (Figure 5) (23).

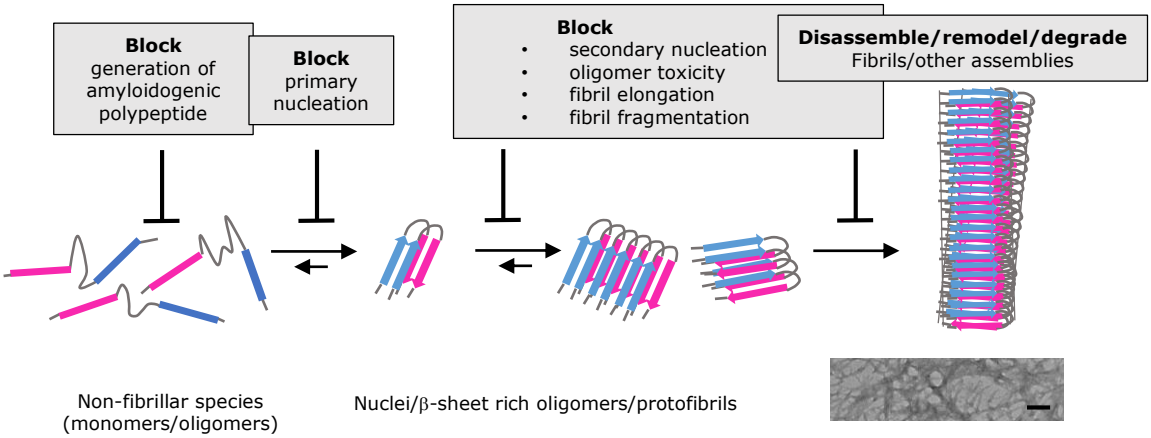

Figure 5. Amyloid fibril formation and strategies to block its aggregation. The figure is taken from ref. (23).

A commonly used approach to design inhibitors is to use amyloid self-recognition segments as a template and apply chemical tools to optimize them. After identifying IAPP(22-27) (NFGAIL) as a minimum length sequence sufficient to self-associate into β-sheet containing fibrils, the double N-methylated NFGAIL-GI was designed and found to be an effective suppressor of IAPP amyloidogenicity and cytotoxicity (24). In addition, several full-length IAPP based inhibitors were designed following a similar approach. IAPP-GI ([(N-Me)G24,N-Me)I26]-IAPP) was obtained using minimalistic conformational restrictions and found to be a highly soluble, non-amyloidogenic, and non-cytotoxic IAPP molecular mimic and an IAPP receptor antagonist. IAPP-GI interacts with IAPP with a low nanomolar affinity and blocks its fibrillogenesis and cytotoxicity. Also, this inhibitor dissociates cytotoxic IAPP oligomers and fibrils and is able to reverse their cytotoxicity (25). Moreover, Andretto et al. proposed a "hot-segment" linking approach to design a series of IAPP cross-amyloid interaction surface mimics (ISMs) as highly potent inhibitors of amyloid self-assembly of Aβ, IAPP, or both polypeptides (26). A novelty for the design of amyloid inhibitors was introduced by Vendruscolo's group (27). A computational method of rational design procedure was applied to obtain antibodies that specifically bind target epitopes within disordered regions of peptides or proteins. The amyloid core segments or complementary peptides were included in antibody-derived scaffolds, called "gammabodies" (23, 27). This new class of inhibitors can bind with a good affinity and specificity target regions of several disordered peptides, including IAPP, and effectively reduce their aggregation (27). Several examples of inhibitors designed based on molecular recognition features of amyloid self-assembly have been reported in the literature. In this approach, the atomic structure of short amyloidogenic segments was taken as a template, which was rationally modified with the application of the Rosetta strategy to design short inhibitors that cap fibril ends (23). The design of the inhibitors is based on the assumption that the short amyloidogenic sequences form the steric zipper structure as in the fibrils of their corresponding full-length proteins (23). The two peptides Aβ(24-34) WT and hIAPP(19-29) S20G were obtained and found to be inhibitors of both IAPP and Aβ fibril formation and reduced the cytotoxicity of both proteins (28). In 2011, Gazit et al. showed the ability of hybrid molecules composed of an aromatic moiety and the α-aminoisobutyric acid β-sheet breaker elements to act as inhibitors of amyloid fibril formation. In particular, the D-Trp-Aib is a potent inhibitor of diverse amyloids, such as calcitonin, α-synuclein, and IAPP (29). Inhibitors can be also designed without having sequence similarity to their targets, but mimicking their structural features (23). The Andersen lab reported that β-hairpin peptides bearing both Trp and Tyr residues inhibit fibril formation by human pancreatic amylin (hAM). These peptides expose Trp and Tyr residues at varying positions along the β-strands of the hairpin structure, facilitating an intermolecular association and formation of pre-amyloid states, preventing their oligomerization and aggregation (30).

1.3 Alzheimer's disease (AD)

Alzheimer's disease (AD) is recognized as a global health priority by the World Health Organization (31). The disease was first reported by the German psychiatrist and neuropathologist Alois Alzheimer in 1907 (32). Despite many attempts, no disease-modifying treatment could be developed to date (31). Dementia is a major cause of dependence and mortality and has an impact on all the activities of daily life. Estimates show that currently 44 million people are affected by dementia worldwide.

In western countries cases of dementia have been declining and this might correspond to the better treatment of vascular risks. Also, the most significant increase of dementia is expected in countries with low or middle income, where cases of cardiovascular disease, hypertension, and diabetes are increasing (31). AD is the biggest cause of dementia and it is mainly a later life condition, doubling in prevalence every 5 years after age 65 (31). AD can occur in a sporadic form in the majority of the cases, but also in a rare (<0.5 % of the cases) familial form, based on the mutation of three genes; amyloid precursor protein (APP), presenilin 1 (PSEN1) and presenilin 2 (PSEN2) (33). Risk factors for sporadic AD are attributed to environmental and genetic factors, and the latter one is believed to cause circa 70% of the cases. In particular, the APOE gene, which has three variants (ε2, ε3, and ε4) is the biggest genetic risk factor for AD. E4 increases the risk in heterozygotes

by 3 times and in homozygotes by 12 times, compared to non-ε4 carriers (34). Pathology of Alzheimer's disease is characterized by the presence of amyloid plaques and neurofibrillary tangles and consequent neurodegeneration with synaptic and neuronal loss leading to macroscopic atrophy (35). The extracellular amyloid plaques are composed of abnormally folded Aβ made of 40 or 42 amino acid residues (Aβ40 and Aβ42). Plaques contain majorly Aβ42, due to its insolubility and its ability to form fibrils. Neurofibrillary tangles are composed of hyperphosphorylated Tau. Consequently, the formation of the neurofibrillary tangles leads to the neuronal and synaptic loss typical of AD (36). In fact, memory loss and difficulties in acquiring new information are the first symptoms of AD which evolve into a progressive decline of cognitive functions when the dementia is in an advanced state (37).

1.3.1 Amyloid-beta (Aβ)

The extracellular deposits of amyloid beta (Aβ) peptide in the senile plaques are one of the pathological features of AD and are known to affect brain function and cause neuronal death. Although the neurotoxicity of this peptide is known, it is still not clear how it participates in the progressive cognitive decline in patients. It is also to be clarified whether Aβ plays a role in normal physiology since it is also detected in the cerebrospinal fluid and plasma of healthy individuals (38).

The type I integral membrane glycoprotein, APP, is the precursor of the amyloid-β peptides. This protein comprises an amyloid-β domain with cleavage sites for the secretase enzymes. The protein can be processed following two different pathways, which can lead to an amyloidogenic or a non-amyloidogenic product. When the non-amyloidogenic pathway occurs, the cleavage of APP in the amyloid-β domain by α-secretase (a member of the ADAM, a disintegrin, and a metalloprotease) releases the soluble ectodomain sAPPα and the C-terminal fragment CTFα. The following cleavage of CTFα by γ-secretase produces a soluble extracellular p3 peptide and the APP intracellular domain (39, 40). In the amyloidogenic pathway, the cleavage of APP by the β-secretase generates the soluble ectodomain sAPPβ and CTFβ. Cleavage of CTFβ by γ-secretase yields amyloid-β peptides of varying lengths as well as the AICD fragment (Figure 6). Amyloid-β peptides have different lengths. Aβ40, which is circa 90% abundant in basal conditions, is less toxic and amyloidogenic than Aβ42 (39).

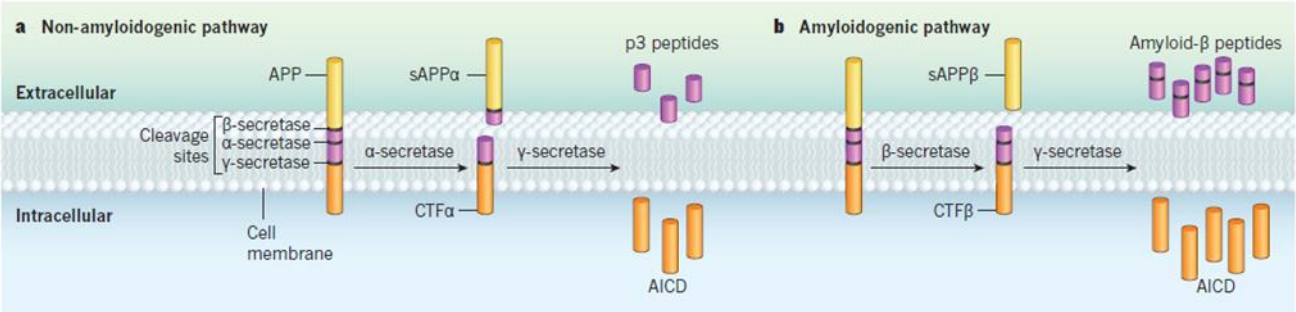

Figure 6. Non-amyloidogenic and amyloidogenic processing pathways of the APP protein. a) Non-amyloidogenic pathway, in which α-secretase cleaves APP in the amyloid-β domain, resulting in sAPPα and CTFα. The latter is cleaved by γ-secretase leading to the production of p3 peptides and AICD; b) amyloidogenic pathway, in which β-secretase cleaves APP into aAPPβ and CTFβ. The sequential cleavage of CTFβ by γ-secretase leads to the formation of amyloid-β peptides. The figure is taken from ref. (40).

Throughout time, several experimental approaches were applied for the determination of the structures of the fibrils of Aβ40 and Aβ42 peptides, due to their insoluble and non-crystalline nature. In 2006, Petkova et al. determined the structure of Aβ40 using solid-state NMR (41). The model proposed that residues 1-9 are structurally disordered, residues 10-22 and 30-40 form β-strands, and residues 23 to 29 form a loop (Figure 7a). Aβ40 fibrils exhibited in-register parallel β-sheets (42). The presence of a salt bridge between D23 and K28 was confirmed. Finally, side chains of L17, F19, I32, L34, and V36 create a hydrophobic cluster that

apparently stabilizes the fold of a single molecular layer. G33, G37, and G38 create grooves into which the side chains of I31 and M35 fit at the interface between molecular layers. Charged and polar side chains are outside the hydrophobic core of the protofilament (41). Aβ42 is the most toxic and amyloidogenic peptide among the Aβ species and is the dominant species in the plaques of AD patients. Combining data from electron microscopy (EM) and solid-state NMR (ssNMR), Riek's lab determined the structure of a relevant polymorph of Aβ42. The Aβ42 obtained fibril is made of subunits made of two molecules, with C_2 symmetry along the fibril axis. In the 3D structure, each Aβ42 unit is formed of five in-register parallel intermolecular β-strands winding in a horseshoe manner around two hydrophobic cores, involving residues 15-42. Residues 1-14, instead, are partially ordered and not completely rigid (Figure 7b) (43). In 2017, Schröder et al. determined the atomic structure of Aβ42 fibrils using cryo-electron microscopy (cryo-EM). As previously found, the fibril, which exhibits a 2_1 symmetry, comprises two twisted protofilaments of Aβ42 molecules stacked in in-register parallel intermolecular β-strands (Figure 7c). Each Aβ42 molecule presents an LS shape, of which the N-terminus is L and the C-terminus is S-shaped. The stability of the fibril structure is given by three hydrophobic clusters: (i) Ala2, Val36, Phe4, and Leu34; (ii) Leu17, Ile31, and Phe19; and (iii) Ala30, Ile32, Met35, and Val40. The identified salt bridges are between Asp1 and Lys28; Asp7 and Arg5; and Glu11 and both His6 and His13. Investigation of the structure of the amyloid beta fibrils is a task of high importance since it will help to understand the mechanism of fibril growth and how to possibly interfere with it (44).

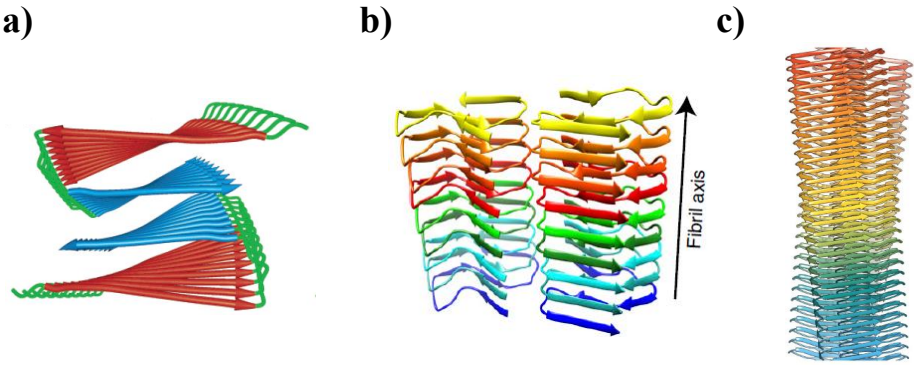

Figure 7. Overview structures of amyloid-β fibrils a) Representation of Aβ40 fibrils determined via ssNMR. Picture taken from ref. (41); b) representation of Aβ42 fibrils determined via 3D ssNMR. Picture taken from ref. (43); c) atomic model of Aβ42 fibril determined via cryo-EM. Picture taken from ref. (44).

1.4 Connection of type 2 diabetes and Alzheimer's disease

T2D and AD have been traditionally considered as two independent diseases. Nevertheless, in recent years it has been shown that they are epidemiological, cognitive, and neuropathological linked, although the mechanism is still the object of studies (45, 46). On the one hand, it has been shown that rodent models of T2D and insulin resistance exhibited memory loss and dysfunction and on the other hand diabetic phenotype was present in AD mouse models. Mouse model containing phenotypes of both diseases showed metabolic and neuronal dysfunction (45). Experiments conducted by McGeer's group showed that Aβ aggregates and hyperphosphorylation of tau, fundamental features of AD, are also characteristics in T2D. This indicates the existence of common features between the two neurodegenerative diseases and that aggregation of Aβ and hyperphosphorylation of tau may take place not only in the brain (47). In 2013, Jackson et al. showed that amylin produced by pancreatic cells accumulates and precipitates in the temporal lobe in diabetic patients, forming a complex with Aβ. This accumulation might also contribute to the etiology of AD by altering the cerebrovascular system and precluding the elimination of amyloid beta from the brain (48). Studies indicate that glucose dysregulation and insulin resistance may be driven by Aβ (45). It has been shown that the pathology of AD may be led by the malfunction of insulin metabolism. Insulin can interfere with the levels of Aβ, promoting its release in neuronal cells and inhibiting its degradation via the insulin-degrading enzyme (IDE). IDE, a metalloprotease that catabolizes insulin, is expressed in the brain, muscle, liver, and kidneys and

has a key role in the clearance of Aβ in the brain and is involved in the degradation of intracellular Aβ and extracellular Aβ in the cerebrospinal fluid (CSF), although in AD its activity is reduced. It has been proven that infusions of insulin enhance the level of CSF insulin and increase CSF Aβ42 concentrations in older individuals (49). From a molecular point of view, IAPP and Aβ have similar sequences. The alignment of the two sequences shows that the two peptides present 50% similarity and 25% identity (50) (Figure 8).

```
        1         10        20        30        40
Aβ40 DAEFRHDSGYEVHHQKLVFFAEDVGSNKGAIIGLM VGGVV

                1 ┌──────┐  10          22    27        37
IAPP            KCNTATCATQRLANFLVHSSNNFGAILSSTNVGSNTY
```

Figure 8. Primary structure of Aβ40 and IAPP. Identical residues are indicated in blue and similar residues are shown in red. The figure is taken from ref. (51).

The cross-amyloid interaction of these two peptides involves regions that are also involved in their self-association into amyloid fibrils. Regarding IAPP, the two segments involved in the interaction with Aβ are IAPP(8-18) and IAPP(22-28), while the IAPP binding Aβ segments are Aβ(19-22), Aβ(27-32), and Aβ(35–40(42)) (52).

The link between these two peptides proven by our research group has been used as a basis to design peptides as potential therapeutics to intervene with amyloid aggregation (26). Another molecular link between IAPP and Aβ was reported by Westermark's group. IAPP transgenic mice were treated with injections of IAPP, proIAPP, and Aβ and results showed that IAPP aggregation in the islet of Langerhans is accelerated via homo and hetero-seeding effects. Studies of patient tissues also revealed the colocalization of IAPP and Aβ in the brain, although deposits in the endocrine pancreas do not contain any Aβ (53).

1.5 Antimicrobial peptides (AMPs)

Antimicrobial peptides have a fundamental role in the innate immune system. More than 1300 AMPs have been identified in a wide range of natural species such as amphibians, mammals, fungi, and bacteria (54). The study of antimicrobial agents started back in 1922 when Alexander Fleming recognized the presence of bactericidal species in the nasal secretion of an acute coryza patient. He first named the species lysozyme, due to their ability to lyse bacterial lawns (55, 56). Subsequently, a similar effect was identified in different tissues and fluids from both humans and animals, suggesting a protective role in the immune system. Further studies of Alexander Fleming with Howard Florey led to the discovery of *Penicillium notatum*, and its antibiotic effect was applied for therapeutic aims. In 1945, the two scientists shared the Nobel Prize in Medicine for the discovery of penicillin (56). The first discovery of a bactericidal agent in prokaryotic cells dates back to 1939 when Renè J. Dubos identified an antimicrobial agent from a soil *Bacillus* that attacked and lysed several Gram-positive species (57, 58). The antimicrobial agent was then furthered studied and named gramicidin in 1941 (59), but it was later shown that it was a mixture of AMPs with a high anti-infection role (56, 60). Since then, several species of antimicrobial peptides have been reported and their role in health and mechanism of action were widely investigated. The structure-function model of Shai-Matsuzaki-Huang explains how AMPs exert their antimicrobial function (61-63). The model proposes the interaction of the AMP with the lipid bilayer of the cytoplasmic membrane with electrostatic forces, followed by the displacement of the lipids, disruption of the cell wall, and the formation of vacancies through which cell components can be lost. In general, peptides operating with this mechanism can kill microbes at micromolar concentrations (64, 65). The function of these peptides is not limited to an antimicrobial function, but increasing reports underline the immunoregulatory function (66), as well as chemotaxis stimulation, suppression of proinflammatory cytokine production, wound

healing, and promotion of angiogenesis (67). In the case of microbial infection, Toll-like receptors (TLRs) signaling is activated from the innate immune system, and antimicrobial peptides and cytokines are produced to eradicate the pathogens. Toll-like receptors are transmembrane proteins that play a crucial role in the case of infections and inflammations (68). The stimulation of the immune system by injuries or infection by pathogens causes the release of AMPs *in situ*. The function of the AMPs in these cases is to block microbial growth, recruit leukocytes, and stimulate the production of cytokines or chemokines as CXCL8 (IL-8), CCL2, and IFN-α. These, in turn, promote indirectly the solicit of effector cells such as macrophages, T cells, monocytes, neutrophils, and immature dendritic cells (64).

In humans, there are three main groups of antimicrobial peptides: defensins, histatins, and cathelicidins (Table 1) (69). Defensins are cationic non-glycosylated peptides comprising intramolecular disulfide bridges formed by cysteine residues. They are divided into α- and β-defensins. The α-defensins are made of 29-35 amino acids and form a triple-stranded β-sheet structure with a β-hairpin loop containing the positively charged molecules. The β-defensins are larger than α-defensins, but they exhibit a similar secondary structure (69, 70). Histatins are small, cationic, helical, histidine-rich peptides present in human saliva, important for protection against oral infections. Cathelicidins are represented in humans by only one peptide, LL-37. This amphipathic helical peptide can be found in a plethora of cells and is the only human cathelicidin known nowadays. All these peptides have different structures and biochemical properties, however, they are all involved in the recognition of pathogens and the prevention of infections (69).

Table 1. Primary structure of main α-defensins, β-defensins, the cathelicidin LL-37, and of the main histatins. The table is taken from ref. (69).

Peptide	**Sequence**	**Number of amino acids**
α-defensins		
HNP-1	ACYCRIPACIAGERRYGTCIYQGRLWAFCC	30
HNP-4	VCSCRLVFCRRTELRVGNCLIGGVSFTYCCTRVD	34
HD-5	ARATCYCRTGRCATRESLSGVCEISGRLYRLCCR	34
HD-6	RAFTCHCRRS-CYSTEYSYGTCTVMGN-HRFCCL	32
β-defensins		
HBD-1	DHYNCVSSGGQCLYSACPIFTKIQGTCYRGKAKCCK	36
HBD-2	DPVTCLKSGAICHPVFCPRRYKQIGTCGLPGTKCCKKP	38
HBD-3	QKYYCRVRGGRCAVLSCLPKEEQIGKCSTRGRKCCRRKK	39
HBD-4	LDRICGYGTARCRKK-CRSQEYRIGRCPNTYA-CCLRKPWDESLLNRTK	47
Cathelicidin		
LL-37	LLGDFFRKSKEKIGKEFKRIVQRIKDFLRNLVPRTES	37
Histatins		
Hst1	DSHEKRHHGYRRKFHEKHHSHREFPFYGDYGSNYLYDN	38
Hst3	DSHAKRHHGYKRKFHEKHHSHRGYRSNYLYDN	32
Hst5	DSHAKRHHGYKRKFHEKHHSHRGY	24

1.5.1 Cathelicidins

Cathelicidins are a family of mammalian proteins known for their antimicrobial properties (71). They are encoded by a gene consisting of 4 exons. Exon 1 is encoding the signal peptide made of 29/30 residues. Exons 2 and 3 encode the cathelin domain, which is highly conserved within the cathelicidin family. Last, exon 4 encodes the mature peptide, which retains the immunoregulatory and antimicrobial properties (72). Within this group of peptides, cathelin was first found in pig leukocytes and is called after its property to inhibit the cysteine proteinase cathepsin L (66). Cathelicidin peptides are characterized by the way they are produced and

stored in cells. In fact, they are produced as pre-pro-proteins, stored in cell granules of neutrophils, and secreted upon cell activation (71). At this point, the cleavage of the preprotein occurs, which is formed by a central signal peptide, flanked by an N-terminal signal peptide and the C-terminal antimicrobial region (54, 72). Peptides with a cathelin-like-pro-peptide sequence have been found in diverse species, such as cow pig, rabbit, sheep, human, mouse, monkey, and horse (73). Cathelicidins are found in a plethora of cells and tissues, as they are found in epithelial cells, mucosal surfaces, keratinocytes, and bone marrow cells (74). The biological role of these peptides covers a wide range of functionalities. In fact, they are known for their potent antimicrobial function against Gram-positive and Gram-negative bacteria, but other important roles were brought to attention. They were found to stimulate the degranulation of immune cells, regulate the expression of pro-inflammatory and anti-inflammatory cytokines, stimulate the phagocytosis of pathogens, and modify immune responses of immune cells (72). Many studies have been carried out for the characterization of the secondary and tertiary structure of these peptides. Prediction studies via the Shiffer-Edmunson wheel projections suggest that many of the cathelicidins have an amphipathic α-helical conformation, and results have been confirmed with circular dichroism studies (71). The helical conformation of observed for most of them in conditions mimicking biological membranes, while most of them are random coiled in water except for LL-37 and PMAP-37 which adopt a helical conformation also in aqueous buffers (71, 74). Results show that the structural features such as size, charge, degree of helicity, and amphipathicity of cathelicidins are of great relevance for their microbicidal function (73).

1.5.2 LL-37, the only human cathelicidin

LL-37 is the only identified human cathelicidin. It was first identified as a “pro-peptide” hCAP-18 in granules of human neutrophils and predicted from a cDNA clone (75). It was further proved that the peptide is encoded by the CAMP gene and it is stored as a preprotein in the neutrophil granules and epithelial cells and is turned extracellularly into its active form by the proteinase 3, a serine proteinase (54). For the cells that do not contain LL-37, it is not known how the peptide is released from the pro-form, but studies indicated that it might occur in the extracellular environment. hCAP18 is expressed by different types of cells, including immune cells like neutrophils, monocytes, macrophages, dendritic cells, NK cells, lymphocytes, and mast cells, but also by epithelial cells. The expression pathway is complex and diverse and it is modulated by exogenous microbial factors and/or by endogenous signal molecules. Its release can be a response to stimulation of toll-like receptors (TLRs) or to cytokines release after the TLRs stimulation (76). Koeffler et al. have also shown that vitamin D3 upregulates the expression of the human cathelicidin antimicrobial peptide (CAMP) (77).

1.5.2.1 Structure of LL-37

The human cathelicidin LL-37 has the following primary structure: LLGDF-FRKSK-EKIGK-EFKRI-VQRIK-DFLRN-LVPRT-ES. The peptide is an amphiphilic α-helix and presents a charged nature (54). In fact, under physiological conditions, LL-37 has a net charge of +6, due to 11 positive charges of 6 Lys and 5 Arg residues and 5 negative charges, attributable to 3 Glu and 5 Asp residues. As shown in the helical wheel diagram in Figure 9, LL-37 assumes mainly a helical secondary structure except for its N-terminus, which exhibits a more unordered structure (66).

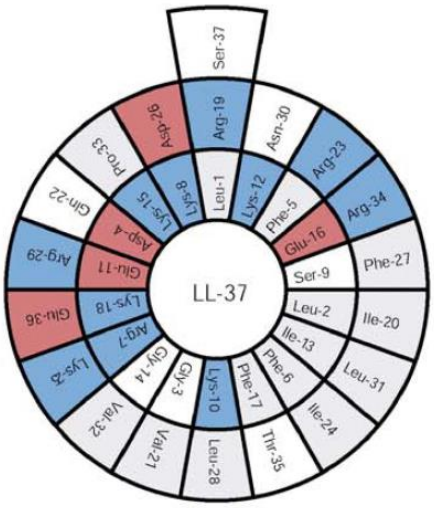

Figure 9. Helical wheel diagram of the human cathelicidin LL-37. Positively charged (blue), negatively charged (red), polar (white), and hydrophobic (grey) amino acids are highlighted. The figure is taken from ref. (66).

The structure of LL-37 in dodecylphosphocholine (DPC) micelles was determined by Veglia et al. (78) via NMR. In the membrane mimicking environment, it was found that LL-37 adopts a "helix-break-helix" conformation, made of flexible helical N-terminus, a break at Lys12, a more stable conformation from residue 13 to 33, and an unstructured C-terminus. The hydrophobic residues of LL-37 were found to interact with DPC, while the hydrophilic residues were exposed to the aqueous environment. The break between the helices is stabilized by contacts between I13, F17, and I20 which stabilize the hydrophobic core, and by a salt bridge between K12 and E16 that confers a 120° curvature to the structure. At the N-terminus, the phenylalanine residues were identified as important for the insertion of the peptide into lipid membranes (78).

In 2017, Sancho-Vaello et al. reported the crystal structure of LL-37. It has been reported that in absence of detergents, LL-37 displays an anti-parallel dimer formed by two α-helices without supercoiling (Figure 10b). The monomers are stabilized by a backbone of salt bridges and H-bonds between Asp4 and Arg7, Glu16 and Arg19 and Asp26 and Arg29, Gln22 and Asp26 (Figure 10a). The dimer covers an area of 670 $Å^2$ involving residues from Leu1 to Phe27 and its interface extends for 3.5 nm with the antiparallel helices shifted by two turns. The stability of the dimer is given by hydrophilic contacts at the dimer interface involving Ser9, Lys12, and Glu16 and by the hydrophobic core involving Leu2, Phe5, Phe6, Ile13, Phe17, Ile20, Ile24, and Phe27. Additionally, it was shown that, in the presence of detergents, dimers can assemble into tetramers, and then fiber-like oligomeric assemblies via head-to-tail arrangement (Figure 10b). This supramolecular structure is held together by contacts between the aromatic residues, Phe5, 6, and 27. These fibers are hydrophobic belts with interaction regions for the detergents at the N-terminus and in the central region. The formation of the fiber-like structures was confirmed using gold-labeled LL-37. Experiments on *E. coli* proved the perforation of the outer membrane, while experiments carried out with a simplified system, the unilamellar vesicles, highlighted the presence of fibers along the surface of the vesicles in a parallel alignment (79).

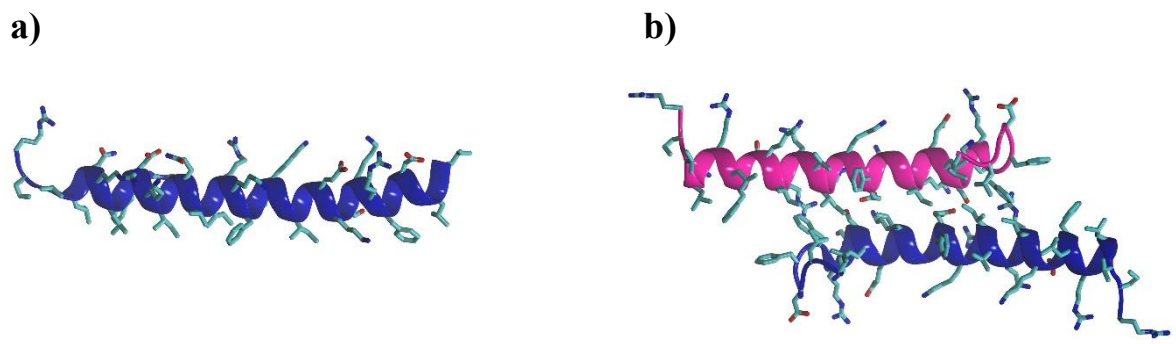

Figure 10. Crystal structures of LL-37. a) X-ray diffraction of monomeric LL-37 in presence of detergents (PDB: 5NMN) (79). b) X-ray diffraction of dimeric LL-37 in absence of detergents displaying an anti-parallel dimer formed by two α-helices. (PDB: 5NNM) (79).

An extended study of LL-37 structural features by CD spectroscopy was carried out by Johansson and coworkers. It has been shown that the conformation of LL-37 is salt, pH, and concentration-dependent. Monomeric LL-37 adopts an unordered structure at concentrations < 10^{-5} M and has an α-helix structure in its oligomeric state, in which the hydrophilic residues are exposed to the aqueous solution (Hofmeister effect). A similar effect is observed in the presence of anions, which induce the oligomerization of LL-37 into helical assemblies. The unfolding of LL-37 at low pH values is explained by the protonation of the side chains and by the loss of the contacts between ion pairs, while the α-helix is retained at neutral and basic pH values. Finally, LL-37 requires the α-helical oligomeric structure to have a more effective antibacterial activity (80).

1.5.2.2 Bioactivity

LL-37 was first known for its antibacterial activity, but studies evidenced its antifungal and antiviral roles, its ability to inhibit the formation of biofilms, and its roles in wound healing and angiogenesis (54, 64, 66, 81, 82). LL-37 is active against Gram-positive and negative bacteria and other pathogens. In general, due to the different membrane compositions, antimicrobial peptides target specifically bacteria rather than mammalian cells (54). In fact, bacterial membranes present a negatively charged nature, as the Gram-positive bacteria present a membrane surface of teichoic acids and the Gram-negative contain negatively charged lipopolysaccharides. Differently, mammalian cell membranes result neutral, due to their zwitterionic nature. As discussed above, the antimicrobial activity of LL-37 depends on its α-helical secondary structure and on the ability to make oligomers. Many studies have been carried out to explain how LL-37 interacts with membranes to perform its antimicrobial function. Two main mechanisms, previously studied for other antimicrobial polypeptides, have been proposed for their action: the toroidal pore carpet-like model and the barrel-stave model (83) (Figure 11). In the carpet mechanism, considered as the most plausible one, the peptides coat the membrane reaching a critical concentration until toroidal pores are formed by the binding of the peptide to the phospholipidic headgroups of the membrane; in the barrel-stave model, the peptide perpendicularly inserts the membrane, causing leakage through pores in the bilayer (54, 84) (Figure 11). LL-37 is known to oligomerize and self-associate when bound to zwitterionic phospholipid vesicles and it is protected from enzymic degradation. When associated with negatively charged vesicles, it dissociates into monomers keeping its resistance to degradation. LL-37 has diverse properties from those of other native α-helical antimicrobial peptides. In fact, these peptides are monomeric when they interact with both zwitterionic phospholipid or negatively charged vesicles and are not proteolytically resistant when bound to zwitterionic phospholipids (85).

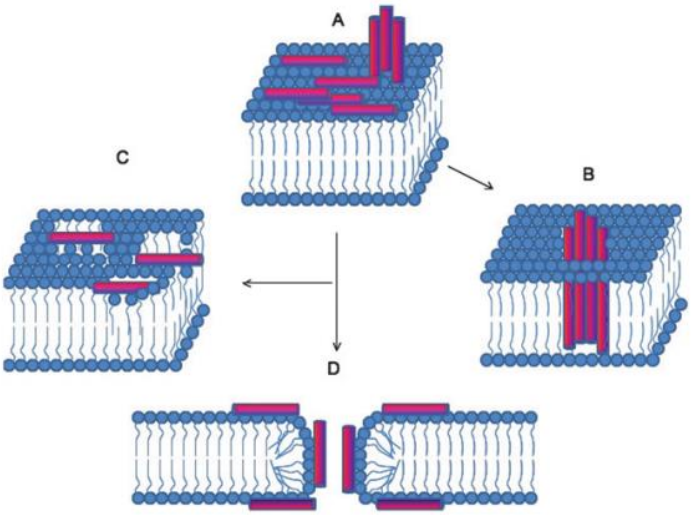

Figure 11. Suggested mechanisms for the insertion of LL-37 into membranes. a) LL-37 is permeating the membrane as an oligomer or a monomer. b) Barrel-stave model. The peptide forms a cylindrical pore in the membrane by its perpendicular insertion in the bilayer. c, d) Carpet model. LL-37 coats the surface of the membrane until a critical concentration is reached. At this point, the membrane is disrupted in a detergent-like manner (c) or by the formation of toroidal pores (d). The figure is taken from ref. (54).

LL-37 also presents a potent antifungal activity. Using *Candida albicans* as a model organism, den Hertog et al. showed that LL-37 interacts with the cell wall, affecting the morphology of the membrane and disrupting it into discrete vesicles, followed by an efflux of vital cellular compounds, such as ATP and NAD, and causing cell death (86). LL-37 can also target viruses like the influenza virus, vaccinia virus, herpes simplex 1 virus, and HIV-1 (84). In 2007, Bergman et al. showed for the first time that LL-37 inhibits HIV-1 replication by target cells in vitro (87). Furthermore, Wang et al. LL-37 derived fragments that exhibit the anti-HIV effect. In particular, FK-13 was identified as the minimal anti-HIV region of LL-37, extending from residues 17 to 29, also known for its anti-cancer properties. The engineered GI-20 peptide had the highest efficacy against the HIV-1 virus. The antiviral effect of these peptides is related to the sequence, the presence of aromatic Phe residues, as well as the helical secondary structure (88). Furthermore, the human cathelicidin LL-37 (as well as the murine cathelicidin mCRAMP) were found to have a potent anti-viral effect against the influenza virus both in vitro and in vivo. In fact, it has been shown that administration of LL-37 to influenza virus-infected mice led to a decrease of the concentration of pro-inflammatory cytokines in the lung than the untreated infected mice (89).

LL-37 was shown also to be involved in the immunity and the pathogenesis of cancer (90). For instance, studies suggest that the overexpression of LL-37 positively regulates ovarian cancer progression. It appears that LL-37 promotes tumor progression by promoting the engraftment of multipotent mesenchymal stromal/stem cells (MSCs) to the tumor stroma and that the neutralization of its effect with anti-LL-37 antibody can reduce the tumor growth and disrupt the fibrovascular network (91). LL-37 can also have a suppressing effect: it was found to inhibit gastric tumor cell proliferation through the activation of bone morphogenetic protein (BMP) via a proteasome-dependent mechanism (92). In additional studies, overexpression of LL-37 was found to promote breast and lung cancer and suppress colon cancer as well (90).

As with other cathelicidins, LL-37 can affect chemoattraction and cytokine release from neutrophils, monocytes, dendritic, and T-cells of the immune system (93). In fact, LL-37 is stored in granules of neutrophils and released at the site of the infection protecting from microbial effects. It was shown that LL-37 induces the secretion of the chemokine IL-8 by macrophages, epithelial cells, and fibroblast modulating the immune response. Moreover, LL-37 stimulates primary monocytes to produce CCL4, CXCL1, and CCL20, chemokines with the ability to attract neutrophils (84). Furthermore, LL-37 balances the action of the neutrophils in the production of anti-inflammatory cytokines in different cell types. For example, it causes the

production of IL-2, IL-4, and IL-6 in mast cells, IL-1β, IL-10, and CCL3 in monocytes, and IL-6 in epithelial cells, human gingival fibroblasts, and keratinocytes (84). Besides the production of cytokines, LL-37 presents an important modulatory function. In fact, it modulates the activation of TLRs, and consequently the cytokine production, upon recognition of pathogen associated molecular patterns (PAMPs) or of cell and tissue damage, balancing out the anti-inflammatory and pro-inflammatory responses. Abnormal levels of LL-37 expression can lead to an increase in the chance of tuberculosis (94), psoriasis (95), dermatitis (96), or reduced wound healing (84).

Host defense peptides were found to be involved also in type 1 diabetes (T1D). In this disease, autoimmune destruction of the pancreatic β-cells occurs and consequently loss of insulin production and hyperglycemia. The gut lumen contains microbes and antigens that have an effect on the gut immune system and T1D incidence in humans, NOD mice, and diabetes-prone BBdp rats (97). Scott et al., have shown that host defense peptides have a protective role in T1D in the BBdp rat. CAMP, the encoding gene of CRAMP (cathelicidin-related antimicrobial peptide), is expressed in pancreatic β-cells. The CRAMP expression is decreased in diabetes-prone BBdp rats before the onset of insulitis. Also, CAMP can act as a regulator of intraislet communication and glucoregulation by stimulating the secretion of insulin and glucagon. It was proved that levels of CRAMP expression decrease in rats with inflamed islets and that CAMP/LL-37 treatments enhance β-cell regeneration in rats, suggesting this treatment as a therapy in T1D patients (97).

Additional studies show that CRAMP production is also reduced in pancreatic β-cells of NOD mice and that the administration of CRAMP to prediabetic NOD mice has a protective role in T1D, converting inflammatory into regulatory immune cells in the pancreas (98).

1.5.3 AMPs as inhibitors of amyloid self-assembly

LL-37 has proven to be a multifunction antimicrobial peptide and it is expressed by immune and non-immune cells (66). A novel function of this peptide was reported by the Barron research group, as LL-37 was shown to bind amyloid beta and interfere with its aggregation into cytotoxic species. It has been shown that LL-37 not only has a high affinity for low-MW Aβ species but also can inhibit its fibril formation until 9 days. Also, LL-37 was shown to prevent the folding of Aβ42 into its characteristic β-sheet via circular dichroism. Studies on the microglial-mediated cytotoxicity to SH-SY5Y cells proved that both peptides Aβ42 and LL-37 have a cytotoxic effect. On the contrary, the mixture of the two showed higher cell viability suggesting that the formation of a complex might attenuate the toxic effects (99). The direct link between Alzheimer's disease and the expression of the human LL-37 has to be yet clarified, but studies report that their functions are related. In fact, the human cathelicidin antimicrobial peptide gene (CAMP) is strongly upregulated by vitamin D3 (77). Vitamin D3, in turn, has been shown to have neuroprotective properties against AD, by reducing the cerebral Aβ40 levels and favoring its efflux, and improving cognition in an AD mouse model (100). The retinoid X receptors (RXR) are also known to be related to AD. Cederlund et al. showed that activation of RXR attenuated neuronal loss in AD mouse model and it was also proven that activation of RXR receptors is involved in the regulation of LL-37 levels (101).

The amphibian host-defense peptide caerin 1.8 was also found to be an inhibitor of amyloid beta fibril formation (102). Caerin 1 peptides, isolated from the skin of amphibians, have been shown to be membrane-active and to have antimicrobial properties (102). Similar to the human cathelicidin, caerin peptides are unstructured in water, but α-helical in a membrane-mimicking environment (103). In their work, Liu et al. proved that caerin 1.8 inhibits aggregation of Aβ42 via the formation of a 1:1 adduct and that the N-terminal residues play an important role in the inhibitory function more than those belonging to the C-terminus (102).

It has been recently shown that the aggregation into amyloid fibrils of α-synuclein, a 140 amino acid protein involved in the pathogenesis of Parkinson's disease (PD), is inhibited by two antimicrobial peptides, the bacterial PMSα3, and the human LL-37 (104). Santos et al. proved that these two AMPs can selectively interact

with toxic α-synuclein oligomeric assemblies, while their interaction with non-toxic monomers is marginal. Moreover, PMSα3 and LL-37 efficiently suppressed the aggregation of α-synuclein into amyloid fibrils and protected human SH-SY5Y cells from oligomer-induced toxicity by reducing intracellular reactive oxygen species (ROS) (104). In the case of these peptides, the mechanism of inhibition of amyloid formation does not rely on the primary structure, but on their amphipathicity and cationic characters. Peptides with high sequence homology to PMSα3, but no amphipathic or cationic character had no inhibitory effect (104).

2 Aims of the thesis

The interaction of LL-37 with amyloids is a recent discovery that opens up a field of research that remains to be explored. In 2017, the Barron research group reported that the human cathelicidin LL-37 is a binding partner of Aβ of Alzheimer's disease and it can inhibit its fibrillogenesis and neuroinflammation in vitro (99). Furthermore, the mouse LL-37 orthologue, CRAMP, is secreted by the pancreatic β-cells, and it was shown to successfully convert inflammatory cells into regulatory ones in type 1 diabetes mouse models (98). Based on the above, the overarching aim of my thesis was to investigate whether and how LL-37 might interact with IAPP and to characterize its potential effects on IAPP amyloid self-assembly and cytotoxicity.

Based on these assumptions, the aims of the first part of this work were:

1. Address the question whether LL-37 interacts with IAPP and, if yes, whether and how it may affect IAPP amyloidogenesis and cytotoxicity.
2. Biophysical characterization of the LL-37/IAPP interaction and the effect of LL-37 on IAPP conformation misfolding.
3. Identification of the IAPP and the LL-37 regions mediating the IAPP/LL-37 interaction interface.
4. Characterization of the LL-37/IAPP hetero-complexes and their role in the inhibitory function of LL-37.

After proving that LL-37 is an inhibitor of IAPP fibril formation and cytotoxicity, the second aim of my work had the following objectives:

1. Identification of the shortest LL-37 derived sequence which can still efficiently suppress the aggregation of IAPP into cell-damaging assemblies and fibrils.
2. Studies of the structure-activity relationship of the truncated LL-37 segments. Biochemical and biophysical studies were performed to study whether a correlation between inhibitory function and secondary structure may exist.

These aims should become achieved by the rational design, synthesis, and biochemical and biophysical characterization of truncated LL-37 sequences (Scheme 1).

Finally, the third part of my work focused on the identification of key residues for the inhibitory potency of LL-37. In particular, the effects of alanine substitutions of phenylalanine residues on the structure, function, and inhibitory properties of LL-37 should become investigated.

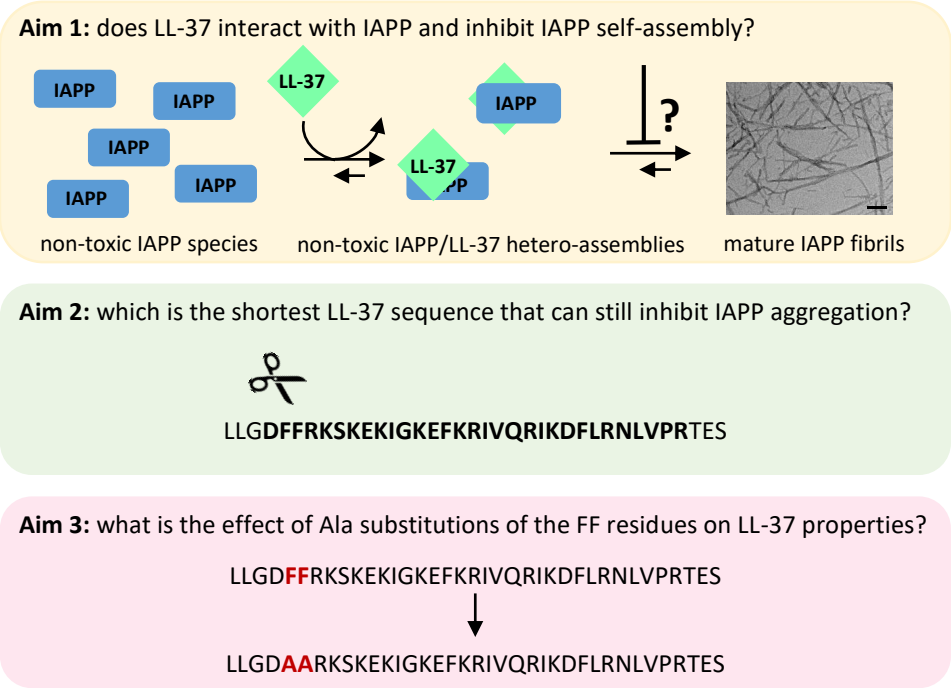

Scheme 1. Schematic representation of the aims of this work. Aim 1 focused on the inhibitory potency of LL-37 as an inhibitor of IAPP amyloid formation. Aim 2 focused on the shortening of the interacting LL-37 sequence to identify the shortest segment that retains inhibitory potency. Aim 3 focused on the investigation of the role of Phe5 and Phe6 on the structure, function, and inhibitory properties of LL-37.

3 Material and methods

3.1 Materials

3.1.1 Chemicals

Table 2. Chemicals

Chemicals	**Company (city or country)**
Acetaldheyde	Roth (Karlsruhe, DE)
Acetic anhydride	Sigma-Aldrich (St. Louis, USA)
Acetonitrile (ACN)	VWR (DE)
Ammonium acetate	Merck (Darmstadt, DE)
2-(7-Aza-1H-benzotriazole-1yl)-1,1,3,3-tetramethyluronium (HATU)	Iris Biotech (Marktredwitz, DE)
2-(1H-Benzotriazol-1-yl)-1,1,3,3-tetramethyluronium hexafluorophosphate (HBTU)	Iris Biotech (Marktredwitz, DE)
4-Benzyloxybenzyl Alcohol Resin (Wang resin)	Iris Biotech (Marktredwitz, DE)
Bovine serum albumin fraction V (BSA)	Roth (Karlsruhe, DE)
5(6)-Carboxyfluorescein (Fluos)	Sigma-Aldrich (St. Louis, USA)
5(6)-Carboxytetramethylrhodamine (TAMRA)	Merck (Darmstadt, DE)
α-Cyano-4-hydroxycinnamic acid (HCCA)	Sigma-Aldrich (St. Louis, USA)
Chloranil	Fluka (Seelze, DE)
7-Diethylaminocoumarin-3-carboxylic acid (Dac)	Invitrogen (Eggenstein ,DE)
Diethyl ether (Et_2O)	Roth (Karlsruhe, DE)
N,N-Diisopropylcarbodiimide (DIC)	Fluka (Seelze, DE)
N,N-Diisopropylethylamine (DIEA)	Biosolve (Valkenswaard, NL)
3-(4,5-dimethylthiazol-2-yl)-2,5-diphenyltetrazolium bromide (MTT)	Sigma-Aldrich (St. Louis, USA)
N,N-Dimethylformamide (DMF)	CLN (Niederhummer, DE)
DL-Dithiothreitol (DTT)	Sigma-Aldrich (St. Louis, USA)
Formic acid	Sigma-Aldrich (St. Louis, USA)
Glutaraldehyde	Sigma-Aldrich (St. Louis, USA)
Glycin	Fluka (Seelze, DE)
Guanidinium-HCl	Roth (Karlsruhe, DE)
Hellmanex	Hellma Analytics (Müllheim, DE)
1,1,1,3,3,3-Hexafluor-2-propanol (HFIP)	Sigma-Aldrich (St. Louis, USA)
Hydrochloric acid (HCl)	Roth (Karlsruhe, DE)
1-Hydroxybenzotriazol (HOBt)	Sigma-Aldrich (St. Louis, USA)
Isopropanol	Roth (Karlsruhe, DE)
Methanol (MeOH)	VWR (DE)
Milk powder (not-fat, dried)	Applichem (Darmstadt, DE)
Ninhydrin	Fluka (Steinheim, DE)
NuPAGE™ LDS Sample Buffer (4x)	Invitrogen (DE)
Phenol	Sigma-Aldrich (St. Louis, USA)
Piperidine	Iris Biotech (Marktredwitz, DE)
Polylysin	Sigma-Aldrich (St. Louis, USA)
Potassium chloride (KCl)	Merck (Darmstadt, DE)
ProLong™ Diamond Antifade Mountant	Invitrogen (DE)

Protected amino acids (AA)	Iris Biotech (Marktredwitz, DE)
Proteinmarker-Multimark TM	Invitrogen (DE)
Sodium borohydride ($NaBH_4$)	Roth (Karlsruhe, DE)
Sodium chloride (NaCl)	Merck (Darmstadt, DE)
Sodium dihydrogen phosphate (NaH_2PO_4)	Merck (Darmstadt, DE)
Sodium dodecyl sulfate (SDS)	Roth (Karlsruhe, DE)
Sodium hydrogen phosphate dihydrate (Na_2HPO_4 x 2 H_2O)	Merck (Darmstadt, DE)
Sodium hydroxide (NaOH)	Roth (Karlsruhe, DE)
Super signal duration ECL staining solution	Sigma-Aldrich (St. Louis, USA)
TentaGel R PHB	Rapp Polymere GmbH (Tübingen, DE)
Thioanisol	Fluka (Seelze, DE)
Thioflavin T (ThT)	Sigma-Aldrich (St. Louis, USA)
Trichloracetic acid (TCA)	Roth (Karlsruhe, DE)
Trifluroacetic acid (>99.5%) (TFA for synthesis)	Sigma-Aldrich (St. Louis, USA)
Trifluoracetic acid (>99.5%) (TFA for HPLC)	Sigma-Aldrich (St. Louis, USA)
2-Amino-2-(hydroxymethyl)-1,3-propanediol, hydrochloride (Tris-HCl)	Roth (Karlsruhe, DE)
Triton X-100	Sigma-Aldrich (St. Louis, USA)
Trypsin/EDTA	Invitrogen (DE)
Tween 20	Roth (Karlsruhe, DE)
Uranyl acetate	Sigma-Aldrich (St. Louis, USA)

3.1.2 Peptides

Table 3. Synthetic peptides purchased or provided by others

Peptides	**Manufacturer/supplier**
Aβ(1-40)	Synthesis by the group of Prof. Kapurniotu
Aβ(1-42)	Synthesis by the group of Prof. Kapurniotu
Dac-Aβ(1-40)	Synthesis by the group of Prof. Kapurniotu
Glucagon	Bachem (DE)
hIAPP	Synthesis by the group of Prof. Kapurniotu
Fluos-IAPP	Synthesis by the group of Prof. Kapurniotu
LL-37	Bachem (DE)/Anaspec (USA)
FAM-LL-37	Bachem (DE)/Anaspec (USA)
Scrambled LL-37	Anaspec (USA)

3.1.3 Assay kits

Table 4. Assay Kits

Assay kit	**Company (city or country)**
Micro Bicinchoninic acid (BCA) protein assay kit	ThermoFischer Scientific (DE)
SuperSignal West Dura extended duration substrate	ThermoFischer Scientific (DE)

3.1.4 Materials and devices

Table 5. Materials

Materials	**Company (city or country)**
96 well plate, Cellstar, sterile, F-bottom	Greiner Bio-One (Frickenhausen, DE)
96 well plate, CellGradeTM plus, sterile	B. Braun (Melsungen, DE)
Cell culture flasks 250 ml	Greiner Bio-One (Frickenhausen, DE)
Cellstar® Tubes, 15 ml	Greiner Bio-One (Frickenhausen, DE)
Cellstar® Tubes, 50ml	Greiner Bio-One (Frickenhausen, DE)
Cuvette, quartz	Hellma Analytics (Müllheim, DE)
Filter, Millex-FG, 0.2µm	Merck (Darmstadt, DE)
Microtiter plate, 96 well, F-bottom, black	ThermoFischer Scientific (DE)
Pasteur pipettes, glass, 145mm	BRAND (Wertheim, DE)
Pipette tips, 2-200µl, yellow	BRAND (Wertheim, DE)
Pipette tips, 100-1000µl, blue	BRAND (Wertheim, DE)
Pipette tips, 0.5-10µl	Axygen (Union City, USA)
Reaction vessel, 1.5ml	Sarstedt (Nümbrecht, DE)
Reagent reservoir	VWR (Ismaning, DE)
Syringe, BD Discardit II, sterile, 10ml	Becton Dickinson (Franklin Lakes, USA)
Syringe, BD Discardit II, sterile, 20ml	Becton Dickinson (Franklin Lakes, USA)
Syringe, BD Discardit II, sterile, 2ml	Becton Dickinson (Franklin Lakes, USA)
TEM grids, FCF300-Cu, 300 mesh	Electron Microscopy Sciences (Hatfield)

Table 6. Devices

Devices	**Company (city or country)**
Analytical balance	Denver Instrument Sartorius (Göttingen, DE)
Centrifuge Labofuge Ae	Heraeus Sepatech (Osterode, DE)
CO_2 Incubator MCO-17AIC	Sanyo Electric Co (J)
Dry freezer Alpha 1-2 LDplus	CHRIST (Osterode, DE)
Eppendorf centrifuge 5417C	Netheler-Hinz GmbH (Hamburg, DE)
Heating block neoBlock 1	NeoLab (Heidelberg, DE)
HPLC Dionex UltiMate 3000 pump	ThermoFischer scientific (DE)
HPLC Dionex UltiMate 3000 RS variable wavelength detector	ThermoFischer scientific (DE)
Incubator T6 Heraeus	ThermoFischer scientific (DE)
JEOL 1400 Plus electron microscope (120 kV)	Jeol (Tokio, J)
LAS-4000 mini Fujifilm	FujifilmEurope GmbH (Düsseldorf, DE)
Magnetic stirrer Topolino	Carl Roth (DE)
MALDI-TOF Mass Spectrometer	Bruker Daltonics (Bremen, DE)
Microscope model CKX41	Olympus (Shin juku, J)
Multichannel pipette	BRAND (Wertheim, DE)
Multilabel plate reader 2030 VictorTM X3	PerkinElmer, Life and analytical sciences (FN)
Nucleosil 100 C18, 250mm length, ID8mm, 7µm particle size	Dr Maisch GmbH, (Ammerbuch, DE)
2-photon Leica TCSPC SP8 DIVE microscope	Leica (DE)
Peptide synthesizer CS336X	CSBio Co. (California, USA)
pH-Meter	Mettler Toledo (Greifensee, CH)

SDS X cell sure Lock BIO RAD	Invitrogen (Carlsbad, USA)
Shaker CAT S20	CAT (Staufen, DE)
Spectrofluorometer FP-6500	Jasco (Gross-Umstadt, DE)
Spectropolarimeter J-715	Jasco (Gross-Umstadt, DE)
Ultrapure water unit TKA MikroPure	TKA (Niederelbert, DE)
Ultrasonic bath SONOREX	Bandelin (Berlin, DE)
UV-Vis spectrophotometer V630	Jasco (Gross-Umstadt, DE)
Vortex Mixer Vortex Genie 2	Scientific Industries (New York, USA)

3.1.5 Cell culture media

Table 7. Cell culture media

Cell culture	**Company (city or country)**
Dimethyl sulfoxide	Sigma-Aldrich (St. Louis, USA)
Fetal calf serum (FCS)	GIBCO™ by Life Technologies, Thermo Fischer Scientific (DE)
Glutamine	GIBCO™ by Life Technologies, Thermo Fischer Scientific (DE)
Horse serum	GIBCO™ by Life Technologies, Thermo Fischer Scientific (DE)
L-glutamine	GIBCO™ by Life Technologies, Thermo Fischer Scientific (DE)
MEM NEAA	GIBCO™ by Life Technologies, Thermo Fischer Scientific (DE)
Penicillin/Streptomycin	GIBCO™ by Life Technologies, Thermo Fischer Scientific (DE)
RPMI-1640	GIBCO™ by Life Technologies, Thermo Fischer Scientific (DE)
Sodium pyruvate	GIBCO™ by Life Technologies, Thermo Fischer Scientific (DE)
Triton™ X-100	Sigma-Aldrich (St. Louis, USA)
Trypsin	GIBCO™ by Life Technologies, Thermo Fischer Scientific (DE)

3.1.6 Antibodies

Table 8. Antibodies

Antibodies	**Company (city or country)**
Goat anti-mouse IgG-POD	Abcam (NL)
Goat anti-rabbit IgG-POD	GE Healthcare (USA)
Monoclonal mouse anti-IAPP fibrils antibody	Synaptic Systems (Göttingen, DE)
Monoclonal mouse anti-LL-37 antibody	Santa Cruz Biotechnology (USA)
Polyclonal rabbit anti-IAPP antibody	Peninsula (USA)

3.2 Methods

3.2.1 Solid phase synthesis using SPPS Fmoc strategy

The synthesis of the peptides was carried out using solid-phase peptide synthesis (SPPS) with Fmoc/tert-butyl strategy on Wang or TentaGel resin. Fmoc-cleavage was done using a solution of DMF containing 25% of piperidine or 20% of piperidine with 0.1 M HOBt in the case of sequences containing aspartic acid to avoid any formation of aspartimide as a side product (105). According to the difficulty of the coupling, amino acids (Table 9) were coupled with at least a 3-fold molar excess of amino acid, a 3-fold excess of HBTU or HATU, and a 4.5-fold excess of DIEA (Table 10). The amounts of coupling reagents were calculated according to the substitution level of the first amino acids on the Wang or TentaGel resin. The efficiency of the couplings was

verified by the Kaiser test (106, 107). To verify the accomplishment of difficult couplings, a small sample of resin was subjected to Fmoc-cleavage, followed by treatment with TFA to cleave the peptide from the resin. The crude product was analyzed via reverse-phase high performance liquid chromatography (RP-HPLC) in combination with MALDI-TOF analysis.

Table 9. Amino acids and their side chain protecting groups.

Amino acids (a.a.)	**Side chain protecting group**
Arg	Pbf
Asn	Trt
Asp	tBu
Gln	Trt
Glu	tBu
Gly	-
Ile	-
Leu	-
Lys	Boc
Phe	-
Pro	-
Ser	tBu
Thr	tBu
Val	-
Ala	-

Table 10. Fmoc chemistry SPPS protocol.

Synthesis step	**Time**	**Reagents**
Fmoc cleavage	1x5 min, 1/2x20 min	25% piperidine in DMF/20% piperidine or 0.1 M HOBt in DMF
Wash	4x1 min	DMF
Kaiser Test		
Coupling	2/3x40 min	Fmoc-a.a/HATU or HBTU/DIEA
Wash	3x1 min	DMF
Kaiser test		
Acetylation	1x15 min	Ac_2O/DIEA
Wash	3x 1 min	DMF

3.2.1.1 Kaiser test

The Kaiser test is a colorimetric test to evaluate the presence or not of the Fmoc group of primary amino acids on a peptide resin (107). The test is made by three solutions:

- Ninhydrin in ethanol (5 g in 100 ml ethanol)
- Phenol in ethanol (40 g in 10 ml ethanol)
- Potassium cyanide in water in pyridine (2 ml of aqueous 0.001 M KCN in 100 ml pyridine)

To carry out the test, a minimal amount of resin is transferred into a test tube and two drops of each of the solutions above described are added, mixed, and heated for 5 minutes at 110° C. The test is negative when the Fmoc-protected amino acid is successfully coupled and the test appears as a yellow solution with colorless beads. When the beads have a blue or brown color, the test is positive and the Fmoc group is cleaved from the N-terminus of the amino acid. The blue color (Ruhemann's purple) is generated by the reaction of the free primary amines with ninhydrin in a transamination-decarboxylation reaction (108, 109).

3.2.1.2 Peptide cleavage from the resin and side chain deprotection

The peptide cleavage from the Wang or TentaGel resin and the final side chain deprotection was carried out using a solution of TFA:ddH_2O (95:5, v:v). For this reaction, 20 or 40 mg of peptide resin were treated with 500 µl or 1 ml respectively of the cleavage solution above described for 3 hours at room temperature. After the reaction time was over, the cleaved peptide was transferred in a glass vial containing water to have a final amount of TFA < 10%. Subsequently, the suspension was lyophilized.

3.2.1.3 Synthesis of N-terminal labeled peptides with 5,6-carboxyfluorescein

For fluorescence spectroscopic binding and 2-photon microscopy studies, peptides were N-terminally carboxyfluorescein (Fluos) labeled. For their synthesis, 20 mg of peptide-resin were Fmoc-deprotected using DMF containing 25% of piperidine or 20% of piperidine with 0.1 M HOBt and thereafter washed with DMF (3 times for 1 minute each). The coupling was performed using 3 equivalents of 5,6-carboxyfluorescein, 3 equivalents of HATU, and 4.5 equivalents of DIEA at room temperature for 2 hours. Couplings were repeated two times. Peptides were cleaved as previously described in 3.2.1.2.

3.2.2 Purification and characterization of peptides

3.2.2.1 Purification of peptides via reverse-phase high performance liquid chromatography (RP-HPLC)

Peptide crudes were purified using reverse-phase HPLC, which exploits a hydrophobic stationary phase and an elution in gradient to separate the peptides from eventual side products. RP-HPLC purifications were performed using a Nucleosil 100 C18 (250 mm x 8 mm; particle size, 7 µm) column and gradient programs as shown in Table 11. Peptides were detected at 214 nm. Elution buffers used were the following:

1. Buffer A: 0.058% (v:v) TFA in ddH_2O
2. Buffer B: 0.05% (v:v) TFA in 90% ACN:ddH_2O

Eluates were frozen on dry ice directly after collection and thereafter lyophilized.

Table 11. Gradients of HPLC programs that are used to purify the synthetic peptides.

HPLC program	Time (min)	% Buffer A	% Buffer B
SchnellAβ	0	90	10
	1	90	10
	31	10	90
10-100% B stay at 100% B for 10 min	0	90	10
	1	90	10
	20	0	100
	31	0	100
LangsamAβ 40–70%B	0	60	40
	7	60	40
	37	30	70
40% B for 7 min-40-80% B in 23 min	0	60	40
	7	60	40
	31	20	80
30% B for 7 min-30-100% B in 30 min	0	70	30
	7	70	30
	37	0	100
	44	0	100
LangsamAβ	0	70	30
	7	70	30
	37	40	60

3.2.2.2 Matrix-assisted laser desorption-ionization mass spectroscopy (MALDI-TOF)

Peptide purity was verified by MALDI-TOF MS at the BayBioMS (Bayerisches Zentrum für Biomolekulare MassenSpektrometrie) facility at TUM. A sample of the solid peptide was dissolved in a mixture of isopropanol:formic acid:ddH_2O (17%:33%:50%, v:v) and then mixed with a saturated solution of the same solvent containing HCCA matrix (1:1). Of this mixture, 0.5 µl were then spotted onto a target and washed with 3 µl of a 10 mM $NH_4H_2PO_4$ solution in ddH_2O with 0.1% TFA to quench the signal of adduct ions such as sodium or potassium. Monoisotopic masses were recorded as $[M+H]^+$.

3.2.3 Peptide stock preparation and determination of their concentration

- IAPP stock solution

IAPP was synthesized using the Fmoc-solid phase synthesis strategy on Rink resin, oxidized with air, and purified. Stock solutions were made by dissolving the peptide in HFIP (at 4°C) and filtering the solution with a 0.2 µm filter; IAPP concentration was determined by UV spectroscopy (tyrosine absorption at 274 nm, ε=1440 $M^{-1}cm^{-1}$) applying the Lambert-Beer law.

- Aβ42 stock solution

Aβ42 was synthesized using Fmoc-solid phase synthesis on TentaGel resin, purified via RP-HPLC by Peptide specialty laboratories GmbH, and disaggregated via size exclusion chromatography (SEC) (110, 111). Briefly, aliquots of 400 µg of pure Aβ42 were dissolved in a solution of 5 M guanidinium chloride in 10 mM Tris/HCl (pH 8). The Aβ42 aliquots were then disaggregated using a Superdex 75 10/300 GL column and an isocratic gradient of a 50 mM ammonium acetate solution (pH 8.5). The concentration of the stock solutions in 50 mM ammonium acetate buffer (pH 8.5) was determined by UV spectroscopy (tyrosine absorption at 274 nm, ε=1440 $M^{-1}cm^{-1}$) applying the Lambert-Beer law.

- Fluorescein-labeled peptide stock solutions

A sample of purified N-terminal Fluos-peptide or DAC-Aβ was dissolved in HFIP (at 4°C) and then filtered (0.2 µm filter). Absorbance in the UV was measured between 600 and 200 nm. The absorbance at 432 nm (with a corresponding ε of 22770 $M^{-1}cm^{-1}$) for Fluos-peptides, and at 445 nm (with a corresponding ε of 75940 $M^{-1}cm^{-1}$) for DAC-Aβ (112) were used for the determination of the concentration using the Lambert-Beer law.

- LL-37 and LL-37 segments stock solutions

Stock solutions of LL-37 and its segments were made by dissolving them in HFIP (at 4°C); concentrations were determined by weight or by BCA assay.

- Determination of the peptide concentrations via bicinchoninic acid (BCA) assay (113)

The bicinchoninic acid assay exploits a reduction of Cu^{2+} to Cu^{+} carried out by proteins in alkaline solutions combined with sensitive and colorimetric detection of the Cu^{+} by BCA. At 562 nm, the BCA/Cu complex has a linear absorbance with the increase of protein concentration.

3.2.4 Thioflavin T (ThT) binding assays

Thioflavin T (ThT) binding assay was applied to investigate the effects of LL-37 and the other peptides on the kinetics of IAPP fibrillogenesis, using a protocol previously described (26). IAPP alone (16.5 µM) and its mixtures with LL-37 or the other LL-37 derived segments were incubated in ThT assay buffer (aqueous 50 mM sodium phosphate buffer, pH 7.4, containing 100 mM NaCl and 0.5% HFIP) at 20°C, and at the indicated molar ratios in non-stirring conditions (26). Aliquots were mixed with the ThT solution consisting of 20 µM ThT in 0.05 M glycine/NaOH (pH 8.5) at the indicated time points and the binding to the dye was determined

by measuring fluorescence emission at 486 nm upon excitation at 450 nm using a Multilabel reader VictorX3 (26, 114).

To study the effect of LL-37 on nucleation of IAPP fibril formation in the presence of IAPP fibrils (fIAPP), IAPP (16.5 µM), and its mixtures with LL-37 (1/1) were incubated at room temperature as described above. An aliquot of a solution consisting mostly of IAPP fibrils (fIAPP, 7 days aged IAPP (16.5 µM) prepared as above) was added to the incubations with a final fIAPP concentration of 1.65 µM (10%). Control incubations of IAPP alone (16.5 µM) and 10% fIAPP alone were included. ThT binding was determined at the indicated time points as above (114).

The investigation of the effect of LL-37-treated IAPP fibrils (LL-37-treated fIAPP) on the kinetics of IAPP fibrillogenesis compared to the seeding effect of fIAPP was carried out as well. "LL-37-treated fIAPP" were obtained by adding an aliquot of a solution consisting mostly of fIAPP (16.5 µM fIAPP, 7 days aged; made as above) to a 10-fold molar excess of solid LL-37, and the mixture was incubated for 24 hours. An aliquot of the fIAPP, treated in the same way as the LL-37-treated aliquot, was used to determine the seeding effect of fIAPP. Incubations containing IAPP alone (16.5 µM), IAPP seeded with fIAPP (10%), and IAPP seeded with LL-37-treated fIAPP (10%) were prepared in the ThT assay buffer and kinetics of fibrillogenesis were determined by the ThT binding assay as described above (114).

Thioflavin T (ThT) binding assay was also applied to investigate the effects of LL-37 and LL-37A5,6 on the kinetics of Aβ42 fibril formation. Aβ42 (5 µM) and its equimolar mixture with LL-37 or LL-37A5,6 were incubated in 50 mM ammonium acetate buffer (pH 8.5), containing 10% of a 100 µM solution of ThT dye in 0.05 M glycine/NaOH (pH 8.5) in a Fluoro-Nunc black 96-well plate. Incubations were kept at 37°C for 5 hours shaking at 500 rpm. After 5 hours, samples were kept at 37°C without shaking. Samples were measured at the indicated time points and the binding to the dye was determined by measuring fluorescence emission at 486 nm upon excitation at 450 nm using a Multilabel reader VictorX3 (Perkin Elmer Life Sciences).

3.2.5 Assessment of cell damage by the MTT reduction assay

Peptide solutions made for the ThT binding assays were also applied to evaluate the effects of LL-37 and the other peptides on the formation of β-cell damaging IAPP assemblies studied in the rat insulinoma cell line RIN5fm (25, 26). Briefly, RIN5fm cells were cultured in RPMI 1640 medium containing 10% heat-inactivated calf serum, 2 mM L-glutamine, 100 U/ml penicillin/streptomycin, 0.1 mM non-essential amino-acid (NEAA), 1 mg/ml glucose, and 1 mM sodium pyruvate. RIN5fm cells were treated with trypsin and plated at a density of 6×10^5 cells/ml in 96-well plates (115). Solutions of IAPP alone and its mixtures with peptides were aged in ThT assay buffer as described in section 3.2.4. At 24 h or 7 days, aliquots were diluted with cell culture medium and added to the cells. After a ~20 h incubation time with the cells at 37°C in a humidified atmosphere containing 5% CO_2, cell damage was verified by the MTT reduction assay (25, 26, 114, 115).

In this work, the MTT reduction assay was also used to study the effects of LL-37 and LL-37A5,6 on the cytotoxic effects of Aβ42 on pheochromocytoma cancer cells (PC-12) from adrenal medulla granules from rats. PC-12 cells were cultured in RPMI 1640 medium containing 10% heat-inactivated horse serum, 5% fetal calf serum, and penicillin/streptomycin (25U/ml). PC-12 cells were treated with trypsin and plated with a density of 1×10^5 cells/ml in 96-well polylysine coated plates (51). At 6 days, aliquots were diluted with cell culture medium and added to the cells. After a ~20 h incubation time with the cells at 37°C in a humidified atmosphere containing 5% CO_2, cell damage was verified by the MTT reduction assay for 90 minutes at 37°C, and cells were successively lysed with 10% SDS in 20mM HCl, pH 4.5 and the plate was shaken for 24 hours. Finally, the absorbance at 570 nm was determined with a 2030 Multilabel Reader VictorX3.

100% of MTT reduction was set to the absorbance value of the cells containing medium alone, while 0% cell viability was defined as the absorbance value of the cells containing 0.1% Triton-X in H_2O. Normalization of the obtained absorbance values was done following the formula:

$$\%\, MTT\ reduction = \frac{\mathrm{Abs(sample)} - Abs(0.1\%\ Triton - X)}{\mathrm{Abs(medium)} - Abs(0.1\%\ Triton - X)} \cdot 100$$

where Abs= absorbance value obtained in wells
To determine the IC_{50} of the inhibitory effect of LL-37 and its segments on the formation of cytotoxic IAPP aggregates, 24 h aged IAPP (100 nM) alone and its mixtures with various amounts of LL-37 (prepared as under section 3.2.4) were added to the cells and cell viability was determined by the MTT reduction assay as above (26, 79).

3.2.6 Spectroscopic methods

1. UV/Visible spectroscopy

Concentrations of peptides (c) and IAPP were determined, as previously described in 3.2.3, using a Jasco V630 spectrophotometer by UV spectroscopy and applying the Lambert-Beer law.

$$\mathrm{A} = \varepsilon \cdot \mathrm{c} \cdot \mathrm{b}$$

where A= absorbance, ε= molar extinction coefficient, c= molar concentration, b= path length

2. Fluorescence spectroscopic titrations

A JASCO FP-6500 fluorescence spectrophotometer was used for the fluorescence spectroscopic titration studies using a previously described experimental protocol (25, 26, 112). Briefly, excitation was carried out at 492 nm and emission spectra were recorded between 500 and 600 nm for titrations of Fluos-IAPP. For DAC-Aβ, excitation was carried out at 430 nm and emission spectra were recorded between 440 and 550 nm. Titrations of synthetic Nα-amino-terminal fluorescein-labeled IAPP (5 nM) or with N-terminal fluorescently labeled Aβ40 (7-diethylaminocoumarin-3-carbonyl-Aβ40) (20 nM) and with various amounts of each of the peptides were carried out to determine the apparent (app.) K_ds of the interactions of IAPP or Aβ40 with LL-37 and its segments. Freshly prepared stocks of peptides and their fluorescently labeled analogs in HFIP were used. Measurements were carried out at room temperature in 10 mM sodium phosphate buffer (pH 7.4) containing 1% HFIP within 2-5 min following solution preparation. Of note, under these conditions freshly prepared Fluos-IAPP (5 nM) or DAC-Aβ (20 nM) solutions consist mostly of monomers (25). Apparent (app.) K_ds were calculated using 1/1 binding models as previously described and are means (± SD) of three binding curves (25, 26, 52, 116). Fitting of the sigmoidal curves was done by using Origin software, applying the following formula:

$$F = \mathrm{F_0} + \frac{\mathrm{F_{max}} - \mathrm{F_0}}{1 + 10^{[(\log \mathrm{K_d} - \mathrm{L}) \cdot m]}}$$

where:
F= fluorescence intensity
F_0= fluorescence intensity of the Fluos-labeled peptide
F_{max}= maximal fluorescence intensity
$\log K_d$= logarithm of the dissociation constant
L= concentration of the ligand
M= slope of the curve

To calculate binding affinities for app. K_d values below 100 nM another formula was applied using the Grafit version 5 program (25, 117):

$$F = \mathrm{F_{min}} + (\mathrm{F_{max}} - \mathrm{F_{min}}) \cdot \sqrt[2]{\frac{\frac{[E_0] + [L_0] + [K_d]}{2} - \frac{([E_0] + [L_0] + [K_d])^2}{4} - [E_0] \cdot [L_0]}{[L_0]}} + S \cdot [E_0]$$

where:
F= fluorescence emission
$F_{min/max}$= minimal fluorescence emission /maximal fluorescence emission
L_0= concentration of the labeled peptide
E_0= concentration of the unlabeled peptide
S= slope
K_d= dissociation constant (app. K_d)

3. Far-UV CD spectroscopy

Far-UV CD studies were performed using a Jasco 715 spectropolarimeter. Spectra were recorded directly after the solution preparation at room temperature between 195 and 250 nm, at 0.1 nm intervals, and with a response time of 1 second. Each spectrum is an average of 3 spectra. All CD measurements were performed at room temperature, in aqueous 10 mM sodium phosphate buffer (pH 7.4) (1xb buffer) with or without 1% HFIP; this assay system has been earlier developed and found to be suitable for following the kinetics of IAPP (5 µM) misfolding into β-sheets and amyloid fibrils alone or in the presence of inhibitors. All peptide stocks were freshly made in HFIP at 4°C and diluted within the cuvette in CD assay buffer at room temperature and in the indicated concentrations. Spectra were measured after gentle mixing immediately or at the indicated incubation time points. Interaction studies between IAPP and peptides alone or in 1/1 molar ratio mixtures were carried out preparing solutions in HFIP at 4°C and diluted within the cuvette in CD assay buffer at room temperature. CD spectra were measured as above. The CD spectrum of the buffer was always subtracted from the CD spectra of the peptide solutions before converting the raw data into mean residue ellipticity (MRE).

$$MRE\left[\frac{deg \cdot cm^2}{dmol}\right] = \frac{100 \cdot \theta}{\mathrm{c} \cdot \mathrm{d} \cdot \mathrm{n}}$$

where c is the concentration in mol/L, d is the path length in cm, n is the number of amino acids and θ is the ellipticity in deg. The MRE is plotted versus the wavelength.

3.2.7 Microscopy methods

1. Transmission electron microscopy (TEM)

To confirm fibril formation or peptide inhibitory activities, transmission electron microscopy was applied. Samples were prepared applying 10 µl aliquots of the solutions used in the ThT binding and MTT reduction assays on carbon-coated grids at the indicated time points. Following a washing step using ddH_2O, grids were stained with aqueous 2% (w/v) uranyl acetate solution (25, 26, 51, 118). Examination of the grids was done with a JEOL 1400 Plus electron microscope at 120 kV at the division for electron microscopy of the department of chemistry of TUM.

2. 2-Photon microscopy and FLIM imaging

For the 2-photon microscopy, TAMRA-IAPP (16.5 µM), its mixture with N-terminal fluorescein-labeled LL-37 (FAM-LL-37) or with N-terminal fluorescein-labeled peptides (Fluos-peptides) in the indicated molar ratios, were incubated at 20°C in 1xb buffer (10 mM sodium phosphate buffer, pH 7.4) for 7 days. Thereafter, samples were spotted onto SuperFrost Plus adhesion slides, air-dried, and then embedded with Prolong Diamond Antifade Mountant using a high precision microscopy cover glass. Examination of the samples was

carried out at the Institute for Stroke and Dementia Research (ISD) at LMU using a two-photon Leica TCSPC SP8 DIVE microscope equipped with an HC PL IRAPO 25x/1.0 WATER objective. A tunable laser from 680 nm to 1300 nm was coupled with the instrument and images were collected using hybrid diode detectors and a sequential scanning mode (HyD-RLD, reflected light detection) (TAMRA: excitation at 1100 nm/emission at 560-630 nm; Carboxyfluorescein: excitation at 920 nm/emission at 480-560 nm). Images were processed with the LAS-X software package, while deconvolutions were performed using Huygens Professional or the Leica Lightning application. For some samples, fluorescence lifetime imaging (FLIM) was carried out. For this, up to 1000 photons per pixel were captured in a time-correlated single photon counting (TC SPC) mode. A Leica FALCON software was applied to fit the fluorescence decay curves utilizing multi-exponential models. The number (n) of components used for the fittings was manually fixed between 2 and 4 to minimize the χ^2 statistics and consequently to have the best fit of the data. The fluorescence lifetime of the donor fluorescent molecule in absence of an acceptor was always analyzed as a control. The amplitude-weighted average lifetime was calculated with the following formula:

$$\tau = \frac{\Sigma(\alpha_i t_i)}{\Sigma a_i}$$

where α_i is the amplitude of each lifetime τ_i.
The FLIM-FRET efficiency was calculated with the following formula:

$$FRET\ efficiency = 1 - \frac{T_{DA}}{T_D}$$

where T_{DA} is the lifetime of the donor in the presence of the acceptor and T_D is the lifetime of the donor without the acceptor.

3.2.8 Cross-linking, NuPAGE, and Western Blot analysis

Cross-linking studies were carried out using a previously developed assay system (26). Briefly, solutions of IAPP alone (30 µM) and its mixtures with LL-37 or its derived peptides at the described molar ratios, or peptides alone (30 µM) were prepared in aqueous sodium phosphate buffer, pH 7.4, and incubated at room temperature for the indicated time (30 minutes or 7 days). Solutions were cross-linked with 25% aqueous glutaraldehyde and 10% aqueous TCA was used to precipitate cross-linked peptides (25, 52). The obtained pellets were dissolved in reducing NuPAGE sample buffer, boiled for 5 min at 95°C, and subjected to NuPAGE electrophoresis in 4-12% Bis-Tris gels with MES running buffer. 20 µl of all samples were loaded in the lanes. Peptides were then blotted using an XCell II Blot Module blotting system. The detection of IAPP or LL-37 was done with a polyclonal rabbit anti-IAPP antibody or a monoclonal mouse anti-LL-37 antibody in combination with suitable peroxidase (POD)-coupled secondary antibodies and the Super Signal West Dura Extended Duration Substrate (114).

3.2.9 Dot blot analysis

To carry out the dot blot assay, solutions of IAPP monomers or IAPP fibrils (fIAPP) (different amounts up to 40 µg) were spotted onto a nitrocellulose membrane. Solutions were prepared by incubating an IAPP solution (1 mg/ml) in ThT assay buffer for 0 h ("monomers") or 24 h ("fibrils"). The membrane was then washed with TBSn (20 mM Tris/HCl, 150 mM NaCl and 0.05% Tween-20), blocked with 5% milk powder in TBSn overnight at 10°C, and washed again with TBSn. The following step is the incubation of the membrane with N-terminal fluorescein-labeled LL-37 (FAM-LL-37) at 200 nM concentration in ThT assay buffer containing 1% HFIP overnight at 10°C. After washing with incubation buffer and TBSn, bound FAM-LL-37 was visualized with a LAS-4000mini instrument (Fujifilm). As a control for the binding specificity of FAM-LL-

37 to fIAPP, glucagon fibrils were spotted. Glucagon fibrils were made by incubating glucagon in 10 mM HCl (2 µg/µl) (10 days) followed by neutralization with 10 mM NaOH; ThT binding assay was used to verify the fibril formation. As a control for non-specific binding (NSB), the ThT buffer alone was spotted as well. Finally, to evaluate the interference of the fIAPP autofluorescence a membrane containing spotted fIAPP which had been incubated in buffer alone was included in each assay. The contribution of the fibrils to the total amount of fluorescence of FAM-LL-37 bound to IAPP fibrils observed was up to 25% (114).

3.2.10 Determination of LL-37 binding sites by using peptide arrays

LL-37 decamers covering the full-length LL-37 sequence and shifted by one residue were synthesized using a peptide array on a modified cellulose membrane using stepwise SPOT synthesis protocols and a MultiPep RSi (Intavis) peptide synthesizer (52, 119, 120). SPPS with Fmoc-strategy was used: Fmoc cleavage was performed using 20% piperidine in DMF, followed by the amino acid coupling with 1.1 M HOBt and 17% (v:v) DIC in DMF. After each coupling, a capping step with acetic anhydride was performed. The decamers were dispensed on an activated glass surface applying a droplet-depositing system. Following, peptides were chemo-selectively immobilized and purified by reaction of the peptides with the modified glass surface resulting in the formation of a covalent bond that allowed the removal of acetylated side products via several washing steps. After all peptides were arrayed on the glass surface, active residues were passivated. Subsequently, glass slides were blocked using 1% BSA in TBSn (20 mM Tris/HCl, 150 mM NaCl and 0.05% Tween-20) for 4 h at room temperature and then incubated with a solution of Fluos-IAPP (1 µM in TBSn containing 1% BSA) for ~12 h at 10°C, followed by washing steps with TBSn. Bound Fluos-IAPP was visualized with a LAS-4000mini instrument (Fujifilm)(114).

3.2.11 Molecular docking simulations

Molecular docking simulations were carried out by Dr. Andrea Di Luca at the University of Fribourg to study the 1:1 IAPP/LL-37 and 1:2 IAPP/LL-37 complexes. The structures of IAPP (PDB ID: 2L86) (121), LL-37 monomer (PDB ID: 5NMN) (79), and LL-37 dimer (PDB ID: 5NNM) (79) were used to generate a peptide-peptide docked structure using Rosetta. The Monte Carlo docking protocol included in Rosetta (rosetta_src_2020.08.61146 version) was applied, using the rosetta2015 scoring function (122) and standard input parameters (123, 124). The PDB structures were prepared assigning standard protonation states to protonatable amino acids. For both complexes, 20000 docked structures were initially generated and ranked by their Rosetta score. The top 1% (200 structures) were then refined (minimized the structure). 500 structures were generated for each conformation using the Rosetta refining protocol with standard parameters, and the lowest refined score for each of the 200 structures was finally selected. The results are shown for the absolute lowest score, or most stable, structure. Only sidechains were kept flexible during the docking procedure, while for the minimization procedure both the sidechain and backbone atoms were allowed to relax. Energy breakdown analysis was performed using the residue_energy_breakdown tool included in the Rosetta package.

3.2.12 Sequence alignment using LALIGN

The sequence alignment of IAPP and LL-37 was done with the program LALIGN (Author: Bill Pearson; https://embnet.vital-it.ch/software/LALIGN_form.html). The comparison of the Aβ and IAPP sequences was previously performed with this program (50). A global alignment method was used with 3 reported sub-alignments; E-value threshold was set to 10.0, the scoring matrix used is BLOSUM50, opening gap penalty was set to -12, and extending gap penalty to -2 (default values) (114). The LALIGN program implements the algorithm of Huang and Miller (125).

4 Results

4.1 The human LL-37 as a potent inhibitor of IAPP self-assembly

The first chapter of my work addresses the question whether LL-37 is a binding partner of IAPP and if it can block its aggregation into cytotoxic amyloid fibrils.

4.1.1 IAPP/LL-37 sequence alignment

The first part of this work focused on the study of the ability of LL-37 to bind and suppress IAPP self-association and its cytotoxicity to pancreatic β-cells. In fact, previous studies carried out by Barron's group showed that LL-37 is a binding partner of amyloid-β involved in AD and intervenes in its fibrillogenesis and into the formation of neurotoxic aggregates (99). A sequence alignment of the sequences of LL-37 and IAPP performed with the software LALIGN showed that the two peptides share a pronounced sequence similarity (42%) and slight sequence identity (5%), as shown in Figure 12 (114). Based on the above we asked if LL-37 could interact with IAPP. Additionally, to study the properties of the C- and N- termini of this peptide, the sequence was dissected into two parts, leading to LL-37(1-14) and LL-37(15-37). A scrambled LL-37 sequence was used as control.

```
IAPP            KC-NTATCATQRLANFLVHSSNNFGAILSSTNVGSNTY

LL-37           LLGDFFRKSKEKIGKEFKRIVQRIKDFLRNL-VPRTES

LL-37(1-14)     LLGDFFRKSKEKIG

LL-37(15-37)    KEFKRIVQRIKDFLRNLVPRTES

scrLL-37        GLKLRFEFSKIKGEFLKTPEVRFRDIKLKDNRISVQR
```

Figure 12. Sequences of IAPP, LL-37, LL-37 segments, and scrambled LL-37 (IAPP C-terminal amide; LL-37 and derived peptides C-terminal COOH). Similar residues between IAPP and LL-37 are marked in blue and identical residues in green. Sequence alignment was performed with LALIGN (125). The figure is taken from Armiento et al. (ACIE, 2020) (114).

4.1.2 Studies on the inhibitory activities on fibrillogenesis and cytotoxicity of IAPP

We first addressed the question whether LL-37 could interfere with IAPP aggregation and the formation of cytotoxic species utilizing the ThT assay in combination with TEM and MTT reduction assay. IAPP at a final concentration of 16.5 μM was incubated alone and with LL-37 (1/1). Kinetics of the fibril formation was followed by ThT fluorescence until 168 hours (Figure 13a). After 24 hours (Figure 13b) and 7 days (Figure 13c), solutions were added to RIN5fm cells and the effect on the cytotoxicity was monitored via MTT reduction assay. LL-37 effectively suppressed IAPP self-association and its cell-damaging effect at a 1/1 molar ratio for 7 days. In addition, an incubation of LL-37 alone (16.5 μM) was included, showing neither fibrillogenesis nor cytotoxicity. These findings were also supported by TEM images which revealed that the 1/1 mixture presents amorphous aggregates as the main species, in contrast with IAPP alone that exhibits mainly fibrils. TEM images of LL-37 alone showed fibrils in addition to the abundant amorphous aggregates (Figure 13d). Importantly, a scrambled sequence of LL-37 was not effective in the inhibition of self-assembly and cytotoxicity of IAPP both in 1/1 (Figure 13a, b, c, d) and in 1/10 ratios (Appendix Figure A 1). In fact, the ThT binding assay clearly shows that IAPP forms fibrils already after 24 hours when it is co-incubated with scrLL-37 (1/1). This mixture reduces the cytotoxicity slightly at 24 hours, but this effect is completely lost after 7 days. The presence of fibrils as the main species was also confirmed by TEM, supporting the obtained results (114).

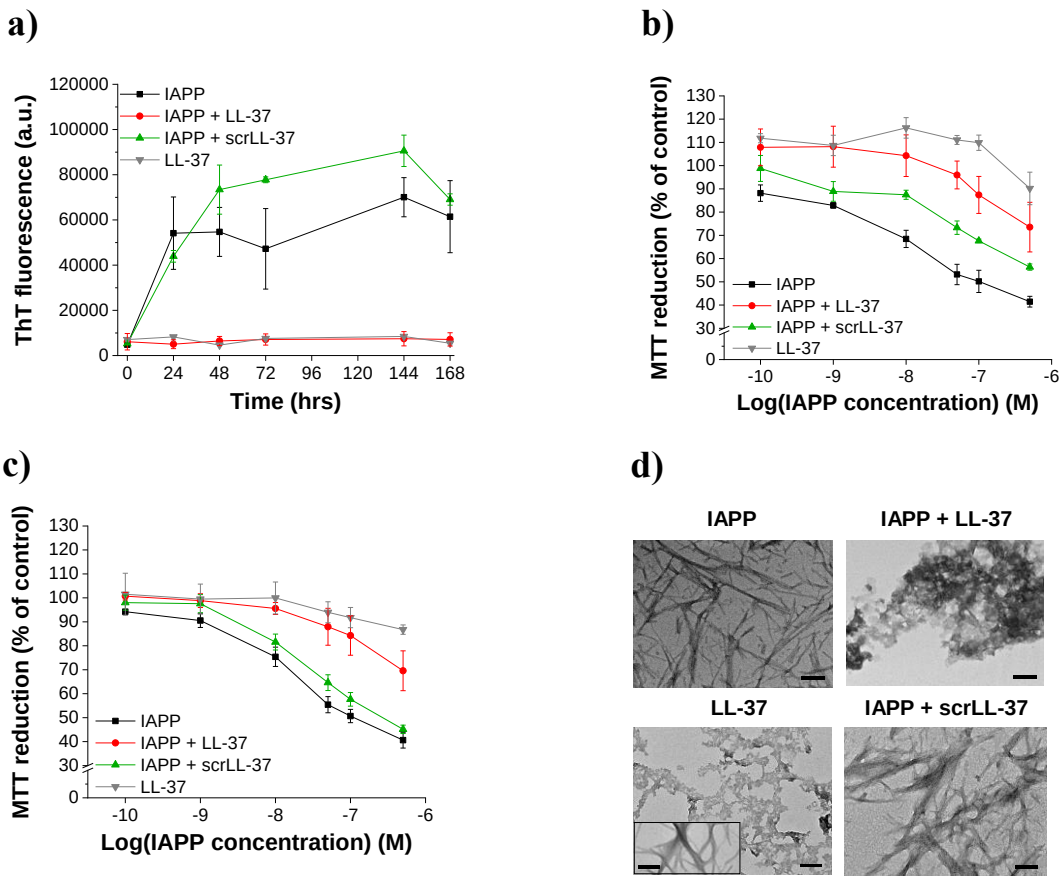

Figure 13. Effects of LL-37 on IAPP amyloid formation and cytotoxicity. a) Fibrillogenesis of IAPP (16.5 μM) and its mixtures with LL-37 (1/1) or scrambled LL-37 (1/1) (means (±SD), 3 assays); amyloidogenicity of LL-37 (16.5 μM) was tested (1 assay). b) Effects on cell viability: solutions from a) were added to cultured RIN5fm cells (24 hours aged). c) effects on cell viability: solutions from a) were added to cultured RIN5fm cells (7 days aged). Cell viability was determined by MTT reduction (means (±SD), 3 assays, n=3 each); cytotoxic effects of LL-37 were also tested (1 assay, n=3). d) TEM images of solutions of a) (7 days aged) as indicated (bars, 100 nm). The figure is taken from Armiento et al. (ACIE, 2020) (114).

Interestingly, when IAPP was mixed with LL-37 in higher molar ratios, a different effect on cytotoxicity was observed. In Figure 14a it is shown that the fibril formation of IAPP is efficiently suppressed when LL-37 is present in equimolar ratio, and in 5-fold excess to IAPP. MTT reduction assay results correlate with the kinetics studies, as the inhibitory effect on the cytotoxicity to RIN5fm cells at 24 hours is very similar for both ratios, as shown in Figure 14b. Notably, the effectiveness of the inhibition of IAPP cytotoxicity depends on the intrinsic toxicity that IAPP retains when it is not aged (time zero). In fact, the profile of the curves strictly depends on how cell-damaging IAPP is when it is not aged yet (Figure 14b). After 7 days the effect on the cytotoxicity was different: while the 1/1 mixture could suppress the toxicity, the mixture containing the 5-fold excess of LL-37 was toxic, although LL-37 alone (82.5 μM) exhibited no toxicity (Figure 14c). TEM images revealed that the 1/5 mixture contained fibrils as the main species. Their morphology is clearly different from IAPP alone, as they result longer and thicker than IAPP fibrils. This result might explain the cytotoxicity at 7 days. Of note, LL-37 alone at 5-fold excess mainly showed amorphous aggregates, a result which correlates with the MTT reduction assay findings (Figure 14d). To evaluate the inhibitory potency of LL-37, studies on the half-maximal inhibitory concentration (IC_{50}) on the formation of cytotoxic IAPP species were carried out. An IC_{50} of 17 (± 1.7) nM was found for LL-37 (Figure 15), leading to the conclusion that LL-37 is a nanomolar inhibitor of IAPP aggregation (114).

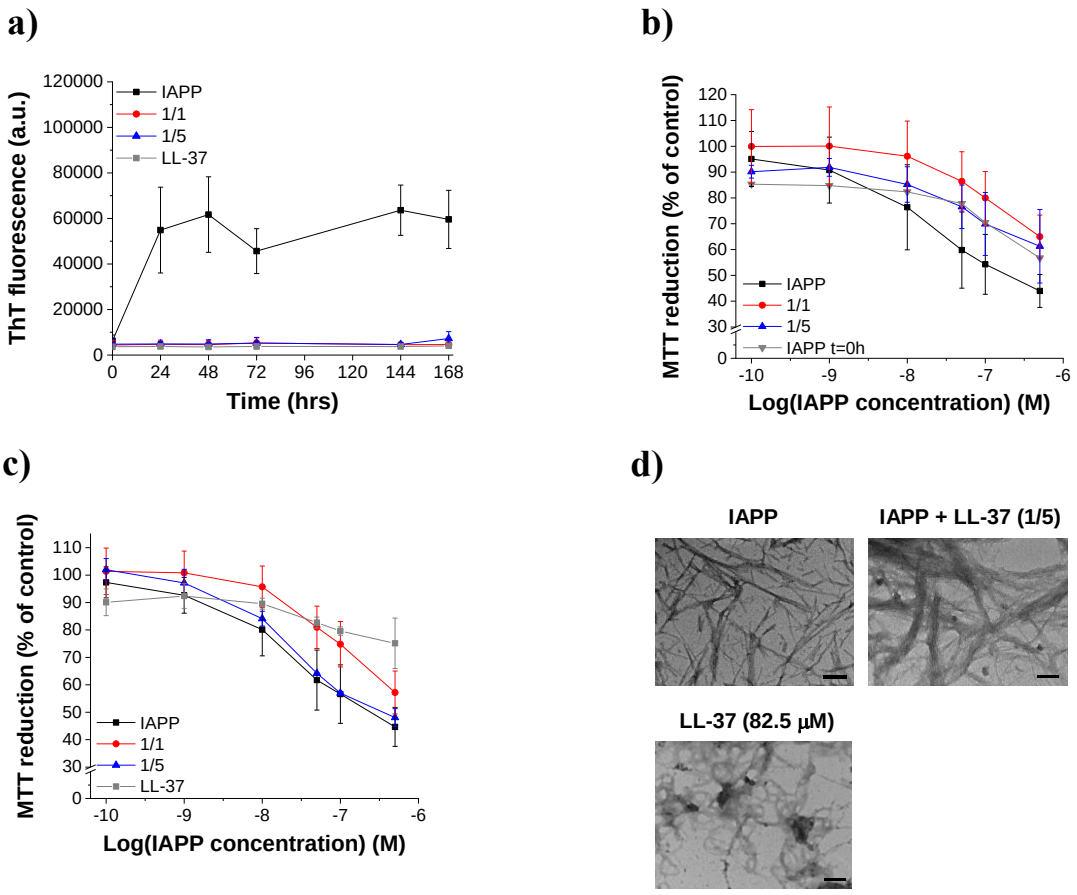

Figure 14. Different effects of LL-37 on IAPP amyloid formation and cytotoxicity. a) Fibrillogenesis of IAPP (16.5 µM) and its mixtures with LL-37 in equimolar ratio or 5-fold excess (means (±SD), 3 assays); amyloidogenicity of LL-37 (82.5 µM) was tested (1 assay). b) Effects on cell viability: solutions from a) were added to cultured RIN5fm cells (24 hours aged). Cytotoxicity of non-aged IAPP was tested (1 assay shown); c) effects on cell viability: solutions from a) were added to cultured RIN5fm cells (7 days aged). Cell viability was determined by MTT reduction (means (±SD), 3 assays, n=3 each); cytotoxic effects of LL-37 were also tested (1 assay, n=3). d) TEM images of solutions of IAPP and its 1/5 mixture with LL-37 (7 days aged) as indicated (bars, 100 nm).

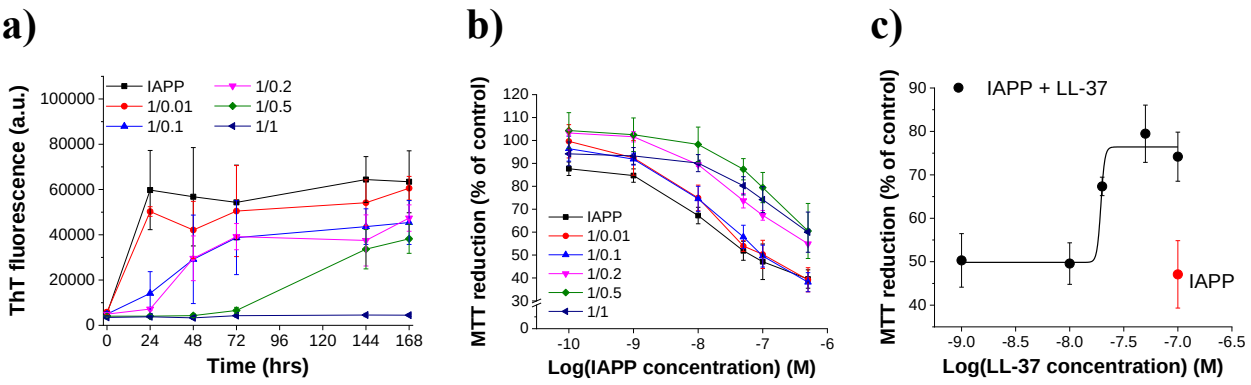

Figure 15. Dose-dependence of the inhibitory effect of LL-37 on IAPP fibrillogenesis and cytotoxicity. a) Fibrillogenesis of IAPP (16.5 µM) alone or with different molar ratios of LL-37 as indicated (means (±SD), 3 assays); b) effects on cell viability: solutions from a) were added to cultured RIN5fm cells (24 hours aged). c) IC50 of the inhibitory effect of LL-37 on cytotoxic effects of IAPP determined by titration of IAPP (100 nM) with LL-37(means (±SD), 3 assays, n=3 each). The figure is taken from Armiento et al. (ACIE, 2020) (114).

We also addressed the question whether LL-37 could intervene with the nucleation of IAPP induced by the presence of fibrillar IAPP (fIAPP). For this study, an aliquot of 7 days aged fIAPP (10%, final concentration

of 1.65 µM) was added to IAPP (16.5 µM) and its mixture with LL-37 (1/1). Incubations of IAPP alone, and 10% fIAPP were included as controls. Kinetics of the fibril formation were followed via ThT binding assay. Non-seeded IAPP had a lag phase of 24 hours, while seeded IAPP exhibited a lag phase of circa 6 hours. In the presence of LL-37 in an equimolar ratio, the seeding effect of fIAPP was fully suppressed, as no increase of the ThT fluorescence signal could be observed (Figure 16a) (114).

Next, we asked if fIAPP treated with 1x and 10x of LL-37 could still seed IAPP and enhance its fibril formation. For this experiment, 7 days aged fIAPP were added with solid, pure LL-37 in a 1/1 or 1/10 ratio. The treated fibrils were further aged for 24 hours and then used to seed IAPP (final concentration of 1.65 µM, 10% in both cases). IAPP alone (16.5 µM) and IAPP seeded with 10% fIAPP, as described above, were added as controls. Kinetics of the fibril formation was followed via ThT binding assay. IAPP alone exhibited a lag phase of 24 hours and seeded IAPP (10% fIAPP) exhibited a 6 hours lag phase as described previously. When IAPP was seeded with 10% LL-37-treated fIAPP, where the fIAPP were incubated with 10x of LL-37, the seeding effect was fully inhibited. Studies suggest that the binding of LL-37 to IAPP fibrils converts them into seeding incompetent species. TEM images of the solutions at 6 hours revealed a different fibril morphology of fIAPP compared to fIAPP treated with 10x LL-37. Different species were found also for the IAPP seeded with 10% fIAPP and the IAPP seeded with 10% of 10x LL-37 treated fIAPP. The first exhibited fibril as the main species, while the latter showed mainly amorphous aggregates (Figure 16b, c) (114).

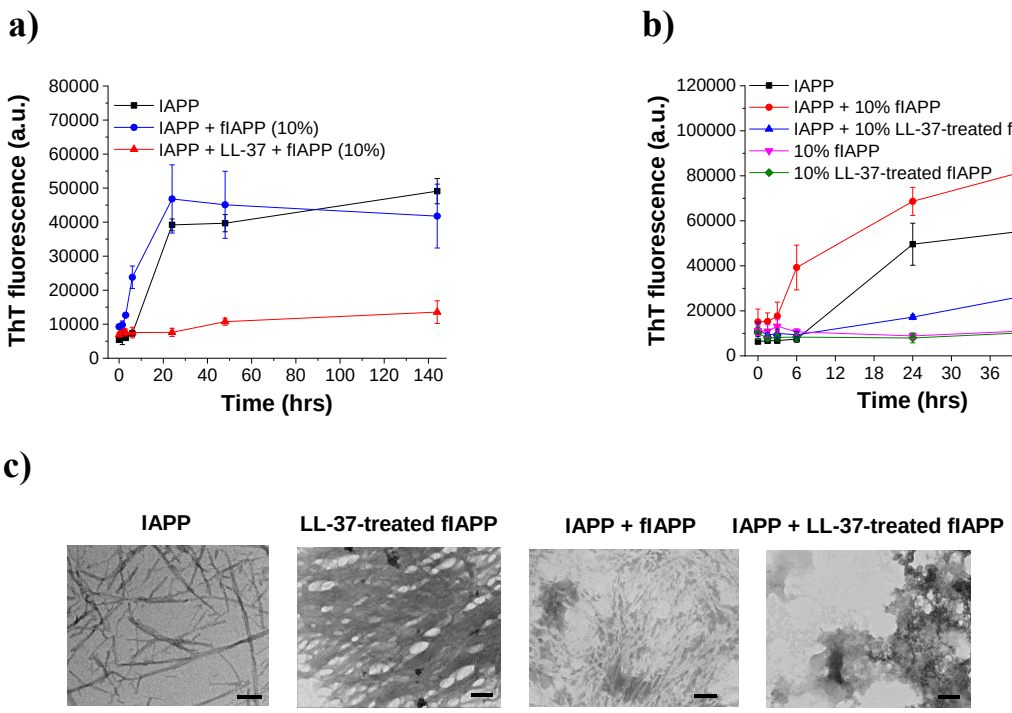

Figure 16. Effects of LL-37 on IAPP amyloid self-assembly kinetics. a) Amyloidogenicity of IAPP (16.5 µM) alone or mixed with LL-37 (1/1) in the presence of fIAPP (10%) determined by ThT binding (means (±SD), 3 assays). b) Amyloidogenicity of IAPP (16.5 µM) alone, in the presence of fIAPP (10%), or in the presence of LL-37 (10x) treated fIAPP (10%) determined by ThT binding (means (±SD), 3 assays). c) TEM images of solutions from 3b): IAPP fibrils, LL-37 (10x) treated fIAPP, IAPP seeded with 10% fIAPP and IAPP seeded with 10% LL-37 (10x) treated fIAPP. The figure is taken from Armiento et al. (ACIE, 2020) (114).

When the same experiment was carried out using fIAPP fibrils treated with 1x LL-37, a different result was observed. Kinetics of fibril formation followed via ThT binding assay show that, when IAPP was seeded with 10% LL-37-treated fIAPP, no inhibition of the seeding effect occurs. In fact, IAPP seeded with both fIAPP or 1x LL-37-treated fIAPP have a lag phase of six hours (Figure 17a). Incubation of IAPP with 10% LL-37 was added as control. Next, the question arose whether the excess of LL-37 in the 10x treated-fIAPP could cause the inhibitory effect. To answer this inquiry, the experiment described above was carried out using treated-

fIAPP with 10x LL-37 after separating them from the unbound LL-37 by centrifugation before using them to seed IAPP. Incubation of IAPP seeded with 10% LL-37 was added as control. Results were very similar to the experiment carried out without any centrifugation (Figure 17b).

To confirm the actual presence of the fIAPP and the LL-37-treated fIAPP in the pellets after centrifugation, a dot blot assay was carried out. IAPP fibrils, centrifuged fIAPP, and LL-37-treated fIAPP were spotted onto a nitrocellulose membrane. The detection of fIAPP was done with a monoclonal mouse anti-fIAPP antibody in combination with suitable peroxidase (POD)-coupled secondary antibodies and the Super Signal West Dura Extended Duration Substrate. No difference between the non-centrifuged and centrifuged fibrils was detected, confirming the presence of fibrils in the pellets (Figure 17c). Last, to confirm the presence of the unbound LL-37 in the supernatant of the above described centrifuged fibrils, a dot blot assay was carried out. For this purpose, untreated LL-37 (165 µM), the supernatant of a centrifuged 165 µM LL-37 solution, and the supernatant of the LL-37-treated fIAPP were spotted onto a nitrocellulose membrane. The detection of LL-37 was done with a monoclonal mouse anti-LL-37 antibody in combination with suitable peroxidase (POD)-coupled secondary antibodies and the Super Signal West Dura Extended Duration Substrate. Figure 17d clearly shows that the unbound LL-37 remains in the supernatant and its 10-fold excess is not responsible for the suppression of the seeding ability of LL-37.

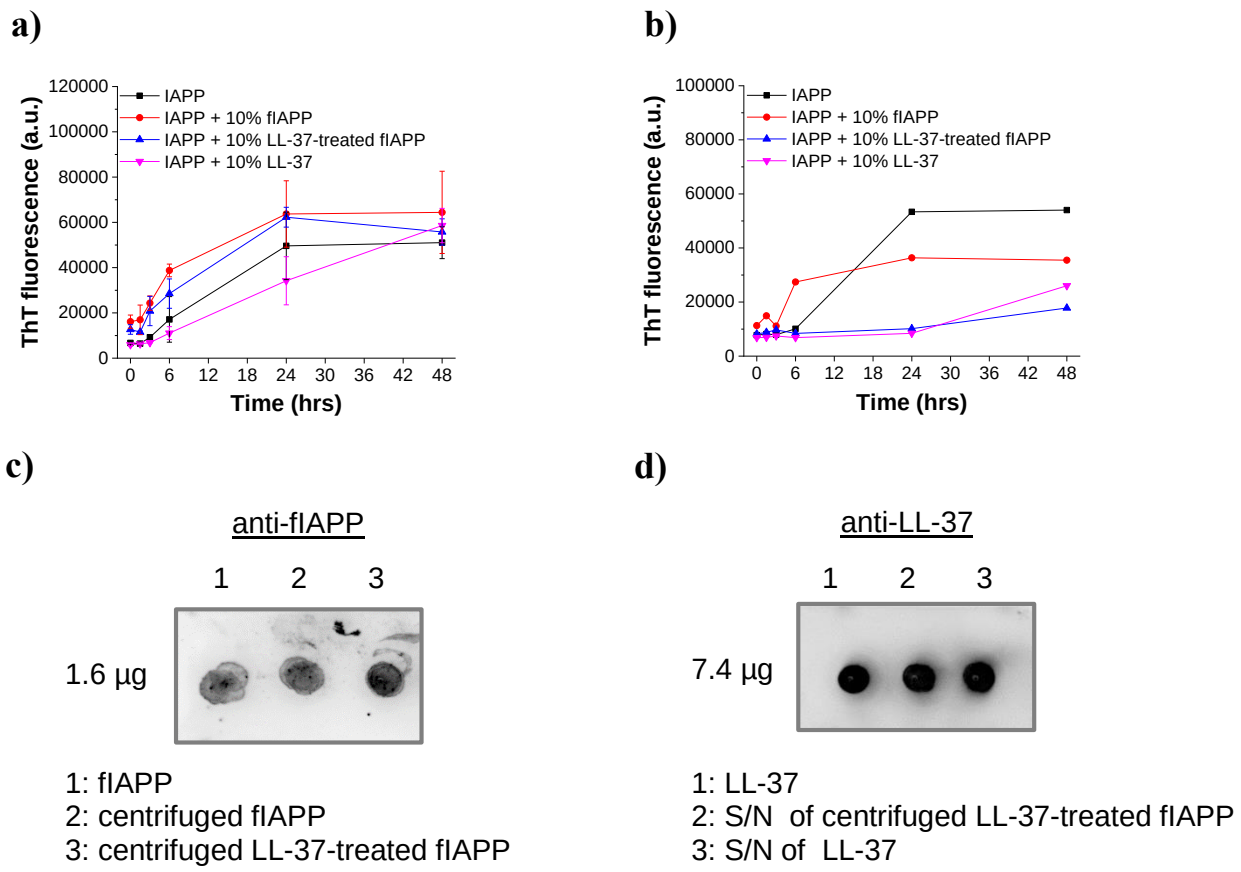

Figure 17. Effects of LL-37-treated fIAPP on IAPP amyloid self-assembly kinetics. a) Amyloidogenicity of IAPP (16.5 µM) alone, in the presence of fIAPP (10%), in the presence of LL-37 (1x) treated fIAPP (10%) or in the presence of LL-37 (10%) determined by ThT binding (means (±SD), 3 assays). b) Amyloidogenicity of IAPP (16.5 µM) alone, in the presence of fIAPP (10%), in the presence of LL-37 (10x) treated fIAPP (10%) or in the presence of LL-37 (10%) determined by ThT binding. IAPP fibrils, LL-37-treated fIAPP, and LL-37 were centrifuged prior use (n= 1 assay). c) Binding of anti-fIAPP antibody to centrifuged fIAPP or LL-37-treated fIAPP used in b). d) Binding of the anti-LL-37 antibody to supernatants of LL-37 or LL-37-treated fIAPP used in b).

Results of this section showed that LL-37 can efficiently suppress IAPP fibril formation in an equimolar ratio, with a half-maximal inhibitory concentration (IC_{50}) of 17 (± 1.7) nM. A scrambled LL-37 sequence did not

have any effect on the fibril formation also in 10-fold excess, underlining the importance of the primary structure of LL-37. Furthermore, LL-37 intervenes with the nucleation of IAPP induced by the presence of IAPP seeds (fIAPP), fully suppressing the seeding effect.

LL-37 could intervene with the nucleation of IAPP induced by the presence of fibrillar IAPP, fully suppressing the seeding effect. Last, when fIAPP were treated with LL-37 the seeding ability of these species was lost, suggesting that LL-37 converts IAPP fibrils into seeding incompetent species (Figure 18).

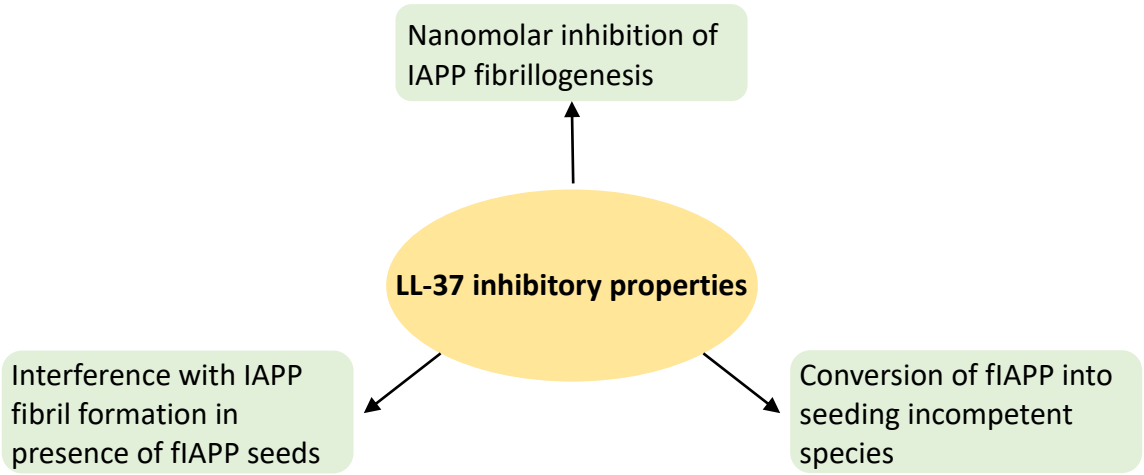

Figure 18. Schematic representation of the inhibitory properties of LL-37 on IAPP amyloid formation.

4.1.3 Determination of binding affinity towards IAPP

To evaluate the binding affinity towards IAPP, fluorescence spectroscopic titrations were carried out. N-terminal fluorescein-labeled IAPP (Fluos-IAPP, 5 nM) was titrated with increasing amounts of LL-37. The interaction with 100-fold excess of the titrant led to an increase of the fluorescence emission of 322%. The obtained app. K_d of 88.1 (± 12.0) nM confirmed the high affinity interaction between the two peptides (Figure 19a, b) (114).

Moreover, app. K_d of the interaction of oligomeric species of IAPP with LL-37 was determined by titrating N-terminal fluorescein-labeled LL-37 (FAM-LL-37, 5 nM) with various amounts of IAPP. The value of the app. K_d was > 2.5 μM (Figure 19c, d).

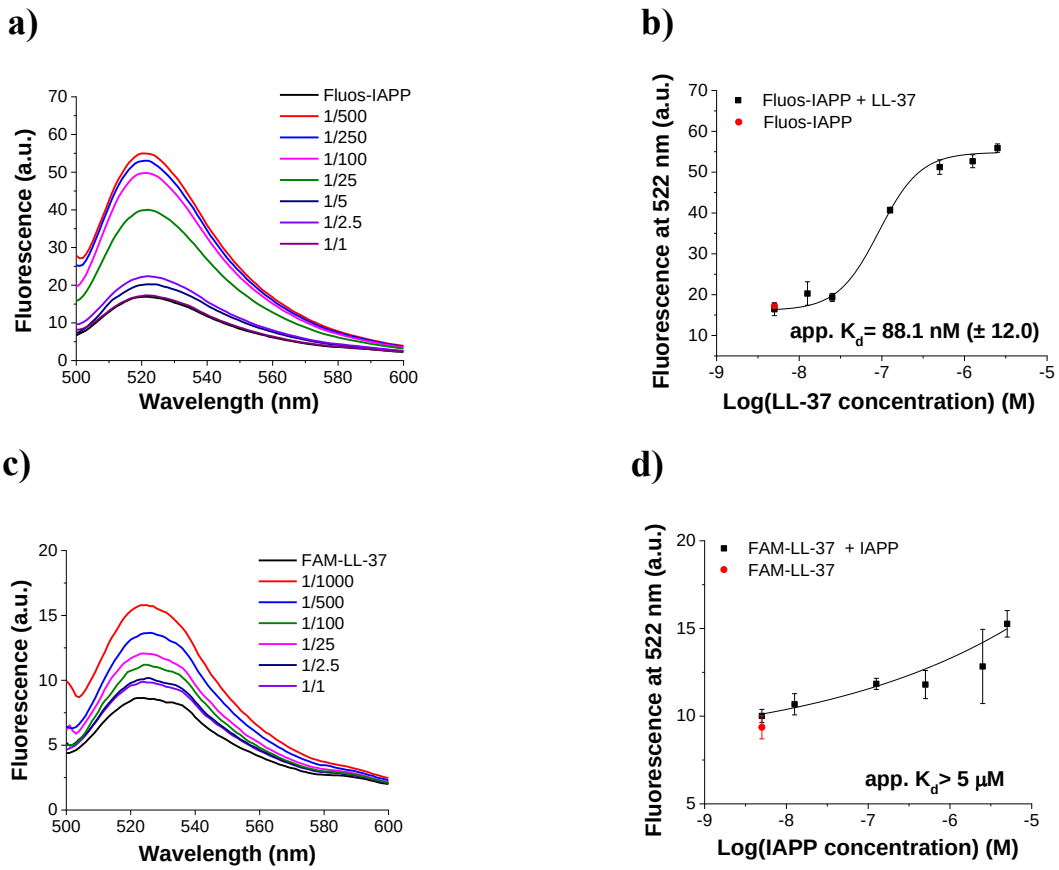

Figure 19. Determination of app. K_ds of interactions of LL-37 with monomeric and oligomeric IAPP by fluorescence titrations. a) Fluorescence emission spectra of Fluos-IAPP (5 nM) alone and its mixtures with increasing amounts of LL-37. b) Binding curve of LL-37. c) Fluorescence emission spectra of FAM-LL-37 (5 nM) alone and its mixtures with increasing amounts of IAPP. d) Binding curve of IAPP. Binding curves are means of 3 assays (±SD) (aqueous buffer 1×b, pH 7.4, containing 1% HFIP). Figures a) and b) are taken from Armiento et al. (ACIE, 2020) (114).

4.1.4 Interactions with IAPP monomers and fibrils by Dot Blot

To evaluate the capability of LL-37 to bind to monomeric IAPP or IAPP fibrils, dot blot experiments were carried out (114). Different amounts of IAPP monomers and fIAPP were spotted onto a nitrocellulose membrane, then the membrane was incubated with N-terminal fluorescein-labeled LL-37 (FAM-LL-37). Results show that LL-37 can bind both IAPP fibrils and monomers (Figure 20 top). The affinity of LL-37 to fIAPP is higher, as a signal could be detected up to 1 µg of fIAPP, whereas the monomer is binding detectable only until 10 µg of IAPP. Of note, to verify the specificity of the binding of FAM-LL-37 to fIAPP, glucagon fibrils were spotted onto the membrane as well, confirming the absence of binding of FAM-LL-37 to glucagon (Figure 20 bottom). As control, nitrocellulose membranes with the same amounts of IAPP monomers and fIAPP were incubated with assay buffer to exclude eventual intrinsic fluorescence signals of the amyloid fibrils (126, 127), as shown in Appendix Figure A 3.

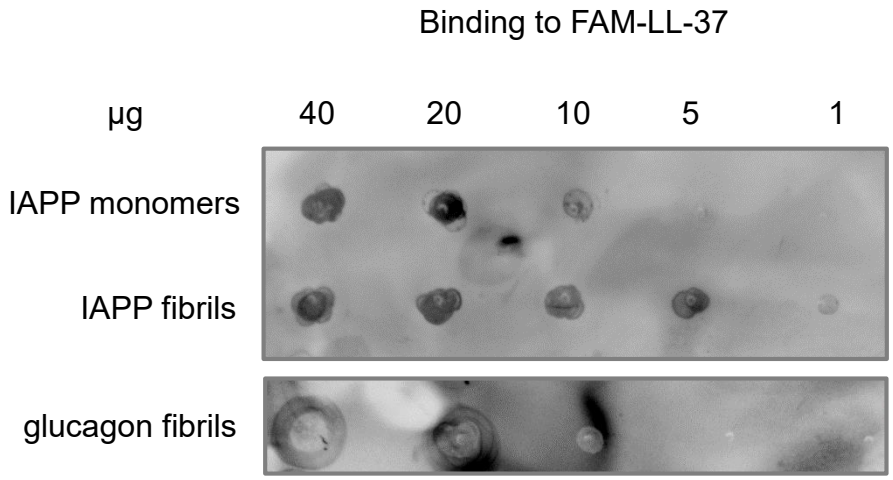

Figure 20. Binding of FAM-LL-37 to IAPP monomers and fibrils. IAPP monomers, fIAPP, and glucagon fibrils were spotted onto a nitrocellulose membrane and probed with 0.2 µM FAM-LL-37. Representative membrane is reported (n=3).

4.1.5 Interactions with IAPP by CD spectroscopy

To further characterize the effect of LL-37 on the misfolding of IAPP, far-UV CD spectroscopy was carried out. Spectra of IAPP, LL-37 (5 µM each), and of their 1/1 mixture were recorded at different time points (Figure 21). At 0 h, IAPP presents an unordered structure characterized by a strong minimum at ~ 200 nm. LL-37 exhibits an α-helix and β-sheet/turn structure, with two minima at ~ 210 nm and ~ 227 nm (n→π*) and a maximum at ~ 198 nm. Of note, the spectrum of the 1/1 mixture clearly differs from the sum of the spectra of the single peptides, indicating an interaction between the two (Figure 21a). The spectrum of IAPP recorded over time shows a transition to a β-sheet structure, an indication of the aggregation of the peptide resulting in precipitation at 24 hours (Figure 21b). The 1/1 mixture instead showed no precipitation and an increase in the unordered content (Figure 21c). Of note, the spectra of LL-37 alone were measured over time. The peptide undergoes a transition to a α-helical structure and loses the β-sheet/turn content, as the two minima shift from 210 nm to 206 nm, and from 227 nm to 222 nm. An overall decrease of the signal is visible, although no precipitation occurred after 24 hours (Appendix Figure A 4). A control experiment using scrLL-37 showed no interaction between IAPP and the peptide, as the sum of the single spectra is the same as the spectrum of the 1/1 mixture (Figure 21d). These results show that the interaction of IAPP and LL-37 leads to the formation of partially disordered assemblies that block the fibrillogenesis of IAPP (114).

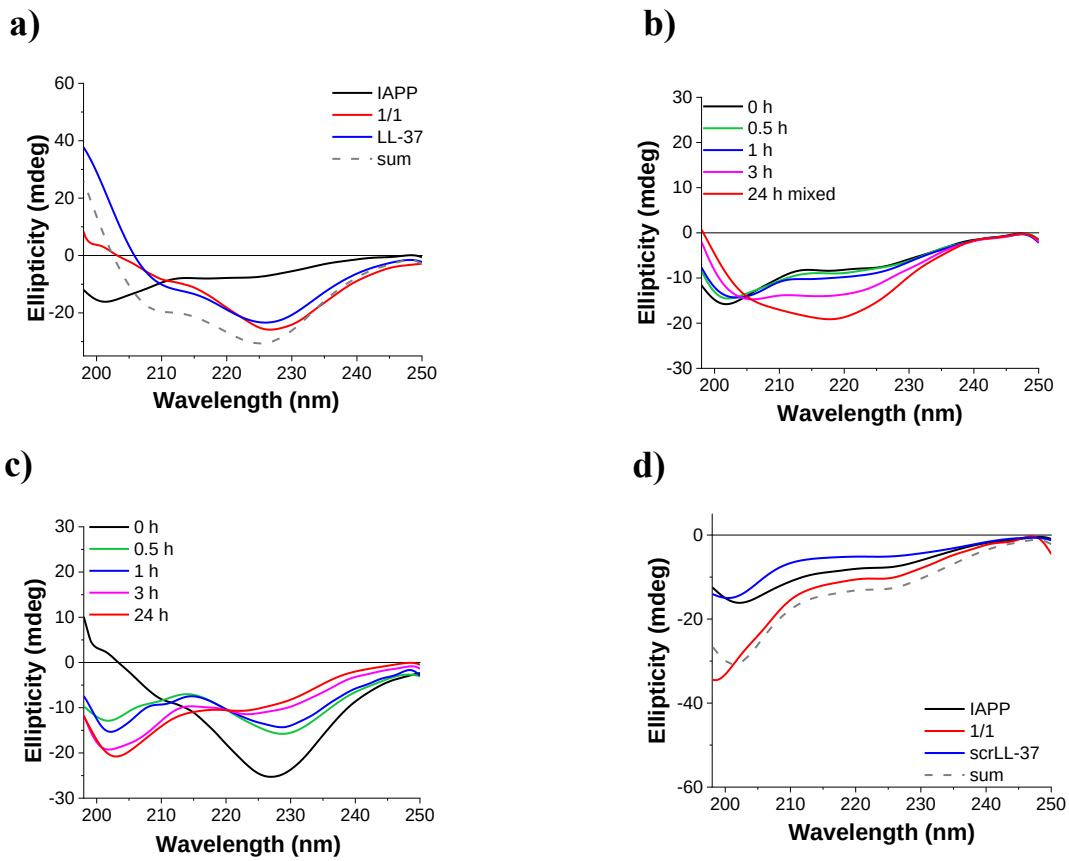

Figure 21. Characterization of the IAPP/LL-37 interaction. a) Far-UV CD spectra of IAPP (5 µM), IAPP/LL-37 mixture (1/1, 5 µM each), and LL-37 (5 µM), the mathematical sum of IAPP and LL-37 is shown (dashed gray line). b, c) Kinetics of IAPP misfolding (b) and in the presence of LL-37 (c). d) Far-UV CD spectra of IAPP (5 µM), IAPP/scrLL-37 mixture (1/1, 5 µM each), and scrLL-37 (5 µM), the mathematical sum of IAPP and scrLL-37 is shown (dashed gray line). Measurements were performed in aqueous buffer 1×b, pH 7.4, containing 1% HFIP. The figure is taken from Armiento et al. (ACIE, 2020) (114).

4.1.6 Characterization of the IAPP/LL-37 hetero-assemblies by cross-linking

NuPAGE electrophoresis followed by Western Blot (WB) was performed to investigate the formation of the LL-37/IAPP hetero-complexes. IAPP (30 µM) and its mixtures with LL-37 or with the control scrLL-37 in different molar ratios were incubated for 30 minutes. Figure 22 shows that IAPP contains low MW oligomers, consisting of di- to hexamers and high MW assemblies. Similar bands are visible in the mixtures of IAPP with scrLL-37 (1/0.1, 1/1, and 1/2) (Appendix Figure A6a), and in the presence of LL-37 at non-inhibitory molar ratios (1/0.1). In the IAPP/LL-37 1/1, 1/2, and 1/5 mixtures, where the inhibition of IAPP fibrillogenesis is observed, a band at circa 15 kDa is visible, a clear indication of a hetero-complex which corresponds to a hetero-tetramer between the two peptides. The band in the WB was visible with both anti-IAPP and anti-LL-37 antibodies. In addition, the incubation of LL-37 alone (30, 60, and 150 µM) showed a band at 15 kDa, indicative of the formation of homo-tetramers. In general, the incubation of LL-37 alone exhibits bands due to homo-assemblies extending from dimers to hexamers, as well as high molecular weight aggregates (Appendix Figure A6b). Together, these results identified the hetero-tetrameric species as a necessary condition for the inhibitory effect of LL-37 of IAPP amyloid self-assembly (114).

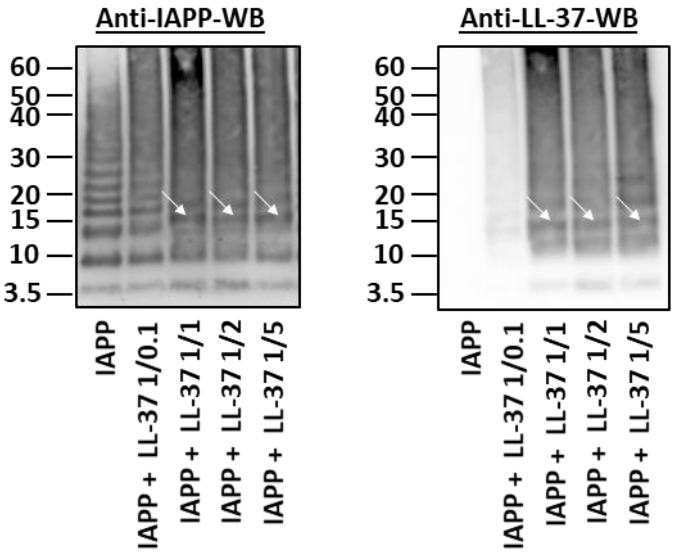

Figure 22. Characterization of the LL-37-IAPP hetero-assemblies via cross-linking (pH 7.4). NuPAGE and WB with IAPP (30 μM) and its mixtures with LL-37 (1/0.1, 1/1, 1/2, and 1/5) is shown. Representative gel is reported (n>5).

To further characterize the LL-37/IAPP hetero-assemblies, trials with size exclusion chromatography (SEC) were carried out, although no successful result was obtained due to no elution of the high molecular weight peptide aggregates of the IAPP/LL-37 mixture and IAPP or LL-37 alone (data not shown).

4.1.7 Molecular docking of IAPP/LL-37 complex

As the results of cross-linking experiments suggested the formation of an IAPP/LL-37 hetero-complex, we studied the association of the two peptides and the possible geometries of interaction. For this aim, protein-protein docking using Rosetta (122) was kindly performed by Dr. Andrea Di Luca (unpublished). The crystal structures of LL-37 show that the peptide folds into an amphipathic α-helix, and its helicity increases with the increase in the concentration of the peptide or salt (79). On the other hand, IAPP which is natively disordered was found to be helical in a transient pre-fibrillar state (15, 17). With the assumption from circular dichroism studies of the two peptides retaining their helical structure during the first association, the IAPP/LL-37 interaction in their monomeric form was studied. 20000 structures were generated using the Rosetta protocol (section 3.2.11) while maintaining a rigid backbone structure and selected the best poses after the relaxation of both the sidechains and backbone atoms. The lowest-score (best) dimer structure shows that IAPP interacts mainly with the central/C-terminal region of LL-37, with the IAPP-kink region accommodating the LL-37 helix and forming a hydrophobic surface between the two peptides. Breakdown of the residue-residue interaction energies between the two peptides shows that in particular residues Phe17, Leu28, Arg29, Leu31, Val32, Pro33 of LL-37 and Ala8, Leu12 and Asn22 of IAPP are important stabilizers of the interaction (Figure 23).

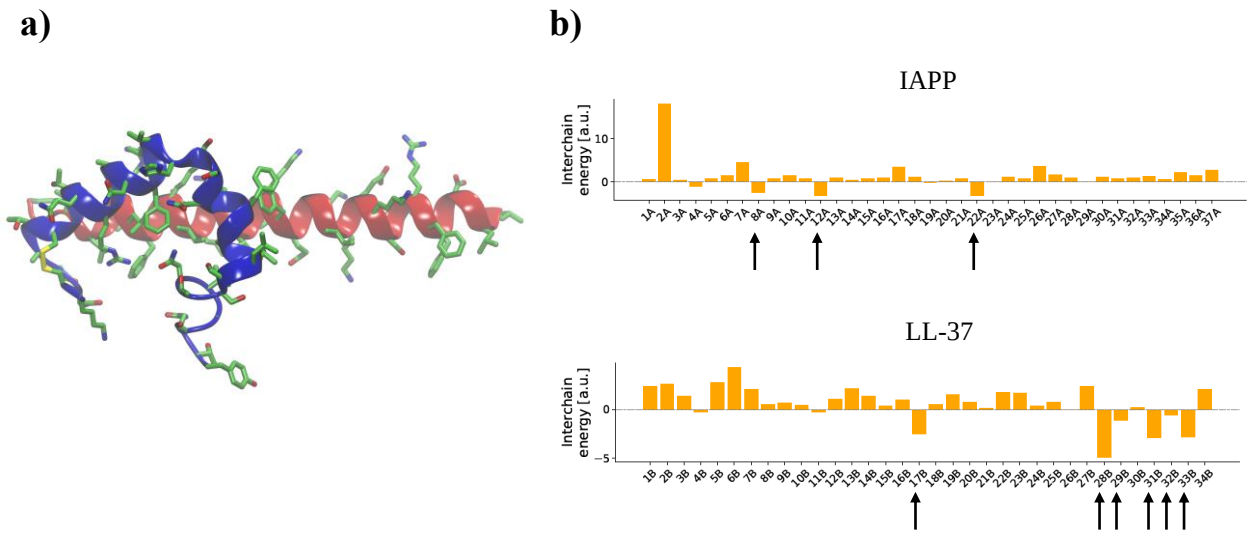

Figure 23. Computational docking experiment of the geometry of interaction of IAPP and LL-37 in 1/1 stoichiometry using Rosetta protocol. a) Lowest score dimer out of 20000 generated structures. IAPP (blue) interacts with the central/C-terminal region of LL-37 (orange); b) Interchain energy of the residue-residue interaction energies between IAPP and LL-37. Residues stabilizers of the interaction are highlighted by black arrows.

Crystal structures of LL-37 without detergents showed that LL-37 is mainly found as a dimer, composed of two helices without supercoiling (79). To study the effect of the dimerization of LL-37 on the LL-37/IAPP interaction, a protein-protein docking was performed using the same protocol of the IAPP:LL-37 1:2 complex (Figure 24). The best pose shows the IAPP interacting principally with one of the two LL-37 helices, with the interaction region focusing in the central segment and involving amino acids Leu12, Phe15, Leu16, Ser19, Phe23, Ile26, Leu27, Asn31, and Val32 (Figure 24b, c). These amino acids are mostly apolar, except for Ser19 and Asn21. As for the 1:1 case, LL-37 interacts mainly with its C-terminal region, extending from position 17 to 27 (Figure 24c). Of note, also residues Leu1 and Leu2 of LL-37 (N-terminus), seem to be important for the interaction with IAPP. Importantly, the mobility of these terminal amino acids is expected to be higher than the rest of the peptides, and rearrangement to different conformations upon binding are not captured by the docking protocol. Overall, the results support the findings of the interaction studies done via fluorescence spectroscopic titrations, which will be presented in section 4.2.4, and the membrane-bound peptide array which are shown next (section 4.1.8).

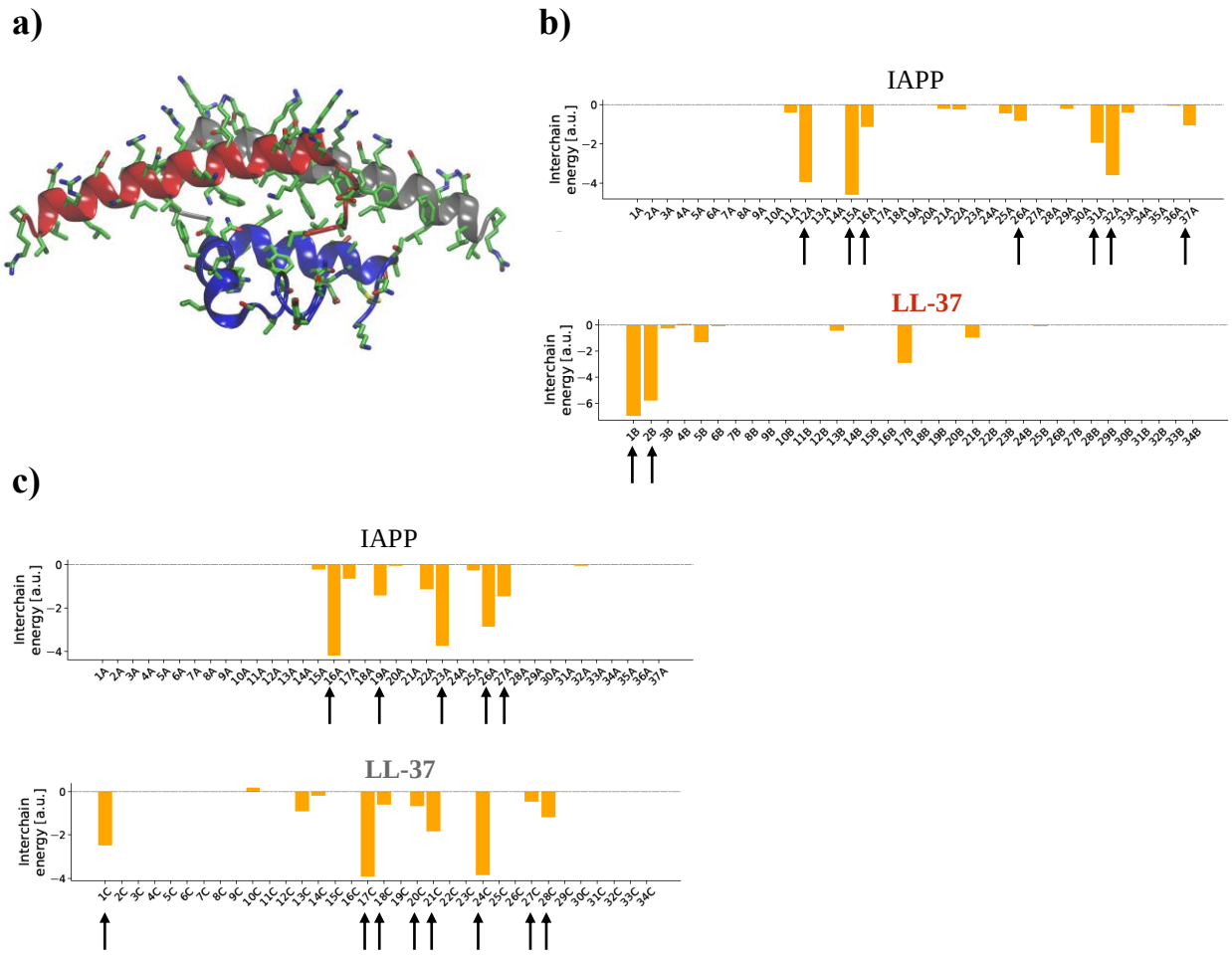

Figure 24. Computational docking experiment of the geometry of interaction of IAPP and LL-37 in 1/2 stoichiometry using Rosetta protocol. a) Lowest score dimer out of 20000 generated structures. IAPP (blue) mainly interacts with the C-terminal region of one of the two LL-37 helices (gray); b) Interchain energy of the residue-residue interaction energies between IAPP and LL-37 helix 1 (orange); c) Interchain energy of the residue-residue interaction energies between IAPP and LL-37 helix 2 (gray). Residues stabilizers of the interaction are highlighted by black arrows.

4.1.8 Identification of LL-37 regions mediating its interaction with IAPP by using peptide arrays

To have a first indication of the LL-37 regions important for its interaction with IAPP, a peptide array was utilized. Briefly, decamers covering the full sequence of LL-37 were covalently attached on glass slides and then incubated with 1 µM Fluos-IAPP. Developments revealed two different regions binding to IAPP: the N-terminus, extending from residue 1 to residue 15 (LL-37(1-15)), and LL-37(18-34), corresponding to the C-terminal region of the antimicrobial peptide. Within these two regions, two common “binding cores” were identified: FRKSK (LL-37(6-10)) and KDF (LL-37(25-27)) (Figure 25) (114). Quantification of the bound Fluos-IAPP to each decamer extending the LL-37 sequence is also shown. Signals were normalized to the highest value obtained. As previously stated, an evident decrease of the signal occurs when the Phe residues 5 and 6 are neglected from the sequence of the decamer suggesting the importance of these two aromatic residues for the interaction of LL-37 with IAPP. The second binding core (LL-37(25-27)) contains a Phe residue as well. Data suggest that the hydrophobic contact might be crucial for the interaction interface of the two peptides.

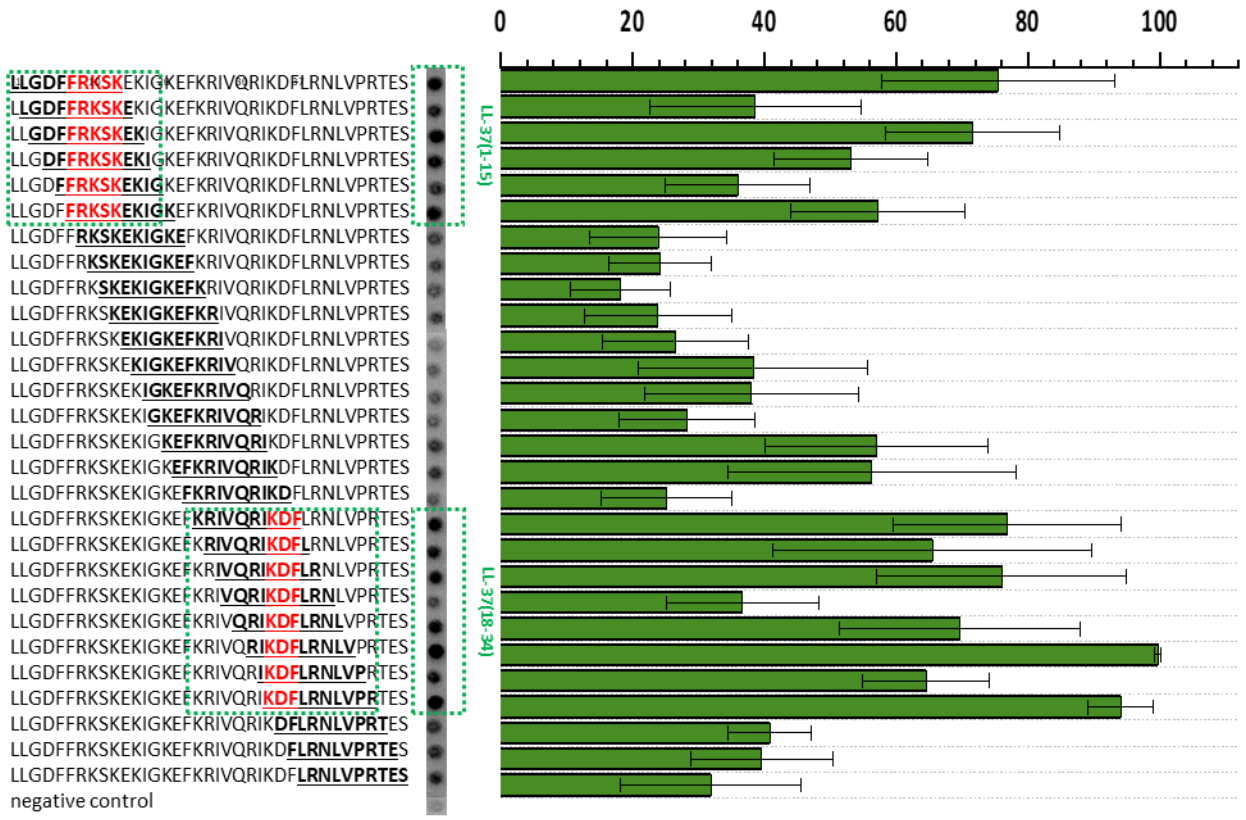

Figure 25. Identification of LL-37 regions interacting with IAPP determined by peptide arrays. Glass slides containing LL-37 decamers shifted by one residue were incubated with Fluos-IAPP. Binding regions are evidenced by green boxes, "binding cores" in red letters. Quantification of the binding of Fluos-IAPP to decamers extending the LL-37 sequence (n= 4 assays). The left figure is taken from Armiento et al. (ACIE, 2020) (114).

4.1.9 Identification of IAPP regions and residues involved in the IAPP/LL-37 interaction interface via fluorescence spectroscopic titration

To determine the IAPP regions involved in the IAPP/LL-37 cross-interaction interface, fluorescence spectroscopic titrations were carried out. Using a rational approach, the sequence of IAPP was dissected into different segments (52). Similarly, LL-37 was used to titrate two N-terminal carboxyfluorescein-labeled IAPP segments which result in a dissection of the full sequence into two parts, which are Fluos-IAPP(1-18) and Fluos-IAPP(19-37) at 5 nM concentration. The binding affinities were carried out by titration of the N-terminal carboxyfluorescein-labeled IAPP segments with an increasing amount of LL-37. All titrations were carried out in 1xb, pH 7.4 containing 1% of HFIP. The app. K_d obtained for the spectroscopic titration of Fluos-IAPP(1-18) with LL-37 was above 1.25 µM, indicating that the region between residues 1 and 18 is partially responsible for the binding to the native IAPP (Appendix Figure A 7). When Fluos-IAPP(19-37) was titrated with LL-37, no binding until 1.25 µM was found (Appendix Figure A 7). Next, to evaluate whether the LL-37 binding region of IAPP includes parts of both IAPP segments, Fluos-IAPP(8-28) was titrated with increasing amounts of LL-37 leading to an app. K_d> 1.25 µM (Appendix Figure A 7). Since the region 8-28 of IAPP is known to have amyloidogenic properties (52), for easier handling, its N-methylated and more soluble analog Fluos-(8-28)GI (26) was used to carry out the same experiment. The obtained app. K_d was 372.4 (± 64.3) nM (Appendix Figure A 7), which is a 4-fold weaker binding compared to the app. K_d of the binding affinity to Fluos-IAPP (88.1 (± 12.0) nM). This result shows that the region of IAPP majorly responsible for the binding affinity to IAPP is IAPP(8-28). It has been shown that IAPP(8-18) and IAPP(22-28) are hot regions of both the IAPP/IAPP and IAPP/Aβ40 interaction interfaces (52). Similarly, we asked if these two segments are singularly involved in the IAPP/LL-37 interface. To address this issue, Fluos-IAPP(8-18) or Fluos-IAPP(22-

28) were titrated with LL-37. Both segments showed no binding until 1.25 µM, meaning that their co-presence is required to interact with LL-37 (Appendix Figure A 8). Finally, Fluos-IAPP(1-7) was also titrated with LL-37, to investigate the contribution of the N-terminus of the IAPP interaction. No binding until 1.25 µM was found in this case (Appendix Figure A 8), suggesting that the N-terminus is not involved in the interaction with LL-37 (Table 12).

Table 12. Identification of IAPP regions that bind full-length LL-37 and determination of apparent binding affinities (K_d, app.) by fluorescence titration assays.

Fluos-IAPP segments	**$K_{d,app}$ (±SD) (for LL-37)[a]**
Fluos-IAPP(1-18)	> 1.25 µM
Fluos-IAPP(1-7)	n.b. [b]
Fluos-IAPP(19-37)	n.b. [b]
Fluos-IAPP(8-28)	> 1.25 µM
Fluos-IAPP(8-28)GI	372.4 (± 64.3) nM
Fluos-IAPP(8-18)	n.b. [b]
Fluos-IAPP(22-28)	n.b. [b]

[a] App. K_ds, means (±SD) from 3 binding curves. Determined via titrations of fluorescein-labeled peptides (Fluos-peptides, 5nM) with non-labeled LL-37. [b] n.b., no binding at peptide concentrations ≤ 1.25µM, (aq. buffer 1×b, pH 7.4, containing 1% HFIP).

Previous studies carried out in our group identified four key residues of the IAPP sequence for its self-interaction and cross-interaction with Aβ40 and itself: Phe15, Leu16, Phe23, and Ile26. In fact, the simultaneous substitution of these residues with alanine drastically reduced the binding affinity of IAPP to both IAPP and Aβ40 (128). To determine if these four residues affect the interaction between IAPP and LL-37, N-terminal carboxyfluorescein-labeled IAPP with alanine substitutions in the positions 15, 16, 23, 26 (Fluos-4A) was titrated with different amounts of LL-37 in 1xb, pH 7.4 containing 1% of HFIP. Results revealed a weak binding affinity between the two peptides with an app. K_d> 1.25 µM (Figure 26), indicating that Phe15, Leu16, Phe23, and Ile26 are crucial for the IAPP/LL-37 interaction interface.

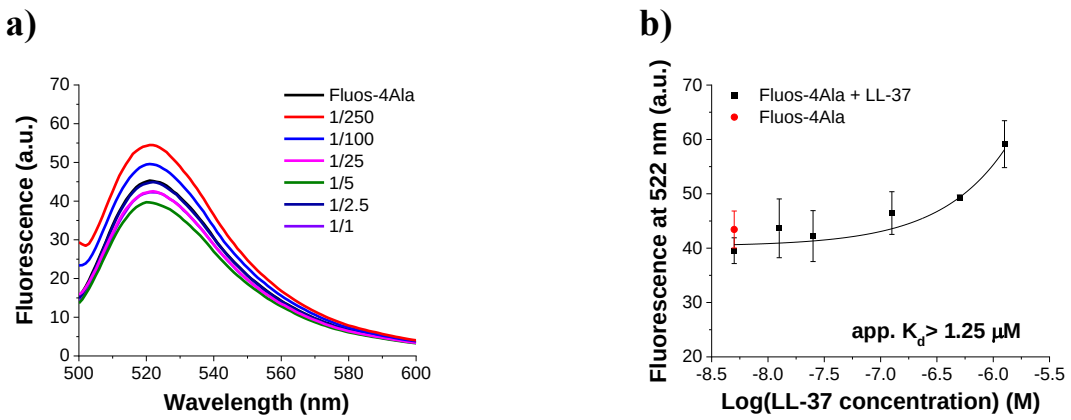

Figure 26. Determination of app. K_ds of interactions of LL-37 with monomeric 4Ala by fluorescence titrations. a) Fluorescence emission spectra of Fluos-4Ala (5 nM) alone and its mixtures with increasing amounts of LL-37. b) Binding curve of LL-37. Binding curves are means of 3 assays (±SD) (aqueous buffer 1×b, pH 7.4, containing 1% HFIP).

To verify if the effect of these residues is cooperative, N-terminal carboxyfluorescein IAPP with only two substitutions at a time were tested in the same experimental conditions. Titration of Fluos-A15,23 with LL-37 lead to an app. K_d of 110.6 ± 46.1 nM, a value which is comparable to the binding of Fluos-IAPP to LL-37 and indicating that Phe15 and Phe23 are not crucial residues of the IAPP/LL-37 interaction. Next, Fluos-

A15,16 was titrated in the same conditions by Linus Wollenweber (129). In this case, the obtained app. K_d was 129.2 nM which shows that Phe15 and Leu16 alone do not have any effect on the interaction. Similarly, titration of Fluos-A23,26 with LL-37 led to an app. K_d value of 169.9 ± 58.9 nM confirming that there is no effect when Phe23 and Ile26 are replaced with alanine (Appendix Figure A 9). These results indicate that only the replacement of all four residues disrupts the interaction between IAPP and LL-37 (Table 13).

Table 13. Identification of key IAPP residues for the binding of full-length LL-37 and determination of apparent binding affinities (K_d, app.) by fluorescence titration assays.

Fluos-IAPP alanine mutants	**$K_{d,app}$ (±SD) (for LL-37)[a]**
Fluos-A15,23	110.6 ± 46.1 nM
Fluos-A15,16	129.2 nM [b]
Fluos-A23,26	169.9 ± 58.9 nM
Fluos-4Ala	> 1.25 µM

[a] App. K_ds, means (±SD) from 3 binding curves. Determined via titrations of fluorescein-labeled peptides (Fluos-peptides, 5nM) with non-labeled LL-37 (aq. buffer 1×b, pH 7.4, containing 1% HFIP). [b] Preliminary experiment carried out by Linus Wollenweber (129). App. K_d, representative from 2 binding curves.

4.1.10 Peptide synthesis on N- and C-termini of LL-37 segments

To investigate if the inhibitory role of LL-37 is localized in specific regions, the sequence of the peptide was dissected into two parts, LL-37(1-14) and LL-37(15-37) respectively containing segments of the N-terminus or the C-terminus. The LL-37 partial segments were synthesized on Wang-resin using a Fmoc-SPPS strategy. Couplings were carried out two or three times in DMF using 3-fold excess of HBTU or HATU as coupling reagents, 3-fold excess of Fmoc-protected amino acid, and a 4.5-fold excess of DIEA. The syntheses were carried out manually and with an automatic synthesizer.

The synthesis of LL-37(1-14) was carried out by Sophie von Schönberg. Briefly, the synthesis was carried out on Wang resing with a substitution level of the first amino acid equal to 0.31 mmol/g. For this synthesis, Gly^{14} and Ile^{13} were coupled manually, while the rest of the sequences with an automatic synthesizer. Most of the couplings were carried out using HBTU, but for the coupling of Lys^{10}, Glu^{11}, and Lys^{12} HATU was used for the first of the two couplings. Furthermore, three times coupling was performed for residues Phe^{5}, Phe^{6}, and Arg^{7} using HATU for the first one. Similarly, the synthesis of LL-37(15-37) was carried out on Wang resin using an automatic synthesizer, with 0.6 mmol/g as the final substitution level. For this sequence, most couplings were performed three times using HATU for the first one, and HBTU for the second and the third ones. Only in the case of Lys^{25}, Asp^{26}, Pro^{33}, and Arg^{34} coupling reactions were performed twice (114). Additionally, LL-37(15-37) was N-terminally carboxyfluorescein (Fluos) labeled, as described in section 3.2.1.3. Cleavages of peptides from the resin were carried out for 3 hours using TFA:ddH_2O (95:5 v:v). Crude products were purified by RP-HPLC (Figure 27a, c, and e). In the case of LL-37(1-14) two steps of purification were required. Peptide purity was confirmed by MALDI-TOF MS (Figure 27b, d, and f).

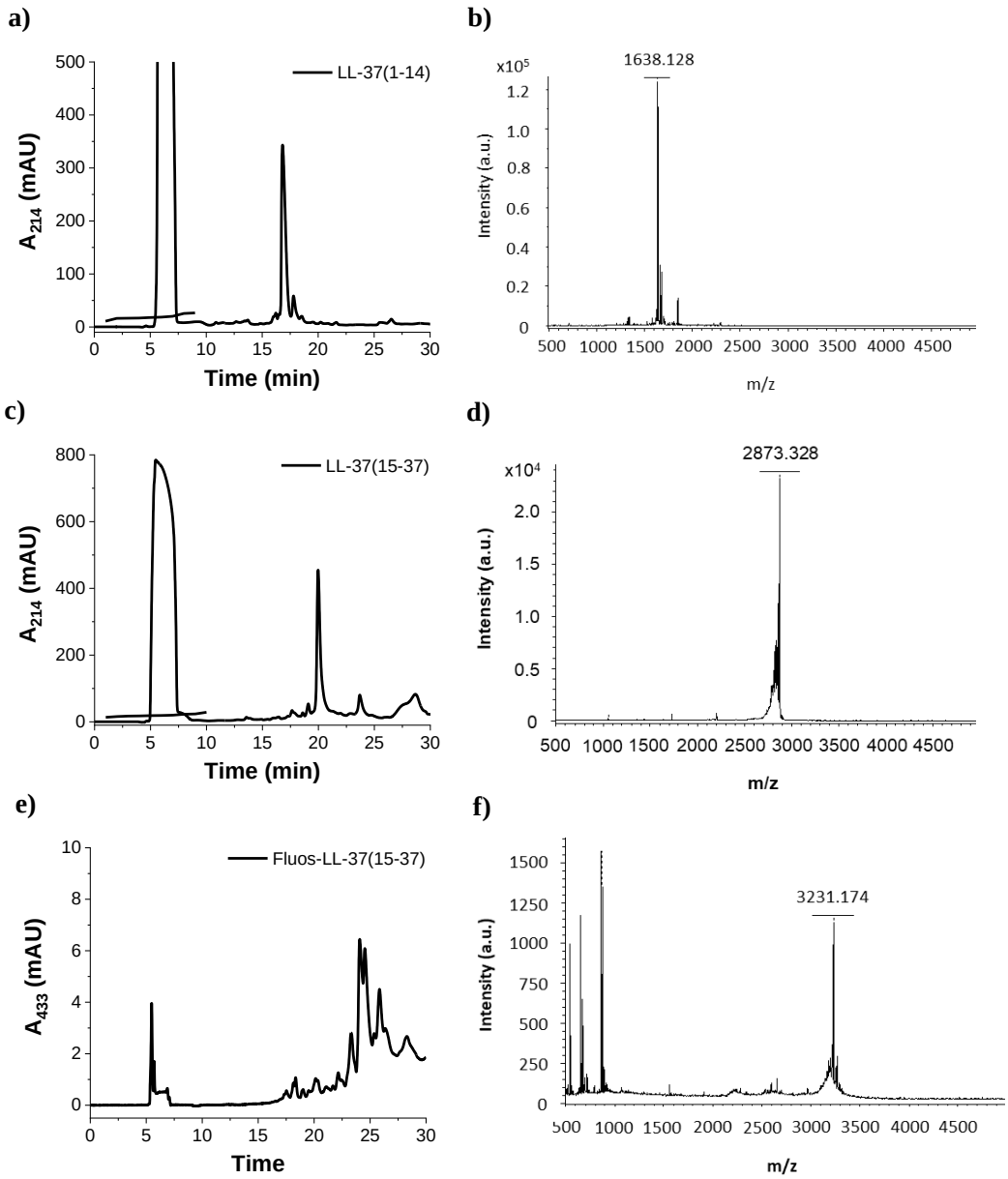

Figure 27. Characterization of LL-37(1-14), LL-37(15-37), and Fluos-LL-37(15-37) via RP-HPLC and MALDI-TOF. Representative chromatogram at 214 nm of a) LL-37(1-14) crude, c) LL-37(15-37) crude, and e) Fluos-LL-37(15-37) crude, with retention time of the peptides at 16.7, 20.1, and 24.5 min respectively. MALDI-TOF-MS spectra of HPLC purified b) LL-37(1-14), d) LL-37(15-37), and f) Fluos-LL-37(15-37) with $[M-H]^+$ found masses. Data regarding LL-37(1-14) was produced by Sophie von Schönberg.

HPLC gradients applied for the purification of the peptides and yields of the purifications resulted in respect of crude peptides are reported in Table 14.

Table 14. Characterization of the synthetic peptides via RP-HPLC and MALDI-TOF

Abbreviation	**HPLC program**	**t_R (min)[a]**	**HPLC program for 2nd purification**	**t_R (min)**	**Yield[b]**	**$[M+H]^+$ expected[c]**	**$[M+H]^+$ found[c]**
LL-37(1-14)	SchnellAβ	16.7	SchnellAβ	16.7	19%	1638.9	1638.3
LL-37(15-37)	SchnellAβ	20.1	-	-	11%	2873.6	2873.3
Fluos-LL-37(15-37)	SchnellAβ	24.5	-	-	n.d. [d]	3229.6	3231.2

Peptides were synthesized with free C- and N-terminus. [a] t_R, HPLC retention time; [b] % yield with regard to crude peptide, and [c] monoisotopic molar mass $[M+H]^+$ expected and $[M+H]^+$ found; [d] not determined.

4.1.11 Effect of the N- and C-termini of LL-37 on IAPP fibrillogenesis, cytotoxicity, and cross-interaction

Previous works showed that LL-37(17(18)-29) and LL-37(13-32) segments, extending mainly in the central and C-terminal regions of LL-37, have been used for drug design due to their antiviral, antimicrobial, and immunoregulatory role (54, 76, 130). We addressed the question whether the inhibitory function of LL-37 is contained in the N-terminus or the central/C-terminal part of the antimicrobial peptide. The sequence was dissected into two parts, LL-37(1-14) and LL-37(15-37), as described in 4.1.10. The two peptides were tested to evaluate whether they could interfere with the aggregation of IAPP into cytotoxic aggregates via ThT binding and MTT reduction assays (Figure 28). IAPP at a final concentration of 16.5 μM was incubated alone and in its 1/1 mixture with LL-37(1-14) or LL-37(15-37) and the fibril formation was followed by ThT fluorescence determination until 168 hours (Figure 28a). At 24 hours, solutions were added to RIN5fm cells and the effect on the cytotoxicity was monitored via MTT reduction assay. Results clearly show that the two segments are not sufficient to have an inhibitory effect on the aggregation of IAPP into β-cell damaging species (Figure 28b) (114). TEM of the samples was performed at 24 hours. Images show co-presence of both fibrils and amorphous aggregates for both species, confirming the ThT assay results (Figure 28c).

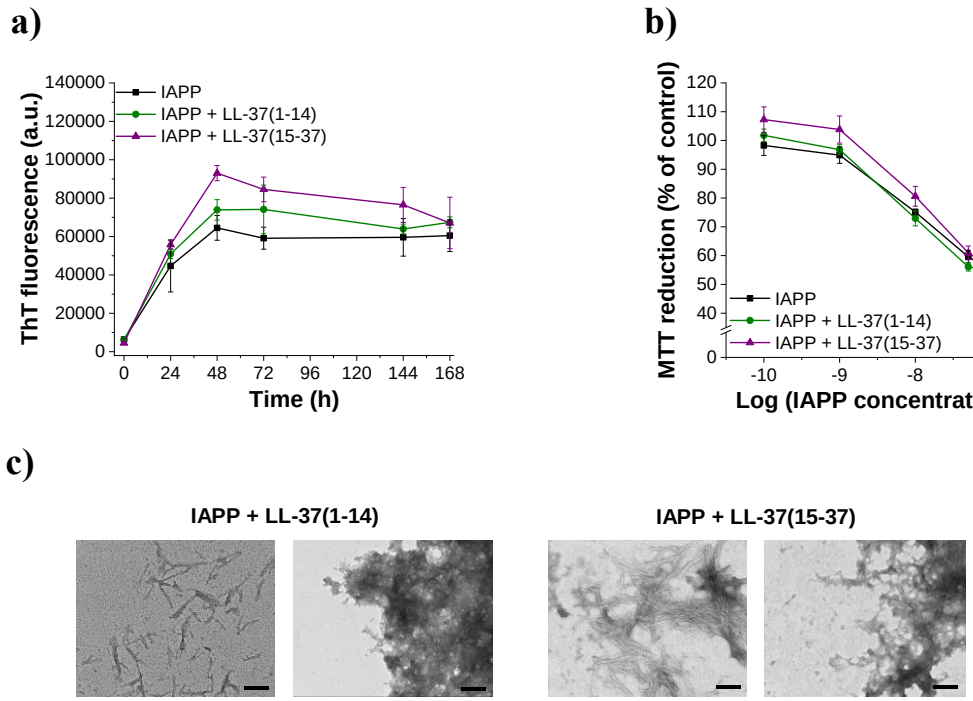

Figure 28. Effects of the N- and C-termini of LL-37 on IAPP amyloid formation and cytotoxicity. a) Fibrillogenesis of IAPP (16.5 μM) and its mixtures with LL-37(1-14) or LL-37(15-37) (1/1) (means (±SD), 3 assays); b) effects of LL-37(1-14) and LL-37(15-37) on cell viability: solutions from a) were added to cultured RIN5fm cells (24 hours aged). Cell viability was determined by MTT reduction (means (±SD), 3 assays, n=3 each). c) TEM images of solutions of a) (24 hours aged) as indicated (bars, 100 nm). The figure is taken from Armiento et al. (ACIE, 2020) (114).

Next, binding affinity studies were carried out. Fluorescence spectroscopic titrations of Fluos-IAPP (5 nM) with increasing amounts of both peptides led to the app. K_d values of 39.1 (± 2.2) nM for LL-37(15-37) and of 2.54 (± 0.5) μM for LL-37(1-14) (Figure 29). As a result, the C-terminus has high interaction with the monomeric IAPP as the native LL-37, and it is most likely mediating the interaction with IAPP since the N-terminus exhibits a weaker binding, although it has no effect on the inhibition of the IAPP fibril formation and toxicity (114).

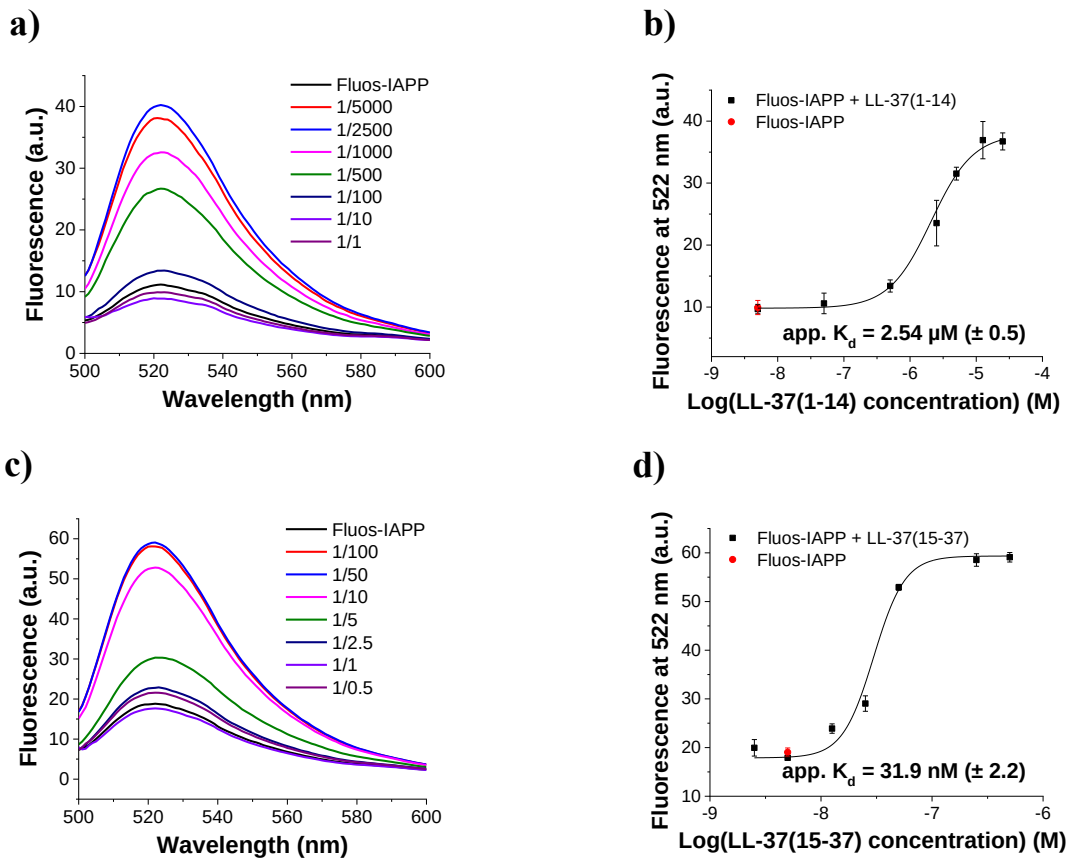

Figure 29. Determination of app. K_ds of interactions of N- and C-termini of LL-37 with monomeric IAPP by fluorescence titrations. a) Fluorescence emission spectra of Fluos-IAPP (5 nM) alone and its mixtures with increasing amounts of LL-37(1-14). b) Binding curve of LL-37(1-14). c) Fluorescence emission spectra of Fluos-IAPP (5 nM) alone and its mixtures with increasing amounts of LL-37(15-37). d) Binding curve of LL-37(15-37). Binding curves are means of 3 assays (±SD) (aqueous buffer 1×b, pH 7.4, containing 1% HFIP). Figure taken from Armiento et al. (ACIE, 2020) (114).

These results empirically confirm what was found with the Rosetta docking, as the central/C-terminal region of LL-37 gave the main contribution to the IAPP/LL-37 interaction. It is clear that the co-presence of the termini is required for having an anti-amyloid effect.

4.1.12 Conformational studies via CD spectroscopy

The conformation of LL-37 and its derived peptides was determined via circular dichroism. For these measurements, peptides were diluted from their HFIP stocks in aqueous 10 mM sodium phosphate buffer (pH 7.4) containing 1% HFIP. Spectra were recorded between 2 µM and 100 µM to evaluate their aggregation propensity. The spectra of LL-37 exhibited a maximum at 198 nm and two minima, one at 210 nm and a more pronounced one at 227 nm, indicative of β-sheet/turn and α-helix secondary structure (Figure 30a). Results show that the oligomerization of the peptide starts at 10 µM and aggregates at higher concentrations, as the signal for the 20 µM concentration decreases drastically. By contrast, the spectra of scrLL-37, LL-37(1-14), and LL-37(15-37) exhibited a similar structure (Figure 30b, c, d). In particular, LL-37(1-14) exhibited a minimum at 200 nm, indicative of random coil conformation (experiment carried out by Sophie von Schönberg). Only for scrLL-37 and for LL-37(15-37), additionally to the minima at 198 nm, a non-marked minimum is present at 226 nm, indicating a minimal amount of β-sheet structure. In general, all peptides are mainly unstructured, with a minimum around 198 nm, and have no concentration dependence on the intensity of their signals.

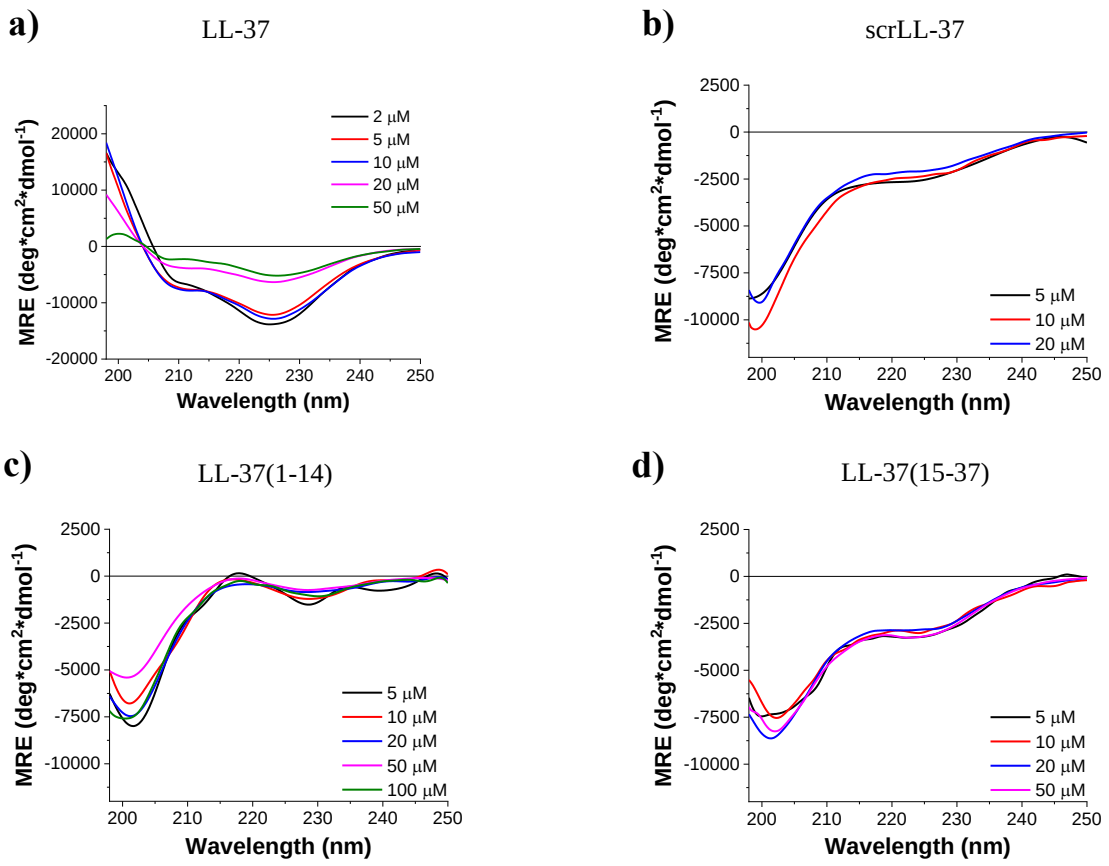

Figure 30. Concentration dependence of LL-37 and LL-37 derived segments assessed by far-UV CD spectroscopy. a) LL-37, b) scrambled LL-37, c) LL-37(1-14), Sophie von Schönberg's data, d) LL-37(15-37). Measurements were performed in aqueous buffer 1×b, pH 7.4, containing 1% HFIP.

To study the effect of HFIP on the secondary structure of LL-37, LL-37(1-14), and LL-37(15-37) spectra at 5 µM were also recorded in aqueous 10 mM sodium phosphate buffer (1xb, pH 7.4) (Figure 31). LL-37 exhibited an α-helical secondary structure with two minima, one at 206 nm and one at 224 nm. Compared to its structure in the presence of HFIP, the minimum at 224 nm is less pronounced. This result suggests that in the presence of HFIP LL-37 assumes a β-sheet/turn content. In these conditions, LL-37(1-14) had a minimum at circa 200 nm, confirming its unordered structure. The spectra of LL-37(15-37) in 1xb had an intense minimum at 203 nm and a less evident one at 226 nm which suggest mainly random coil structure of the peptide and a minimum amount of β-sheet/turn content.

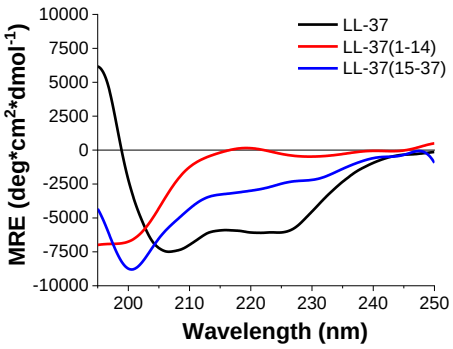

Figure 31. Effect of the absence of HFIP on the secondary structure of LL-37, LL-37(1-14), LL-37(15-37) assessed by far-UV CD spectroscopy. Measurements were performed at a concentration of 5 μM in aqueous buffer 1×b, pH 7.4.

Furthermore, the effect of 2,2,2-trifluoroethanol (TFE) on the secondary structure of the inhibitor LL-37 and of the non-inhibitor scrLL-37 was investigated (Figure 32). TFE promotes protein unfolding and at high concentration induces α-helical structures in peptides with helical propensities (131). As previously described, LL-37 in aqueous buffer exhibits a β-sheet/turn and α-helix secondary structure, with a maximum at 198 nm and two minima at 210 nm and 227 nm. As the amount of TFE increases, the signal at 198 nm increases, and the two minima shift to lower wavelengths, 208 and 222 nm respectively, indicating an α-helix formation, with a transition point (T_M) at circa 8% TFE (Figure 32a, b). The CD profile of scrLL-37 is mainly a random coil, with a minimum at 198 nm. The titration of this peptide with increasing amounts of TFE led to a two-state transition, from unordered to an α-helix secondary structure (minima at 208 and 222 nm). The middle point of the transition was found at approximately 21% TFE, indicating a lower helical propensity compared to LL-37. For this peptide, an isodichroic point at 200 nm was observed indicating the two-state transition (Figure 32c, d). Additionally, studies carried out by Linus Wollenweber showed that the transition point for the two segments LL-37(1-14) and LL-37(15-37) are different (129). In fact, LL-37(1-14) appears unfolded without any TFE and reaches its transition point at 20% TFE (Appendix Figure A 5a, b), while LL-37(15-37), which is also a random coil in absence of TFE, exhibits a transition point at 5% TFE (Appendix Figure A 5c, d), indicating that the central/C-terminus of LL-37 has a slightly higher helical propensity than LL-37 and a more pronounce helical propensity than the N-terminus. Results are summarized in Table 15.

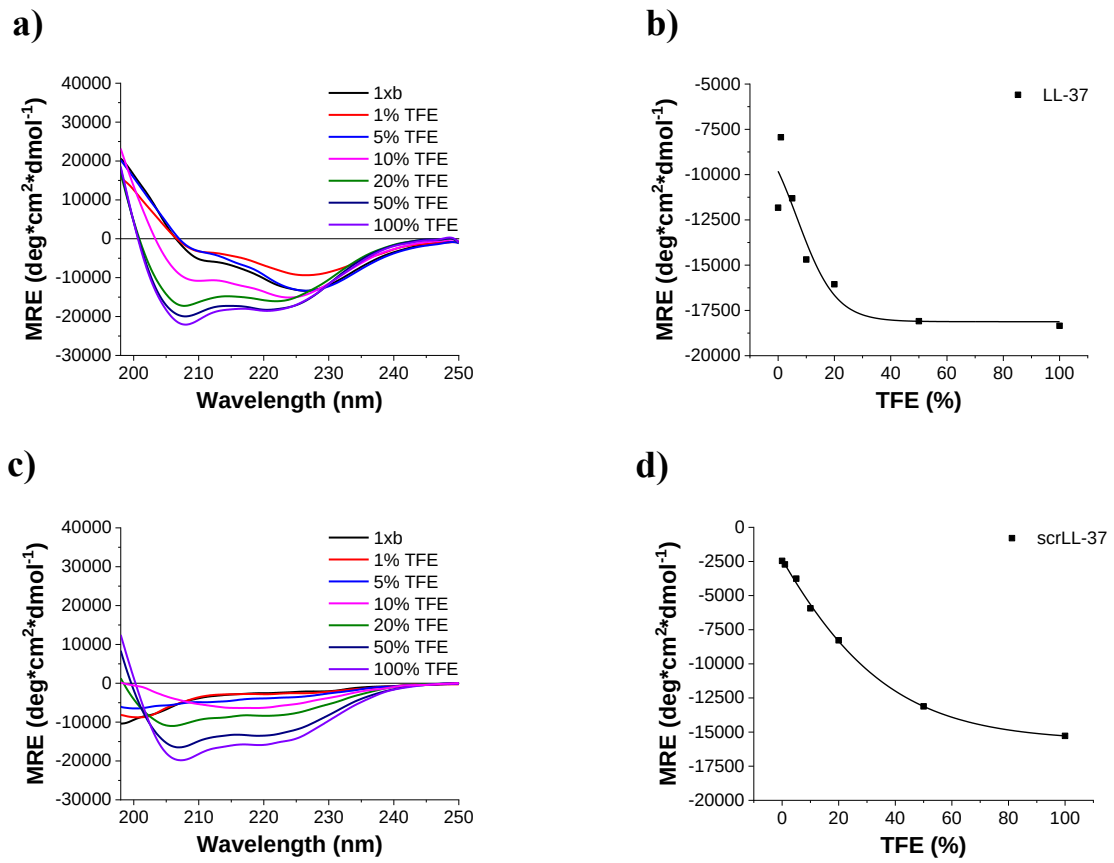

Figure 32. Effects of TFE on the conformation in aqueous solution of a) LL-37, c) scrambled LL-37 assessed by far-UV CD spectroscopy. Experiments were performed at peptide concentrations of 5 µM in aqueous buffer 1×b, pH 7.4, containing 1% HFIP with the indicated amounts of TFE. b), d) plots of minima at 222 nm versus the TFE amounts (%) of the CD spectra of the peptides shown in a) and c) respectively.

Table 15. Characterization of the secondary structure of LL-37, scrLL-37, LL-37(1-14), and LL-37(15-37).

Peptide	**Secondary structure in 1xb[a] + 1% HFIP**	**Secondary structure in 1xb[a]**	**Concentration of oligomerization**	**TFE % T_M**
LL-37	α-helix/β-sheet,β-turn	α-helix	20 µM	8 %
scrLL-37	random coil/β-sheet,β-turn	-	no oligomerization	21%
LL-37(1-14)	random coil	random coil	no oligomerization	20%*
LL-37(15-37)	random coil/β-sheet,β-turn	random coil/β-sheet,β-turn	no oligomerization	5%*

[a] 1xb, aq. buffer, pH 7.4, containing 1% HFIP. * Linus Wollenweber's data (129).

4.1.13 Effect of the primary and secondary structure of LL-37 on the inhibition of IAPP fibril formation

As previously described, LL-37 is an inhibitor of IAPP fibrillogenesis. We asked whether this property is related to the amino acid sequence, to the secondary structure of the peptide, or both factors. To address the question, a ThT binding assay and an MTT reduction assay were utilized. IAPP (16.5 µM) was incubated alone and in a mixture with both LL-37(1-14) and LL-37(15-37) (16.5 µM each peptide) (Figure 33a, b). Kinetics of the fibril formation was followed by ThT fluorescence for 7 days. At 24 hours and 7 days solutions were added to RIN5fm cells to evaluate their effect on the cytotoxicity via MTT assay. Results show that the mixture of LL-37(1-14) and LL-37(15-37) is not able to inhibit the aggregation of IAPP and its cytotoxic effects already at 24 hours, although the two peptides together contain the full amino acid sequence of the native peptide.

Next, the secondary structure of the mixture of these two peptides was studied via CD spectroscopy (Figure 33c). As previously described, the two peptides have an unordered structure with a minimum at 198 nm. The CD spectrum of the mixture of the two peptides (5 µM each) diluted in 10 mM sodium phosphate buffer (pH 7.4) containing 1% HFIP was measured. The mixture of the two peptides exhibited a random coil secondary structure, with a signal intensity that is comparable to the sum of the spectra of LL-37(1-14) and LL-37(15-37), indicating that there is no interaction between the two peptides and no change of their secondary structure when mixed in solution. Results show that the primary structure of LL-37 is not sufficient to inhibit IAPP self-assembly.

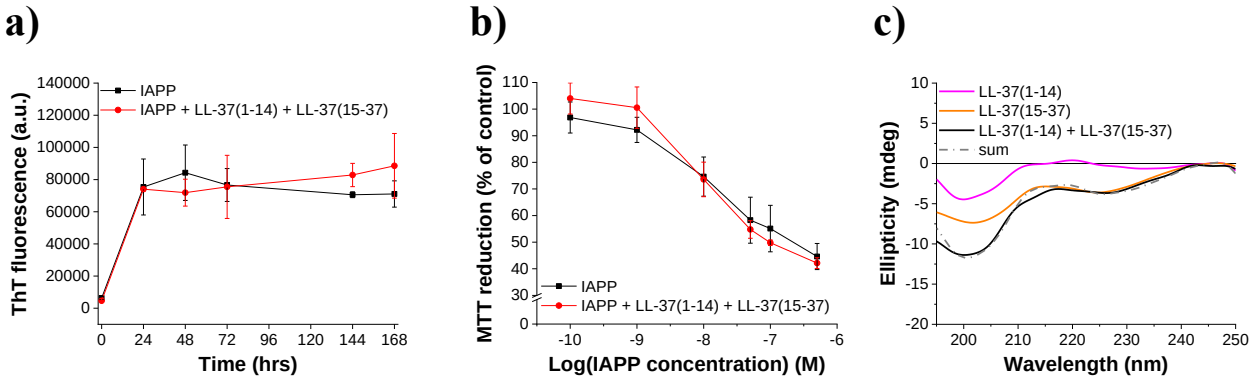

Figure 33. Effects of the primary and secondary structure of LL-37 on IAPP amyloid formation and cytotoxicity. a) Fibrillogenesis of IAPP (16.5 µM) and its mixtures with LL-37(1-14) and LL-37(15-37) (1/1/1) (means (±SD), 3 assays); b) effects of the mixture of LL-37(1-14) and LL-37(15-37) on cell viability: solutions from a) were added to cultured RIN5fm cells (24 hours aged). Cell viability was determined by MTT reduction (means (±SD), 3 assays, n=3 each). c) Far-UV spectra of LL-37(1-14) (5 µM), LL-37(15-37) (5 µM) and their mixture (1/1, 5 µM each), the mathematical sum of LL-37(1-14) and LL-37(15-37) is shown (dashed grey line).

4.1.14 Two-photon microscopy (2-PM) for the characterization of IAPP- LL-37 assemblies

To address the possibility of hetero-complexes formation involving IAPP and LL-37, 2-photon microscopy was applied. Briefly, TAMRA-IAPP (16.5 µM), its 1/1 and 1/5 mixtures with FAM-LL-37, or its 1/1 mixture with Fluos-LL-37(15-37) were incubated at 20°C in 1xb buffer (10 mM sodium phosphate buffer, pH 7.4) for 7 days. After the spotting and embedding procedures, samples were analyzed via a 2-photon microscope. TEM imaging showed that 7 days-aged IAPP incubation presents fibrils as the major species. Similarly, when TAMRA-IAPP was incubated for 7 days and then analyzed, fibrillar species were found, confirming our TEM findings, as shown in Figure 34 (Karin Tas's data).

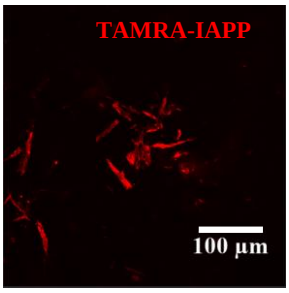

Figure 34. Two-photon microscopy for the characterization of TAMRA-IAPP fibrillar assemblies. TAMRA-IAPP (red) (16.5 µM) after 7 days aging (bars, 100 µm). Karin Tas's data is shown.

The 1/1 IAPP/LL-37 mixture presented mainly amorphous aggregates, as already proved by TEM experiments. These aggregates were also visible in the 2-PM images. In particular, results show that FAM-LL-37 clusters aggregates of TAMRA-IAPP (Figure 35a). This might explain the inhibitory potency of LL-37. In fact, IAPP might not be able to form amyloid fibrils because LL-37 surrounds it, blocking its elongation. In addition,

Förster resonance energy transfer (FRET) could be observed between TAMRA-IAPP and FAM-LL-37 in this aggregation state. A shift of the amplitude value from 2.47 ns to 0.16 ns was present when the donor FAM-LL-37 was in the presence of the acceptor TAMRA-IAPP (Figure 35b, c). These results confirm the presence of hetero-complexes, which were also observed in cross-linking experiments.

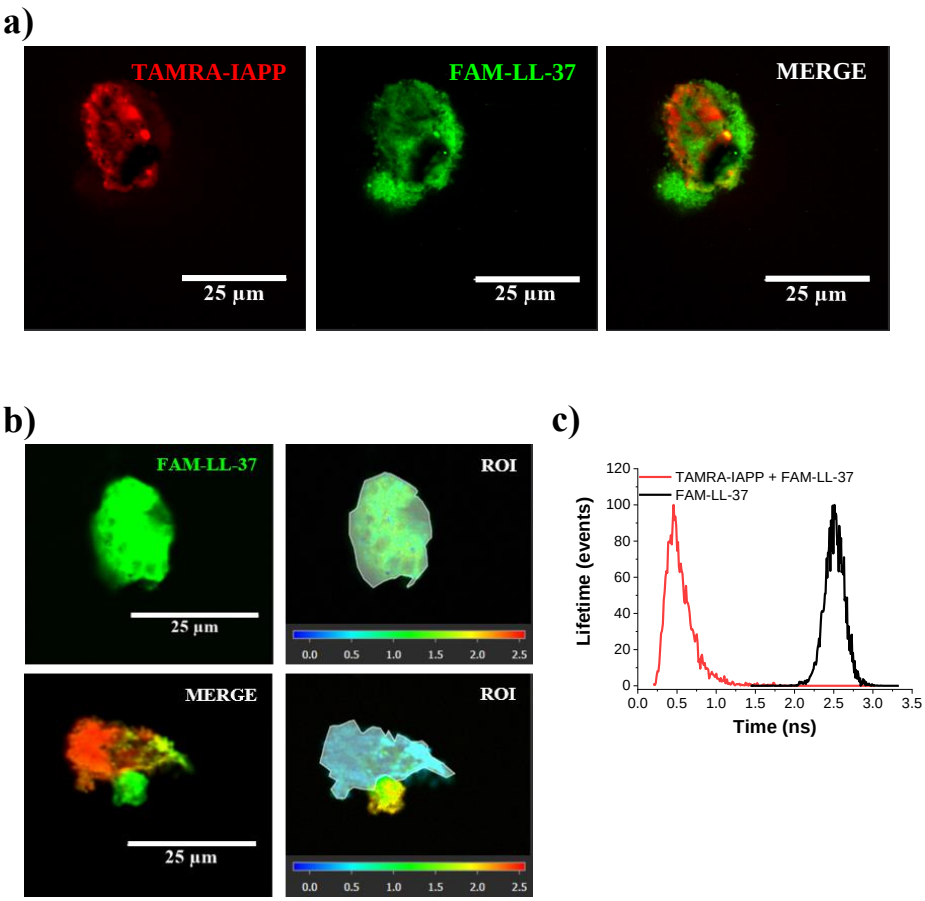

Figure 35. Two-photon microscopy for the characterization of IAPP/LL-37 co-assemblies. a) TAMRA-IAPP (red) (16.5 µM) and its mixture with FAM-LL-37 (green) (1/1) after 7 days aging (bars, 25 µm). Merge image is also shown. b) ROI selections for FAM-LL-37 (16.5 µM) and its mixture with TAMRA-IAPP (1/1) after 7 days aging (bars, 25 µm). c) Fluorescence lifetime imaging (FLIM) of FAM-LL-37 and its 1/1 mixture with TAMRA-IAPP shown in b).

The 1/5 IAPP/LL-37 mixture presented the same amorphous aggregates found for the 1/1 mixture. Again, the TAMRA-IAPP was clustered by the FAM-LL-37, a result that correlates with the ThT binding assay findings, which suggests no amyloid formation. On the other hand, also fibrils containing both colors were found. The dimension of these species resembles the ones found via TEM imaging and may be responsible for the cytotoxicity of these hetero-aggregates (Figure 36).

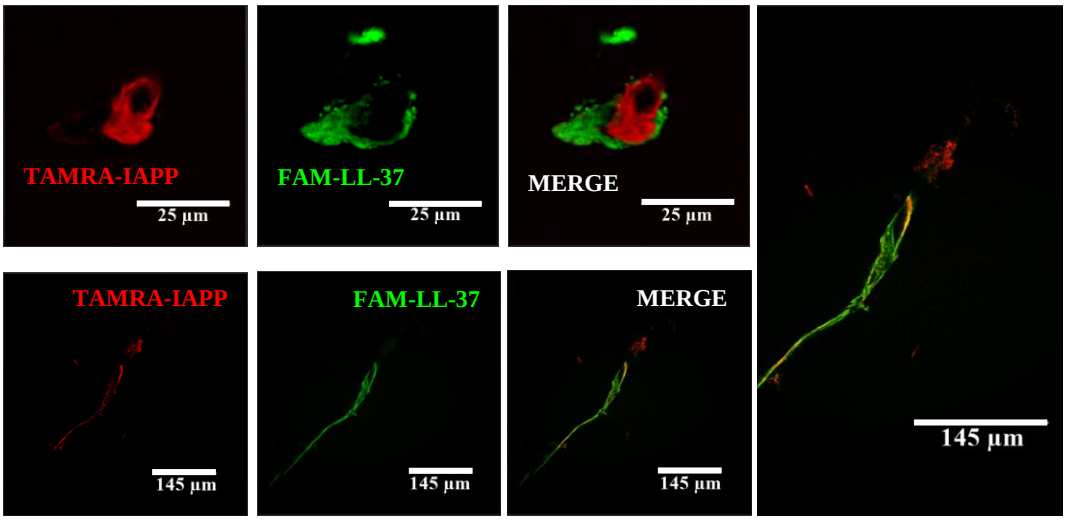

Figure 36. Two-photon microscopy for the characterization of IAPP/LL-37 hetero-assemblies. TAMRA-IAPP (red) (16.5 µM) and its mixture with FAM-LL-37 (green) (1/5) after 7 days aging (bars, 25 µm). Merge and zoom images of fibrillar species are also shown.

Of note, TAMRA-IAPP was also incubated with LL-37(15-37) as a negative control as previously described. It has been previously shown that LL-37(15-37) has no inhibitory potency against the IAPP fibril formation, so we asked whether this could be also proven with 2-PM experiments. Figure 37 shows that the two peptides do not interact with each other. In fact, LL-37(15-37) forms amorphous aggregates, and fibrils containing mainly TAMRA-IAPP and a minimum amount of Fluos-LL-37(15-37). No aggregates with the TAMRA-IAPP/FAM-LL-37 morphology could be found, as well as FRET between the two peptides. Results support the findings of ThT binding assays as well as TEM images, as amorphous complexes containing both peptides should form when an inhibitory effect is observed.

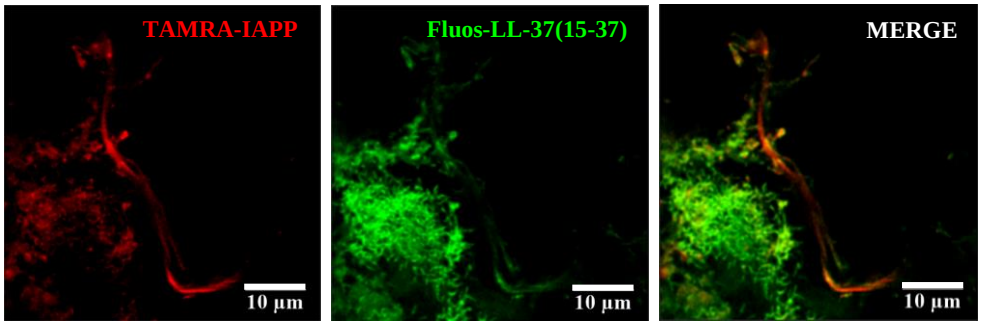

Figure 37. Multiphoton microscopy for the characterization of IAPP/LL-37(15-37) assemblies. TAMRA-IAPP (red) (16.5 µM) and its mixture with Fluos-LL-37(15-37) (green) (1/1) after 7 days aging (bars, 25 µm). Merge image is also shown.

4.1.15 Conclusions: LL-37 as inhibitor of IAPP amyloid formation

In summary, the studies of this chapter showed that LL-37 and IAPP, which share 42% of sequence similarity and 5% of sequence identity, interact with nanomolar affinity. Moreover, LL-37 was shown to interact not only with monomeric IAPP in the nanomolar range, but also with its fibrillary state. In vitro experiments proved that LL-37 can effectively suppress the aggregation of IAPP into cytotoxic species. The inhibitory ability of LL-37 interferes with the aggregation of IAPP by sequestering prefibrillar species and converting them into soluble and non-amyloidogenic species and by converting fIAPP into species with no more seeding ability. Mechanistic studies showed that IAPP and LL-37 form hetero-tetramers, formation of which was not observed when LL-37 was present in sub-equimolar ratio or when IAPP was mixed with the non-inhibitor scrLL-37. These results suggest that the presence of this hetero-complex is required to have inhibitory activity, as confirmed also by 2-PM studies. LL-37(6-10) and LL-37(25-27) were identified as the binding core regions for the interaction with IAPP and subsequently, the LL-37 sequence was dissected into LL-37(1-14) and LL-37(15-37) to study if the presence of only one of the binding regions was sufficient to have inhibitory activity. Fluorescence titrations revealed that the C-terminal segment LL-37(15-37) mainly mediates the interaction with Fluos-IAPP with a nM range binding affinity, while the N-terminal segment LL-37(1-14) exhibits only a weak interaction. These results correlate with the Rosetta Docking findings, which suggested that the regions involved in the IAPP/LL-37 interaction interface are the central region of IAPP and the C-terminus of LL-37.

Additionally, the primary structure of LL-37 was proved to be not sufficient to inhibit IAPP fibrillogenesis, as the equimolar mixture of the LL-37(1-14) and LL-37(15-37) segments did not affect the aggregation of IAPP. Via fluorescence spectroscopy titrations, IAPP(8-28) was found to be the binding core region for the interaction with LL-37. A schematic representation of these results is shown in Figure 38. Based on these findings, next the shortest LL-37 segment with inhibitory potency for IAPP aggregation was identified.

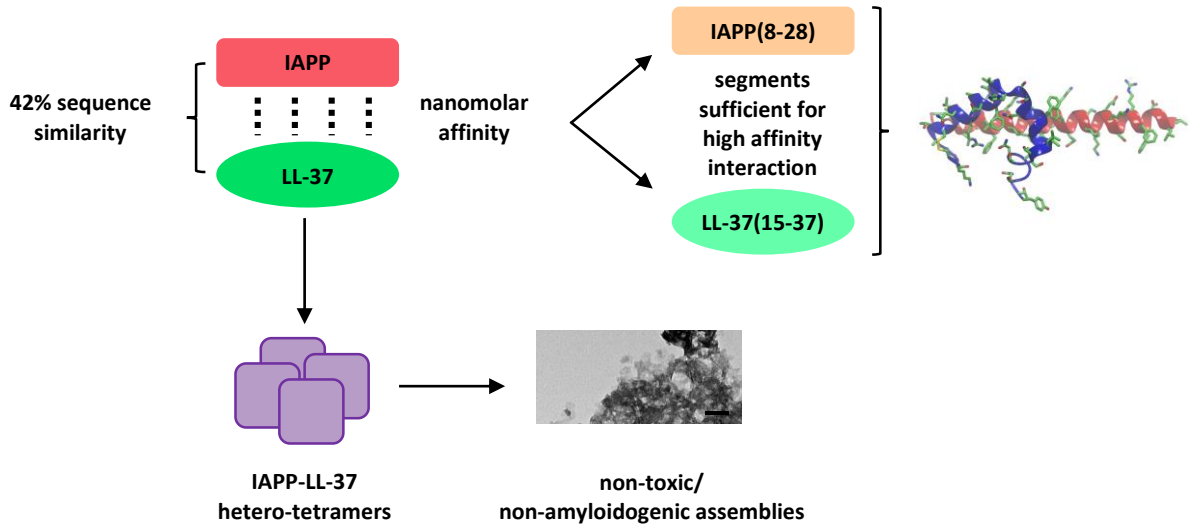

Figure 38. Schematic representation of the functions of LL-37 as binding partner and inhibitor of IAPP self-assembly. LL-37 binding IAPP with nanomolar affinity, and IAPP(8-28) and LL-37(15-37) regions are mediating the interaction. LL-37 forms hetero-complexes when mixed with IAPP, leading to the formation of non-toxic and non-amyloidogenic species.

4.2 Identification of partial LL-37 segments able to inhibit IAPP fibrillogenesis and cytotoxicity

The second part of my work aimed at the identification of the shortest LL-37-derived sequence, which can efficiently suppress the self-association of IAPP into cytotoxic assemblies.

4.2.1 Peptide design and synthesis

The aim above described was achieved by the rational design, followed by biochemical and biophysical characterization, of C-terminal and/or N-terminal truncated LL-37-derived segments. As a first approach, the design was based on the identified regions of LL-37 mediating its interaction with IAPP, which were found to be LL-37(6-10) and LL-37(25-27) (section 4.1.8). Based on these findings, the segments LL-37(1-10) and LL-37(20-31) were synthesized. Preliminary results obtained by Vincenz Buschinger showed that these two segments containing the core regions of LL-37 for their interaction with IAPP were not sufficient to interfere with IAPP aggregation into cytotoxic species. Additionally, circular dichroism experiments showed that the two segments are random coiled with no concentration-dependent oligomerization propensity. The app. K_ds for the interaction with IAPP of LL-37(1-10) and LL-37(20-31), obtained by Vincenz Buschinger and Stefanie Grümbel respectively, were determined via fluorescence spectroscopic titration. The N-terminal segment LL-37(1-10) exhibited a weak binding affinity (micromolar range), while a nanomolar binding affinity was found for LL-37(20-31), suggesting that the central/C-terminal region is mainly involved in the interaction with IAPP (Table 16).

Table 16. Preliminary studies on LL-37(1-10) and LL-37(20-31).

Abbreviation	**Peptide sequence**	**Inhibition of IAPP amyloid formation**	**Secondary structure**	**$K_{d,app}$ (±SD) (for Fluos-IAPP)[a]**
LL-37(1-10)	LLGDFFRKSK	no inhibition	random coil	> 20 μM[b]
LL-37(20-31)	IVQRIKDFLRNLV	no inhibition	random coil	170.0 (± 42.4) nM[c]

[a] App. K_ds, means (±SD) from 3 binding curves. Determined via titrations of fluorescein-labeled IAPP (Fluos-IAPP, 5nM) with non-labeled LL-37 segments. [b] performed by Vincenz Buschinger; [c] performed by Stefanie Grümbel.

Subsequently, with a rational approach, the C-terminus of LL-37 was removed, yielding to several truncated segments: LL-37(1-14), LL-37(1-26), LL-37(1-27), LL-37(1-31), and LL-37(1-34).

LL-37(1-14) was designed by dissecting the native sequence in two parts, as described in section 4.1.10. LL-37(1-26) and LL-37(1-27) were designed to investigate whether Phe27 plays a crucial role in the inhibition of IAPP fibrillogenesis. LL-37(1-31) contains the residues of the peptide known to fold into an α-helical structure (132). LL-37(1-34) contains both of the LL-37 regions identified via peptide array as important for the interaction with IAPP.

With a similar rational approach, the N-terminal truncated peptides were designed to identify the shortest LL-37 segment able to inhibit IAPP self-assembly: LL-37(15-37), LL-37(7-37), LL-37(5-37), and LL-37(3-37).

LL-37(15-37) is the correspondent C-terminal segment to LL-37(1-14), LL-37(7-37), LL-37(5-37) were designed to study the role of Phe5 and Phe6 in the inhibition of IAPP fibril formation. The N-terminus was also elongated in the peptide LL-37(3-37) to achieve similar biophysical and biochemical properties to LL-37 (Figure 39). Finally, after LL-37(3-37) and LL-37(1-34) were found to be respectively the N-terminal and C-terminal shortened segments that are inhibitors of IAPP self-assembly, LL-37(3-34) was synthesized. This peptide combines the features of the two inhibitors, and we asked whether it could still have an inhibitory potency like LL-37.

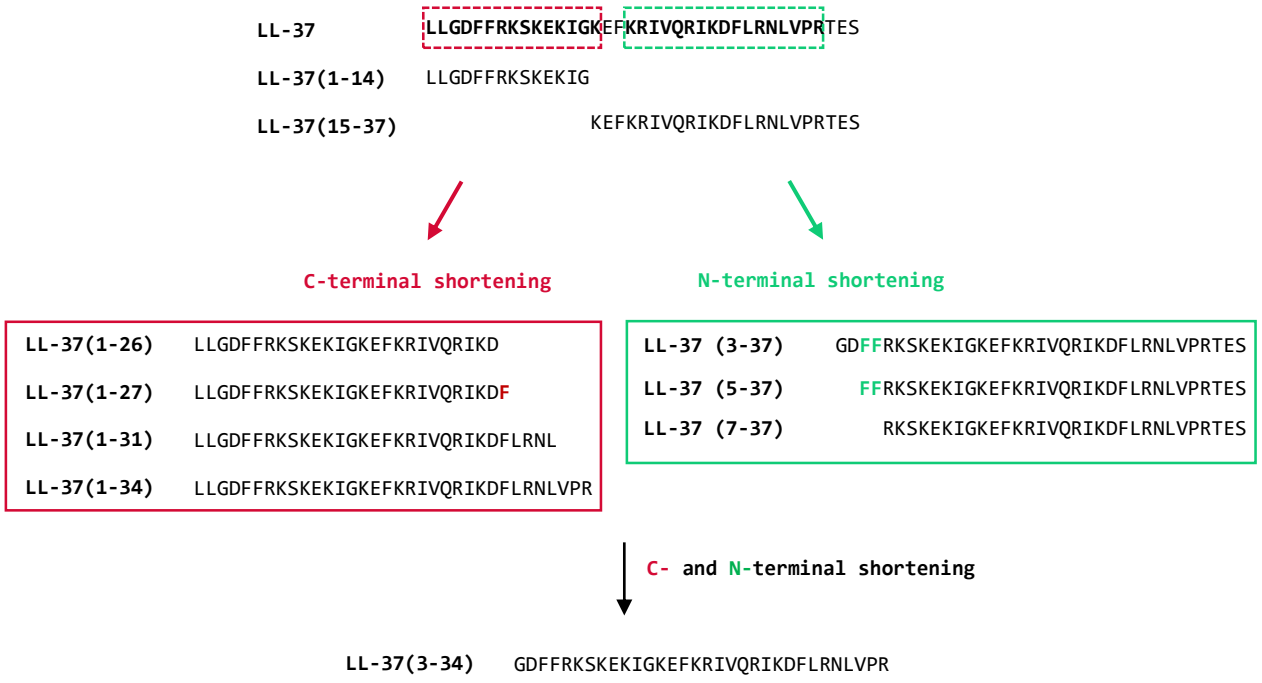

Figure 39. Rational design approach of C- and N-terminal truncated LL-37 segments. Red and green dashed boxes indicate the two regions of LL-37 mediating its interaction with IAPP. Consequently, C-terminal and N-terminal shortening were carried out (red and green boxes respectively) and roles of phenylalanine residues were investigated.

Peptides were synthesized using the Fmoc-SPPS strategy (Table 17) and purified utilizing RP-HPLC.

Table 17. Name and primary structure of LL-37 segments.

Abbreviation	**Peptide sequence**
LL-37(1-14)	LLGDFFRKSKEKIG
LL-37(1-26)	LLGDFFRKSKEKIGKEFKRIVQRIKD
LL-37(1-27)	LLGDFFRKSKEKIGKEFKRIVQRIKDF
LL-37(1-31)	LLGDFFRKSKEKIGKEFKRIVQRIKDFLRNL
LL-37(1-34)	LLGDFFRKSKEKIGKEFKRIVQRIKDFLRNLVPR
LL-37(3-37)	GDFFRKSKEKIGKEFKRIVQRIKDFLRNLVPRTES
LL-37(5-37)	FFRKSKEKIGKEFKRIVQRIKDFLRNLVPRTES
LL-37(7-37)	RKSKEKIGKEFKRIVQRIKDFLRNLVPRTES
LL-37(15-37)	KEFKRIVQRIKDFLRNLVPRTES
LL-37(3-34)	GDFFRKSKEKIGKEFKRIVQRIKDFLRNLVPR

Most of the LL-37 segments were synthesized on Wang resin, using a combination of manual and automated SPPS with the CS336X peptide synthesizer. The synthesis of longer segments was challenging, due to the high amount of difficult couplings which led to the formation of side products that had to be removed via RP-HPLC. For each peptide, Fmoc-cleavage was done using a solution of DMF containing 25% of piperidine or 20% of piperidine with 0.1 M HOBt in the case of sequences containing aspartic acid, and a capping step with acetic anhydride was performed after the complete coupling of each amino acid.

The synthesis and the purification of LL-37(1-14) and LL-37(15-37) are described in detail in section 4.1.10. The synthesis of LL-37(1-26) was carried out on Wang resin with a final substitution level of 0.46 mmol/g. Couplings were performed in DMF two or three times using Fmoc-protected amino acids in 3-fold molar excess, HBTU or HATU as coupling reagents in 3-fold molar excess, and DIEA in 4.5 molar excess. The reaction time for each coupling was 40 minutes. For selected difficult couplings, double amounts of molar

excesses were used for coupling reagents, Fmoc-protected amino acids, and DIEA or HBTU was replaced with HATU. In the case of LL-37(1-26), most of the couplings were performed twice using HBTU as a coupling reagent, with the exception of Phe^{17}, Lys^{15}, Phe^{6}, Phe^{5}, Asp^{4}, Gly^{3}, and Leu^{1} for which HATU was used for the first coupling; additionally, Glu^{16}, Gly^{14}, and Leu^{2} were coupled both times using HATU and Lys^{18} was coupled twice with HATU and for 50 minutes of coupling time. Couplings of Arg^{19} and Lys^{12} were performed 3 times using HATU. Finally, as the coupling of Lys^{10} was particularly challenging 6-fold molar excess of HATU and Fmoc-protected amino acid, and 9-fold excess of DIEA were applied.

Similarly, LL-37(1-27) was synthesized on Wang resin with a final substitution level of 0.48 mmol/g. Most of the couplings of this peptide were performed twice using 3-fold molar excess of Fmoc-protected amino acids, 3-fold excess of HBTU, and 4.5 molar excess of DIEA. In the case of Phe^{17}, Lys^{15}, Phe^{6}, Phe^{5}, Asp^{4}, Gly^{3} the first coupling was carried out with HATU as coupling reagent. Glu^{16}, Gly^{14}, and Leu^{2} were coupled both times using HATU, and Lys^{18} was coupled twice with HATU and for 50 minutes of coupling time. Arg^{19} and Lys^{12} were coupled 3 times using HATU, while Lys^{10} was coupled with a 6-fold molar excess of HATU and Fmoc-protected amino acid and 9-fold excess of DIEA.

LL-37(1-31) was synthesized on Wang resing with 0.40 mmol/g as substitution level. As above, most of the couplings were performed twice using a 3-fold molar excess of HBTU as a coupling reagent, 3-fold molar excess of Fmoc-protected amino acid, and 4.5-molar excess of DIEA. In the couplings of Phe^{17}, Lys^{15}, Phe^{6}, Phe^{5}, Asp^{4}, Gly^{3}, and Leu^{1}, HBTU was replaced with HATU only for the first coupling reaction, as for the previous peptides. Both couplings were carried out with HATU for Glu^{16}, Gly^{14}, and Leu^{2} and in the same conditions, but for 50 minutes coupling time in the case of Lys^{18}. Additionally, the coupling of Asp^{26} was carried out 3 times, while the couplings of Asn^{30}, Arg^{29}, Leu^{28}, and Phe^{27} were also carried out 3 times, but in the first two HATU was applied as a coupling reagent. HATU was also used for the 3-times coupling of Arg^{19}, Lys^{12}, and Leu^{2}, while Lys^{10} was coupled with a 6-fold molar excess of HATU and Fmoc-protected amino acid and 9-fold excess of DIEA.

The synthesis of the longest C-terminal truncated segment, LL-37(1-34) was carried out on Wang resin with 0.29 mmol/g as substitution level. The synthesis of the previous segments was optimized, to avoid the formation of side-products which can be problematic during the purification of the peptides. For this reason, most of the couplings were carried out twice with a 3-fold molar excess of HATU instead of HBTU, 3-fold molar excess of Fmoc-protected amino acid, and a 4.5-fold molar excess of DIEA, except for Ile^{13}, Glu^{11}, Ser^{9}, Lys^{8}, and Arg^{7} which were coupled with HBTU as coupling reagent. Coupling reactions were carried out using HATU only first of the two couplings in the case of Pro^{33}, Phe^{17}, Lys^{15}, Phe^{6}, Phe^{5}, Asp^{4}, Gly^{3}, and Leu^{1}. Difficult couplings were carried out three times. In particular, Arg^{19}, Lys^{12}, Lys^{10}, and Leu^{2} were coupled using only HATU; for Val^{32} and Leu^{31} HATU was applied only for the first coupling and HBTU for the other two. In the coupling of Val^{21} HATU was used for the first two couplings and HBTU only for the third reaction. Finally, Ile^{20} was coupled three times with HATU, and in addition, the first coupling was carried out with a 6-fold molar excess of HATU and Fmoc-protected amino acid and 9-fold excess of DIEA. The N- and C-terminal shortened peptide LL-37(3-34) was synthesized in the same way interrupting the synthesis at Gly^{3} and leaving out Leu^{1} and Leu^{2}.

For the synthesis of the N-terminal truncated segments, several attempts were carried out to optimize the procedure and avoid the formation of truncated sequences. Results led to the conclusion that TentaGel R PBH resin with a substitution level of 0.19 mmol/g gave the best purification yield. For LL-37(3-37), most couplings were performed twice using HATU as a coupling reagent, except for Glu^{36}, Thr^{35}, Arg^{34}, Pro^{33}, for which HBTU was used for the second coupling step. Difficult couplings were performed three times. As in the synthesis of LL-37(1-34), Val^{32} and Leu^{31} were coupled using HATU only for the first coupling and HBTU for the other two, while Val^{21} was coupled with HATU for the first two couplings and HBTU for the last one. Gln^{22}, Lys^{15}, Lys^{12}, Lys^{8}, and Leu^{2} were coupled three times using HATU as coupling reagent. For positions Glu^{11} and Lys^{10}, the three times coupling with HATU was carried out for 50 minutes. In several positions of the sequence, difficult couplings were identified. For Ile^{20}, Arg^{19}, and Lys^{18}, Phe^{17}, and Ile^{13} three coupling

steps of 50 minutes each were carried out with a 6-fold molar excess of HATU and Fmoc-protected amino acid and 9-fold excess of DIEA for the first two. Finally, Gly^{14} and Asp^{4} were coupled three times with a 6-fold molar excess of HATU and Fmoc-protected amino acid and 9-fold excess of DIEA for 50 minutes. The synthesis of LL-37(5-37) and LL-37(7-37) can be carried out similarly interrupting the synthesis after Phe^{5} or Arg^{7} respectively. As described above, the synthesis presented difficulties in the coupling reaction of certain amino acids. A synthetic scheme of the most common capped side products is shown in Table 18.

Table 18. Characterization of the acetylated side products of the LL-37 synthesis via MALDI-TOF.

Difficult couplings	**Identified acetylated side products**	**$[M+H]^+$ expected of acetylated side products [a]**	**$[M+H]^+$ or $[M+Na]^+$ found of acetylated side products [b]**
Ile^{20}	Ac-LL-37(21-37)	2113.2	2113.5
Arg^{19}	Ac-LL-37(20-37)	2226.3	2226.3
Lys^{18}	Ac-LL-37(19-37)	2382.4	2382.5
Phe^{17}	Ac-LL-37(18-37)	2510.5	2510.7
Glu^{16}	Ac-LL-37(17-37)	2657.5	2683.9
Gly^{14}	Ac-LL-37(15-37)	2914.7	2914.6
Ile^{13}	Ac-LL-37(14-37)	2971.7	2971.7
Asp^{4}	Ac-LL-37(5-37)	4135.4	4135.2
Leu^{2}	Ac-LL-37(3-37)	4307.4	4307.2

[a] monoisotopic molar mass $[M+H]^+$ or $[M+Na]^+$ expected and [b] $[M+H]^+$ or $[M+Na]^+$ found.

Cleavages of peptides from the resin were carried out for 3 hours using TFA:ddH_2O (95:5 v:v). The obtained crude products were purified using RP-HPLC. Some of the LL-37 segments required more than one purification cycle to obtain a high purity final product. The purity of each of them was verified by MALDI-TOF MS as shown in Table 19.

Table 19. Characterization of the synthetic peptides via RP-HPLC and MALDI-TOF.

Abbreviation	**HPLC program**	**t_R (min)[a]**	**HPLC program for 2nd purification**	**t_R (min)**	**Yield[b]**	**$[M+H]^+$ expected[c]**	**$[M+H]^+$ found[c]**
LL-37(1-26)	SchnellAβ	17.9	-	-	25%	3178.9	3179.7
LL-37(1-27)	SchnellAβ	19.2	SchnellAβ	19.8	12%	3325.9	3326.6
LL-37(1-31)	10-100% B stay at 100% B for 10 min	16.9	10-100% B stay at 100% B for 10 min	16.9	5%	3822.2	3823.2
LL-37(1-34)	10-100% B stay at 100% B for 10 min	16.6	30% B for 7 min-30-100% B in 30 min	24.8	1%	4174.4	4175.8
LL-37(3-37)	40% B for 7 min-40-80% B in 23 min	19.6	40% B for 7 min-40-80% B in 23 min (2x)	19.6	7%	4265.4	4264.8
LL-37(5-37)	10-100% B stay at 100% B for 10 min	15.4	10-100% B stay at 100% B for 10 min	15.4	13%	4093.4	4093.7
LL-37(7-37)	SchnellAβ	21.4	SchnellAβ	21.4	9%	3799.2	3799.8
LL-37(3-34)	10-100% B stay at 100% B for 10 min	16.0	-	-	18.5%	3948.3	3949.3

Peptides were synthesized with free C- and N-terminus. [a] t_R, HPLC retention time; [b] % yield with regard to crude peptide, and [c] monoisotopic molar mass $[M+H]^+$ expected and $[M+H]^+$ found.

The synthesis steps were optimized throughout time according to the acetylated fragments found when the peptides were characterized via RP-HPLC and MALDI-TOF analysis (Figure 40 and Figure 41).

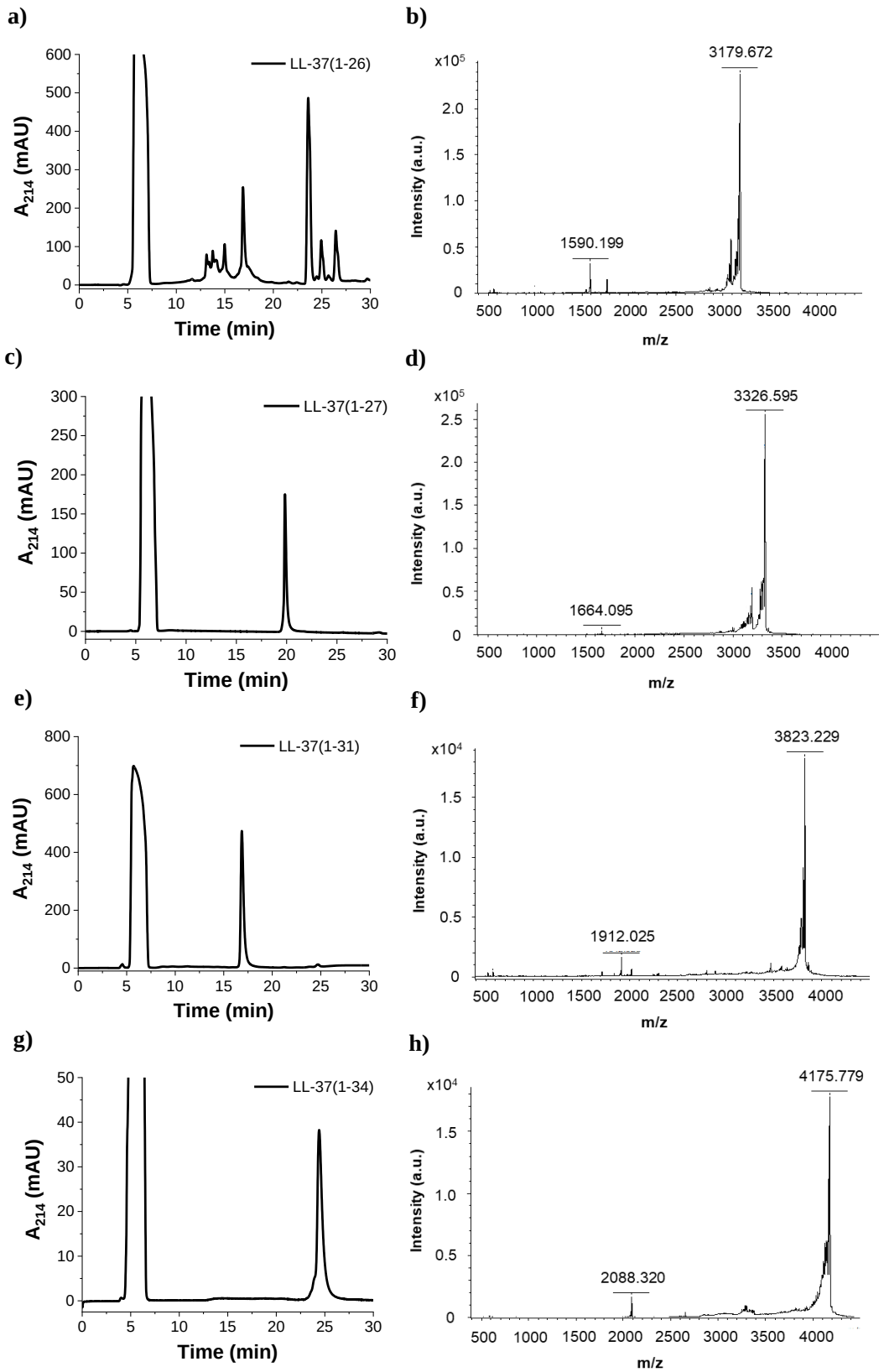

Figure 40. Characterization of LL-37(1-26), LL-37(1-27), LL-37(1-31), and LL-37(1-34) via RP-HPLC and MALDI-TOF. Representative chromatogram at 214 nm of a) LL-37(1-26) crude, c) repurified LL-37(1-27), e) repurified LL-37(1-31), and g) repurified LL-37(1-34) with retention time of the peptides at 17.9, 19.8, 16.9, and 24.8 min respectively. MALDI-TOF-MS spectra of HPLC purified b) LL-37(1-26), d) LL-37(1-27), f) LL-37(1-31), and h) LL-37(1-34) with $[M+H]^+$ and $[M+2H]^{2+}$ found masses.

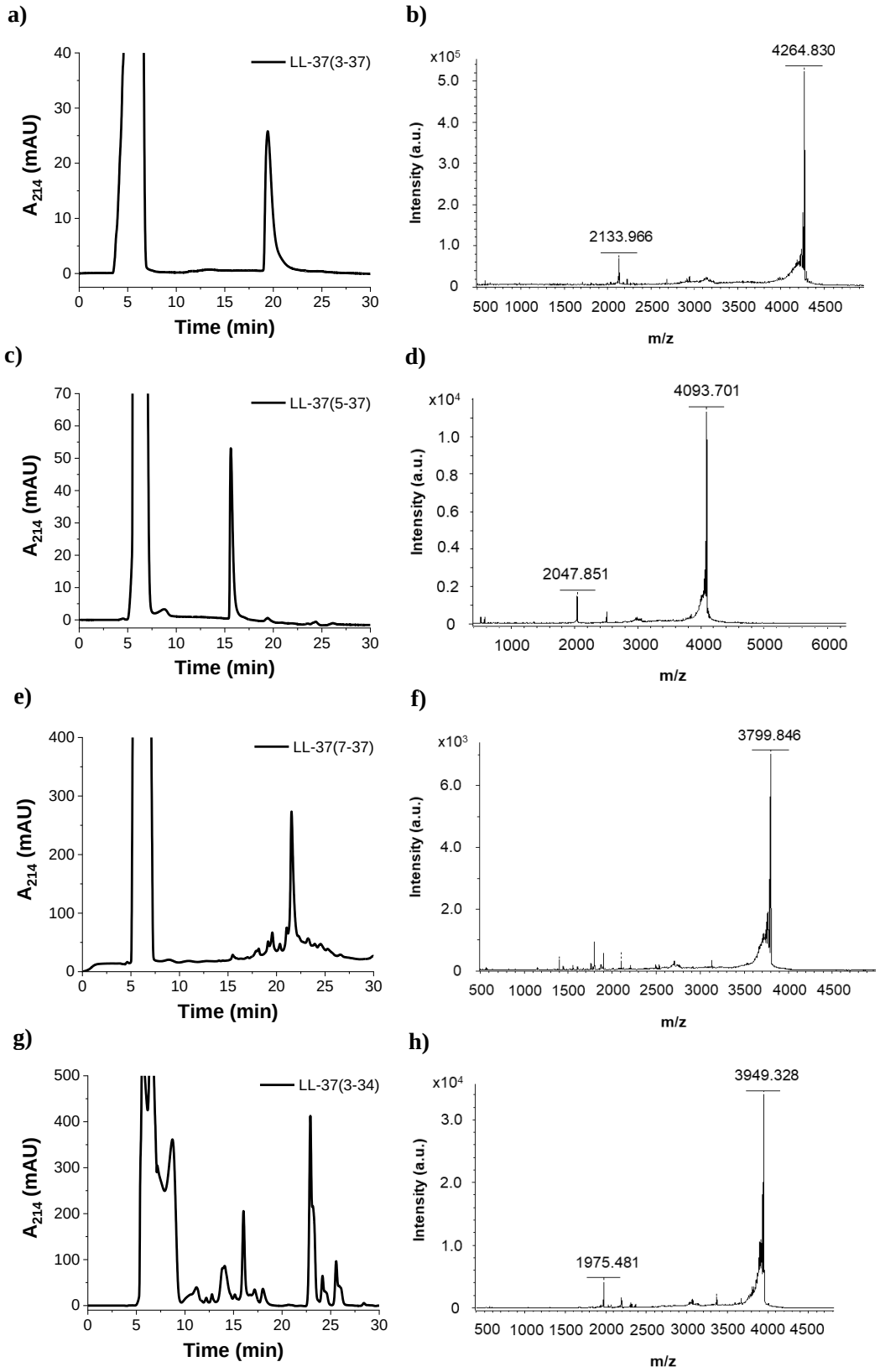

Figure 41. Characterization of LL-37(3-37), LL-37(5-37), LL-37(7-37), and LL-37(3-34) via RP-HPLC and MALDI-TOF. Representative chromatogram at 214 nm of a) repurified LL-37(3-37), c) repurified LL-37(5-37), e) repurified LL-37(7-37), and g) LL-37(3-34) crude with retention time of the peptides at 19.6, 15.4, 21.4, and 16.0 minutes respectively. MALDI-TOF-MS spectra of HPLC purified b) LL-37(3-37), d) LL-37(5-37), f) LL-37(7-37), and h) LL-37(3-34) with $[M+H]^+$ and $[M+2H]^{2+}$ found masses.

4.2.2 Biophysical characterization: conformational studies via CD spectroscopy

The secondary structure of the truncated LL-37 segments was studied via circular dichroism spectroscopy. All spectra were recorded by diluting the peptide of interest from its HFIP stock in aqueous 10 mM sodium phosphate buffer (pH 7.4), for a total of 1% HFIP. To estimate their aggregation propensity, spectra were recorded between 1 μM and 100 μM (Figure 42). Regarding the C-terminal shortened segments, all peptides showed no concentration dependence in their oligomerization propensity. Furthermore, LL-37(1-10), similarly to LL-37(1-14) (section 4.1.12), showed a minimum at 198 nm, typical of disordered peptides (Figure 42a). Elongated sequences such as LL-37(1-26) and LL-37(1-27) exhibited no concentration-dependent signal and mainly random coil structure with a minimum at 198 nm, but also a minimum around 227 nm, indicative of β-sheet/turn and/or α-helix secondary structure (Figure 42b, c). LL-37(1-31) displayed a maximum at 198 nm and two minima, one at 208 nm and a marked one at 226 nm, typical of the β-sheet/turn and α-helix secondary structure (Figure 42d). Also for this peptide, no concentration dependence of the signal was observed. A similar structure was exhibited by LL-37(1-34): two minima at 209 nm and a more pronounced one at 226 nm and a maximum at 198 nm were observed, proof of a β-sheet/turn and α-helix secondary structure as the native peptide. Interestingly, no concentration-dependent signal was visible between 5 and 10 μM, indicating that the peptide already oligomerizes at 10 μM, but at 20 μM the signal is circa two times more intense, although the peptide visibly precipitates (Figure 42e). In general, the shorter segments are unordered with low signal intensities, while LL-37(1-31) and LL-37(1-34) exhibit a β-sheet/turn and α-helix secondary structure. The signal resulted more intense for LL-37(1-34) compared to LL-37(1-31) indicating a higher structural content (Figure 42f).

In contrast, N-terminal truncated segments exhibited aggregation properties dependent on their concentration (Figure 43). LL-37(3-37) showed a reduction of the signal due to oligomerization starting at 10 μM and β-sheet/turn and α-helix secondary structure, with a maximum at 198 nm and two minima, one at 208 nm and a more pronounced one at 226 nm (Figure 43a). The secondary structures observed for LL-37(5-37) and LL-37(7-37) were similar (Figure 43b, c). Both peptides present the maximum at 198 nm and the two minima at 208 nm and 226 nm, but compared to LL-37(3-37) the two minima have similar signal intensities. This correlates with the loss of β-sheet/turn content, which LL-37(3-37) instead shows (Figure 43d). Results indicated an aggregation propensity starting at 10 μM for these two segments. Only the shortest N-terminal truncated segment LL-37(15-37) exhibited an unordered structure with a minimum at 200 nm and no variations of the oligomerization depending on the concentration as shown in section 4.1.12.

Last, the secondary structure of LL-37(3-34) was investigated (Figure 44). The peptide exhibited no concentration dependence, as the signal did not significantly change with increasing concentration. The obtained secondary structure was mainly α-helix, characterized by a maximum at 198 nm and two minima with comparable intensity, one at 208 nm and one at 223 nm which has slightly higher intensity. Nearly no β-sheet/turn content was identifiable in this segment, although it was present in LL-37(1-34) and LL-37(3-37), from which LL-37(3-34) is derived.

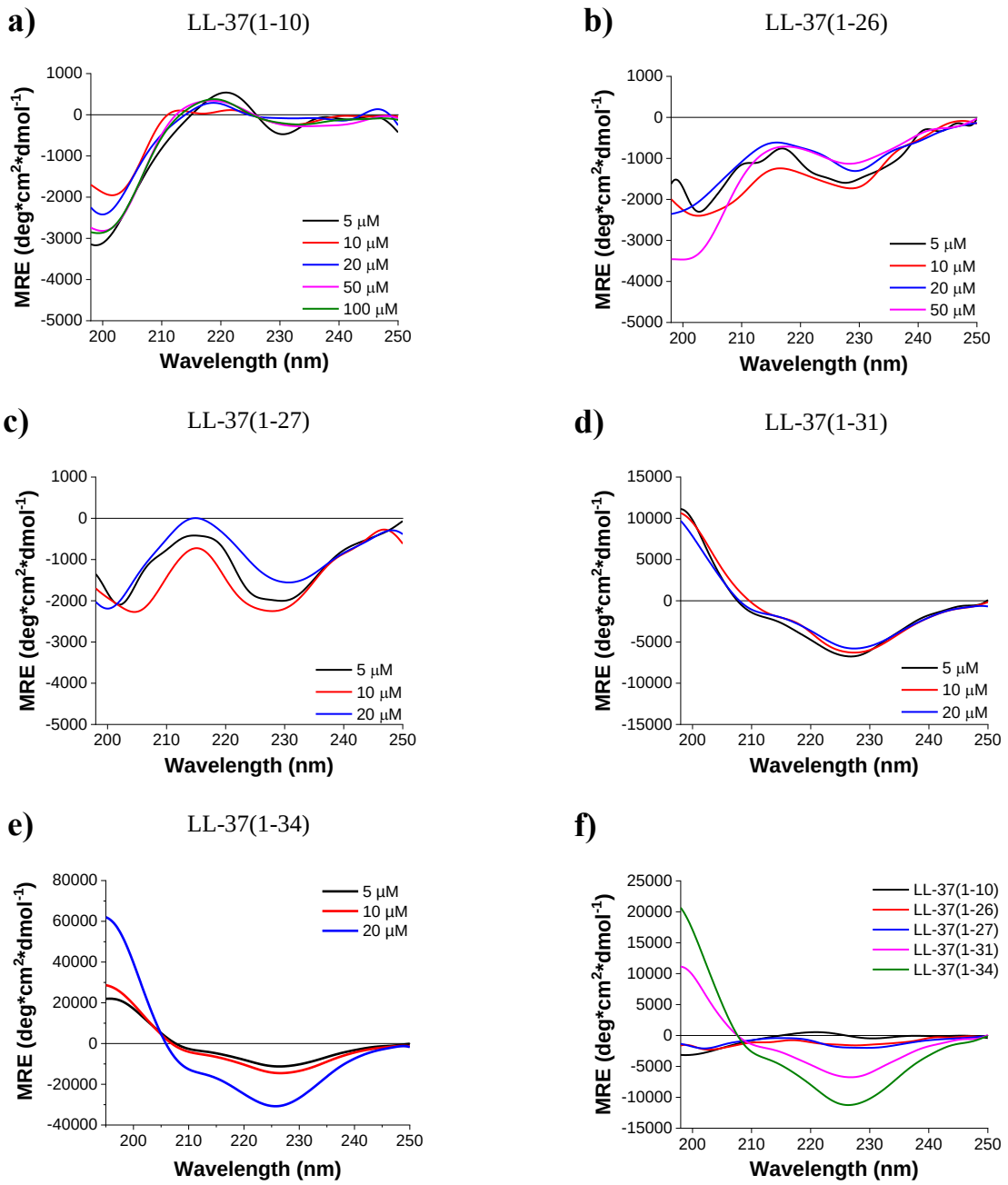

Figure 42. Concentration dependence of C-terminal truncated LL-37 segments assessed by far-UV CD spectroscopy a) LL-37(1-10), Vincenz Buschinger's data, b) LL-37(1-26), c) LL-37(1-27), d) LL-37(1-31), e) LL-37(1-34), and f) overlay at 5 µM of the spectra in a), b), c), d), and e). Measurements were performed in aqueous buffer 1×b, pH 7.4, containing 1% HFIP.

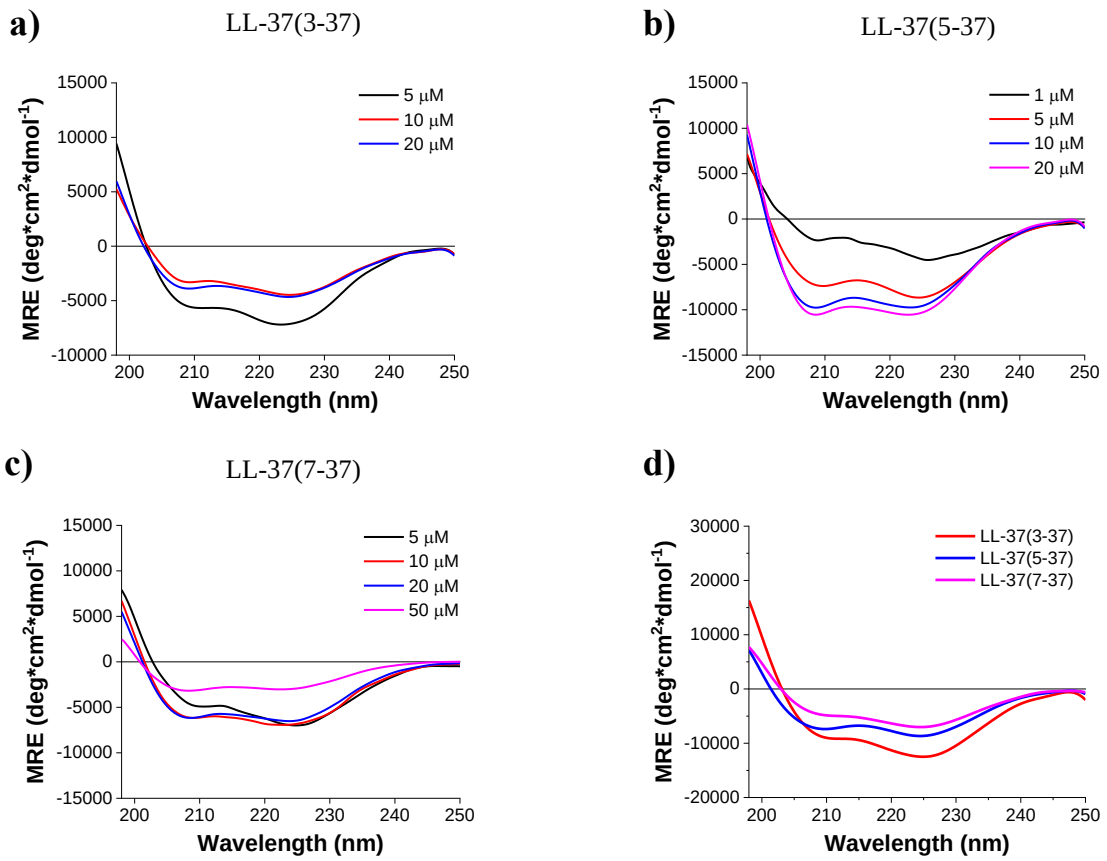

Figure 43. Concentration dependence of N-terminal truncated LL-37 segments assessed by far-UV CD spectroscopy. a) LL-37(3-37), b) LL-37(5-37), c) LL-37(7-37), and d) overlay at 5 µM of the spectra in a), b), and c). Measurements were performed in aqueous buffer 1×b, pH 7.4, containing 1% HFIP.

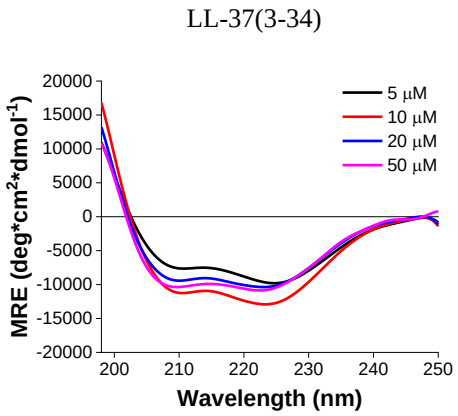

Figure 44. Concentration dependence of C- and N-terminal truncated LL-37 segment, LL-37(3-34) assessed by far-UV CD spectroscopy. Measurements were performed in aqueous buffer 1×b, pH 7.4, containing 1% HFIP.

To evaluate the effect of HFIP on the secondary structure of these peptides, spectra at 5 µM were recorded in aqueous 10 mM sodium phosphate buffer (pH 7.4) (Figure 45). As shown in section 4.1.12, LL-37 exhibits an α-helix with a maximum at 198 nm and two minima at 206 and 224 nm. The LL-37 segments were investigated as well in these conditions. LL-37(1-14) had a minimum at circa 200 nm, indicating a random coil structure. The structure of LL-37(1-26) and LL-37(1-27) were identical in these conditions. With a minimum at 200 nm, both peptides were mainly unstructured.

LL-37(1-31) exhibited a maximum signal at 198 nm and two minima of equal intensities at 206 and 224 nm, indicating a loss of signal intensity at 224 nm in absence of HFIP, which can be attributed to a loss of β-sheet/turn content (Figure 45a). Also for LL-37(1-34) a loss of β-sheet/turn conformation was observed. This peptide is an α-helix, with the characteristic maximum at 195 nm and the two minima at 208 and 222 nm respectively. A similar effect of β-sheet loss was observed for the N-terminal truncated segment LL-37(3-37). In fact, the two minima at 206 and 224 nm have comparable intensities, as for LL-37(1-31). LL-37(5-37) exhibited a minimum at 203 nm and one at 226 nm, indicating an increase of the random coil content when the spectrum is recorded only in aqueous buffer. The secondary structure of LL-37(7-37) was predominantly random coil, with a marked minimum at 200 nm. Finally, LL-37(15-37) had a marked minimum at 203 nm and one at 226 nm, remaining mainly unordered (Figure 45b).

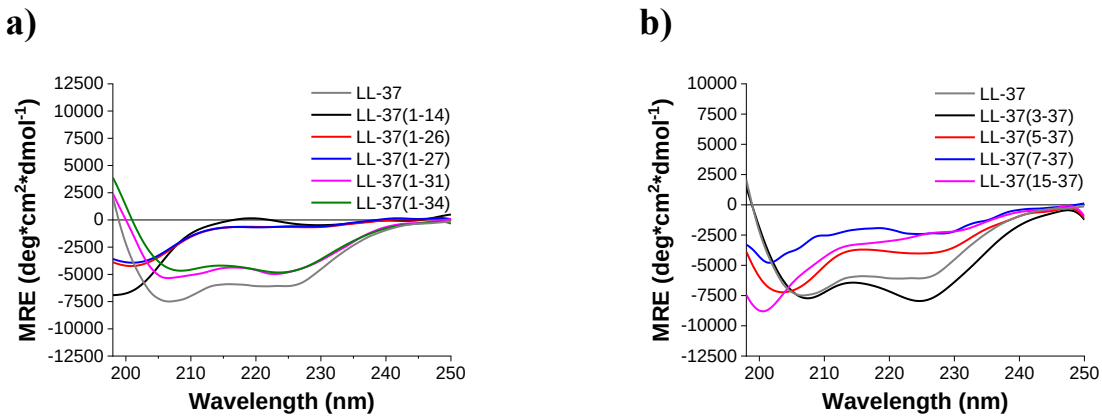

Figure 45. Effect of the absence of HFIP on the secondary structure of LL-37, N- and C-terminal truncated LL-37 segments assessed by far-UV CD spectroscopy. a) LL-37 and C-terminal truncated LL-37 segments, b) LL-37 and N-terminal truncated LL-37 segments. Measurements were performed at a concentration of 5 μM in aqueous buffer 1×b, pH 7.4.

The secondary structure in aqueous buffer without HFIP was investigated also for LL-37(3-34). Although the peptide is still helical, as it exhibits two minima at 204 and 224 nm with the first one with a higher signal intensity, no positive signal at 195 nm was observed, suggesting an increase of unordered structure. Also, the lack of both C- and N-terminus led to a loss of structure, as the longer parent segments LL-37(3-37) and LL-37(1-34) had a higher helical content as shown in Figure 46.

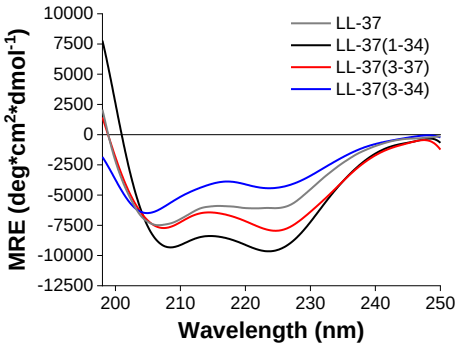

Figure 46. Effect of the absence of HFIP on the secondary structure of LL-37, LL-37(1-34), LL-37(3-37), and LL-37(3-34) assessed by far-UV CD spectroscopy. Measurements were performed at a concentration of 5 μM in aqueous buffer 1×b, pH 7.4.

Next, the effect of 2,2,2-trifluoroethanol (TFE) on the helical propensity of two shortened LL-37 derived peptides was investigated. In absence of TFE, LL-37(1-27) is a random coil with a slight β-sheet/turn secondary structure. The titration with an increasing percentage of TFE led to a radical change in the conformation, as the signal of two minima at 208 and 222 nm increased, indicating the formation of an α-helix with a transition point (T_M) at circa 18% TFE (Figure 47a, b). Results indicate that this truncated sequence exhibits a lower helical propensity than LL-37, underlining the contribution of the C-terminus to the helical structure of the human cathelicidin. As described above, LL-37(1-31) displays a maximum at 198 nm and two minima, one at 208 nm and a marked one at 226 nm, typical of the β-sheet/turn and α-helix secondary structure. Titrations with increasing amounts of TFE led to a two-state structural transition. The β-sheet/turn content was lost, and two minima, at 208 and 222 nm appeared, indicating the α-helix formation (Figure 47c). The transition point (T_M) was found at circa 16% TFE (Figure 47d), indicating a lower helical propensity than the native peptide, which had a transition point at 8% TFE. The longest C-terminal truncated peptide LL-37(1-34) showed a higher helical propensity than the previously described peptides. In fact, the peptide displays a β-sheet/turn and α-helix secondary structure as the native peptide two minima at 209 nm and a more pronounced one at 226 nm and a maximum at 198 nm when no TFE was added to the sample. The titration with TFE led to a two-state structural transition between the β-sheet/turn and α-helix structure to a helical structure, with a T_M at 12% TFE, which is comparable to the transition point of LL-37 (Figure 47e, f). Similarly, LL-37(5-37) shows a maximum at 198 nm and the two minima at 208 nm and 226 nm with comparable signal intensity indicating mainly an α-helix secondary structure. The titration of this peptide with increasing amounts of TFE led to the complete conversion of the secondary structure into an α-helix, with a T_M at 17% TFE (Figure 48a, b). Also in this case the helical propensity of the peptide is lower than the one of LL-37. The longer peptide LL-37(3-37) showed similar behavior. Without TFE, LL-37(3-37) shows a maximum at 198 nm and the two minima at 208 nm and 226 nm, indicating an α-helix and β-sheet/turn structure. The titration with TFE led to a transition to a helical secondary structure with the two minima at 208 and 222 nm (Figure 48c) and a T_M at 11% TFE (Figure 48d), confirming that the longer peptides exhibit similar helical propensity as LL-37. Last, the effect of the TFE of the C-and N-terminal truncated peptide LL-37(3-34) was investigated. This peptide mainly shows an α-helical secondary structure characterized by a maximum at 198 nm and two minima at 208 nm and 223 nm with comparable intensity, indicating less β-sheet/turn folding compared to its parent peptides. The TFE titration led to a transition to an α-helix structure with a transition point at 16% TFE (Figure 49a, b). The removal of both C- and N-termini evidenced the importance of these two regions for the helical propensity of the peptides. In fact, LL-37(3-34) showed a lower helical propensity than LL-37(3-37) and LL-37(1-34). In general, the results suggest that the shorter the sequences are, the lower is the α-helical propensity of the LL-37 derived peptides.

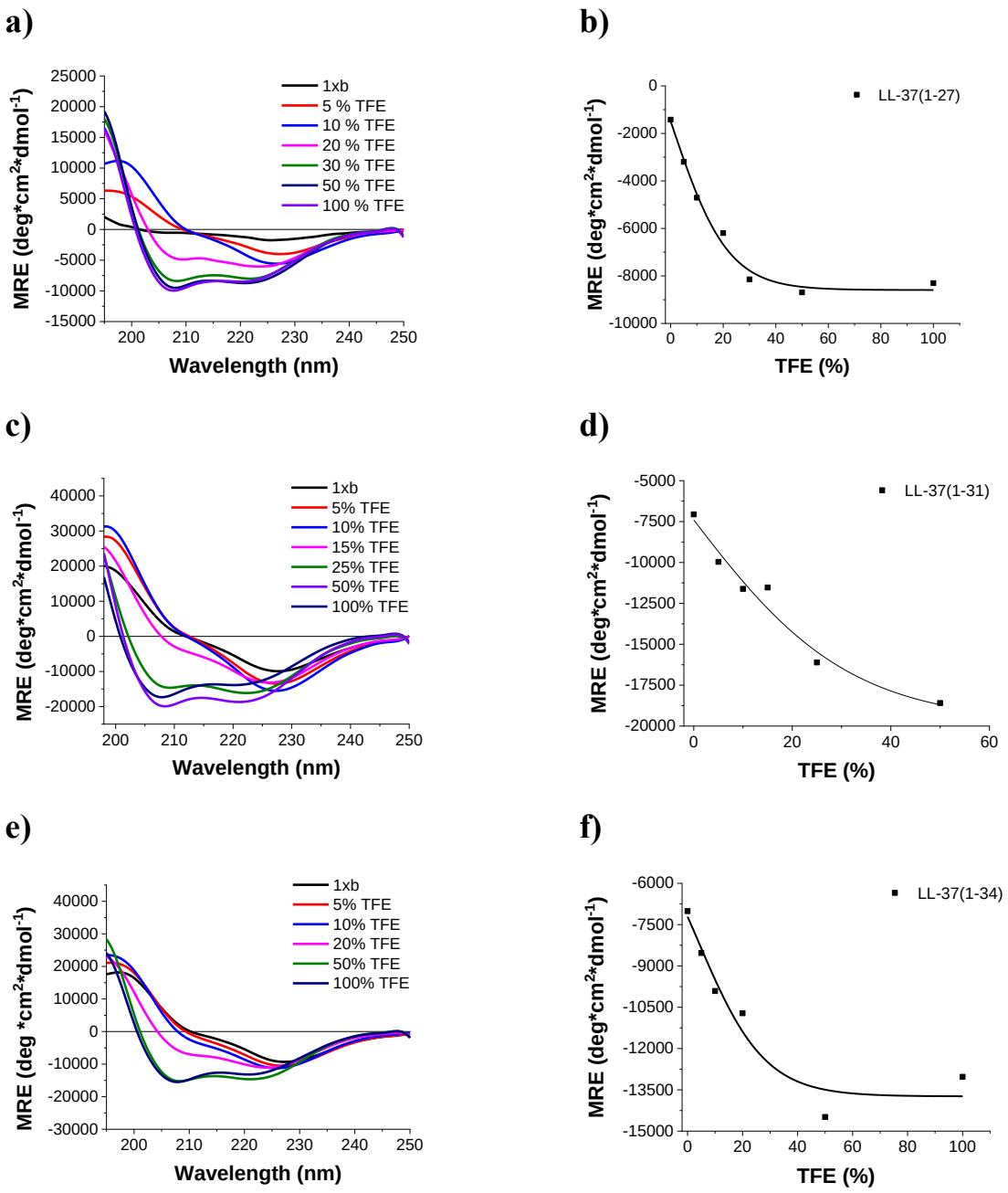

Figure 47. Effects of TFE on the conformation in aqueous solution of a) LL-37(1-27), c) LL-37(1-31), and e) LL-37(1-34) assessed by far-UV CD spectroscopy. Experiments were performed at peptide concentrations of 5 µM in aqueous buffer 1×b, pH 7.4, containing 1% HFIP with the indicated amounts of TFE. b), d), and f) Plots of minima at 222 nm versus the TFE amounts (%) of the CD spectra of the peptides shown in a), c), and e) respectively.

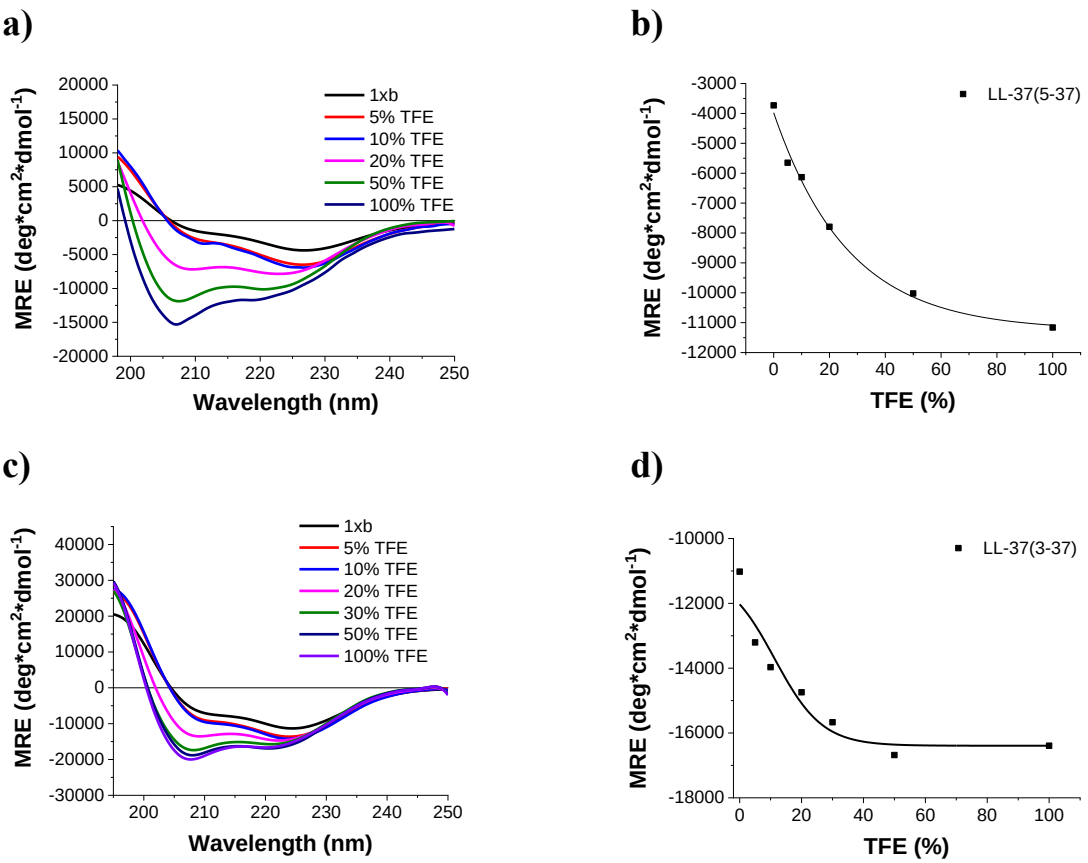

Figure 48. Effects of TFE on the conformation in aqueous solution of a) LL-37(5-37), c) LL-37(3-37) assessed by far-UV CD spectroscopy. Experiments were performed at peptide concentrations of 5 µM in aqueous buffer 1×b, pH 7.4, containing 1% HFIP with the indicated amounts of TFE. b), d) Plots of minima at 222 nm versus the TFE amounts (%) of the CD spectra of the peptides shown in a) and c) respectively.

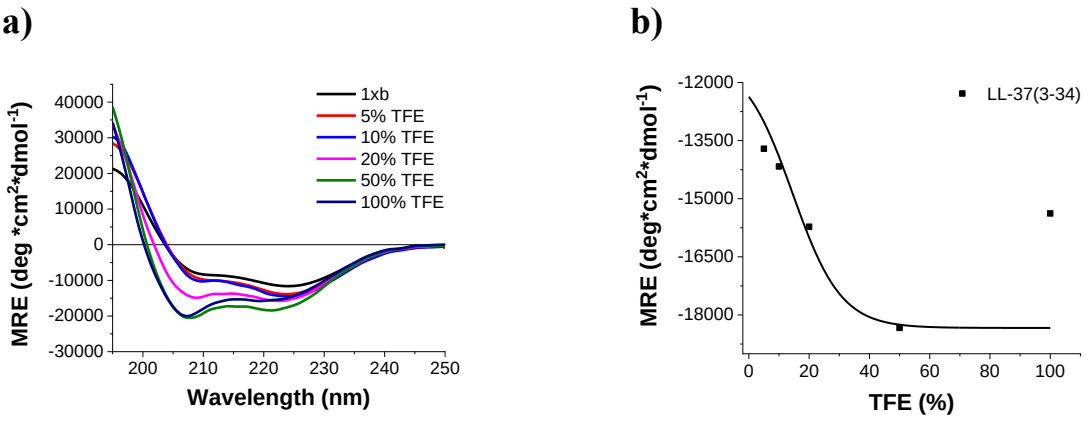

Figure 49. Effects of TFE on the conformation in aqueous solution of a) LL-37(3-34) assessed by far-UV CD spectroscopy. Experiments were performed at peptide concentrations of 5 µM in aqueous buffer 1×b, pH 7.4, containing 1% HFIP with the indicated amounts of TFE. b) Plots of minima at 222 nm versus the TFE amounts (%) of the CD spectra of the peptide shown in a).

In this section, the secondary structure of LL-37 truncated sequences was investigated via circular dichroism. Within the C-terminal truncated sequences, LL-37(1-14), LL-37(1-26), and LL-37(1-27) resulted mainly unstructured and with no oligomerization propensity. LL-37(1-31) and LL-37(1-34) exhibited an α-helix/β-sheet, β-turn structure like the native peptide. LL-37(3-37) is the only peptide truncated at the N-terminus that has an α-helix/β-sheet, β-turn structure like the native peptide with an oligomerization starting at 10 μM. Also LL-37(5-37) and LL-37(7-37) oligomerized at 10 μM, but their structure was only α-helical. The shortest segment, LL-37(15-37), was random coiled and showed no oligomerization. LL-37(3-34), truncated at both termini, was mainly α-helical with no significant oligomerization propensity. TFE titrations carried out for LL-37(1-27), LL-37(1-31), and LL-37(1-34) revealed that the truncated sequences have lower helical propensity than LL-37, as their transition points were identified at 18, 16, and 12% TFE respectively versus only 8% TFE for LL-37. Furthermore, the same conclusion can be drawn for LL-37(5-37) and LL-37(3-37) which exhibited T_M values at 17% and 11% TFE. Last LL-37(3-34), shortened at both termini, showed lower helical propensity than the corresponding peptides with one of the two termini (Table 20).

Table 20. Characterization of the secondary structure of LL-37and LL-37 C-/N-terminal truncated segments.

Peptide	**Secondary structure in 1xb[a] + 1% HFIP**	**Secondary structure in 1xb[a]**	**Concentration of oligomerization**	**T_M (TFE %)**
LL-37	α-helix/β-sheet,β-turn	α-helix	20 μM	8%
LL-37(1-14)	random coil	random coil	no oligomerization	20%*
LL-37(1-26)	random coil/β-sheet,β-turn	random coil	no oligomerization	-
LL-37(1-27)	random coil/β-sheet,β-turn	random coil	no oligomerization	18%
LL-37(1-31)	α-helix/β-sheet,β-turn	α-helix	no oligomerization	16%
LL-37(1-34)	α-helix/β-sheet,β-turn	α-helix	20 μM	12%
LL-37(3-37)	α-helix/β-sheet,β-turn	α-helix	10 μM	11%
LL-37(5-37)	α-helix	α-helix	10 μM	17%
LL-37(7-37)	α-helix	random coil	10 μM	-
LL-37(15-37)	random coil/β-sheet,β-turn	random coil/β-sheet,β-turn	no oligomerization	5%*
LL-37(3-34)	α-helix	α-helix	no oligomerization	16%

[a] 1xb, aq. buffer, pH 7.4, containing 1% HFIP. * Linus Wollenweber's data (129).

4.2.3 Studies on the inhibitory activities of LL-37 truncated segments on fibrillogenesis and cytotoxicity of IAPP

Next, we asked whether the C-terminal/N-terminal truncated LL-37 segments could intervene in the aggregation of IAPP in cytotoxic assemblies and which of them is the shortest sequence that retains the inhibitory properties. ThT binding assay in combination with TEM and MTT reduction assays was carried out to address this issue. Briefly, IAPP alone (16.5 µM) and its 1/1 mixtures with peptides were incubated for 168 hours, following the kinetics of fibril formation via ThT binding assay and the cytotoxicity via MTT reduction assay. TEM was used to evaluate the morphology of aggregates or fibrils at the given time points. In section 4.1.11, it has been shown that the C-terminal truncated segment LL-37(1-14) has no inhibitory properties. In Figure 50a it is shown that when IAPP is mixed with LL-37(1-14) the kinetics of aggregation are the same. After 24 hours fibril formation is observed, as the ThT signal increase for both IAPP alone and the mixture. MTT reduction assays show that there is no inhibition of the cytotoxicity of IAPP after 24 hours, and consequently after 7 days (Figure 50b, c). TEM images from the 24 hours aged sample show the presence of amyloid fibrils, confirming the obtained results (Figure 50d).

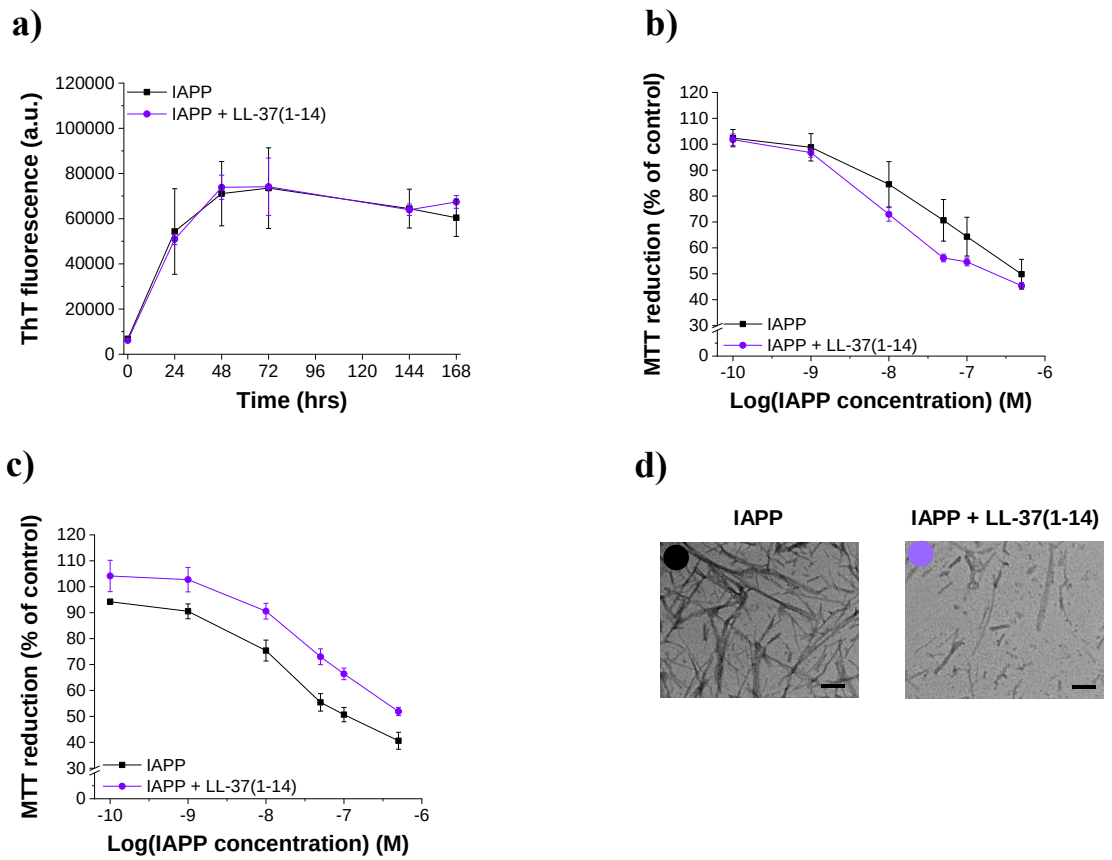

Figure 50. Effects of C-terminal truncated segment LL-37(1-14) on IAPP amyloid formation and cytotoxicity. a) Fibrillogenesis of IAPP (16.5 µM) and its mixtures with LL-37(1-14) (1/1) (means (±SD), 3 assays); b) effects on cell viability: solutions from a) were added to cultured RIN5fm cells (24 hours aged). Cell viability was determined by MTT reduction (means (±SD), 3 assays, n=3 each); c) effects on cell viability: solutions from a) were added to cultured RIN5fm cells (7 days aged). Cell viability was determined by MTT reduction (means (±SD), 3 assays, n=3 each); d) TEM images of solutions of a) (24 hours aged) as indicated (bars, 100 nm). The figure is taken from Armiento et al. (ACIE, 2020) (114).

Subsequently, to evaluate the importance of the Phe27 on the inhibitory potency of LL-37 against IAPP aggregation, the effect of LL-37(1-26) and LL-37(1-27) on IAPP self-assembly into cytotoxic species was tested. LL-37(1-26) had no inhibitory effect on both IAPP fibrillogenesis and cytotoxicity. Kinetics of IAPP

aggregation and the 1/1 mixture of LL-37(1-26) have a similar profile, and fibril formation was present for both incubations already after 24 hours (Figure 51a). MTT assay results correlate with the ThT binding assay, as the cytotoxicity was not blocked by LL-37(1-26) already at 24 hours (Figure 51b). TEM images of the solutions confirmed the presence of fibrils after 7 days of incubation time (Figure 51d).

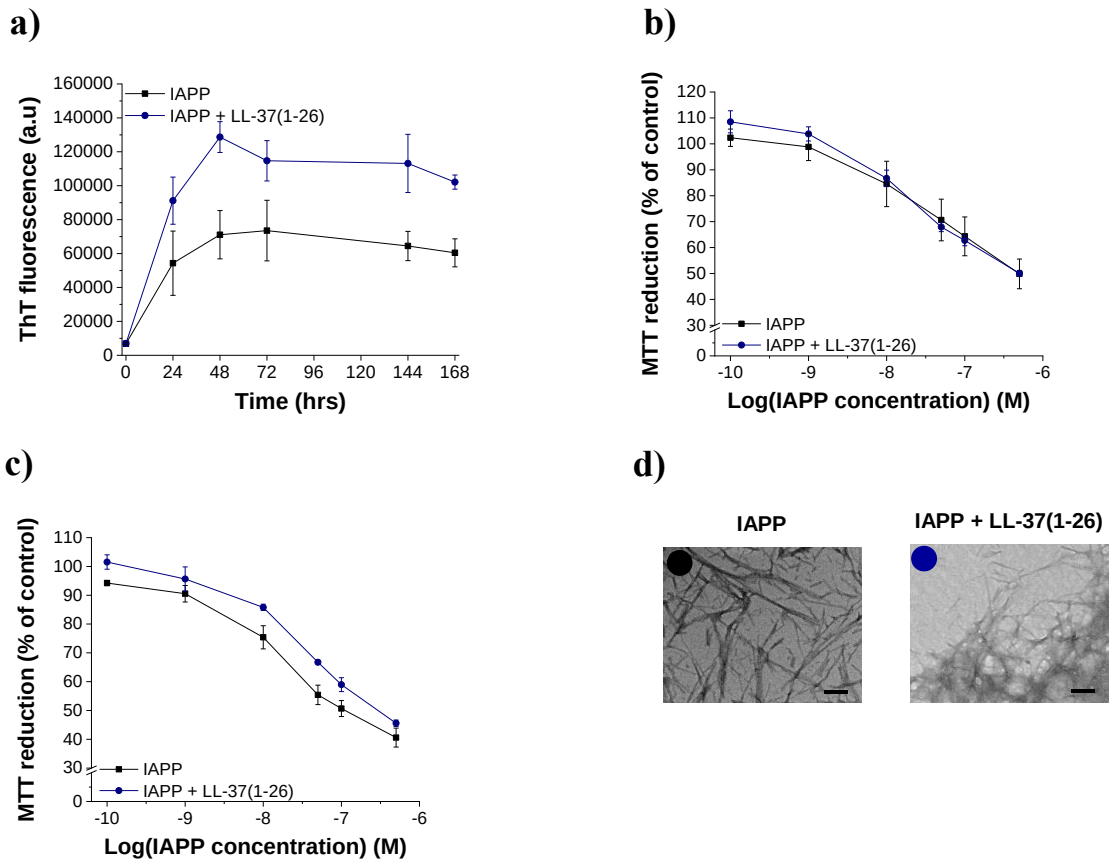

Figure 51. Effects of C-terminal truncated segment LL-37(1-26) on IAPP amyloid formation and cytotoxicity. a) Fibrillogenesis of IAPP (16.5 μM) and its mixtures with LL-37(1-26) (1/1) (means (±SD), 3 assays); b) effects on cell viability: solutions from a) were added to cultured RIN5fm cells (24 hours aged). Cell viability was determined by MTT reduction (means (±SD), 3 assays, n=3 each); c) effects on cell viability: solutions from a) were added to cultured RIN5fm cells (7 days aged). Cell viability was determined by MTT reduction (means (±SD), 3 assays, n=3 each); d) TEM images of solutions of a) (7 days aged) as indicated (bars, 100 nm).

LL-37(1-27) was tested thereafter with the aim to investigate the role of Phe27 in the inhibitory potency of this peptide. Interestingly, the Phe27 residue has no role in interfering with the aggregation of IAPP. In fact, LL-37(1-27) showed no inhibitory ability already at 24 h of both amyloidogenesis and cytotoxicity and TEM confirmed these findings as shown in Figure 52.

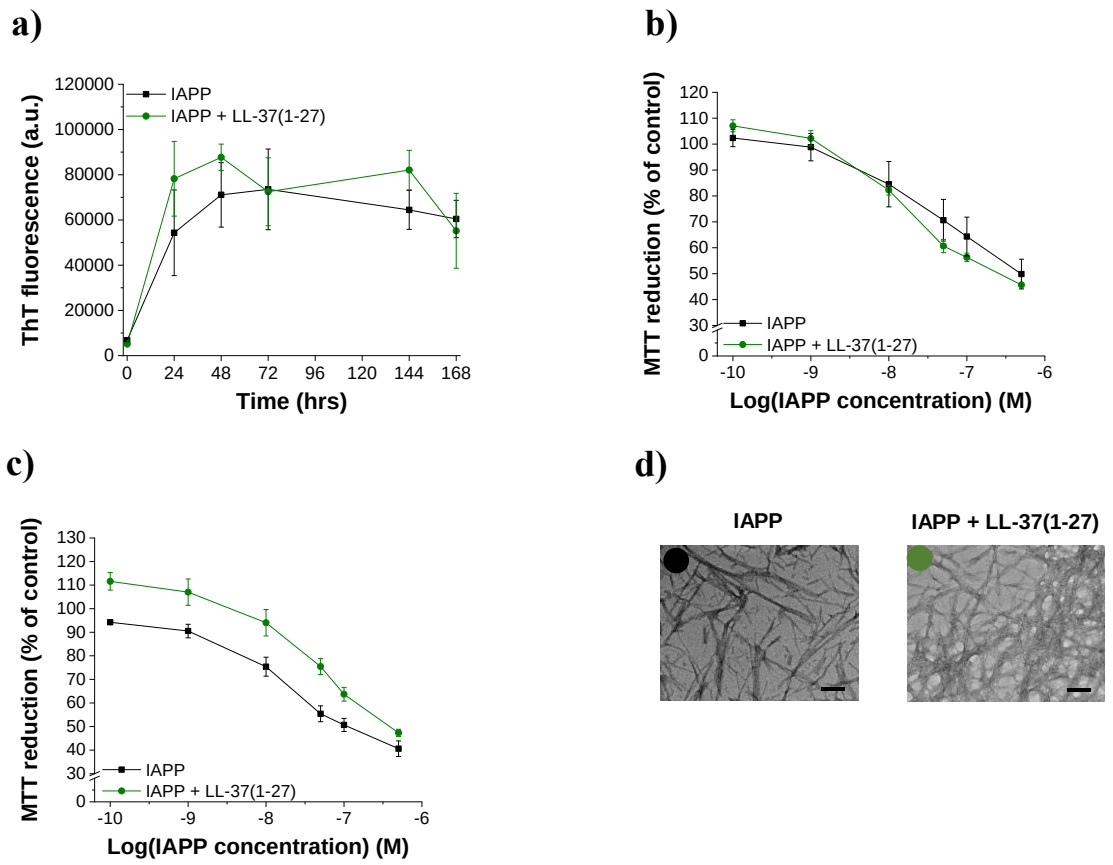

Figure 52. Effects of C-terminal truncated segment LL-37(1-27) on IAPP amyloid formation and cytotoxicity. a) Fibrillogenesis of IAPP (16.5 μM) and its mixtures with LL-37(1-27) (1/1) (means (±SD), 3 assays); b) effects on cell viability: solutions from a) were added to cultured RIN5fm cells (24 hours aged). Cell viability was determined by MTT reduction (means (±SD), 3 assays, n=3 each); c) effects on cell viability: solutions from a) were added to cultured RIN5fm cells (7 days aged). Cell viability was determined by MTT reduction (means (±SD), 3 assays, n=3 each); d) TEM images of solutions of a) (7 days aged) as indicated (bars, 100 nm).

Next, the longer segment LL-37(1-31) was tested. This peptide is known to have an α-helical structure, as found by NMR studies (132). Interestingly, LL-37(1-31) could inhibit IAPP fibril formation until 144 hours, as shown in Figure 53a. Cytotoxicity to RIN5fm cells at 24 h was also inhibited (Figure 53b). At 168 h the ThT fluorescence signal increased, and the inhibitory ability of both fibril formation and cytotoxicity was lost (Figure 53a, c). Additionally, fibrils were the main species in TEM images (Figure 53d). Results underline the importance of the α-helix and β-sheet/turn structure for the inhibitory properties of LL-37. In fact, LL-37(1-31) exhibited a partial α-helix/β-sheet/turn structure in the CD studies and had a higher inhibitory potency compared to the shorter and unstructured segments.

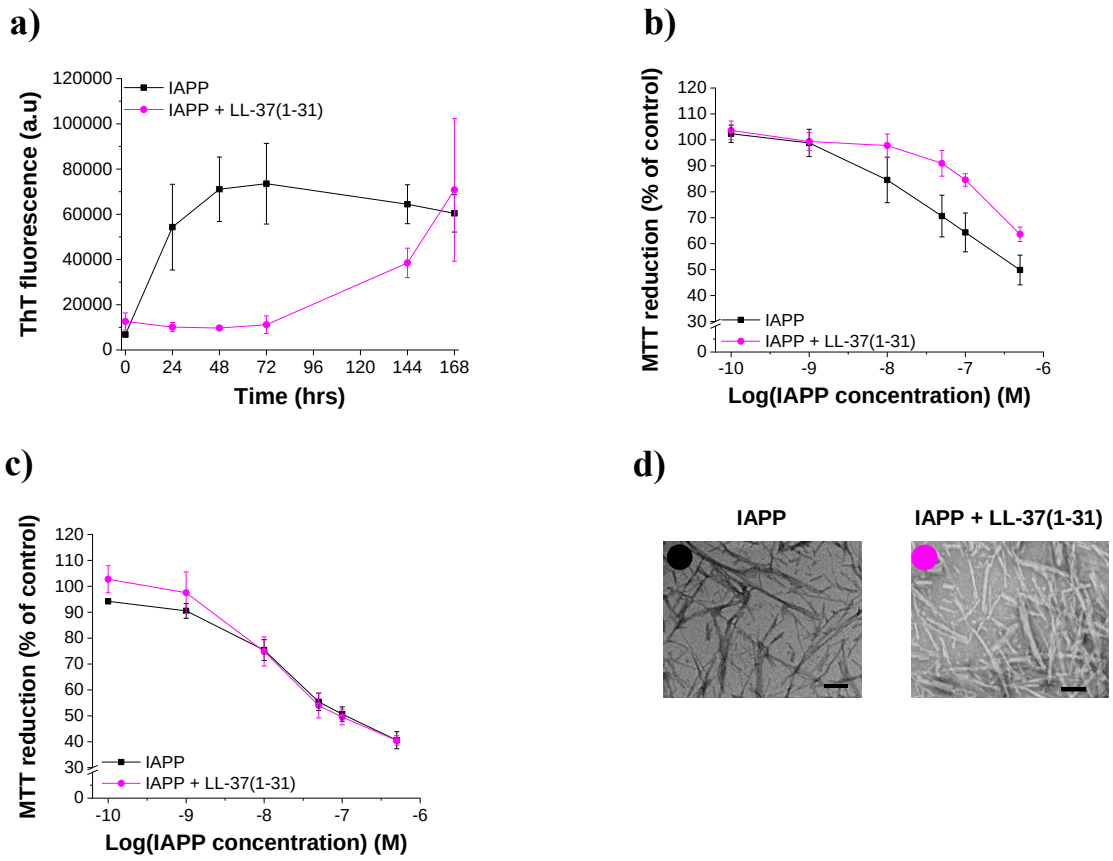

Figure 53. Effects of C-terminal truncated segment LL-37(1-31) on IAPP amyloid formation and cytotoxicity. a) Fibrillogenesis of IAPP (16.5 μM) and its mixtures with LL-37(1-31) (1/1) (means (±SD), 3 assays); b) effects on cell viability: solutions from a) were added to cultured RIN5fm cells (24 hours aged). Cell viability was determined by MTT reduction (means (±SD), 3 assays, n=3 each); c) effects on cell viability: solutions from a) were added to cultured RIN5fm cells (7 days aged). Cell viability was determined by MTT reduction (means (±SD), 3 assays, n=3 each); d) TEM images of solutions of a) (7 days aged) as indicated (bars, 100 nm).

Among the C-terminal shortened sequences, LL-37(1-34) was the only one that showed a potent inhibitory effect on IAPP fibrillogenesis as the native peptide LL-37. In fact, LL-37(1-34) efficiently suppressed IAPP fibril formation until 168 hours, as shown by the ThT binding assay results (Figure 54a). Consequently, also the IAPP cell-damaging effect was blocked. The percentage of the cell viability was significantly higher for the IAPP/LL-37(1-34) mixture compared to IAPP alone, both after 24 or 168 hours of co-incubation time (Figure 54b, c). TEM images support the obtained results: the mixture with LL-37(1-34) presented mainly amorphous aggregates compared to the IAPP incubation, which showed mainly fibrils (Figure 54d). The results indicated the importance of the α-helix/β-sheet/turn structure for the inhibitory properties of LL-37, as the only shortened C-terminal sequence that can inhibit IAPP cell-damaging aggregates is LL-37(1-34). Additionally, the inhibitory potency of LL-37(1-34) was quantified via titrations of cytotoxic IAPP with increasing amounts of the inhibitor to determine the half-maximal inhibitory concentration (IC_{50}). Experiments lead to an IC_{50} of 24 (± 5.9) nM, suggesting that LL-37(1-34) is a nanomolar inhibitor of IAPP self-assembly like the native LL-37 (Figure 55).

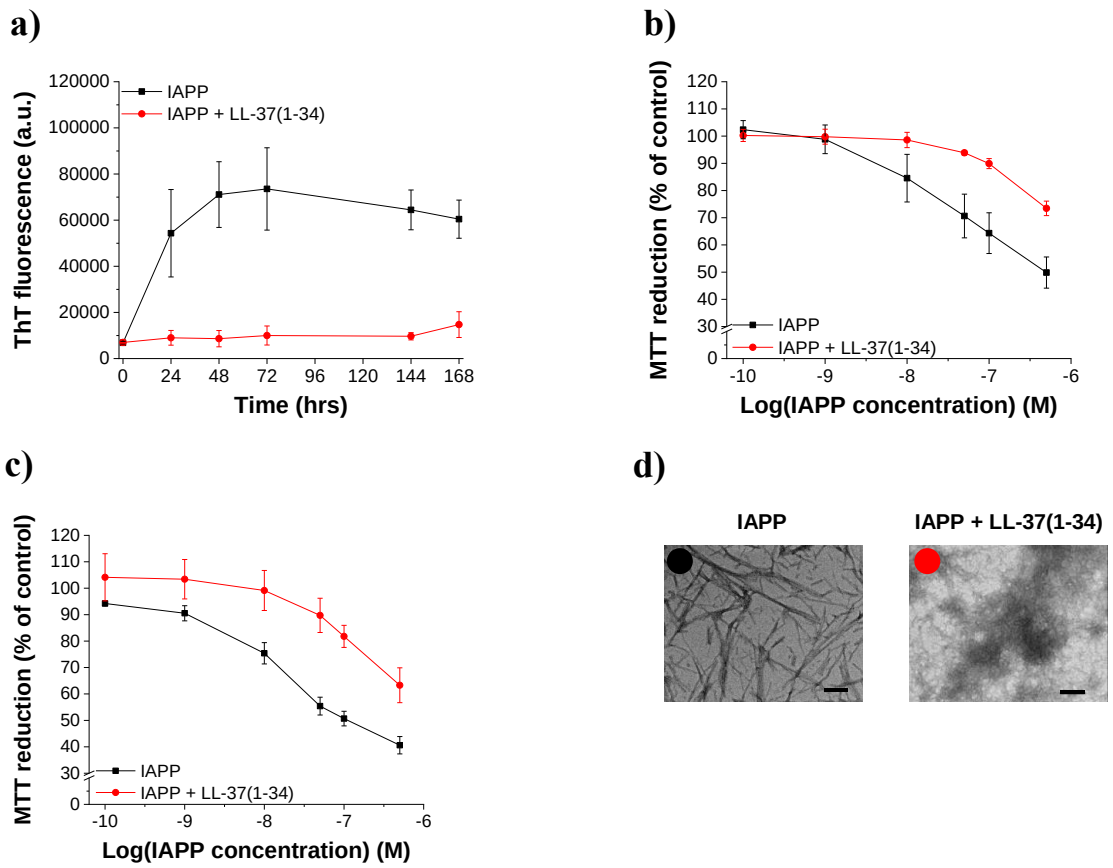

Figure 54. Effects of C-terminal truncated segment LL-37(1-34) on IAPP amyloid formation and cytotoxicity. a) Fibrillogenesis of IAPP (16.5 µM) and its mixtures with LL-37(1-34) (1/1) (means (±SD), 3 assays); b) effects on cell viability: solutions from a) were added to cultured RIN5fm cells (24 hours aged). Cell viability was determined by MTT reduction (means (±SD), 3 assays, n=3 each); c) effects on cell viability: solutions from a) were added to cultured RIN5fm cells (7 days aged). Cell viability was determined by MTT reduction (means (±SD), 3 assays, n=3 each); d) TEM images of solutions of a) (7 days aged) as indicated (bars, 100 nm).

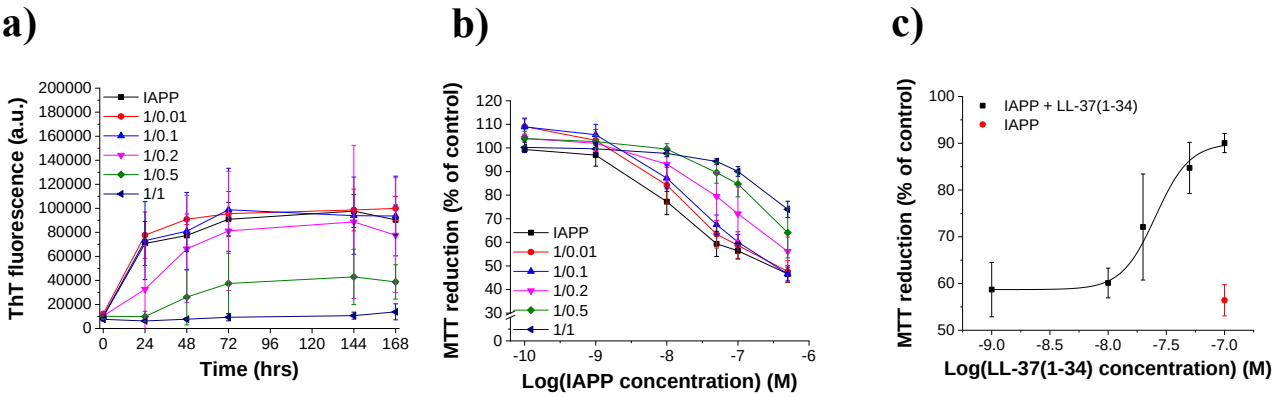

Figure 55. Effects of LL-37(1-34) on IAPP amyloid formation and cell viability. a) Dose-dependence of the inhibitory effect of LL-37(1-34) on IAPP fibrillogenesis. Fibrillogenesis of IAPP alone (16.5 µM) or with different molar ratios of LL-37(1-34) as indicated above determined by the ThT binding assay (means (±SD), 3 assays, n=3 each); b) effects on cell viability: solutions from a) were added to cultured RIN5fm cells (24 hours aged). Cell viability was determined by MTT reduction (means (±SD), 3 assays, n=3 each). d) IC_{50} of the inhibitory effect of LL-37(1-34) on cytotoxic effects of IAPP determined by titration of IAPP (100 nM) with LL-37(1-34) (means (±SD), 3 assays, n=3 each).

Similarly, the N-terminal truncated LL-37 segments were tested to evaluate their ability to inhibit the aggregation of IAPP into cytotoxic species. The shortest tested segment LL-37(15-37) exhibited no inhibitory

properties after 24 hours and could not inhibit the cytotoxicity to RIN5fm cells as well (Figure 56a, b, and c), as shown in section 4.1.11. TEM images confirmed the results. In fact, fibrils are the major species in the 1/1 mixture of the two peptides and the morphology of the fibrils is similar to the fibrils of IAPP alone (Figure 56d).

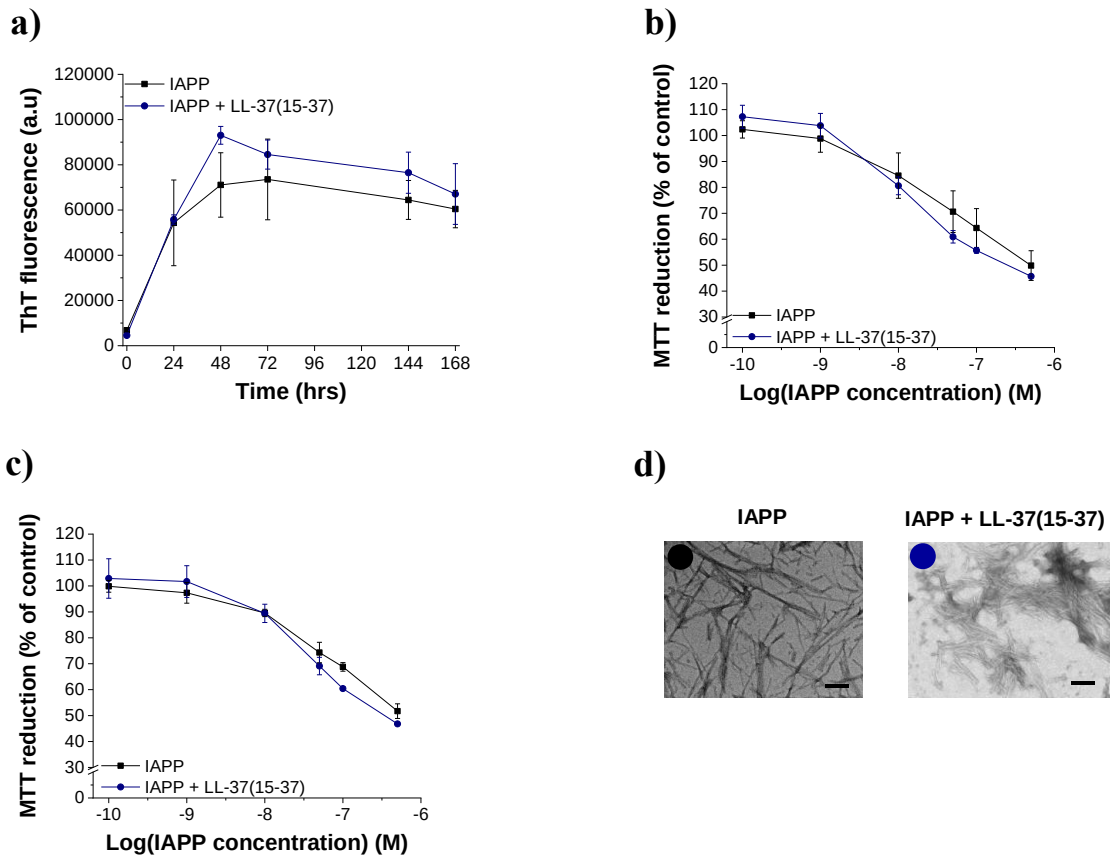

Figure 56. Effects of N-terminal truncated segment LL-37(15-37) on IAPP amyloid formation and cytotoxicity. a) Fibrillogenesis of IAPP (16.5 μM) and its mixtures with LL-37(15-37) (1/1) (means (±SD), 3 assays); b) effects on cell viability: solutions from a) were added to cultured RIN5fm cells (24 hours aged). Cell viability was determined by MTT reduction (means (±SD), 3 assays, n=3 each); c) effects on cell viability: solutions from a) were added to cultured RIN5fm cells (7 days aged). Cell viability was determined by MTT reduction (means (±SD), 3 assays, n=3 each); d) TEM images of solutions of a) (24 hours aged) as indicated (bars, 100 nm). The figure is taken from Armiento et al. (ACIE, 2020) (114).

LL-37(7-37) showed an analog behavior. This peptide could partially inhibit IAPP amyloidogenesis at 24 hours, as the ThT signal of the mixture was significantly lower than the ThT signal of IAPP alone. After 24 hours the inhibitory potency for the fibril formation was completely lost, as shown in Figure 57a. The MTT reduction assay showed that LL-37(7-37) could not block the cytotoxicity of IAPP already at 24 hours, and also at 7 days (Figure 57b, c). TEM images confirmed the findings. Fibrils are the most present species in the 1/1 mixture of IAPP and LL-37(7-37) (Figure 57d).

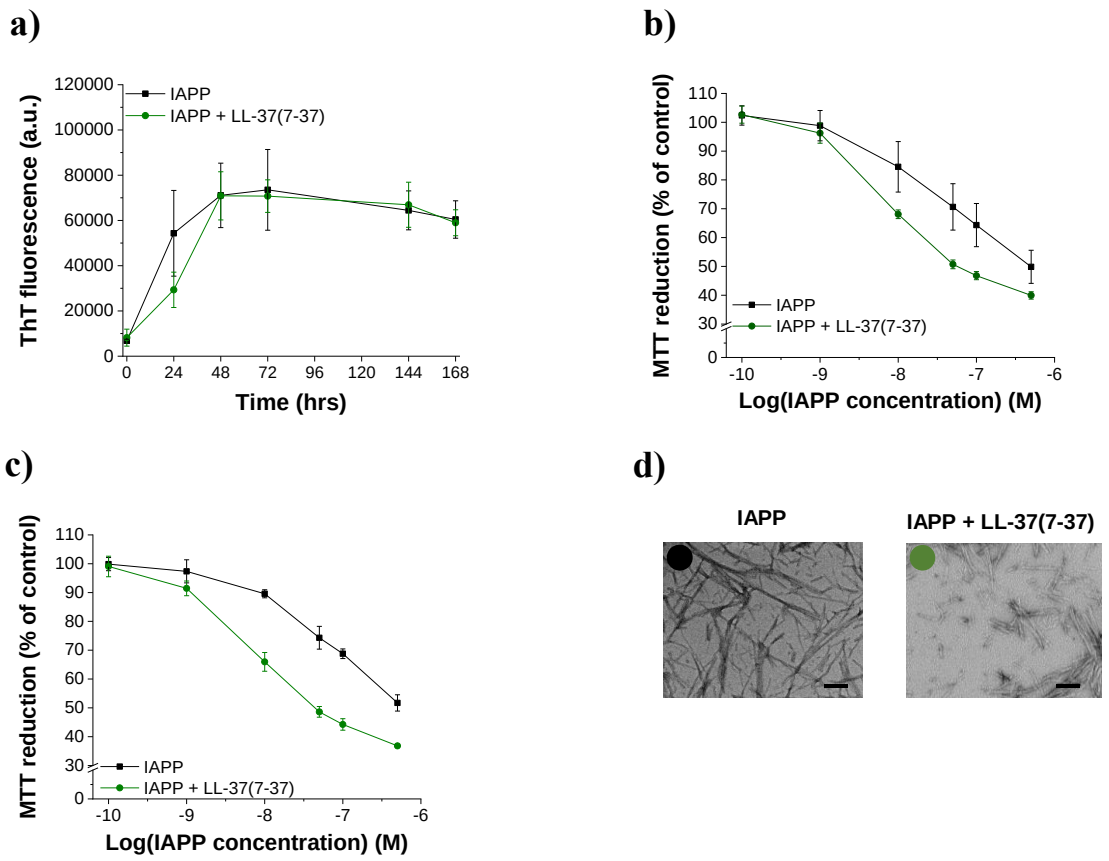

Figure 57. Effects of N-terminal truncated segment LL-37(7-37) on IAPP amyloid formation and cytotoxicity. a) Fibrillogenesis of IAPP (16.5 μM) and its mixtures with LL-37(7-37) (1/1) (means (±SD), 3 assays); b) effects on cell viability: solutions from a) were added to cultured RIN5fm cells (24 hours aged). Cell viability was determined by MTT reduction (means (±SD), 3 assays, n=3 each); c) effects on cell viability: solutions from a) were added to cultured RIN5fm cells (7 days aged). Cell viability was determined by MTT reduction (means (±SD), 3 assays, n=3 each); d) TEM images of solutions of a) (7 days aged) as indicated (bars, 100 nm).

The longer segment LL-37(5-37) exhibited significantly different inhibitory potency than LL-37(7-37). In fact, this peptide could interfere with the aggregation of IAPP until 72 h incubation time. The inhibitory potency is weaker at 144 h, as shown by the partial increase of the ThT fluorescence signal and by the TEM images in which fibrils were found (Figure 58a, d). Additionally, LL-37(5-37) could block IAPP toxicity at 24 hours and also at 7 days, despite the presence of fibrils found by TEM (Figure 58b, c). The results suggest that phenylalanine residues 5 and 6 play a key role in the inhibitory capacity of these peptides. In fact, as soon as they are neglected from the sequence, no inhibition of IAPP fibrillogenesis could be observed.

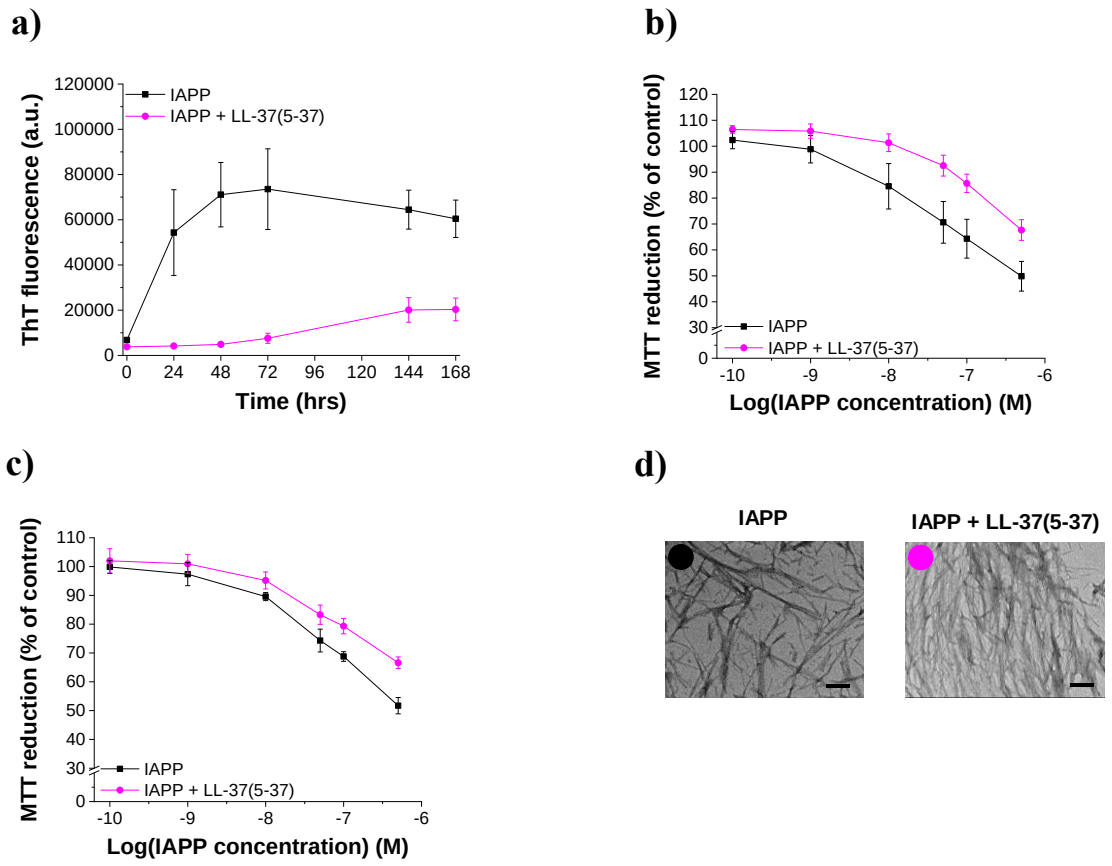

Figure 58. Effects of N-terminal truncated segment LL-37(5-37) on IAPP amyloid formation and cytotoxicity. a) Fibrillogenesis of IAPP (16.5 µM) and its mixtures with LL-37(5-37) (1/1) (means (±SD), 3 assays); b) effects on cell viability: solutions from a) were added to cultured RIN5fm cells (24 hours aged). Cell viability was determined by MTT reduction (means (±SD), 3 assays, n=3 each); c) effects on cell viability: solutions from a) were added to cultured RIN5fm cells (7 days aged). Cell viability was determined by MTT reduction (means (±SD), 3 assays, n=3 each); d) TEM images of solutions of a) (7 days aged) as indicated (bars, 100 nm).

LL-37(3-37) exhibited complete inhibition of IAPP amyloidosis. This peptide is missing only two Leu residues in positions 1 and 2 of the LL-37 sequence and showed inhibitory potency similar to LL-37. ThT binding assay results show that IAPP fibril formation was blocked until 168 hours (Figure 59a). Consequently, the cytotoxic effect of IAPP was efficiently suppressed after 24 hours and 7 days of incubation time (Figure 59b, c). TEM images confirmed the presence of amorphous aggregates as the main species at 168 hours (Figure 59d). Moreover, as LL-37(3-37) is the only N-terminal shortened sequence that can efficiently inhibit IAPP fibril formation and cytotoxicity, the half-maximal inhibitory concentration (IC_{50}) was determined to quantify the inhibitory potency. Titrations of cytotoxic IAPP with peptide were carried out leading to an IC_{50} of 19 (± 0.9) nM, confirming that LL-37(3-37), as the native LL-37, is a nanomolar inhibitor of IAPP self-association in cell-damaging species (Figure 60).

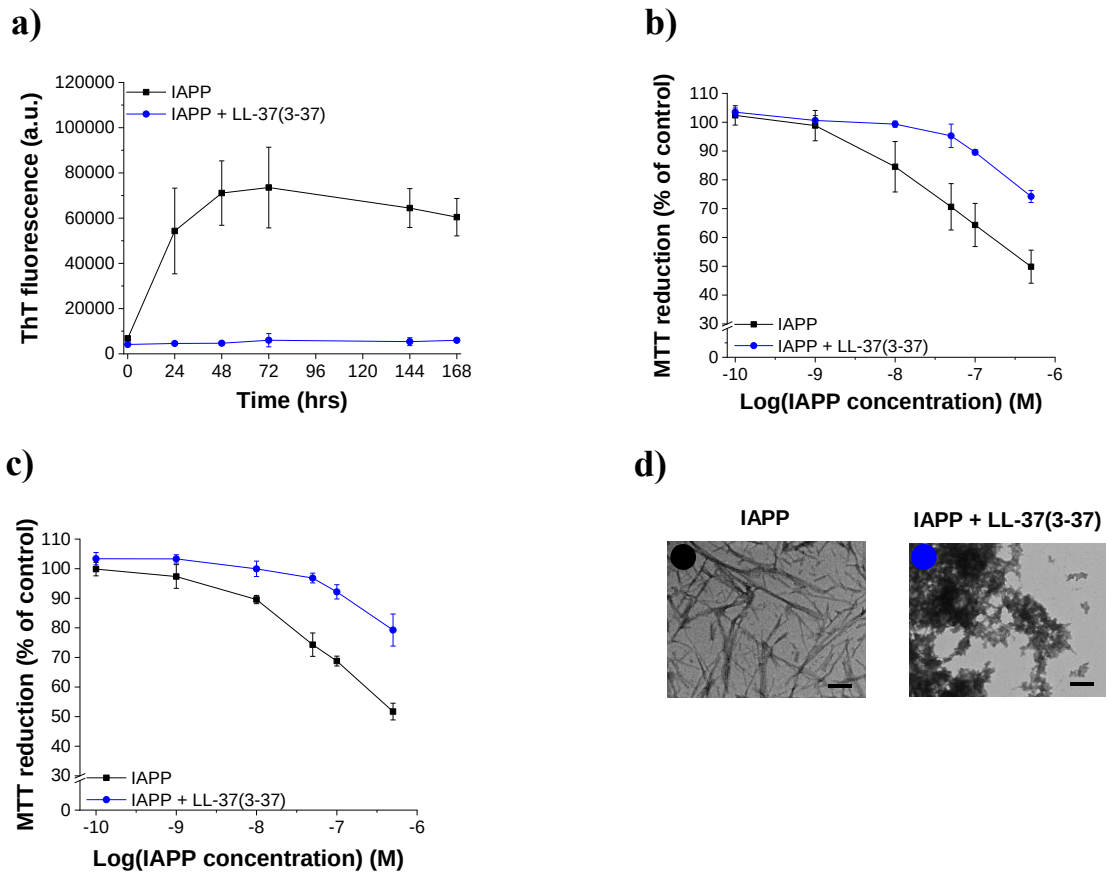

Figure 59. Effects of N-terminal truncated segment LL-37(3-37) on IAPP amyloid formation and cytotoxicity. a) Fibrillogenesis of IAPP (16.5 µM) and its mixtures with LL-37(3-37) (1/1) (means (±SD), 3 assays); b) effects on cell viability: solutions from a) were added to cultured RIN5fm cells (24 hours aged). Cell viability was determined by MTT reduction (means (±SD), 3 assays, n=3 each); c) effects on cell viability: solutions from a) were added to cultured RIN5fm cells (7 days aged). Cell viability was determined by MTT reduction (means (±SD), 3 assays, n=3 each); d) TEM images of solutions of a) (7 days aged) as indicated (bars, 100 nm).

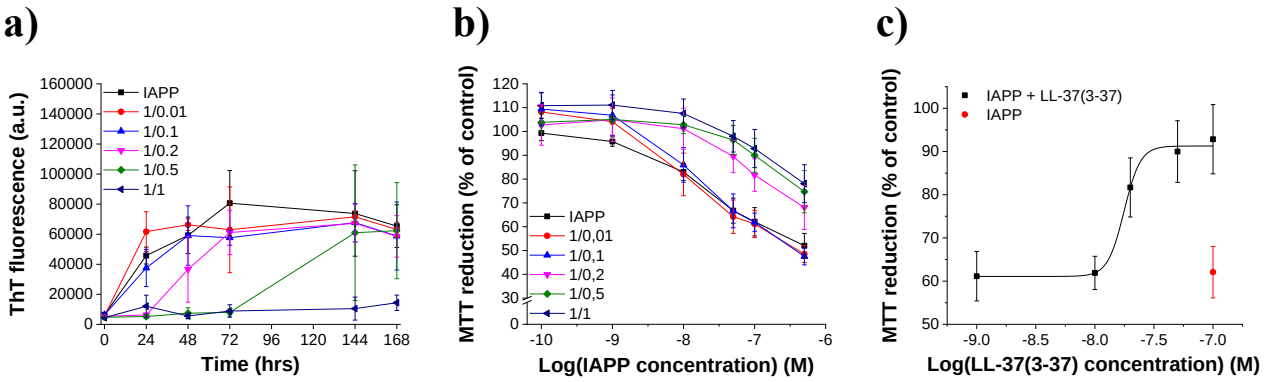

Figure 60. Effects of LL-37(3-37) on IAPP amyloid formation and cell viability. a) Dose-dependence of the inhibitory effect of LL-37(3-37) on IAPP fibrillogenesis. Fibrillogenesis of IAPP alone (16.5 µM) or with different molar ratios of LL-37(3-37) as indicated above determined by the ThT binding assay (means (±SD), 3 assays, n=3 each); b) effects on cell viability: solutions from a) were added to cultured RIN5fm cells (24 hours aged). Cell viability was determined by MTT reduction (means (±SD), 3 assays, n=3 each). d) IC_{50} of the inhibitory effect of LL-37(3-37) on cytotoxic effects of IAPP determined by titration of IAPP (100 nM) with LL-37(3-37) (means (±SD), 3 assays, n=3 each).

The LL-37 segments, which showed no inhibitory effect at a 1/1 ratio were also tested in mixture in a 1/10 ratio with IAPP to study their effect when they are in large excess. For testing the N-terminal truncated peptides, IAPP (16.5 µM) was incubated alone and in mixture with a 10-fold excess of LL-37(5-37), LL-37(7-

37) or LL-37(15-37) (165 μM) each, and the aggregation kinetics was monitored using the ThT binding assay. Regarding LL-37(15-37), no improvement of the inhibitory potency was observed. In fact, the mixture exhibited ThT fluorescence at 24 hours in a similar manner to the 1/1 mixture. In 1/10, LL-37(7-37) could extend the lag phase of IAPP aggregation from 24 to 72 hours but still, this segment could not inhibit IAPP fibril formation until 7 days. Finally, LL-37(5-37) showed a complete inhibition as the native sequence, when mixed in 10-fold excess with IAPP. Results show that the inhibitory potency of LL-37(5-37) is 10-fold weaker compared to LL-37, while the shorter segments LL-37(7-37) and LL-37(15-37) had no strong effect on IAPP fibrillogenesis even at 165 μM (Figure 61a).

In a similar manner, the segments shortened on their C-terminus were tested. LL-37(1-26) had no effect on IAPP aggregation, also in a 10-fold excess to IAPP. In 1/10, LL-37(1-27) extended the lag phase of IAPP self-association for 48 hours, but no effect was observed at later time points. LL-37(1-31) showed a complete inhibition as the native sequence when mixed in 10-fold excess with IAPP. Results show that the inhibitory potency of LL-37(1-31) is 10-fold weaker compared to LL-37, while the shorter segments LL-37(1-27) and LL-37(1-26) have no strong effect on IAPP fibrillogenesis even at 165 μM, so their inhibitory potency is more than 10-times weaker than LL-37 (Figure 61b).

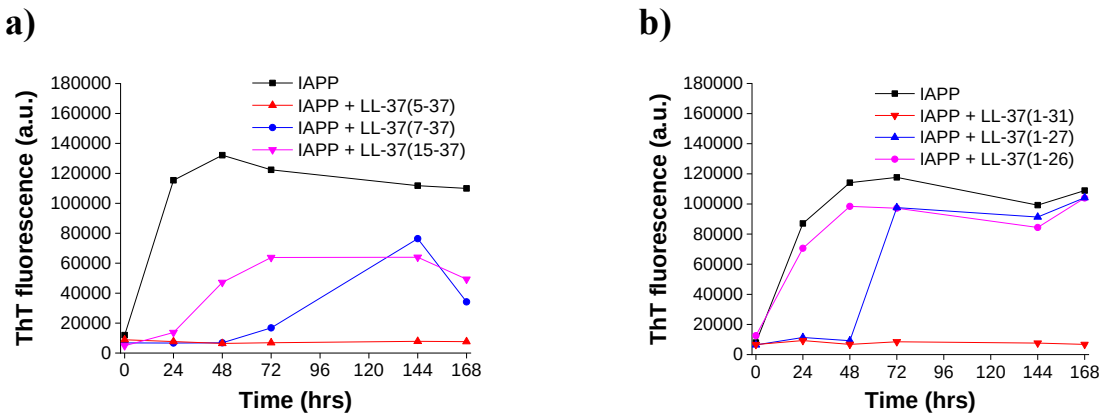

Figure 61. Effects of LL-37 N-terminal truncated segments in 10-fold excess on IAPP amyloid formation. a) Fibrillogenesis of IAPP (16.5 μM) and its mixtures with LL-37(5-37) (1/10), LL-37(7-37) (1/10) or LL-37(15-37) (1/10) (representative experiment is reported (n=2)). b) Fibrillogenesis of IAPP (16.5 μM) and its mixtures with LL-37(1-31) (1/10), LL-37(1-27) (1/10) or LL-37(1-26) (1/10) (representative experiment is reported (n=2)).

The two shortest inhibitors of IAPP fibril formation indentified were LL-37(3-37) and LL-37(1-34), which were truncated at the N-terminus and the C-terminus respectively. Furthermore, LL-37(3-34) was tested, to state which was the core region of LL-37 required for the inhibition of IAPP self-association into cytotoxic species. In fact, this peptide is missing the first two residues at the N-terminus and the last three residues of the C-terminus at the same time. IAPP (16.5 μM) and its 1/1 mixture with LL-37(3-34) were incubated for 168 hours, and ThT binding assay and MTT reduction assay in combination with TEM were used to evaluate the inhibitory properties. The peptide is a partial inhibitor of IAPP fibrillogenesis. In fact, the ThT dye signal indicates that the fibril formation is blocked for 72 hours, and not anymore further in time points (Figure 62a). Correlating with these results, the MTT reduction assay shows that the cytotoxicity of IAPP could be blocked only at 24 hours, but not at 7 days (Figure 62b, c). TEM images of 7 days aged samples confirm that fibrils are the main species present in the 1/1 mixture of the two peptides (Figure 62d). Results suggest that the simultaneous lack of C- and N-terminus of the LL-37 sequence affects the secondary structure, which appeared to be only α-helix, without any β-sheet/turn content, and the inhibitory properties which were not comparable to the native sequence.

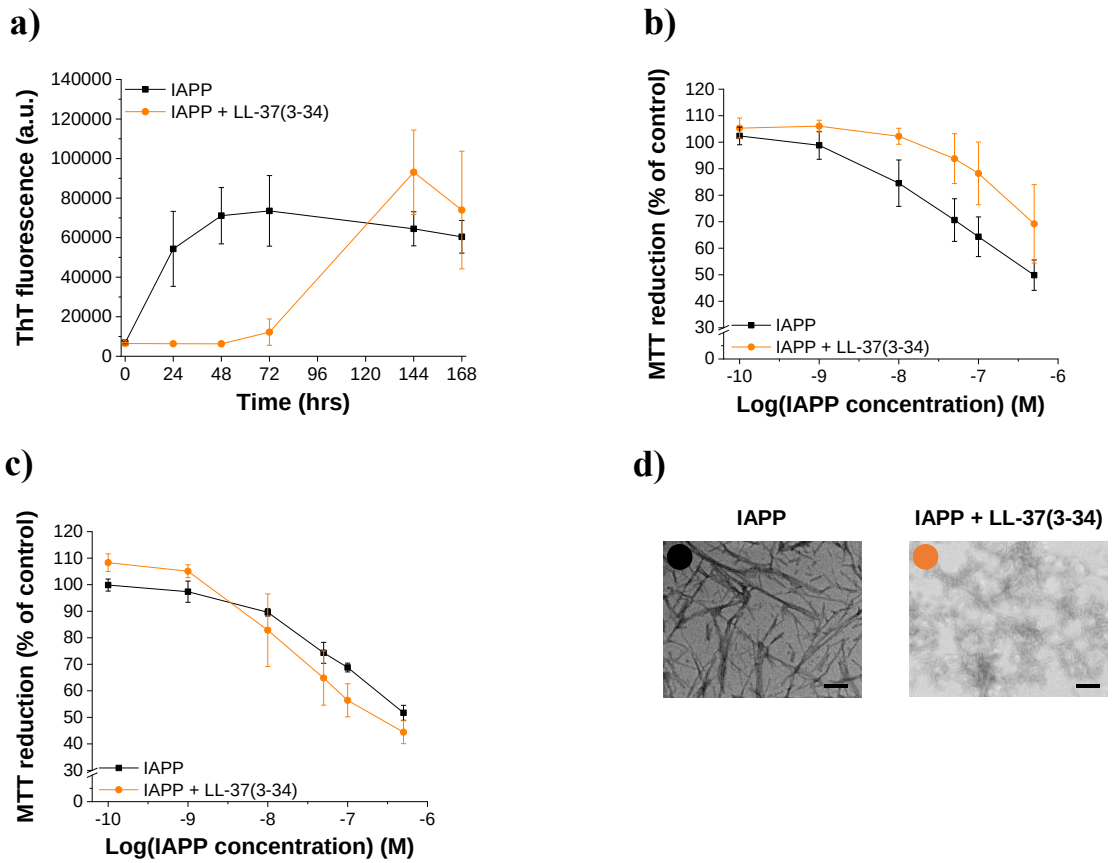

Figure 62. Effects of C- and N-terminal truncated segment LL-37(3-34) on IAPP amyloid formation and cytotoxicity. a) Fibrillogenesis of IAPP (16.5 µM) and its mixtures with LL-37(3-34) (1/1) (means (±SD), 3 assays); b) effects on cell viability: solutions from a) were added to cultured RIN5fm cells (24 hours aged). Cell viability was determined by MTT reduction (means (±SD), 3 assays, n=3 each); c) effects on cell viability: solutions from a) were added to cultured RIN5fm cells (7 days aged). Cell viability was determined by MTT reduction (means (±SD), 3 assays, n=3 each); d) TEM images of solutions of a) (7 days aged) as indicated (bars, 100 nm).

In this section, the inhibitory potency of the LL-37 truncated sequences was studied. Among the C-terminal truncated sequences LL-37(1-14), LL-37(1-26), and LL-37(1-27) did not inhibit IAPP fibril formation, also in 10-fold excess to IAPP. LL-37(1-31) partially inhibited the fibrillogenesis in an equimolar ratio and fully suppressed the aggregation of IAPP in the 1/10 (IAPP/inhibitor) mixture. LL-37(1-34) exhibited similar properties to the native sequence. In fact, it is a nanomolar inhibitor of IAPP fibril formation. Among the N-terminal truncated sequences, LL-37(15-37) and LL-37(7-37) could not interfere with the aggregation of IAPP also when they were present in 10-fold excess. LL-37(5-37), which only partially had an inhibitory effect in 1/1, fully suppressed the aggregation of IAPP in 1/10. Finally, LL-37(3-37) had similar properties to the native sequence, and a comparable IC_{50} could be determined for this peptide. As LL-37(1-34) and LL-37(3-37) were found to be the shortest segments with similar inhibitory potency of LL-37, LL-37(3-34) was tested. This peptide could only partially block the aggregation of IAPP, suggesting that the lack of both termini negatively affects the inhibitory ability (Table 21).

Table 21. Overview of the inhibitory properties of LL-37 and LL-37 truncated segments.

Peptide	**Inhibition of IAPP fibrillogenesis in 1/1**	**IC_{50} at 100 nM**	**Inhibition of IAPP fibrillogenesis in 1/10**
LL-37	✓	17 ± 1.7 nM	-
LL-37(1-14)	✗	-	-
LL-37(1-26)	✗	-	✗
LL-37(1-27)	✗	-	✗
LL-37(1-31)	partially ✓	-	✓
LL-37(1-34)	✓	24 ± 5.9 nM	-
LL-37(15-37)	✗	-	✗
LL-37(7-37)	✗	-	✗
LL-37(5-37)	partially ✓	-	✓
LL-37(3-37)	✓	19 ± 0.9 nM	-
LL-37(3-34)	partially ✓	-	-

Legend: ✓= the peptide is an inhibitor of IAPP amyloid formation; ✗= the peptide cannot block IAPP amyloid formation; - = not determined.

4.2.4 Determination of binding affinities towards IAPP

To characterize the IAPP/LL-37 interaction, fluorescence spectroscopic titrations were carried out. N-terminal fluorescein-labeled IAPP (Fluos-IAPP, 5 nM) was titrated in aqueous 10 mM sodium phosphate buffer (pH 7.4) containing 1% HFIP with different amounts of LL-37 analogs to evaluate the app. K_d value of their binding affinities. The N-terminal segment, LL-37(1-14), weakly bound to Fluos-IAPP, exhibiting an app. K_d of 2.54 (± 0.5) µM, as already shown in section 4.1.11. By contrast, N-terminal segments that comprise the central region of LL-37 bind Fluos-IAPP with nanomolar affinities, such as LL-37(1-26), LL-37(1-27), LL-37(1-31), and LL-37(1-34) (app. K_ds of 227.7 (± 2.1) nM, 24.2 (± 4.2), 18.4 (± 6.8) nM, and 132.4 (± 3.2) nM respectively). Results are summarized in Table 22.

Table 22. Identification of LL-37 C-terminal truncated segments that bind monomeric IAPP and determination of apparent binding affinities ($K_{d,app}$) by fluorescence titration assays.

LL-37 segments	**$K_{d,app}$ (±SD) (for Fluos-IAPP)[a]**
LL-37(1-14)	2.54 (± 0.5) µM
LL-37(1-26)	227.7 (± 2.1) nM
LL-37(1-27)	24.2 (± 4.2) nM
LL-37(1-31)	18.4 (± 6.8) nM
LL-37(1-34)	132.4 (± 3.2) nM

[a] App. K_ds, means (±SD) from 3 binding curves. Determined via titrations of fluorescein-labeled IAPP (Fluos-IAPP, 5nM) with non-labeled LL-37 segments (aq. buffer 1×b, pH 7.4, containing 1% HFIP).

Experiments show that the region between residues 14 and 26 is crucial for the interaction with monomeric IAPP, resulting in a 10-fold increase of the app. K_d value (Figure 63 and Figure 64).

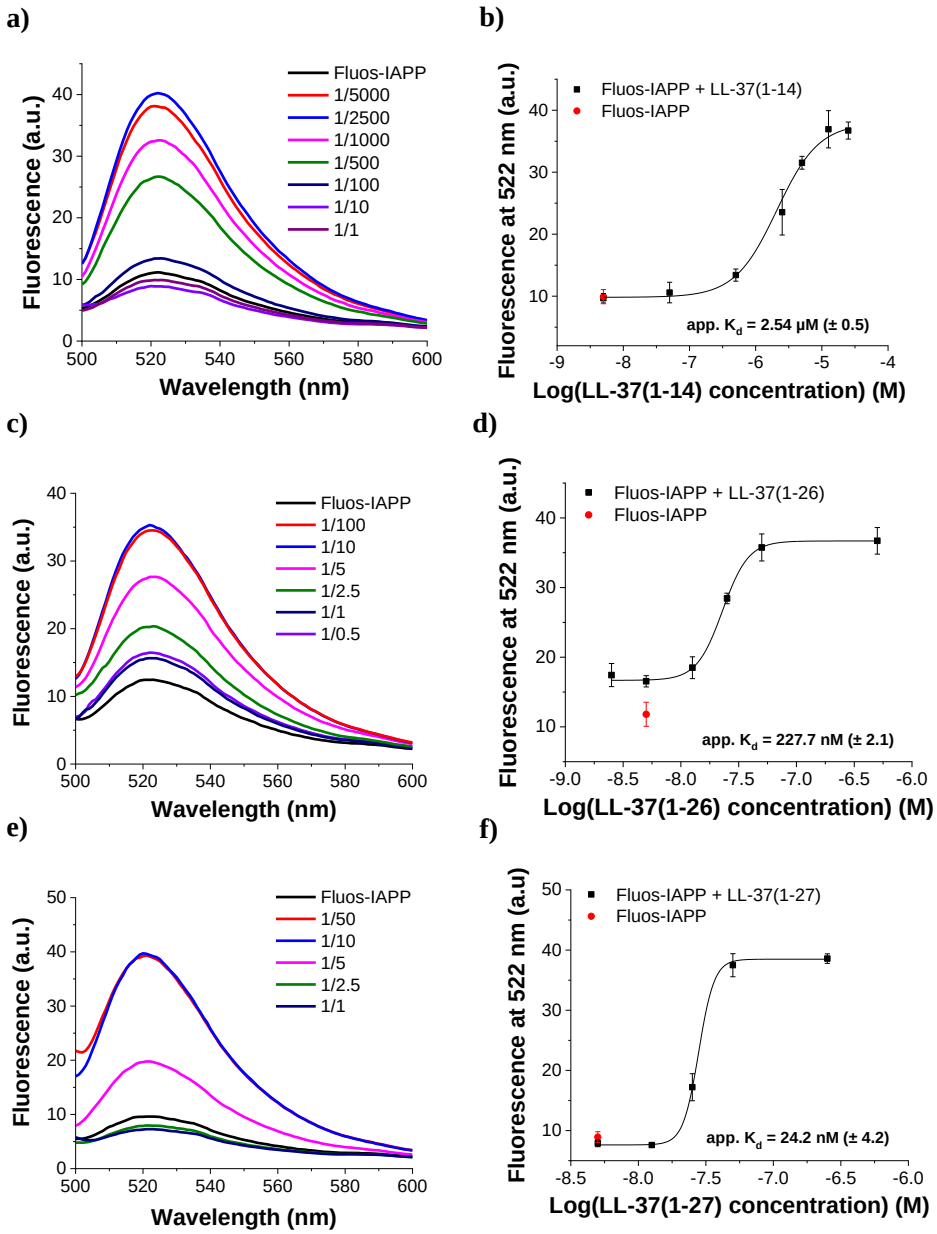

Figure 63. Determination of app. K_ds of interactions of LL-37 C-terminal truncated segments with monomeric IAPP by fluorescence spectroscopy. Panels a), c), e) show fluorescence spectra of Fluos-IAPP (5nM) alone and their mixtures with various amounts of LL-37(1-14) (a), LL-37(1-26) (c), and LL-37(1-27) (e); the molar ratios of Fluos-IAPP/LL-37 segments are as indicated. Panels b), d), f), show the binding curves of LL-37(1-14) (a), LL-37(1-26) (c), and LL-37(1-27) (e) with Fluos-IAPP; app. K_ds are means (±SD) from 3 binding curves. Measurements were performed in aqueous buffer 1×b, pH 7.4, containing 1% HFIP. Figures a) and b) are taken from Armiento et al. (ACIE, 2020) (114).

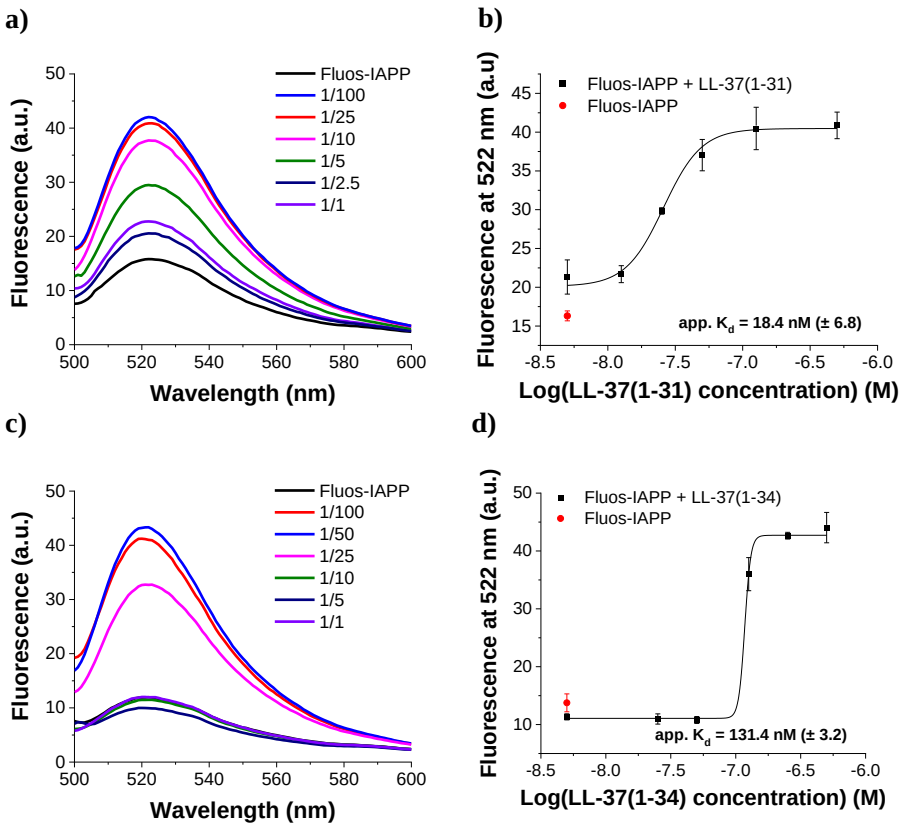

Figure 64. Determination of app. K_ds of interactions of LL-37 C-terminal truncated segments with monomeric IAPP by fluorescence spectroscopy. Panels a), c) show fluorescence spectra of Fluos-IAPP (5nM) alone and their mixtures with various amounts of LL-37(1-31) (a), and LL-37(1-34) (c); the molar ratios of Fluos-IAPP/LL-37 segments are as indicated. Panels b), d) show the binding curves of LL-37(1-31) (a), and LL-37(1-34) (c) with Fluos-IAPP; app. K_ds are means (±SD) from 3 binding curves. Measurements were performed in aqueous buffer 1×b, pH 7.4, containing 1% HFIP.

By contrast, all central/C-terminal LL-37 segments mediate the interaction with IAPP by binding to IAPP monomers in the nanomolar range. As summarized in Table 23, LL-37(3-37) exhibits an app. K_d of 101.9 (± 56.0) nM, LL-37(5-37) exhibits an app. K_d of 51.3 (± 15.0) nM, LL-37(7-37) exhibits an app. K_d of 62.7 (± 17.8) nM and, LL-37(15-37) an app. K_d of 31.9 (± 2.2) nM.

Table 23. Identification of LL-37 N-terminal truncated segments that bind monomeric IAPP and determination of apparent binding affinities ($K_{d,app}$) by fluorescence titration assays.

LL-37 segments	**$K_{d,app}$ (±SD) (for Fluos-IAPP)[a]**
LL-37(3-37)	101.9 (± 56.0) nM
LL-37(5-37)	51.3 (± 15.0) nM
LL-37(7-37)	62.7 (± 17.8) nM
LL-37(15-37)	31.9 (± 2.2) nM

[a] App. K_ds, means (±SD) from 3 binding curves. Determined via titrations of fluorescein-labeled IAPP (Fluos-IAPP, 5nM) with non-labeled LL-37 segments (aq. buffer 1×b, pH 7.4, containing 1% HFIP).

These peptides show a strong binding affinity to Fluos-IAPP, comparable to the native peptide LL-37, and suggest that Phe5 and Phe6 do not contribute to the IAPP/LL-37 interaction (Figure 65).

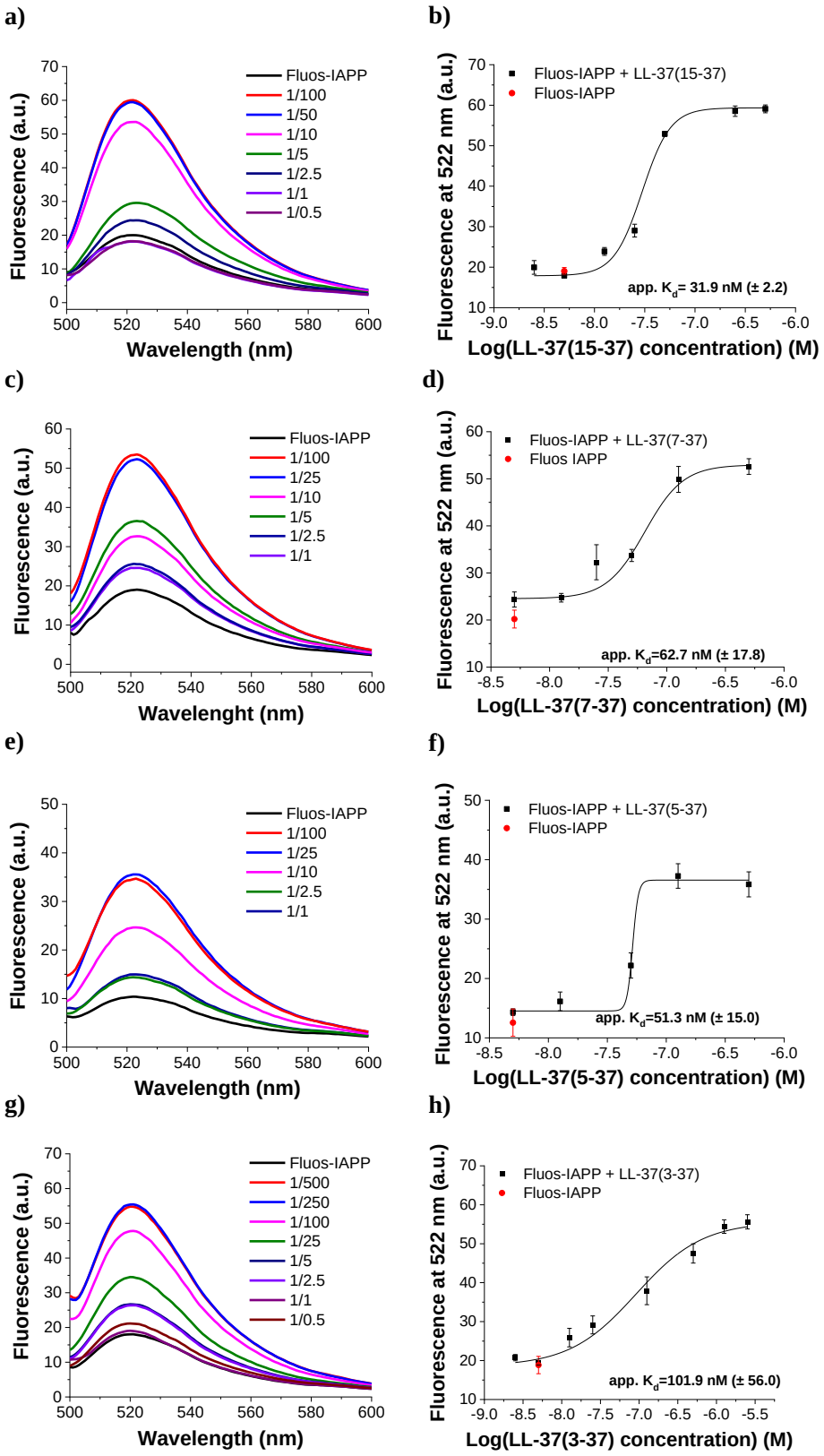

Figure 65. Determination of app. K_ds of interactions of LL-37 N-terminal truncated segments with monomeric IAPP by fluorescence spectroscopy. Panels a), c), e), g) show fluorescence spectra of Fluos-IAPP (5nM) alone and their mixtures with various amounts of LL-37(15-37) (a), LL-37(7-37) (c), LL-37(5-37) (e) and LL-37(3-37) (g); the molar ratios of Fluos-IAPP/LL-37 segments are as indicated. Panels b), d), f), h) show the binding curves of LL-37(15-37) (b), LL-37(7-37) (d), LL-37(5-37) (f), and LL-37(3-37) (h) with Fluos-IAPP; app. K_ds are means (±SD) from 3 binding curves. Measurements were performed in aqueous buffer 1×b, pH 7.4, containing 1% HFIP. Figures a) and b) are taken from Armiento et al. (ACIE, 2020) (114).

Finally, the binding affinity of the C- and N-terminal shortened peptide, LL-37(3-34), to Fluos-IAPP was tested. As expected, the binding affinity is in the nanomolar range, with an app. K_d of 34.7 (± 7.1) nM (Figure 66), confirming that the central/C-terminal region majorly contributes to the interaction with IAPP.

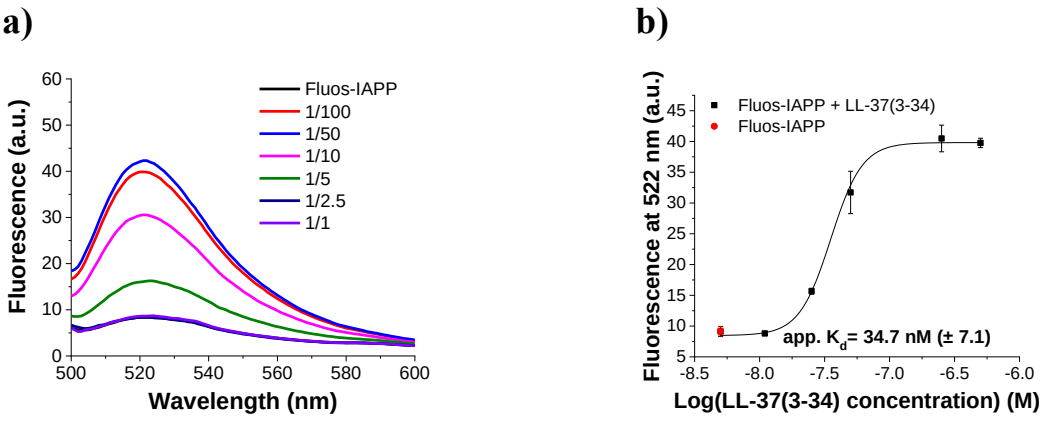

Figure 66. Determination of app. K_ds of interactions of oligomeric LL-37(3-34) with IAPP by fluorescence spectroscopy. a) Fluorescence spectra of Fluos-IAPP (5nM) alone and its mixture with various amounts of LL-37(3-34); the molar ratios of Fluos-IAPP/LL-37(3-34) are as indicated. b) Binding curves of Fluos-IAPP with LL-37(3-34); app. K_ds are means (±SD) from 3 binding curves. Measurements were performed in aqueous buffer 1×b, pH 7.4, containing 1% HFIP.

4.2.5 Characterization of the LL-37 segments/IAPP hetero-assemblies by cross-linking

To investigate the formation of hetero-complexes between IAPP and various LL-37 segments, NuPAGE electrophoresis followed by Western Blot (WB) experiments was carried out. IAPP (30 μM) and its mixtures with LL-37, LL-37(3-37), LL-37(5-37), LL-37(7-37), LL-37(15-37) in equimolar ratio were incubated for 30 minutes. As shown in Figure 67a, IAPP alone contains low MW oligomers, consisting of di- to hexamers and of high MW assemblies. All mixtures with the LL-37 derived analogs contain low MW oligomers and high MW assemblies, but no low oligomeric bands, attributable to toxic IAPP oligomers. Except for the mixture of IAPP with LL-37(15-37), all mixtures exhibit a band around 15 kDa, indicating a hetero-complex which corresponds to a hetero-tetramer, already found in the cross-linking experiment with the native LL-37 and required to have an inhibitory effect. In fact, LL-37, LL-37(3-37) and LL-37(5-37) are inhibitors of IAPP fibril formation at least until 72 hours. LL-37(7-37) can partially still inhibit fibril formation at 24 hours, as shown from the ThT signal of its 1/1 mixture with IAPP and which is not as intense as the IAPP alone, indicating a lower amount of fibrils (section 4.2.3). LL-37(15-37) is not inhibiting the aggregation of IAPP self-association already at 24 hours and presents no hetero-tetramer when cross-linked with IAPP. Additionally, it exhibits a clear random coil secondary structure, whereas the other LL-37 C-terminal segments exhibit at least a partial α-helix/β-sheet, β-turn secondary structure except for LL-37(7-37) which is partially unordered. The formation of the hetero-complex is correlating with the inhibitory properties and with the presence of a clear secondary structure of the peptides. Using the same experimental design, IAPP was incubated also with the N-terminal segments. IAPP (30 μM) and its mixtures with LL-37, LL-37(1-34), LL-37(1-31), LL-37(1-27), LL-37(1-26), LL-37(1-14) in equimolar ratio were incubated for 30 minutes. Results show that IAPP forms, low MW aggregates as well as high MW aggregates, as previously described. As expected, the hetero-band at ~15 kDa, attributable to a hetero-tetramer, is present in the mixtures of IAPP with LL-37, LL-37(1-34), LL-37(1-31), although the separation of the bands in this experiment was not as effective as in the previous ones. These peptides are the ones that could partially or fully intervene with IAPP amyloidogenesis. This band was not visible for the mixtures with the non-inhibitors, like LL-37(1-27), LL-37(1-26), and LL-37(1-14) (Figure 67b).

Notably, these non-inhibitors are also unstructured, confirming that the hetero-complex formation correlates with the inhibitory potency and the secondary structure of these peptides.

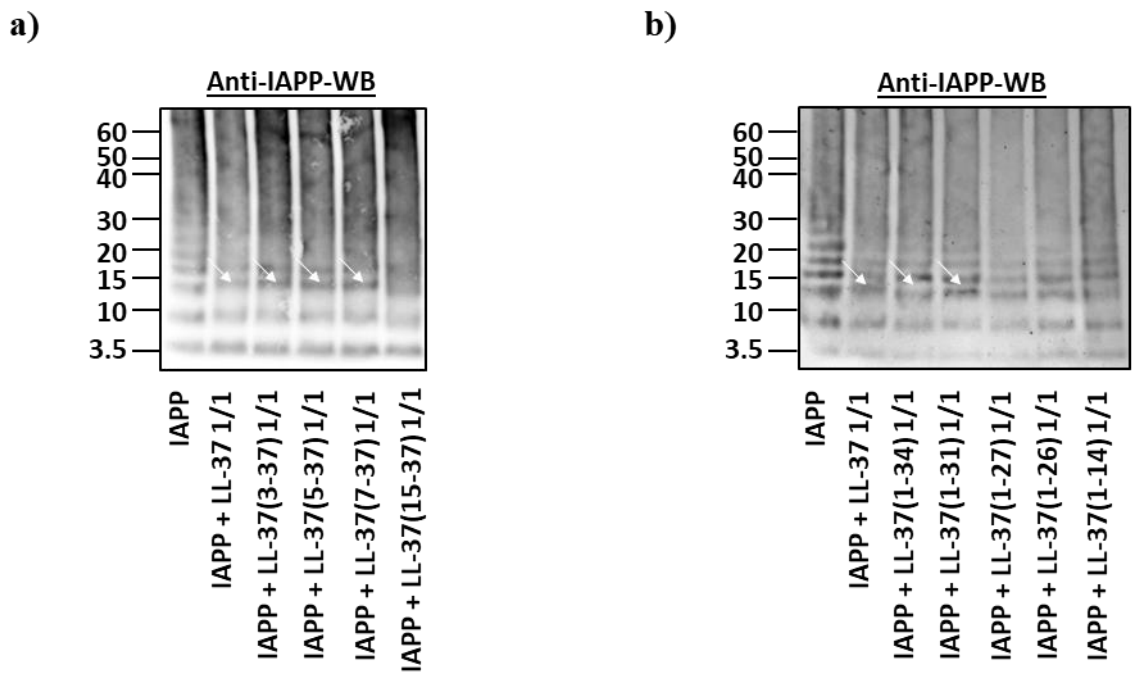

Figure 67. Characterization of the N- and C-terminal truncated LL-37 segments-IAPP hetero-assemblies via cross-linking (pH 7.4). a) NuPAGE and WB with IAPP (30 μM) and its mixtures with LL-37 (1/1), LL-37(3-37) (1/1), LL-37(5-37) (1/1), LL-37(7-37) (1/1), and LL-37(15-37) (1/1) are shown. Representative gel is reported (n=2). b) NuPAGE and WB with IAPP (30 μM) and its mixtures with LL-37 (1/1), LL-37(1-34) (1/1), LL-37(1-31) (1/1), LL-37(1-27) (1/1), LL-37(1-26) (1/1), and LL-37(1-14) (1/1) is shown. Representative gel is reported (n=2).

Of note, the homo-oligomerization of these peptides was characterized. Low MW oligomers, as well as the band at circa 15 kDa, were visible for LL-37(3-37), LL-37(5-37) and, LL-37(7-37). Additionally, higher MW oligomers, for example, hexamers at ~25 kDa were present (133). Only LL-37 presents higher MW oligomers, which are not visible for the shorter segments. LL-37(15-37) is too short to be detected by the antibody against LL-37. A similar pattern to LL-37 was observed for LL-37(1-34). This peptide presents, low and high MW oligomeric assemblies, as well as the homo-tetramer at 15 kDa. This band, together with the low MW assemblies, was visible for the shorter LL-37 C-terminal shortened segments, LL-37(1-31) and LL-37(1-27). Shorter peptides could not be detected by the antibody against LL-37 (Appendix Figure A 12).

4.2.6 Conclusions: identification of LL-37 segments as inhibitors of IAPP amyloid formation

To summarize, the second part of this work focused on the identification of the LL-37 derived shortest sequences, which can efficiently suppress the self-association of IAPP into cytotoxic assemblies. The aim was achieved by the rational design of C- or N-terminal shortened LL-37 sequences. Regarding the N-terminal segments, LL-37(1-14), LL-37(1-26), and LL-37(1-27) exhibited mainly an unordered structure and no inhibitory potency against IAPP fibrillogenesis and cytotoxicity, also when peptides were added in a 10-fold excess compared to IAPP. Results suggested that Phe27 does not contribute to the inhibitory function of LL-37. The α-helical segment LL-37(1-31) was found to be a partial inhibitor of IAPP amyloidogenesis. Only LL-37(1-34), which exhibits the major content of α-helix/β-sheet secondary structure like LL-37, has inhibitory properties comparable to the native peptide.

The C-terminal segments were analyzed as well. LL-37(15-37) and LL-37(7-37) do not interfere with IAPP aggregation and have no ordered structure. By including Phe5 and Phe6 in the sequence, the inhibitory function

was gained. In fact, LL-37(5-37) was found to inhibit partially IAPP self-association and LL-37(3-37) had an inhibitory potency comparable to LL-37. Furthermore, also for these segments a structure-activity relationship was found: LL-37(3-37) is a potent inhibitor with the major α-helix/β-sheet, turn secondary structure compared to the other C-terminal segments. As LL-37(1-34) and LL-37(3-37) were found to be the shortest LL-37 derived inhibitors, the C- and N-termini were both neglected, and LL-37(3-34) was synthesized. Inhibition studies revealed that this peptide could only partially inhibit IAPP aggregation into cytotoxic species and that the region from residue 3 to 34 is not sufficient to have an α-helix/β-sheet secondary structure like the inhibitors display. In fact, a structure-activity relationship was again observed, as the absence of a β-sheet signal at 226 nm correlates with a weaker inhibitory potency. Results of binding affinity studies for monomeric IAPP revealed that the N-terminus is not mediating the interaction with IAPP, while the central/C-terminus is giving the major contribution to the IAPP/LL-37 interaction interface. The binding affinity is not the only requirement to have an inhibitory effect, as the compresence of both termini is required to have an inhibitory effect. Finally, cross-linking studies showed that a hetero-complex of circa 15 kDa, attributable to a hetero-tetramer between IAPP and LL-37 derived sequences, is formed each time inhibition is observed, as already shown in the case of LL-37. This result suggests that the formation of a tetramer between IAPP and the inhibitor might be necessary to avoid the aggregation of IAPP. Results are summarized in Table 24.

Table 24. Overview of the biophysical characterization and interactions of LL-37 segments with IAPP.

Peptide	Inhibition of IAPP fibril formation	Secondary structure (1xb + 1% HFIP)	IAPP/LL-37 hetero-tetramer (~15 kDa)	Binding affinity to monomeric IAPP
LL-37	✓	α-helix/β-sheet	✓	88.1 (± 12.0) nM
LL-37(3-37)	✓	α-helix/β-sheet	✓	101.9 (± 56.0) nM
LL-37(5-37)	partially ✓	α-helix	✓	51.3 (± 15.0) nM
LL-37(7-37)	✗	partially α-helix	✓	62.7 (± 17.8) nM
LL-37(15-37)	✗	unordered	✗	31.9 (± 2.2) nM
LL-37(1-14)	✗	unordered	✗	2.54 (± 0.5) μM
LL-37(1-26)	✗	unordered	✗	227.7 (± 2.1) nM
LL-37(1-27)	✗	unordered	✗	24.2 (± 4.2) nM
LL-37(1-31)	partially ✓	partially α-helix/ β-sheet	✓	18.4 (± 6.8) nM
LL-37(1-34)	✓	α-helix/β-sheet	✓	132.4 (± 3.2) nM
LL-37(3-34)	partially ✓	α-helix	-	34.7 (± 7.1) nM

Legend: ✓= the peptide is an inhibitor of IAPP amyloid formation; ✗= the peptide cannot block IAPP amyloid formation; - = not determined.

4.3 Identification of FF as key residues for the inhibitory effect of LL-37 on IAPP amyloidogenesis and cytotoxicity

In this chapter, the role of the residues Phe5 and Phe6 of LL-37 in the inhibition of the fibrillogenesis of IAPP was investigated.

4.3.1 Peptide design and synthesis

The studies carried out to identify the LL-37 core inhibitor, which can suppress the aggregation of IAPP into cytotoxic species, led to the identification of Phe5 and Phe6 as key residues for the inhibitory properties. Interestingly, when the N-terminal truncated segments LL-37(5-37) and LL-37(7-37) were tested as inhibitors via ThT binding assay, the importance of the FF motif was underlined. To confirm these preliminary results, double and single alanine mutants of LL-37 and its N-terminal truncated segments LL-37(3-37) and LL-37(5-37) were rationally designed and synthesized (Table 25).

Table 25. Name and primary structure of LL-37 single and double alanine mutants.

Abbreviation	**Peptide sequence**
LL-37A5,6	LLGDAARKSKEKIGKEFKRIVQRIKDFLRNLVPRTES
LL-37A5	LLGDAFRKSKEKIGKEFKRIVQRIKDFLRNLVPRTES
LL-37A6	LLGDFARKSKEKIGKEFKRIVQRIKDFLRNLVPRTES
LL-37(3-37)A5,6	GDAARKSKEKIGKEFKRIVQRIKDFLRNLVPRTES
LL-37(5-37)A5,6	AARKSKEKIGKEFKRIVQRIKDFLRNLVPRTES

The synthesis of the LL-37 mutants was carried out on Wang or TentaGel R PBH resins using a combination of manual and automated SPPS with the CS336X peptide synthesizer. The Fmoc-cleavage was performed with a DMF solution containing 20% of piperidine with 0.1 M HOBt, and a capping step with acetic anhydride was carried out after each coupling. Based on the results obtained for the synthesis of the N-terminal truncated sequences, the synthesis using TentaGel R PBH resin led to better results in means of purification of crude peptides via RP-HPLC. The optimized procedure of the synthesis of these sequences was based on the one described in section 4.2.1. Briefly, peptides were synthesized on TentaGel R PBH resin with a substitution level of 0.19 mmol/g. Most of the couplings were performed two times using the coupling reagent HATU, and only for Glu^{36}, Thr^{35}, Arg^{34}, Pro^{33} HBTU was used for the second coupling step. Difficult coupling reactions were performed three times: Val^{32} and Leu^{31} were coupled using HATU only for the first coupling and HBTU for the other two, while Val^{21} was coupled with HATU for the first two couplings and with HBTU for the last one. Three times couplings were carried out for Gln^{22}, Lys^{15}, Lys^{12}, Lys^{8}, and Leu^{2} using HATU as the coupling reagent. For positions Glu^{11} and Lys^{10}, the three times coupling with HATU was carried out for 50 minutes. Additionally, Ile^{20}, Arg^{19}, and Lys^{18}, Phe^{17}, and Ile^{13} were coupled three times for 50 minutes with a 6-fold molar excess of HATU and Fmoc-protected amino acid and 9-fold excess of DIEA for the first two. Finally, Gly^{14} and Asp^{4} were coupled three times with a 6-fold molar excess of HATU and Fmoc-protected amino acid and 9-fold excess of DIEA for 50 minutes. For the synthesis of LL-37A5,6, LL-37(3-37)A5,6, and LL-37(5-37)A5,6 Phe^{5} and Phe^{6} were replaced with alanine, and the synthesis was interrupted at position Gly^{3} and Ala^{5} for LL-37(3-37)A5,6, and LL-37(5-37)A5,6 respectively. For the single alanine mutant LL-37A5 and LL-37A6 Phe^{5} or Phe^{6} were substituted with alanine residues. Crude peptides were obtained by a 3 hour-long cleavage from the resin, using TFA:ddH_2O (95:5 v:v), and then purified utilizing RP-HPLC. For most of the sequences, the purification process had to be repeated two times, to eliminate the side products formed during the SPPS. The purity of each of them was verified by MALDI-TOF MS (Table 26, Figure 68, and Figure 69).

Table 26. Characterization of the synthetic peptides via RP-HPLC and MALDI-TOF.

Abbreviation	**HPLC program**	**t_R (min)**	**HPLC program for 2nd purification**	**t_R (min)**	**Yield**	**$[M+H]^+$ expected**	**$[M+H]^+$ found**
LL-37A5,6	LangsamAβ	32.3	LangsamAβ	32.3	9%	4339.5	4340.3
LL-37A5	LangsamAβ	33.8	LangsamAβ 40–70%B	24.2	9%	4415.6	4417.9
LL-37A6	LangsamAβ 40–70%B	25.1	LangsamAβ 40–70%B	25.1	7%	4415.6	4416.7
LL-37(3-37)A5,6	10-100% B stay at 100% B for 10 min	15.5	-	-	5%	4413.3	4113.7
LL-37(5-37)A5,6	SchnellAβ	21.5	-	-	11%	3941.3	3941.3

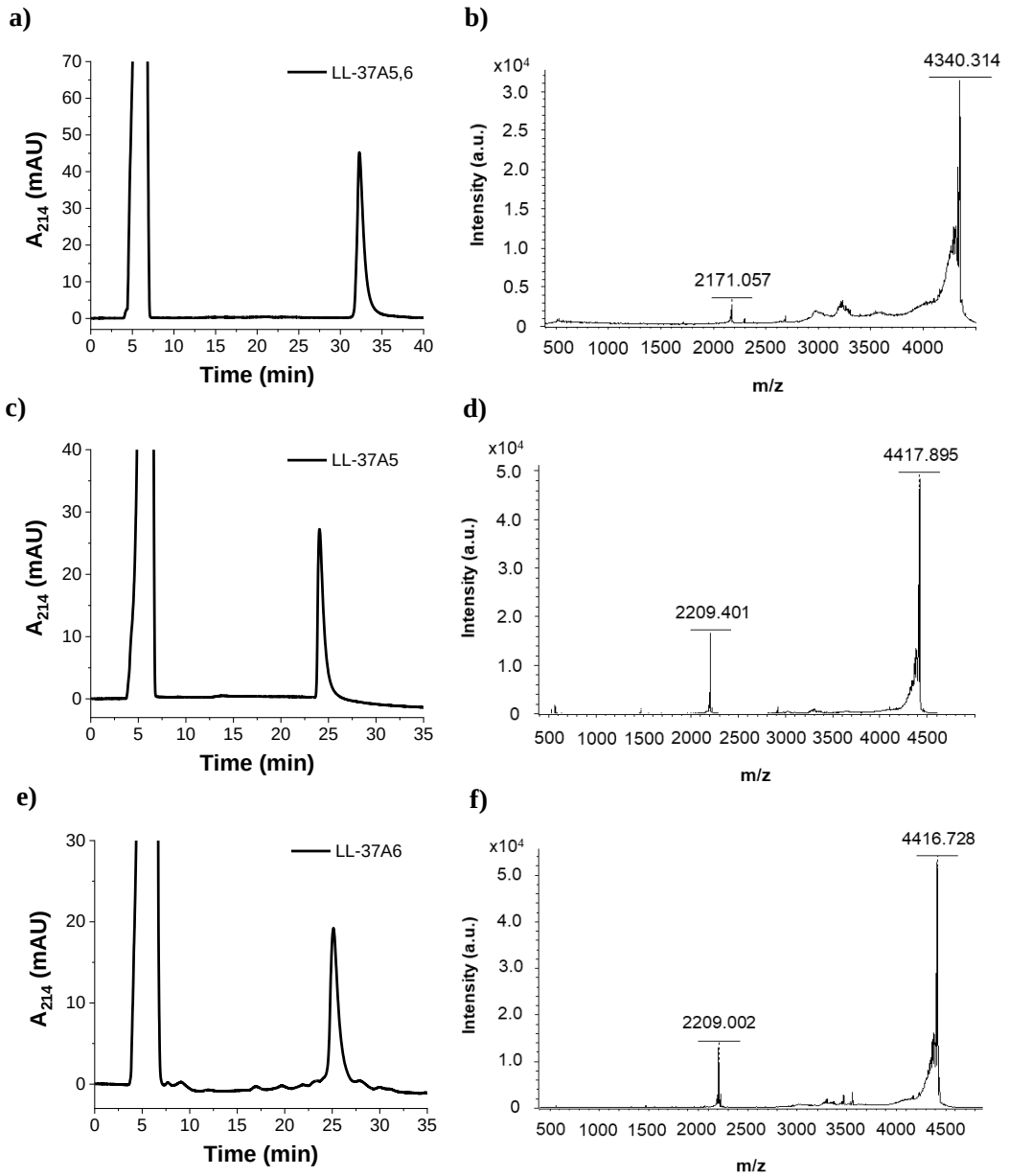

Figure 68. Characterization of LL-37A5,6, LL-37A5, and LL-37A6 via RP-HPLC and MALDI-TOF. Representative chromatogram at 214 nm of a) repurified LL-37A5,6, c) repurified LL-37A5, and e) repurified LL-37A6 with retention time of the peptides at 32.3, 24.2, and 25.1 min, respectively. MALDI-TOF-MS spectra of HPLC purified b) LL-37A5,6, d) LL-37A5, and f) LL-37A6, with $[M+H]^+$ and $[M+2H]^{2+}$ found masses.

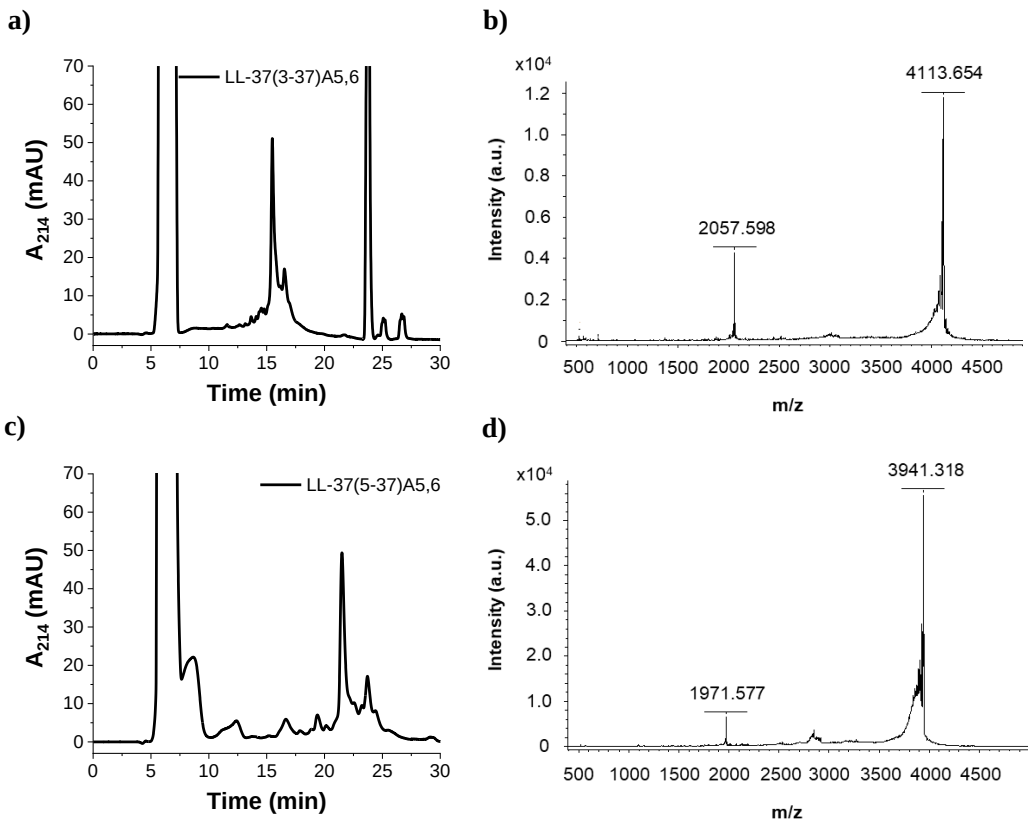

Figure 69. Characterization of LL-37(3-37)A5,6 and LL-37(5-37)A5,6 via RP-HPLC and MALDI-TOF. Representative chromatogram at 214 nm of a) LL-37(3-37)A5,6 crude and c) LL-37(5-37)A5,6 crude with retention time of the peptides at 15.5, and 21.5 min respectively. MALDI-TOF-MS spectra of HPLC purified b) LL-37(3-37)A5,6 and b) LL-37(5-37)A5,6 with $[M+H]^+$ and $[M+2H]^{2+}$ found masses.

4.3.2 Biophysical characterization: Conformational studies via CD spectroscopy

The effect of the alanine mutations of Phe5 and Phe6 on the secondary structure was studied via CD spectroscopy. Briefly, peptides were diluted from their HFIP stock in aqueous 10 mM sodium phosphate buffer (1xb, pH 7.4) containing 1% of final HFIP amount, and subsequently, spectra of these solutions were recorded. The self-association propensity was evaluated by measuring spectra between 5 μM and 100 μM. LL-37A5,6 exhibited mainly an α-helix secondary structure, with two minima showing similar intensities at 208 and 222 nm and a maximum at 198 nm. Furthermore, the peptide showed an oligomerization tendency, as the signal intensity significantly decreases at higher concentrations (20 μM), as shown in Figure 70a. The single alanine mutant LL-37A5 showed an α-helix/β-sheet, β-turn secondary structure, with the two characteristic minima at 208 and 224 nm and a maximum at 198 nm. Unlike the analog peptide with double alanine mutations, in LL-37A5 the minima have different intensities, in fact, the minimum at 222 nm has a more intense signal than the one at 208 nm. Additionally, the peptide showed an oligomerization propensity, with a reduction of the signal intensity starting at 10 μM (Figure 70b). The second single alanine mutant LL-37A6 exhibited no concentration dependence between 5 and 20 μM. Its α-helical/β-sheet, β-turn secondary structure resembles the structure of the native LL-37 with an intense minimum at 226 nm, a less pronounced one at 208 nm, and a maximum at 198 nm (Figure 70c).

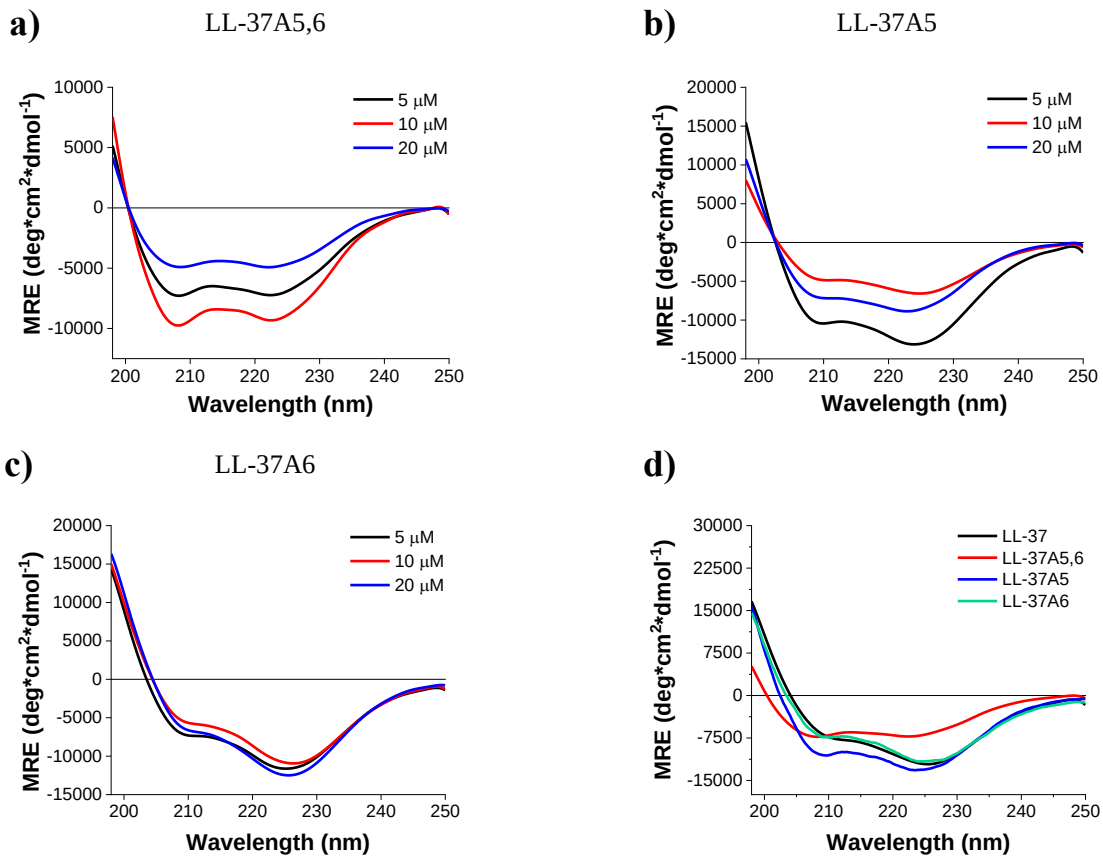

Figure 70. Concentration dependence of LL-37 single and double Phe5 and Phe6 alanine mutants assessed by far-UV CD spectroscopy. a) LL-37A5,6, b) LL-37A5, c) LL-37A6. d) Overlay at 5 µM of the spectra in a), b), and c). Measurements were performed in aqueous buffer 1×b, pH 7.4, containing 1% HFIP.

When the spectra of these peptides were recorded in assay buffer in absence of HFIP, LL-37A5,6 exhibited majorly an α-helix/random coil structure, characterized by a minimum at 203 nm, suggesting that the presence of HFIP induces the secondary structure to this peptide. The difference with the single alanine mutants was striking. In fact, LL-37A5 still exhibits an α-helix and β-sheet/turn structure with a maximum at 198 nm and two minima, one at 208 nm and the more intense one at 224 nm. LL-37A6 presents a similar profile, although the overall signal intensity is slightly lower (Figure 71). In the case of LL-37A5 and LL-37A6, the effect of HFIP on the secondary structure was not as evident as for all the other peptides studied, since the β-sheet/turn content was not induced by the HFIP.

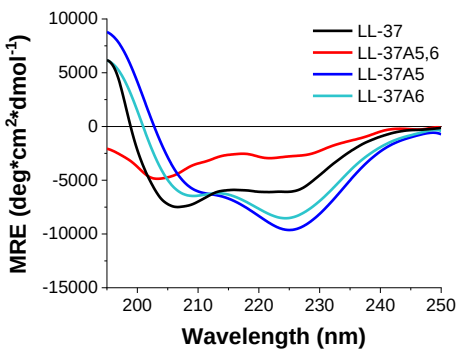

Figure 71. Effect of the absence of HFIP on the secondary structure of LL-3A5,6, LL-37A5, and LL-37A6 assessed by far-UV CD spectroscopy. Measurements were performed at a concentration of 5 µM in aqueous buffer 1×b, pH 7.4.

LL-37(3-37)A5,6 displayed a similar structure to LL-37A5,6. In fact, the peptide showed the typical signal of an α-helix, a maximum at 198 nm and the two minima at 208 and 222 nm but the minimum at 222 nm resulted to be more pronounced (Figure 72a). By increasing the concentration to 10 μM, the signal is circa two times higher, indicating a concentration dependence. Last, at 20 μM, the peptide oligomerizes as the signal intensity drastically decreases. Regarding LL-37(5-37)A5,6, a minimum at 204 nm and a less pronounced one at 224 nm, and a slight maximum at 198 nm were present. This might indicate a transition from a helical to a partially unordered state. The peptide presented no concentration dependence between 5 μM and 20 μM and a strong increase of the signal at 50 μM (Figure 72b).

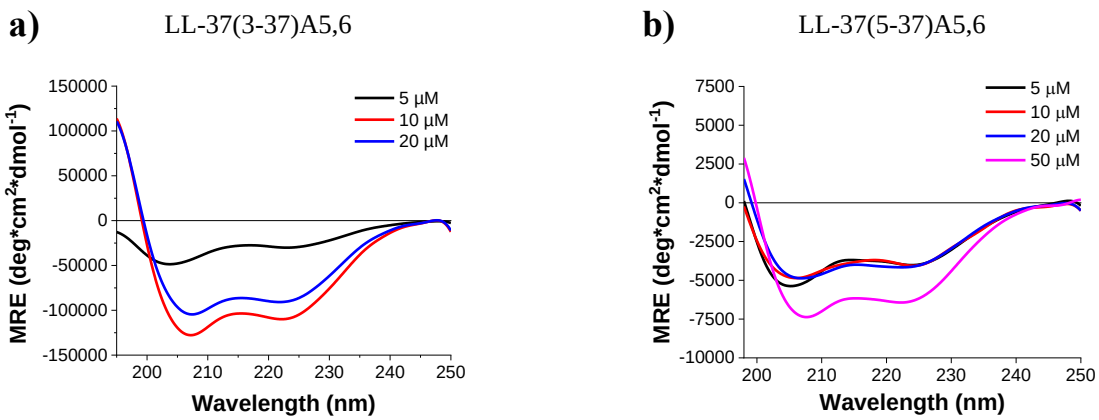

Figure 72. Concentration dependence of LL-37 segments double Phe5 and Phe6 alanine mutations assessed by far-UV CD spectroscopy. a) LL-37(3-37)A5,6, b) LL-37(5-37)A5,6. Measurements were performed in aqueous buffer 1×b, pH 7.4, containing 1% HFIP.

Next, the effect of 2,2,2-trifluoroethanol (TFE) on the helical propensities of LL-37A5,6, LL-37A5, and LL-37A6 were investigated. As described above, in absence of TFE, LL-37A5,6 displays a maximum at 198 nm and two minima, one at 208 nm and one at 226 nm, indicating an α-helix secondary structure. Titration with increasing amounts of TFE slightly increased the helical content (Figure 73a). Due to its initial high helical content, the transition point for LL-37A5,6 is at ~2% TFE (Figure 73b), which is about 4-times lower than LL-37, as its transition point is at 8% TFE. A different behavior was observed for the single alanine mutants. Both LL-37A5 and LL-37A6 exhibit an α-helix and β-sheet/turn secondary structure without TFE with a maximum at 198 nm and the two minima at 208 and a more marked one at 226 nm (Figure 73c, e). The increasing amounts of TFE led to a two-state transition for both peptides with T_M values at 21 and 20% respectively (Figure 73d, f). The single substitution of the Phe5 or Phe6 caused a loss of the helical propensity of LL-37 as the transitions occur for these peptides with 2.5-fold more TFE.

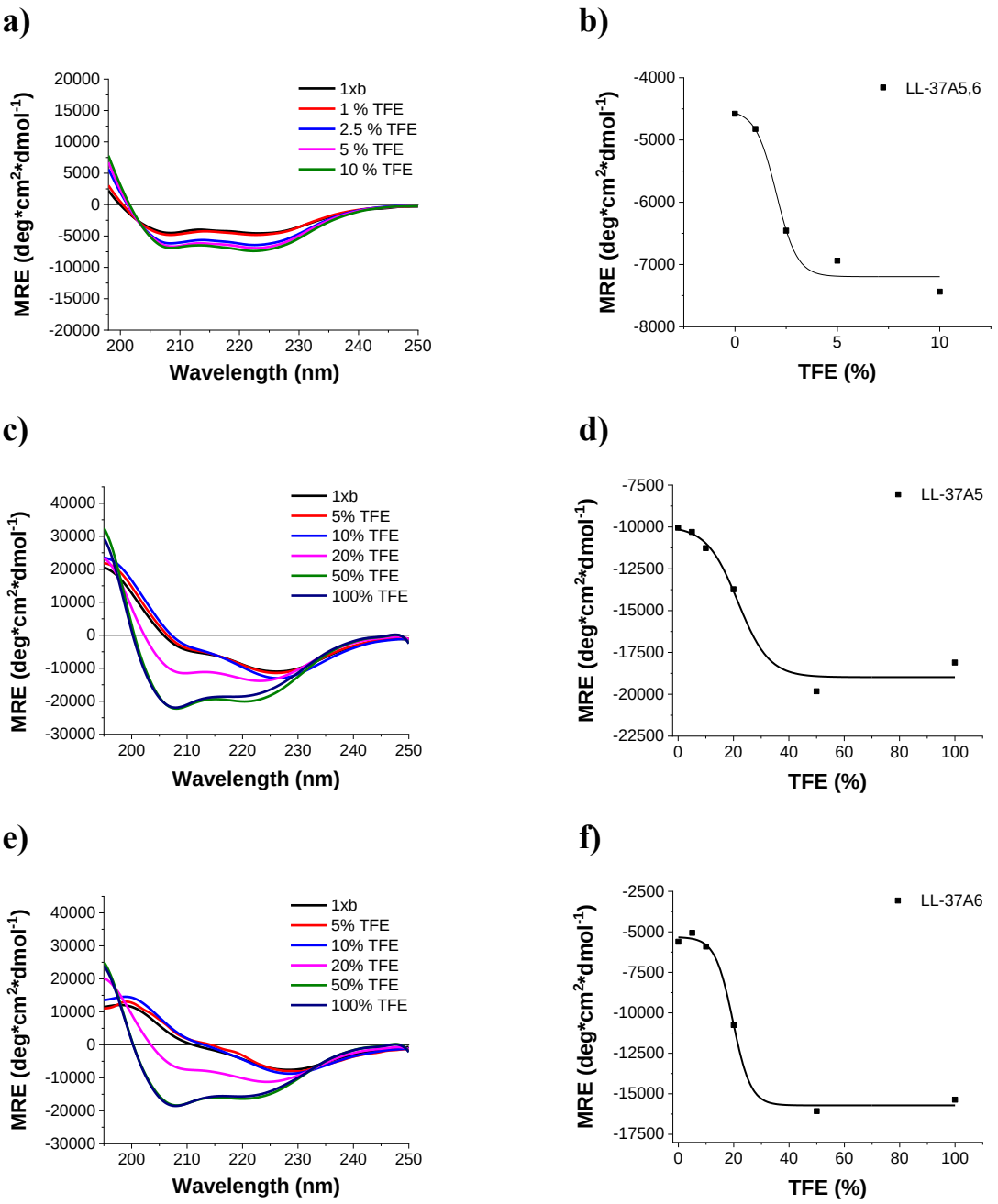

Figure 73. Effects of TFE on the conformation in aqueous solution of a) LL-37A5,6, c) LL-37A5, and e) LL-37A6 assessed by far-UV CD spectroscopy. Experiments were performed at peptide concentrations of 5 µM in aqueous buffer 1×b, pH 7.4, containing 1% HFIP with the indicated amounts of TFE. b), d), and f) Plots of minima at 222 nm versus the TFE amounts (%) of the CD spectra of the peptides shown in a), c), and e) respectively.

In this section, the secondary structure of LL-37 alanine mutants was investigated. In LL-37A5,6 the substitution on Phe5 and Phe6 with alanine residues affected the secondary structure, leading to a loss of β-sheet/turn content. Furthermore, the peptide oligomerized at 20 µM as the native sequence. The TFE titration for this peptide led to a transition point at 2% TFE, as the peptide was already α-helical in absence of TFE. For the single alanine mutants, the titrations suggest that the helical propensity decreases when only one of the two residues is replaced. When the spectrum was recorded in the assay buffer without HFIP, the structure resulted partially disordered due to the presence of the β-sheet/turn structure in the case of LL-37A5,6, but the HFIP had no significant effect on LL-37A5 and LL-37A6. In fact, the two peptides present an α-helical and β-sheet/turn structure also without HFIP. The single alanine mutants had a similar structure to LL-37. In fact,

the two peptides exhibited an α-helix and β-sheet/turn structure, but with different oligomerization propensity. LL-37A5 started to oligomerize at 10 μM, as indicated by the loss of signal, while LL-37A6 showed concentration dependence. Regarding LL-37(3-37)A5,6, an α-helical conformation with oligomerization was observed when the concentration on the peptide was increased. In general, the substitution of the FF motif led to a loss of structure for all peptides compared to their native analogs (Table 27).

Table 27. Characterization of the secondary structure of LL-37 alanine mutants.

Peptide	**Secondary structure in 1xb[a] + 1% HFIP**	**Secondary structure in 1xb[a]**	**Concentration of oligomerization**
LL-37	α-helix/β-sheet,β-turn	α-helix	20 μM
LL-37A5,6	α-helix	α-helix/random coil	20 μM
LL-37A5	α-helix/β-sheet,β-turn	α-helix/β-sheet,β-turn	10 μM
LL37A6	α-helix/β-sheet,β-turn	α-helix/β-sheet,β-turn	no oligomerization
LL-37(3-37)A5,6	α-helix	-	20 μM
LL-37(5-37)A5,6	α-helix	-	no oligomerization

[a] 1xb, aq. buffer, pH 7.4, containing 1% HFIP.

4.3.3 Studies on the inhibitory activity of FF alanine mutated LL-37 analogs on fibrillogenesis and cytotoxicity of IAPP.

Next, we addressed the question whether LL-37A5,6, LL-37A5, LL-37A6, and the truncated sequences, LL-37(3-37)A5,6 and LL-37(5-37)A5,6 could still inhibit the aggregation of IAPP into cytotoxic assemblies when the Phe5 and Phe6 residues are alanine mutated. For this purpose, IAPP alone (16.5 μM) and its 1/1 mixture with the LL-37 Ala mutants were incubated for 7 days and the kinetics of IAPP fibril formation and its cytotoxicity were monitored by ThT binding and MTT reduction assays respectively. TEM was used to confirm the assay results.

LL-37A5,6 showed inhibitory potency towards aggregation only for 48 hours of incubation time. Cytotoxicity of IAPP towards RIN5fm cells was efficiently inhibited at 24 hours. After 48 hours, the ThT signal of the IAPP/LL-37A5,6 mixture increased, indicating the formation of amyloid fibrils. At 7 days, the peptide could not inhibit the cytotoxicity anymore, in fact, the MTT reduction curve looks similar for IAPP alone and the mixture (Figure 74a, b, and c). TEM images at 7 days confirmed the above results. Fibrils were the main species for both IAPP and the mixture with LL-37A5,6 (Figure 74d). These results suggest the key role of the FF motif on the inhibitory potency of LL-37. The removal of these two residues led to a significantly weaker inhibitory potency of the peptide of both fibril formation and cytotoxicity.

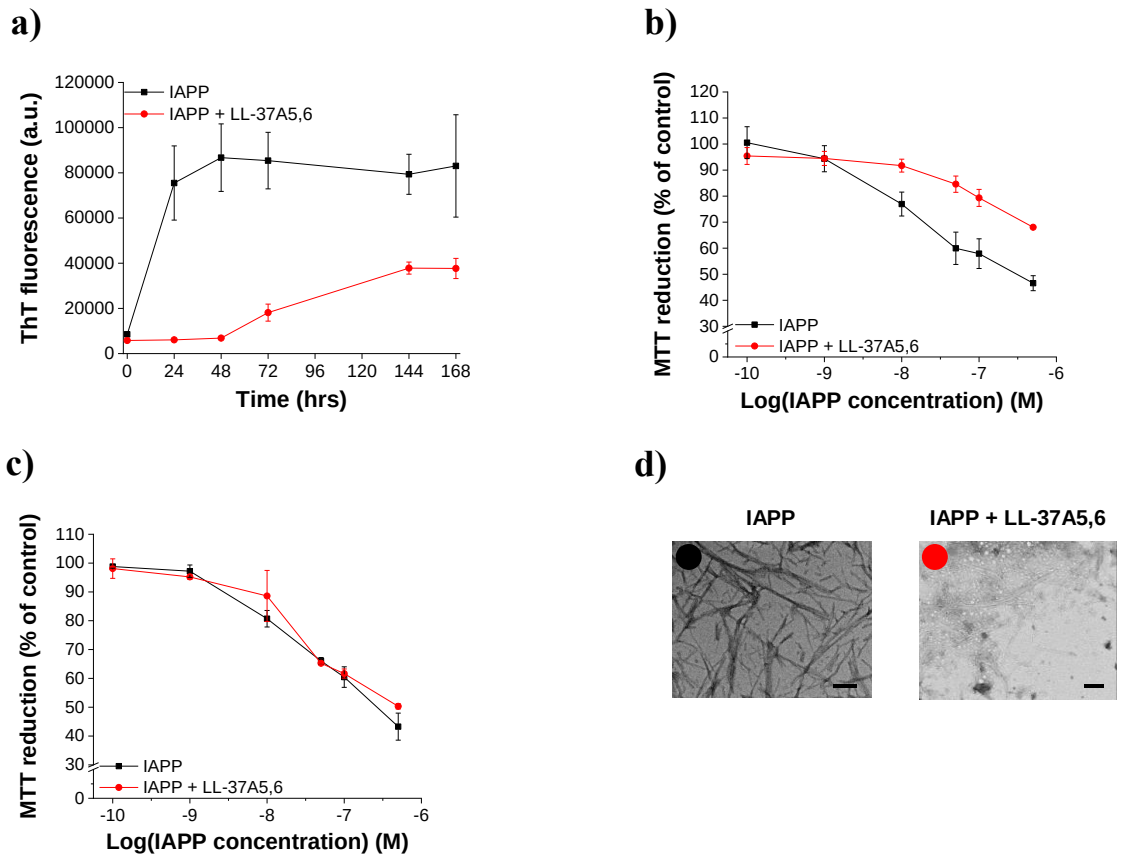

Figure 74. Effects of LL-37A5,6 on IAPP amyloid formation and cytotoxicity. a) Fibrillogenesis of IAPP (16.5 μM) and its mixtures with LL-37A5,6 (1/1) (means (±SD), 3 assays); b) effects on cell viability: solutions from a) were added to cultured RIN5fm cells (24 hours aged). Cell viability was determined by MTT reduction (means (±SD), 3 assays, n=3 each); c) effects on cell viability: solutions from a) were added to cultured RIN5fm cells (7 days aged). Cell viability was determined by MTT reduction (means (±SD), 3 assays, n=3 each); d) TEM images of solutions of a) (7 days aged) as indicated (bars, 100 nm).

Furthermore, ThT binding assay showed that LL-37A5,6 cannot inhibit IAPP aggregation also in 10-fold excess. When IAPP (16.5 μM) is co-incubated with LL-37A5,6 (165 μM), the inhibitory effect is visible only for 48 hours, as the 1/1 incubation of the two peptides (Figure 75). Results suggest that the excess of LL-37A5,6 does not have any effect on IAPP amyloid formation and that the inhibitory potency is at least 10 times worse than the native sequence.

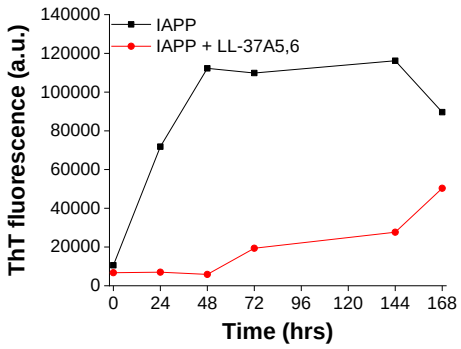

Figure 75. Effects of LL-37A5,6 in 10-fold excess on IAPP amyloid formation. a) Fibrillogenesis of IAPP (16.5 μM) and its mixture with LL-37A5,6 (1/10) (representative experiment is reported (n=2)).

Next, we asked whether a similar effect could be observed in the case of LL-37(3-37). This peptide is an inhibitor of IAPP fibril formation and cytotoxicity and exhibits similar biophysical properties as LL-37. IAPP was co-incubated in an equimolar ratio with the Phe5 and Phe6 alanine mutant of this peptide, LL-37(3-37)A5,6. The effect on the inhibitory properties was dramatic. In fact, the peptide elongated the lag phase of IAPP fibril formation only for 24 hours (Figure 76a). Nevertheless, the peptide could not inhibit IAPP cytotoxicity after 24 hours and, consequently, after 7 days of incubation time (Figure 76b, c). TEM images confirmed the results described. The 1/1 mixture exhibited mainly fibrils after 7 days (Figure 76d).

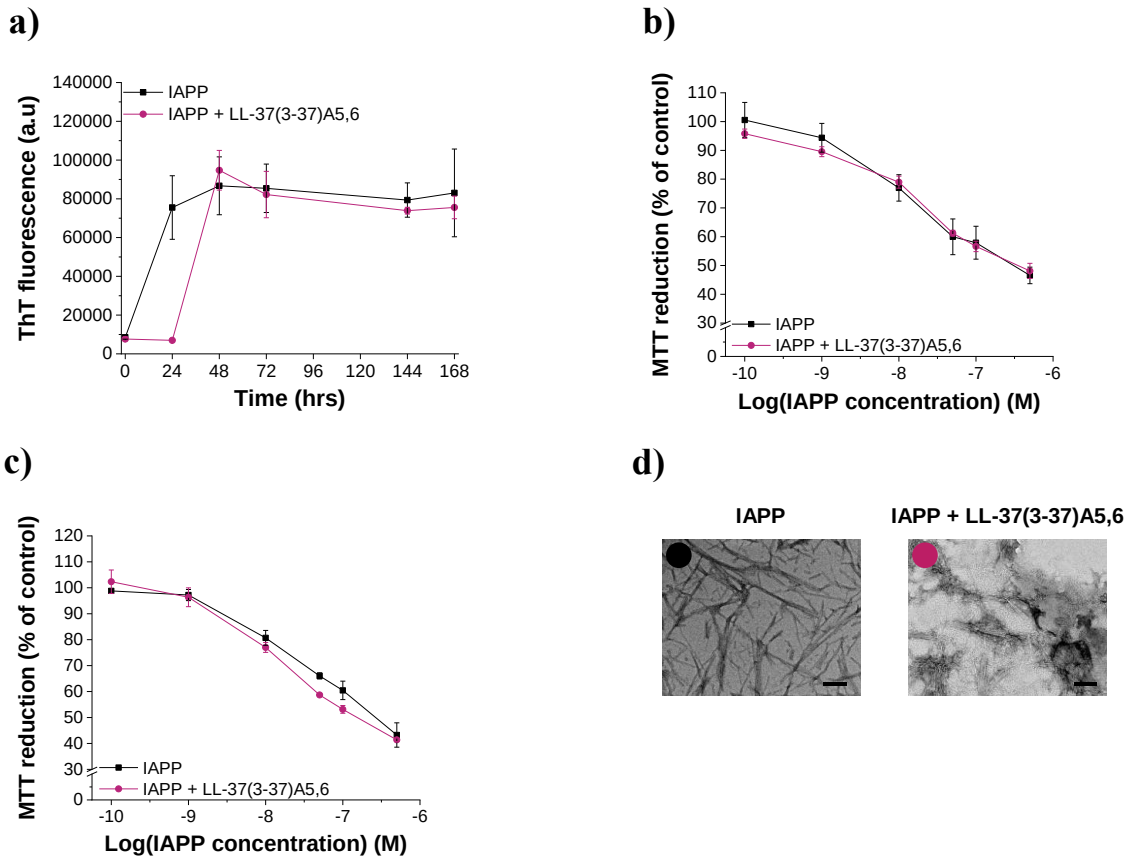

Figure 76. Effects of LL-37(3-37)A5,6 on IAPP amyloid formation and cytotoxicity. a) Fibrillogenesis of IAPP (16.5 μM) and its mixtures with LL-37(3-37)A5,6 (1/1) (means (±SD), 3 assays); b) effects on cell viability: solutions from a) were added to cultured RIN5fm cells (24 hours aged). Cell viability was determined by MTT reduction (means (±SD), 3 assays, n=3 each); c) effects on cell viability: solutions from a) were added to cultured RIN5fm cells (7 days aged). Cell viability was determined by MTT reduction (means (±SD), 3 assays, n=3 each); d) TEM images of solutions of a) (7 days aged) as indicated (bars, 100 nm).

To further confirm the hypothesis that the FF motif is crucial for the inhibitory potency, the two phenylalanine residues were replaced by alanine also in LL-37(5-37). As previously shown, this peptide could block the fibril formation of IAPP for 72 hours. This partial inhibitory role was completely lost for LL-37(5-37)A5,6. In fact, the 1/1 mixture of IAPP and LL-37(5-37)A5,6 had very similar aggregation kinetics to IAPP alone. Additionally, the mixture resulted toxic to the RIN5fm cell line already at 24 hours and TEM images confirmed the presence of amyloid-like fibrils in the mixture of the two peptides (Figure 77).

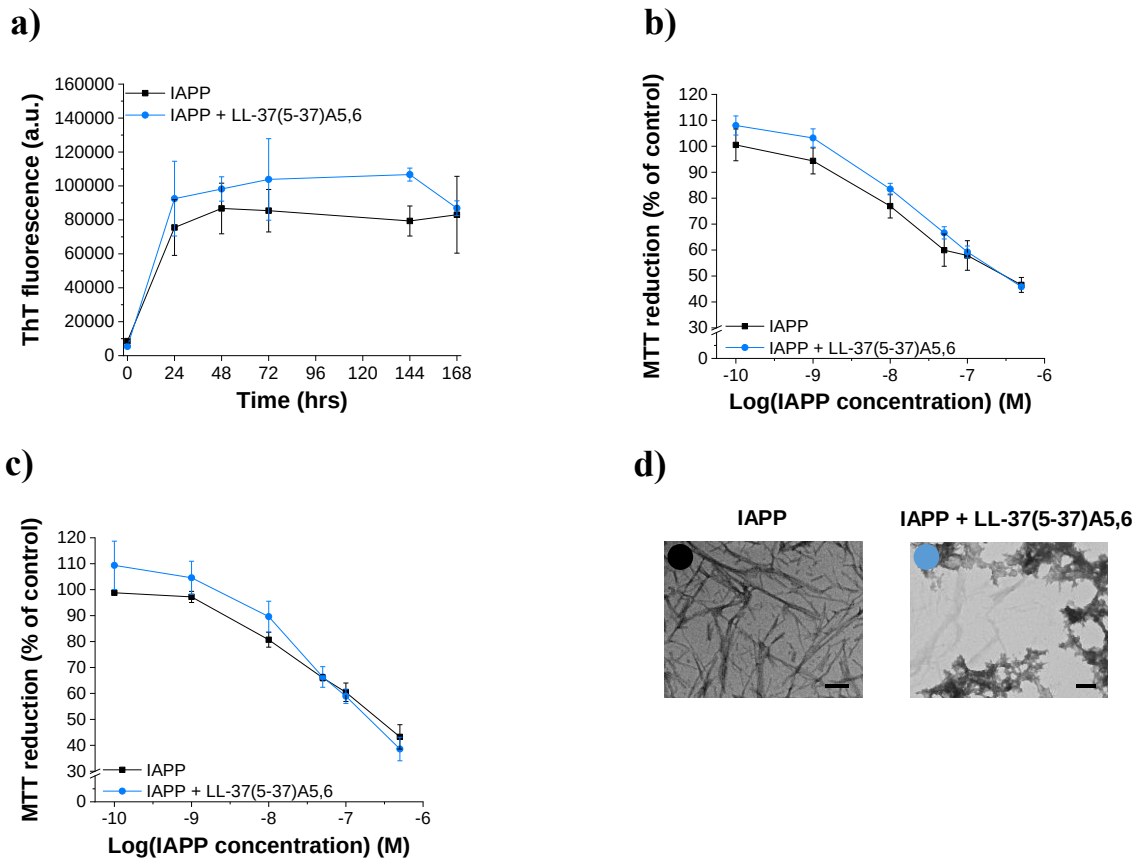

Figure 77. Effects of LL-37(5-37)A5,6 on IAPP amyloid formation and cytotoxicity. a) Fibrillogenesis of IAPP (16.5 μM) and its mixtures with LL-37(5-37)A5,6 (1/1) (means (±SD), 3 assays); b) effects on cell viability: solutions from a) were added to cultured RIN5fm cells (24 hours aged). Cell viability was determined by MTT reduction (means (±SD), 3 assays, n=3 each); c) effects on cell viability: solutions from a) were added to cultured RIN5fm cells (7 days aged). Cell viability was determined by MTT reduction (means (±SD), 3 assays, n=3 each); d) TEM images of solutions of a) (7 days aged) as indicated (bars, 100 nm).

To investigate whether only one of the phenylalanine residues is crucial for the inhibitory potency of LL-37, the single alanine mutants of the native sequence were tested in a similar way. Kinetics of IAPP fibril formation and cytotoxicity were followed by ThT binding and MTT reduction assays as above. Incubations of IAPP and 1/1 mixtures of IAPP and LL-37A5 or IAPP and LL-37A6 were aged 7 days and ThT fluorescence and MTT reduction were measured at given time points.

LL-37A5 partially blocked IAPP aggregation. In fact, the lag phase was extended until 48 hours. Later on, the ThT signal increased, indicating the formation of amyloid fibrils (Figure 78a). In correlation with the ThT results, the MTT reduction assay suggested that the cytotoxicity was blocked only for 24 hours and not after 168 hours of incubation time, as shown in Figure 78b, c. Lastly, TEM images at 168 hours confirmed the presence of fibrils as the main species of the IAPP/LL-37A5 incubation (Figure 78d).

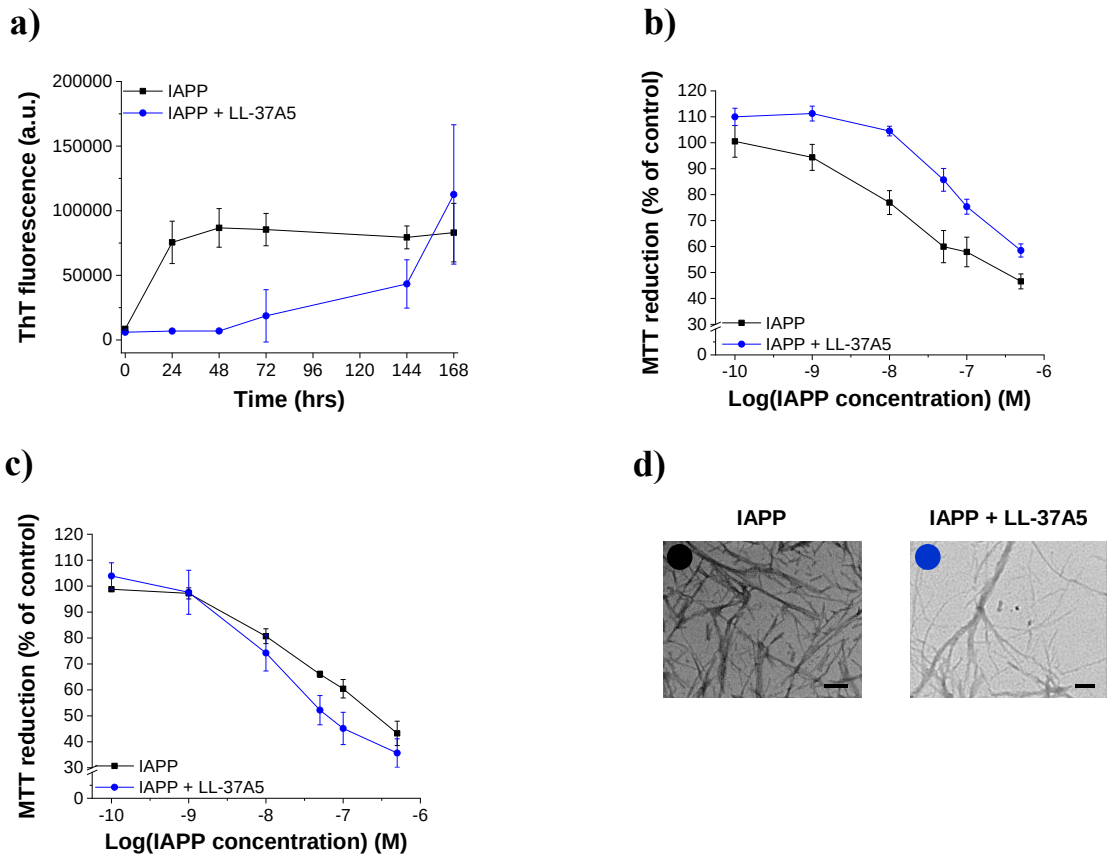

Figure 78. Effects of LL-37A5 on IAPP amyloid formation and cytotoxicity. a) Fibrillogenesis of IAPP (16.5 μM) and its mixtures with LL-37A5 (1/1) (means (±SD), 3 assays); b) effects on cell viability: solutions from a) were added to cultured RIN5fm cells (24 hours aged). Cell viability was determined by MTT reduction (means (±SD), 3 assays, n=3 each); c) effects on cell viability: solutions from a) were added to cultured RIN5fm cells (7 days aged). Cell viability was determined by MTT reduction (means (±SD), 3 assays, n=3 each); d) TEM images of solutions of a) (7 days aged) as indicated (bars, 100 nm).

Results for the second single alanine mutant, LL-37A6, were not significantly different. As shown in Figure 79a, the kinetics of IAPP aggregation were blocked only for 48 hours, as observed for LL-37A5. Additionally, LL-37A6 inhibited the aggregation into cytotoxic species at 24 hours but not at 7 days (Figure 79b, c). In fact, TEM images confirmed the presence of amyloid fibrils at this time point (Figure 79d).

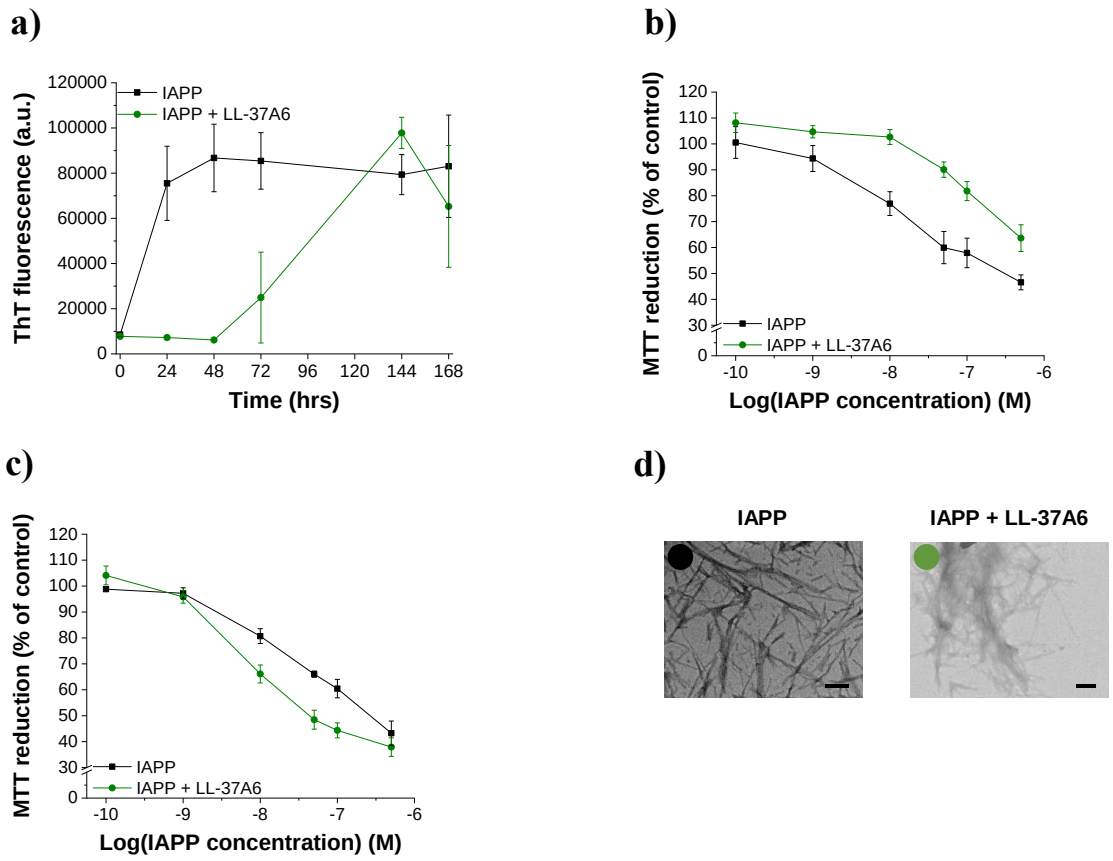

Figure 79. Effects of LL-37A6 on IAPP amyloid formation and cytotoxicity. a) Fibrillogenesis of IAPP (16.5 μM) and its mixtures with LL-37A6 (1/1) (means (±SD), 3 assays); b) effects on cell viability: solutions from a) were added to cultured RIN5fm cells (24 hours aged). Cell viability was determined by MTT reduction (means (±SD), 3 assays, n=3 each); c) effects on cell viability: solutions from a) were added to cultured RIN5fm cells (7 days aged). Cell viability was determined by MTT reduction (means (±SD), 3 assays, n=3 each); d) TEM images of solutions of a) (7 days aged) as indicated (bars, 100 nm).

Results suggest that both phenylalanine residues are important for the inhibitory potency of LL-37, but no additive effect was observed. The two single alanine mutants, LL-37A5 and LL-37A6 delay the IAPP lag phase as LL-37A5,6. Also, LL-37A5,6 has an inhibitory potency that is at least 10-times weaker than LL-37. In the case of the shorter segments, LL-37(3-37)A5,6 and LL-37(5-37)A5,6, the inhibition properties were also weakened compared to their native analogs (Table 28).

Table 28. Overview of the inhibitory properties of LL-37 alanine mutants.

Peptide	Inhibition of IAPP fibrillogenesis in 1/1	Inhibition of IAPP fibrillogenesis in 1/10
LL-37	✓	-
LL-37A5,6	partially ✓	✗
LL-37A5	partially ✓	-
LL-37A6	partially ✓	-
LL-37(3-37)A5,6	✗	-
LL-37(5-37)A5,6	✗	-

Legend: ✓= the peptide is an inhibitor of IAPP amyloid formation; ✗= the peptide cannot block IAPP amyloid formation; - = not determined.

4.3.4 Determination of binding affinities towards IAPP

The effect of alanine mutations on the IAPP/LL-37 interaction was characterized by fluorescence spectroscopic titrations. To evaluate the apparent K_d values of their binding affinities, N-terminal fluorescein-labeled IAPP (Fluos-IAPP, 5 nM) was titrated with different amounts of LL-37 alanine mutants in 1xb buffer (pH 7.4) containing 1% HFIP. LL-37A5,6, LL-37(3-37)A5,6, and LL-37(5-37)A5,6 bound similarly to monomeric IAPP. LL-37A5,6 bound to Fluos-IAPP with an app. K_d of 182.8 (± 29.9) nM (Figure 80). The strong binding is comparable to the binding of LL-37 to Fluos-IAPP indicating that if the Phe5 and Phe6 are replaced with alanine, no effect on the interaction is observed.

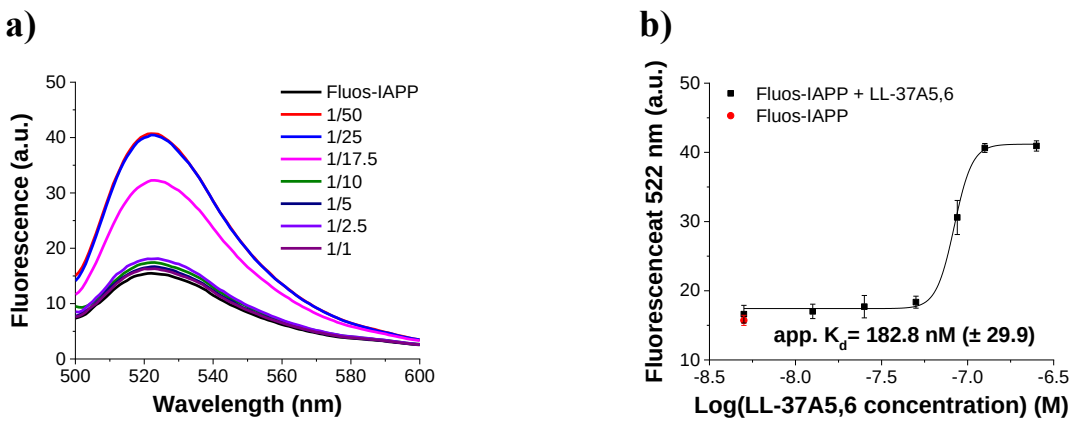

Figure 80. Determination of app. K_ds of interactions of oligomeric LL-37A5,6 species with monomeric IAPP by fluorescence spectroscopy. a) Fluorescence spectra of Fluos-IAPP (5nM) alone and its mixtures with various amounts of LL-37A5,6; the molar ratios of Fluos-IAPP/LL-37A5,6 are as indicated; b) binding curves of Fluos-IAPP with LL-37A5,6; app. K_ds are means (±SD) from 3 binding curves. Measurements were performed in aqueous buffer 1×b, pH 7.4, containing 1% HFIP.

LL-37(3-37)A5,6 bound to monomeric IAPP with an app. K_d of 22.9 (± 4.9) nM (Figure 81). As the previous alanine mutant, also LL-37(3-37)A5,6 showed no influence of the alanine substitutions on the binding affinity to Fluos-IAPP.

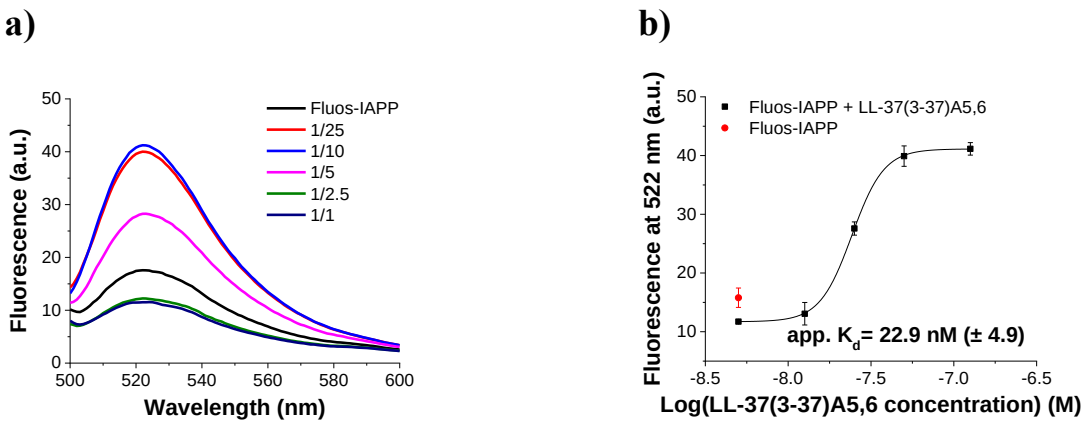

Figure 81. Determination of app. K_ds of interactions of oligomeric LL-37(3-37)A5,6 species with monomeric IAPP by fluorescence spectroscopy. a) Fluorescence spectra of Fluos-IAPP (5nM) alone and its mixtures with various amounts of LL-37(3-37)A5,6; the molar ratios of Fluos-IAPP/LL-37(3-37)A5,6 are as indicated; b) binding curves of Fluos-IAPP with LL-37(3-37)A5,6; app. K_ds are means (±SD) from 3 binding curves. Measurements were performed in aqueous buffer 1×b, pH 7.4, containing 1% HFIP.

Finally LL-37(5-37)A5,6 exhibited a binding affinity towards Fluos-IAPP with an app. K_d of 173.5 (± 106.6) nM (Figure 82). In this case, the binding is circa two times weaker than the app. K_d of the binding of LL-37 to monomeric IAPP.

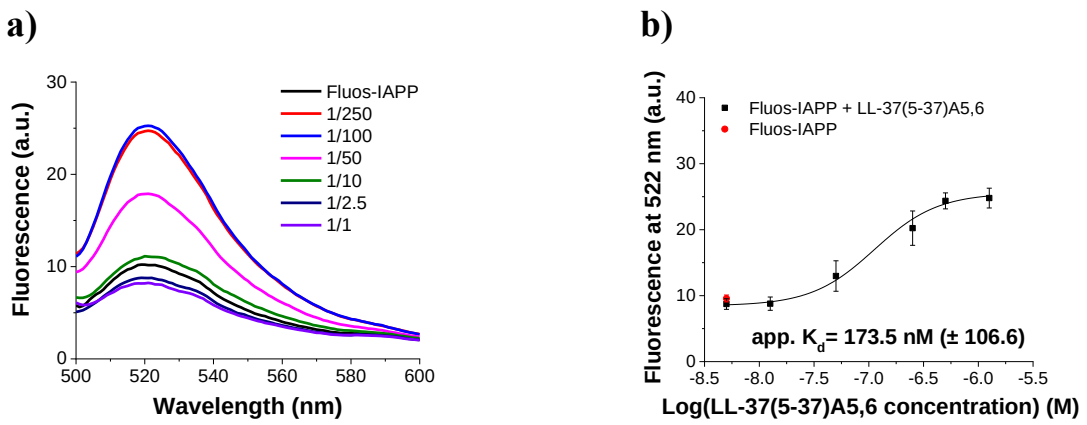

Figure 82. Determination of app. K_ds of interactions of oligomeric LL-37(5-37)A5,6 species with monomeric IAPP by fluorescence spectroscopy. a) Fluorescence spectra of Fluos-IAPP (5nM) alone and its mixtures with various amounts of LL-37(5-37)A5,6; the molar ratios of Fluos-IAPP/LL-37(5-37)A5,6 are as indicated; b) binding curves of Fluos-IAPP with LL-37(5-37)A5,6; app. K_ds are means (±SD) from 3 binding curves. Measurements were performed in aqueous buffer 1×b, pH 7.4, containing 1% HFIP.

Taken together, results provide the evidence that the Phe5 and Phe6 residues do not significantly contribute to the binding potency of LL-37 to IAPP monomers, considering that all obtained app. K_ds are all comparable to the app. K_ds of the correspondent native peptides (Table 29).

Table 29. Effect of alanine mutation of Phe5 and Phe6 on the binding to monomeric IAPP and determination of apparent binding affinities ($K_{d,app}$) by fluorescence titration assays.

LL-37 segments	**$K_{d,app}$ (±SD) (for Fluos-IAPP)[a]**
LL-37	88.1 (± 12.0) nM
LL-37A5,6	182.8 (± 29.9) nM
LL-37(3-37)	101.9 (± 56.0) nM
LL-37(3-37)A5,6	22.9 (± 4.9) nM
LL-37(5-37)	56.5 (± 8.8) nM
LL-37(5-37)A5,6	173.5 (± 106.6) nM

[a] App. K_ds, means (±SD) from 3 binding curves. Determined via titrations of fluorescein-labeled IAPP (Fluos-IAPP, 5nM) with non-labeled LL-37 alanine mutants (aq. buffer 1×b, pH 7.4, containing 1% HFIP).

4.3.5 Role of aromatic residues in the IAPP/LL-37 interaction interface via fluorescence spectroscopic titrations

Via fluorescence spectroscopic titrations we asked whether the phenylalanine residues in positions 5 and 6 of LL-37 are interacting with the phenylalanine residues in positions 15 and 23 of the IAPP sequence. In fact, it has been shown that Phe5 and Phe6 are key residues of LL-37 tetrameric assemblies (79) and we asked whether they could also interact with the two aromatic residues of IAPP to form the hetero-complexes found via cross-linking studies. To address this question, N-terminal fluorescein-labeled IAPP containing alanine mutations in positions 15 and 23 (Fluos-A15,23, 5 nM) was titrated in aqueous 10 mM sodium phosphate buffer (1xb, pH 7.4) containing 1% HFIP with different amounts of LL-37A5,6. The four aromatic residues seem not to mediate the interaction between the peptides. The app. K_d value of 132.3 (± 78.5) nM was in the same range as the app. K_d of the interaction of monomeric IAPP and LL-37 (Figure 83).

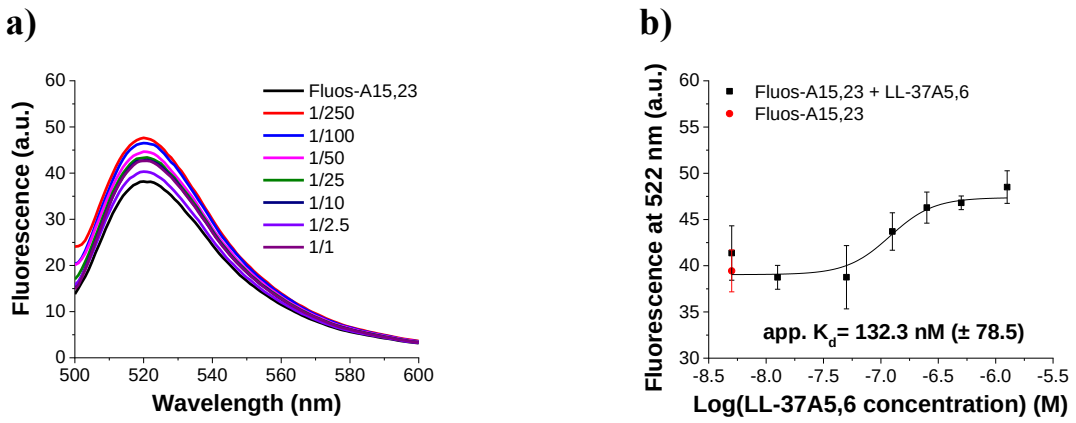

Figure 83. Determination of app. K_ds of interactions of oligomeric LL-37A5,6 species with IAPP alanine mutant, A15,23, by fluorescence spectroscopy. a) Fluorescence spectra of Fluos-A15,23 (5nM) alone and its mixtures with various amounts of LL-37A5,6; the molar ratios of Fluos-A15,23/LL-37A5,6 are as indicated; b) binding curve of Fluos-A15,23 with LL-37A5,6; app. K_ds are means (±SD) from 3 binding curves. Measurements were performed in aqueous buffer 1×b, pH 7.4, containing 1% HFIP.

As the results did not confirm our hypothesis, no further investigations on the role of these four aromatic residues were carried out.

4.3.6 Characterization of the LL-37 Ala mutants/IAPP hetero-assemblies by cross-linking

The formation of the IAPP/LL-37 alanine mutants hetero-complexes was studied via NuPAGE electrophoresis followed by Western Blot (WB). IAPP (30 µM) and its mixtures in a 1/1 molar ratio with LL-37A5,6, LL-37(3-37)A5,6, and LL-37(5-37)A5,6 were incubated for 30 minutes. As controls, 1/1 mixtures with LL-37, LL-37(3-37), and LL-37(5-37) were added to evaluate the effect of the alanine mutations of the hetero-complexes formation. As previously shown, IAPP consists of low MW complexes that go from di- to hexamers, and of high MW aggregates. As shown in section 4.2.5, at 30 minutes, incubations of IAPP with LL-37, LL-37(3-37), and LL-37(5-37) present the band at 15 kDa, which is not visible in IAPP alone and can be attributed to a hetero-tetrameric complex between the two peptides. Low MW species, as well as an intense smear, are also present due to the formation of high MW complexes. When IAPP is mixed with LL-37A5,6 and LL-37(3-37)A5,6, the hetero-complex at 15 kDa is still present, as well as the high MW assemblies. In fact, these two peptides can inhibit IAPP fibril formation for at least 24 hours, therefore the presence of the hetero-complex band was expected. Only the mixture of IAPP with the non-inhibitor LL-37(5-37)A5,6 displayed only high MW complexes and not any hetero-tetramer (Figure 84). The results suggest that the mechanism of inhibition of IAPP self-assembly involves the formation of a tetrameric structure between IAPP and the inhibitor. Of note, WB with anti-LL-37 antibody confirmed the presence of a homo-tetramer in all the peptides alone. Results indicate that although the homo-tetrameric complex is formed by all peptides, the hetero-tetramer is formed only by the inhibitors of IAPP fibril formation (Appendix Figure A 13a).

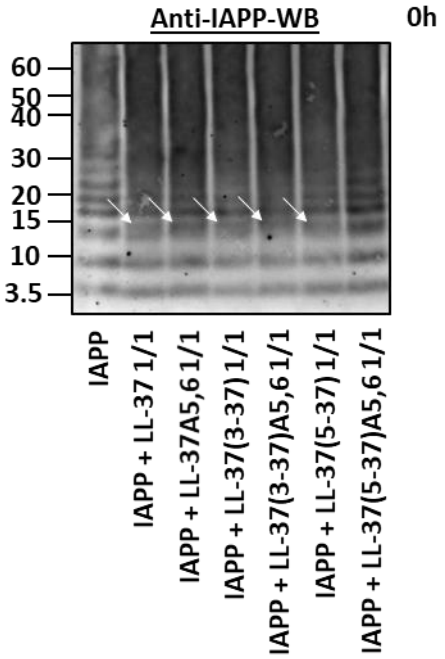

Figure 84. Characterization of the LL-37 double alanine mutants/IAPP hetero-assemblies via cross-linking (pH 7.4). NuPAGE and WB with IAPP (30 μM) and its mixtures with LL-37 (1/1), LL-37A5,6 (1/1), LL-37(3-37) (1/1), LL-37(3-37)A5,6 (1/1), LL-37(5-37) (1/1), and LL-37(5-37)A5,6 (1/1) is shown after aging the incubations for 30 minutes. Representative gel is reported (n>4).

Moreover, the formation of hetero-assemblies between IAPP and LL-37A5 and LL-37A6 was evaluated via NuPAGE electrophoresis and Western blot. For this purpose, IAPP (30 μM) was incubated for 30 min or 7 days alone and with the two single alanine mutants in a 1/1 ratio. As a control, the 1/1 mixture of IAPP with LL-37 or LL-37A5,6 were added. The pattern observed after 30 minutes of incubation time was very similar to the one observed for the double alanine mutant described above. IAPP presented low and high MW complexes, while its mixture with LL-37, LL-37A5,6, LL-37A5, and LL-37A6 presented the hetero-tetrameric structure, as well as high MW assemblies. All these peptides present inhibition capability at least for 24 hours and results confirmed that the hetero-complex formation occurs when inhibition of IAPP fibrillogenesis is observed (Figure 85a). After 7 days of incubation time, the low MW complexes are less prominent, while the high MW complexes are still present. The band at 15 kDa is still clearly present for the mixture of IAPP with LL-37, but for the mixtures with LL-37A5,6, LL-37A5 and LL-37A6 the hetero-complex is diminished. The result correlates with the incapability of these alanine mutants to inhibit IAPP fibril formation until 168 hours (Figure 85b). Additionally, WB with anti-LL-37 antibody confirmed the presence of the hetero-complex at 15 kDa in the 1/1 mixtures, as shown in Figure 85. Of note, all inhibitors, as well as non-inhibitors, form a homo-complex, likely a tetramer, that corresponds to a band at 15 kDa in the incubations of the peptides alone (Appendix Figure A 13b).

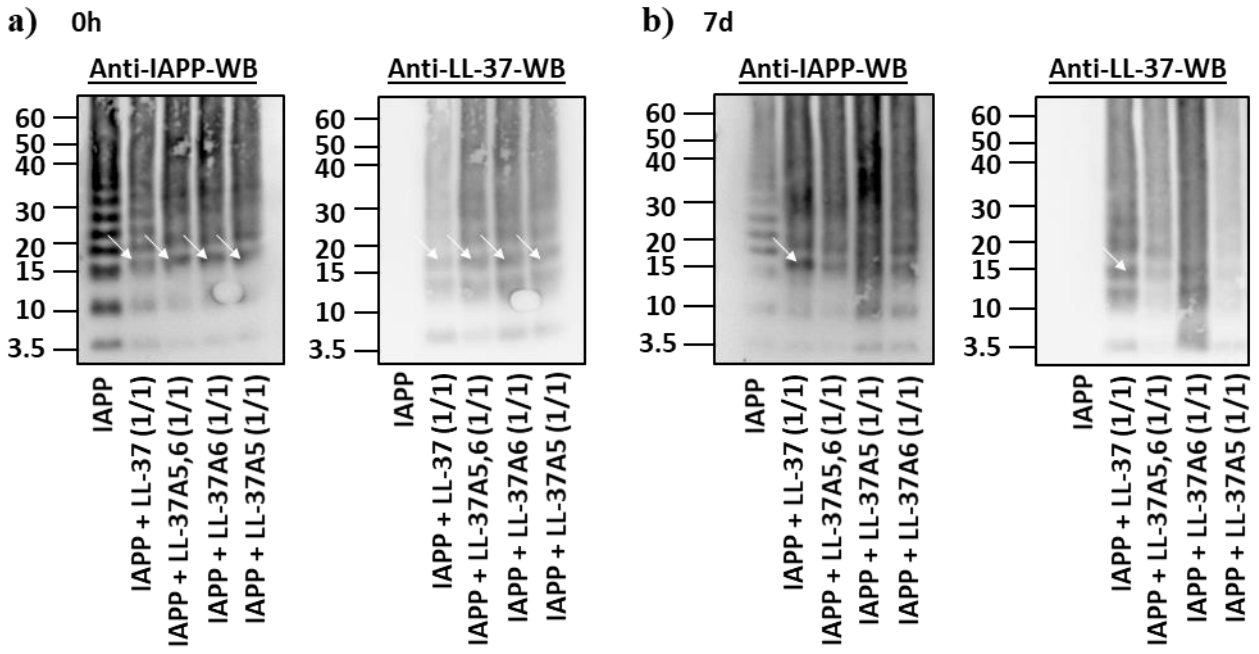

Figure 85. Characterization of the LL-37, LL-37A5,6, LL-37A5, and LL-37A6-IAPP hetero-assemblies via cross-linking (pH 7.4). NuPAGE and WB with IAPP (30 μM) and its mixtures with LL-37 (1/1), LL-37A5,6 (1/1), LL-37A5 (1/1), and LL-37A6 (1/1) is shown after aging the incubations for 30 minutes (a) or 7 days (b). Representative gel is reported (n=2).

4.3.7 Studies on the inhibitory activity of FF alanine mutated LL-37 on fibrillogenesis and cytotoxicity of Aβ42

It has been previously shown that LL-37 is a binding partner of Aβ42. Additionally, LL-37 plays a protective role against microglia-mediated Aβ42 toxicity to SH-SY5Y neuroblastoma cells and efficiently inhibits Aβ42 fibril formation (99). We asked whether LL-37 could inhibit Aβ42 in our system and whether the alanine mutant, LL-37A5,6 has a different inhibitory effect, as the phenylalanine residues were found to be crucial for the inhibitory role against IAPP fibril formation. Briefly, Aβ42 alone (5 μM) and its 1/1 mixture with LL-37 or LL-37A5,6 were incubated for 6 days and the kinetics of Aβ42 fibril formation and its cytotoxicity were monitored by ThT binding and MTT reduction assays respectively. In this system, Aβ42 forms β-sheet rich species that bind the ThT dye within 3 hours. The 1/1 mixture with LL-37 showed full inhibition of the fibril formation for the whole duration of the assay. LL-37A5,6 showed a weaker inhibitory effect. In fact, the profile of the aggregation kinetics has a similar profile to the one of Aβ42, but with a strongly decreased ThT signal, suggesting that the amount of β-sheet aggregates is lower. Of note, LL-37 and LL-37A5,6 alone (5 μM) were added to assure that the peptides do not aggregate in these experimental conditions (Figure 86a, b). After 6 days, PC-12 cells were treated with the incubations above described. Aβ42 exhibited the highest toxicity to PC-12 cells, while its mixture with LL-37 inhibited the cytotoxicity. Also, LL-37A5,6 partially blocked the cytotoxicity, although its effect was lower than the effect of LL-37. Incubations of peptides alone showed no cytotoxicity effect (Figure 86c). TEM images confirm the presence of fibrils in the incubation of Aβ42 alone, while amorphous aggregates were the most abundant species in the 1/1 incubations of Aβ42 and LL-37 and LL-37A5,6 (Figure 86d). These findings correlate with the ThT binding assay results, as both peptides exhibit an effect on the fibrillogenesis of Aβ42. Results of these assays confirm that Phe5 and Phe6 have a significant effect on the inhibitory potency of LL-37 against Aβ42 as well. The effect is more pronounced in the case of the inhibition of IAPP fibrillogenesis, but it is still present for the inhibition of Aβ42.

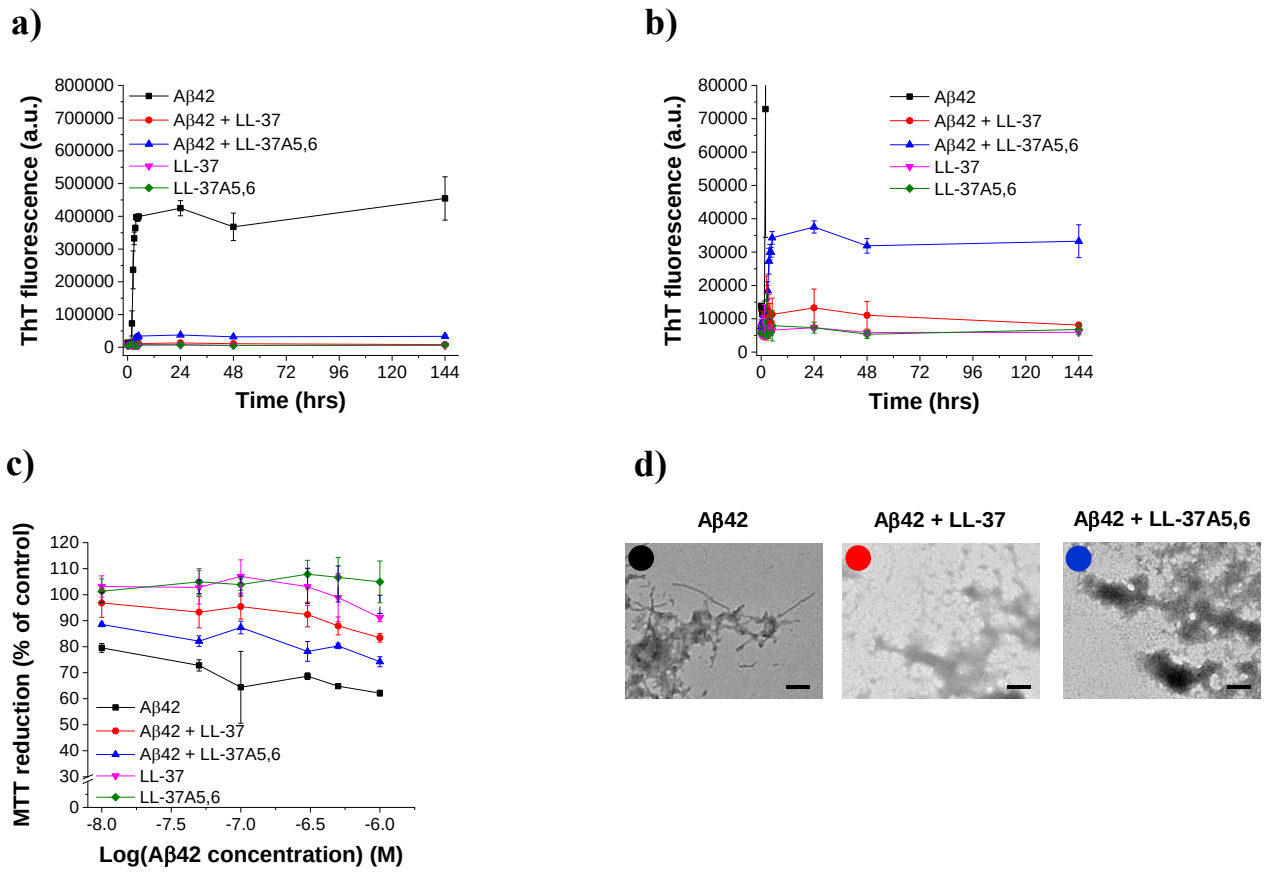

Figure 86. Effects of LL-37 and LL-37A5,6 on Aβ42 amyloid formation and cytotoxicity. a) Fibrillogenesis of Aβ42 (5 µM) and its mixtures with LL-37 (1/1) or LL-37A5,6 (1/1) (means (±SD), 3 assays); b) zoom-in of a); c) effects on cell viability: solutions from a) were added to cultured PC-12 cells (6 days aged). Cell viability was determined by MTT reduction (means (±SD), 1 assay, n=3 each); d) TEM images of solutions of a) (6 days aged) as indicated (bars, 100 nm).

4.3.8 Determination of binding affinity towards Aβ40

Previous studies proved that LL-37 is a binding partner of amyloid beta and that it is able to inhibit its aggregation into neurotoxic species (99). We verified this interaction in our experimental conditions. Fluorescence spectroscopic titrations were carried out to evaluate the binding affinity to Aβ40. N-terminal fluorescently labeled Aβ40 (7-diethylaminocoumarin-3-carbonyl-Aβ40), also named DAC-Aβ (20 nM), was titrated with increasing amounts of LL-37 to evaluate the apparent K_d of their binding affinity. The app. K_d could not be determined although it resulted to be higher than 10 µM, as there is an increase of the fluorescence signal confirming that the two peptides are binding (Figure 87a, b). Additionally, to evaluate if there is an interaction of LL-37 with oligomeric Aβ40, N-terminal fluorescein-labeled LL-37 (FAM-LL-37, 5 nM) was titrated with various amounts of Aβ40. No app. K_d value could be determined until 5 µM of amyloid beta concentration (Figure 87c, d).

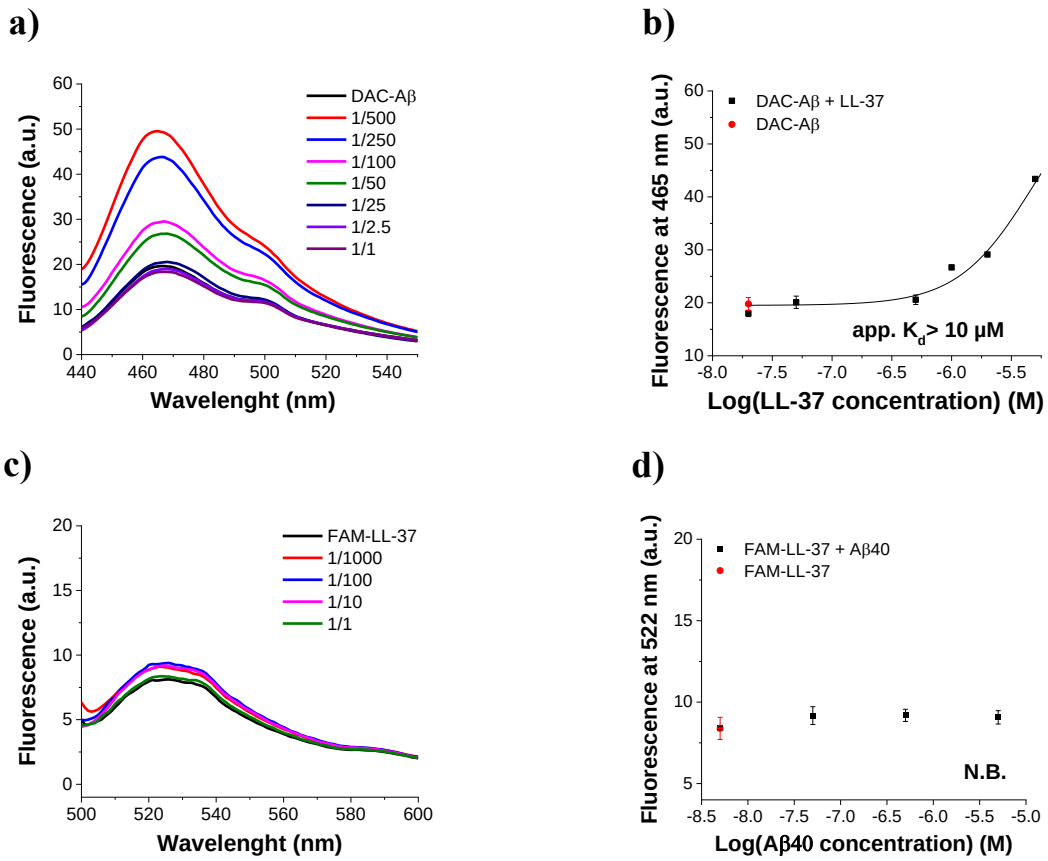

Figure 87. Determination of app. K_ds of interactions of LL-37 with monomeric and oligomeric Aβ40 by fluorescence titrations. a) Fluorescence emission spectra of DAC-Aβ (20 nM) alone and its mixtures with increasing amounts of LL-37. b) Binding curve of DAC-Aβ to LL-37. c) Fluorescence emission spectra of FAM-LL-37 (5 nM) alone and its mixtures with increasing amounts of Aβ40. d) Binding curve of FAM-LL-37 to Aβ40. Binding curves are means of 3 assays (±SD) (aqueous buffer 1×b, pH 7.4, containing 1% HFIP).

4.3.9 Conclusions: identification of FF as key residues for the inhibitory potency of LL-37 on IAPP amyloidogenesis

In this third part of my work, the role of Phe5 and Phe6 in the interaction and inhibitory effect of LL-37 on IAPP was investigated. The studies with partial sequences showed that the removal of these two residues from the sequence entailed the total loss of inhibitory function of IAPP fibrillogenesis. To confirm these findings, double and single alanine mutants of LL-37 were synthesized. LL-37A5,6 could only partially intervene in the aggregation of IAPP, and fibrils were the main species found in the 1/1 mixture of IAPP/LL-37A5,6 after 7 days of incubation. Compared to the native peptide, LL-37A5,6 is at least a 10-fold weaker inhibitor, confirming the crucial role of the two phenylalanine residues. LL-37(3-37)A5,6 exhibited a similar result. Compared to the inhibitor LL-37(3-37), this peptide had almost no effect on IAPP aggregation and cytotoxicity. Last, also LL-37(5-37)A5,6 has no inhibitory potency compared to its native correspondent LL-37(5-37). Taken together, results confirmed that Phe5 and Phe6 are necessary to have an inhibitory effect on IAPP aggregation. As a next step, we investigated the role of each phenylalanine, and LL-37A5 and LL-37A6 were synthesized and characterized. These two peptides exhibited very similar inhibitory potency to LL-37A5,6: the substitution of only one residue delayed the lag phase of the IAPP aggregation in the same way the double alanine mutant does, confirming no additive effect. All double alanine mutants display α-helical structures, the single alanine mutants LL-37A5 and LL-37A6 show an α-helix and β-sheet/turn content, but none is an inhibitor of IAPP self-association.

Next, we asked whether Phe5 and Phe6 have a role in binding monomeric IAPP. All the single and the double alanine mutants bound Fluos-IAPP with an app. K_d in the nanomolar range, as LL-37. Findings showed that these two residues do not influence the binding affinity to IAPP. When cross-linking experiments at time zero were carried out, a hetero-tetrameric complex (~15 kDa) between IAPP and LL-37 alanine mutants was observed only when inhibition at least for 24 hours was observed. LL-37(5-37)A5,6 is the only peptide that has no inhibitory potency at all and consequently formed no hetero-tetramer with IAPP, confirming that this hetero-complex occurs each time there is an inhibitory effect. It has been already shown that LL-37 is an inhibitor of Aβ42 aggregation. We finally asked whether Phe5 and Phe6 have an effect on the inhibitory potency of LL-37 on Aβ42 self-assembly. LL-37A5,6 showed a weaker inhibitory effect than LL-37 on Aβ42 self-assembly and cytotoxicity, indicating that the two phenylalanine residues play a role in the inhibitory potency of LL-37 (Table 30).

Table 30. Overview of the biophysical characterization and interactions of LL-37 Phe5 and Phe6 alanine mutants with IAPP.

Peptide	Inhibition of IAPP fibril formation	Secondary structure (1xb + 1% HFIP)	IAPP/LL-37 hetero-tetramer (~15 kDa)	Binding affinity to monomeric IAPP
LL-37	✓	α-helix/β-sheet	✓	88.1 (± 12.0) nM
LL-37A5,6	partially ✓	α-helix	✓	182.8 (± 29.9) nM
LL-37A5	partially ✓	α-helix/β-sheet	✓	-
LL-37A6	partially ✓	α-helix/β-sheet	✓	-
LL-37(3-37)	✓	α-helix/β-sheet	✓	101.9 (± 56) nM
LL-37(3-37)A5,6	✗	α-helix	✗	22.9 (± 4.9) nM
LL-37(5-37)	partially ✓	α-helix	✓	56.5 (± 8.8) nM
LL-37(5-37)A5,6	✗	partially unordered	✗	173.5 (± 106.6) nM

Legend: ✓= the peptide is an inhibitor of IAPP amyloid formation; ✗= the peptide cannot block IAPP amyloid formation; - = not determined.

5 Discussion

Diabetes type 2 (T2D) is a widespread disease, characterized by insulin resistance and β-cell degeneration (10). Pathogenesis of T2D is also linked to the self-association of amylin (IAPP), which is monomeric and disordered in healthy individuals, leading to pancreatic inflammation, β-cell degeneration, and apoptosis (11). Antimicrobial peptides (AMPs) are part of the mammalian innate immunity and are known for their immunoregulatory and anti-inflammatory roles (54, 66). A subgroup of AMPs is composed of cathelicidins, characterized by the structure of their preprotein, which contains a conserved N-terminal cathelin domain and a C-terminal domain that has antimicrobial properties (54). LL-37 is so far the only human cathelicidin known (66). This 37-residue peptide not only plays a role in innate immunity, but also its mouse orthologue CRAMP was found to suppress inflammation in pancreatic β-cells in a T1D mouse model (98). Moreover, LL-37 was found to be a binding partner of Aβ42, suppressing its aggregation into cytotoxic species (99). Studies prove that polypeptides interact and interfere with amyloid fibril formation (51, 99, 134). The interaction of LL-37 with amyloids is a novel additional function that underlines the biomedical importance of this peptide.

5.1 The human LL-37 as a potent inhibitor of IAPP self-assembly

LL-37 was previously found to be a binding partner and an inhibitor of Aβ42 amyloidogenesis and cytotoxicity (99). In addition, the two amyloidogenic polypeptides, Aβ and IAPP share 50% of sequence similarity and 25% of sequence identity and cross-interact (52). For the reasons described above, the first question that was answered in this work is whether LL-37 could interact with IAPP and interfere with its aggregation into cytotoxic species.

As previously done for Aβ40 and IAPP (50), a sequence alignment was preliminarily performed between the sequences of the two peptides: it was shown that LL-37 and IAPP exhibit similar residues extending the sequence of both peptides, yielding to 42% of sequence similarity, and 5% of sequence identity. Interestingly, the sequence similarities between Aβ40 and IAPP, and LL-37 and IAPP are located in the same IAPP region (Scheme 2).

```
Aβ40 DAEFRHDSGYEVHHQKLVFFAEDVGSNKGAIIGLM VGGVV
          . . .    :. . :.    .: :::.    ::
IAPP      KCNTATCATQRLANFLVHSSNNFGAILSSTNVGSNTY
            .    . ..... . .  . .  .: .  :  .
LL-37    LLGDFFRKSKEKIGKEFKRIVQRIKDF LRNL-VPRTES
```

identity: 25%
similarity: 50%

identity: 5%
similarity: 42%

Scheme 2. Primary structure of Aβ40, IAPP, and LL-37. Identical residues between Aβ40 and IAPP or IAPP and LL-37 are indicated with two dots and similar residues are indicated with one dot.

The inhibitory effect of LL-37 on IAPP amyloid self-assembly was studied via ThT binding and MTT reduction assays in combination with TEM. Assays proved the inhibitory capacity of LL-37 when mixed in equimolar ratio with IAPP (1/1) until 168 hours of both fibrillogenesis and cytotoxicity of IAPP to RIN5fm cells. A scrambled sequence of LL-37 did not have a similar effect on IAPP amyloidogenesis up to 10-fold excess of peptide, as shown in Figure 88, indicating the importance of the primary structure of LL-37.

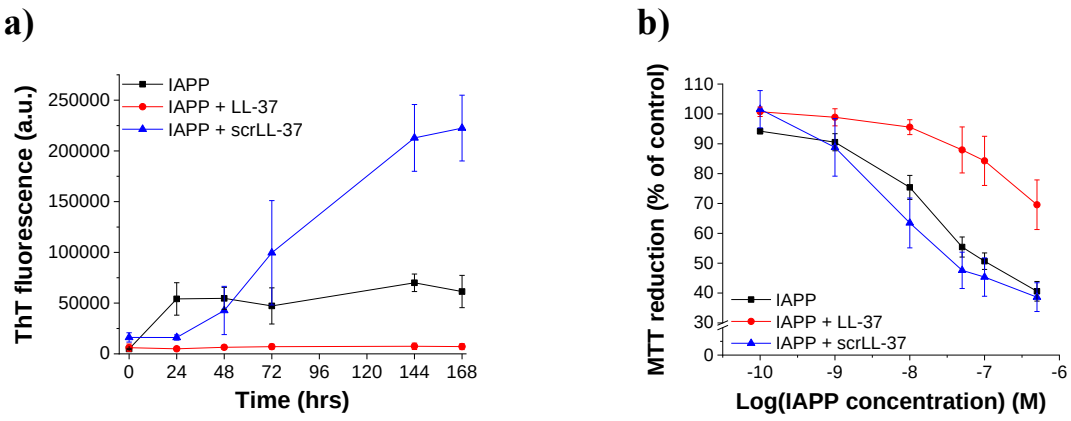

Figure 88. Effects of LL-37 and scrLL-37 on IAPP amyloid formation and cytotoxicity. a) Fibrillogenesis of IAPP (16.5 μM) and its mixtures with LL-37 (1/1) or scrambled LL-37 (1/10) (means (±SD), 3 assays). b) Effects on cell viability: solutions from a) were added to cultured RIN5fm cells (7 days aged). Cell viability was determined by MTT reduction (means (±SD), 3 assays, n=3 each). Data of this figure is taken from Armiento et al. (ACIE, 2020) (114).

Several studies prove that the primary structure of LL-37 is important for LL-37 to perform several of its biological functions (80, 135, 136). Scrambled sequences are inactive in activating receptors that regulate cell proliferation in the site of tissue damage and cell inflammation (135), or in the regulation of proinflammatory responses induced by cytokines (136) due to the lower helical-forming propensity.

ThT assay results were confirmed by TEM images, which revealed amorphous aggregates as the main species at 168 hours for the IAPP/LL-37 1/1 mixture, in contrast to the IAPP/scrLL-37 1/1 and 1/10 mixtures and IAPP alone which presented fibrils with similar morphology as the main species. Consistent with previous findings (79, 137), in addition to amorphous aggregates, fibrils with a different morphology than amylin ones were observed also in LL-37 alone. LL-37 alone was also found not to be cytotoxic and not to bind ThT dye. Several studies were carried out to study the LL-37 fibrils. Microscopy experiments revealed that LL-37 forms fibrous aggregates upon the addition of liposomes. These fibrils exhibited green light birefringence after Congo red staining, revealing their amyloid-like features (138). The ability of LL-37 to destabilize and form pores in membranes is attributed to these fiber-like structures (139). On the other hand, studies showed that the antibacterial core of LL-37, LL-37(17-29), forms supra-helical stable fibrils, lacking amyloid β-sheet structure, and is unable to bind amyloid indicator ThT dye, unlike the cross-α amyloid fibrils of the bacterial cytotoxic PSMα3 (140). This finding might suggest that in our experimental conditions LL-37 forms fibrils composed of amphipathic α-helices, with no amyloid-related feature.

The inhibitory potency of LL-37 was supported by the obtained value of the IC_{50} at 24 hours at 100 nM, which is equal to 17 nM. Results suggest that LL-37 interacts with non-toxic and prefibrillar IAPP species, forming hetero-assemblies which block its aggregation into toxic IAPP oligomers and fibrils (Figure 89).

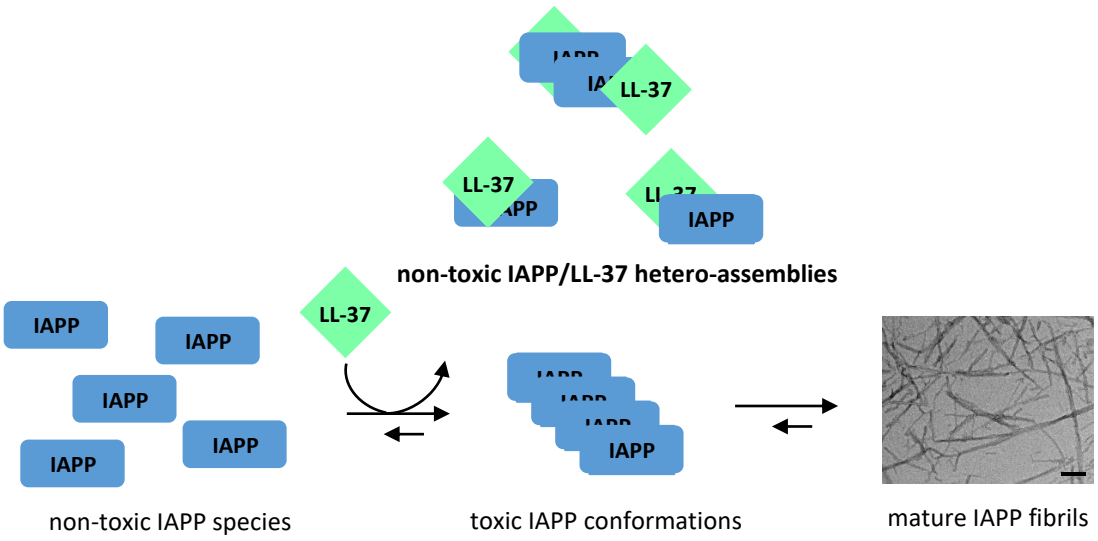

Figure 89. Proposed molecular models of LL-37 with non-toxic IAPP species. LL-37 sequesters early prefibrillar IAPP species resulting in an attenuation of the formation of toxic IAPP assemblies or mature fibrils.

An unexpected result was observed when the same experiment was carried out in a 1/5 molar ratio of IAPP and LL-37 respectively. Although the amyloid fibril formation was completely blocked for the whole duration of the assay, the cytotoxic effect could not be blocked. It seems that the two peptides form cytotoxic assemblies that do not occur when the peptides are mixed in an equimolar ratio. Via TEM it was possible to highlight the presence of large fibrillar assemblies, with a different morphology of IAPP amyloid fibrils. It has been proven that LL-37 is cytotoxic against several eukaryotic cells by the formation of transmembrane pores (80, 85). Of note, LL-37 alone in 5-fold excess showed no fibrillar species in TEM images and had no cytotoxic effect on RIN5fm cells in our studies, results that suggest that the complex between the two peptides confers toxicity to cells. To clarify the mechanism of the formation of toxic species, further studies should be carried out to characterize the structure and the properties of the IAPP/LL-37 hetero-assemblies.

It is known that the kinetics of the aggregation of IAPP into amyloid fibrils is accelerated by the presence of IAPP preformed fibrils, having a seeding effect on amyloidogenesis (118). The presence of LL-37 in an equimolar ratio to IAPP interferes with the nucleation kinetics of IAPP in the presence of 10% fIAPP, suppressing the fibril formation. This result led to the hypothesis that LL-37 could bind to fIAPP, which was verified in a first approach via dot blot assay. Results from dot blot and fluorescence spectroscopic titration studies showed that LL-37 can bind to both IAPP monomeric and fibrillar species. Additionally, LL-37 did not bind glucagon, which forms amyloid-like fibrils (141), consistent with the specific interaction with IAPP fibrils.

As LL-37 was found to bind fIAPP, we incubated fIAPP with LL-37 in 10-fold excess and used these treated fibrils to seed IAPP fibril formation, in comparison to fIAPP. Clearly, the treated fibrils were unable to seed IAPP, leading to the conclusion that LL-37 binds to fIAPP converting them into seeding incompetent species. TEM confirmed a clear difference between the morphology of fIAPP and of the LL-37 treated fIAPP. In fact, the LL-37 treated fibrils form large sheet-like fibrils sticking laterally to each other, while fIAPP do not form these large assemblies. As a control, the same experiment was also carried out by incubating fIAPP with an equimolar ratio of LL-37, and these treated fibrils were used for seeding IAPP. In this case, no inhibition of the seeding effect was shown. In fact, the kinetics of IAPP aggregation resulted similar to when IAPP is seeded with fIAPP. For this reason, we next asked whether the excess of LL-37 used to treat the fIAPP was the reason for this inhibitory effect. To exclude this eventuality, we carried out the same experiment using treated-fIAPP with 10x LL-37 after separating them from the unbound LL-37 by centrifugation before using them to seed IAPP. The presence of the treated fIAPP in the pellet and of the excess of LL-37 in the supernatants were confirmed via dot blot assay. Results of this trial were very similar to the experiment carried out without any

centrifugation confirming that the inhibitory effect was not caused by unbound LL-37. The IAPP seeding studies suggest that LL-37 binds not only to monomeric IAPP but also to IAPP fibrils and converts them into seeding-incompetent species.

The dot blot assay mentioned above showed that LL-37 is also able to bind monomeric IAPP additionally to IAPP fibrils. The app. K_d of the binding affinity to monomeric IAPP determined by fluorescence spectroscopy titration was found to be 88.1 (± 12.0) nM, confirming the high interaction affinity between the two peptides. The titration carried out to determine the binding affinity to IAPP oligomers was found to be in the μM range suggesting a lower affinity between LL-37 and IAPP oligomers (Table 31).

Table 31. Binding of LL-37 to IAPP monomers, oligomers, or fibrils determined via fluorescence spectroscopy titrations or dot blot assays.

IAPP species	**$K_{d,app}$ (±SD) via fluorescence spectroscopy titrations[a]**	**Binding via dot blot[b]**
Monomers	88.1 (± 12.0) nM (for Fluos-IAPP)	Binding
Oligomers	> 2.5 μM (for FAM-LL-37)	-
Fibrils	-	Binding

[a] App. K_ds, means (±SD) from 3 binding curves (aq. buffer 1×b, pH 7.4, containing 1% HFIP). [b] Binding of FAM-LL-37 to IAPP monomers and fibrils. (IAPP monomers and fIAPP were spotted onto a nitrocellulose membrane and probed with 0.2 μM FAM-LL-37).

The effects of LL-37 on IAPP misfolding were studied by far-UV CD spectroscopy (118). Spectra were measured in 1xb in presence of 1% HFIP, an alcohol with denaturing properties that disrupts the self-assembly of amyloid-forming peptides (142). These conditions were applied to follow the kinetics of IAPP fibril formation in aqueous solution. As already shown, the presence of 1% HFIP led to reproducible experimental conditions for IAPP misfolding (118). In fact, at time zero IAPP shows majorly an unordered secondary structure with a minimum at 200 nm. The spectra recorded for IAPP at different time points, clearly indicate that it misfolds into β-sheet rich assemblies, followed by precipitation at 24 hours due to fibril formation (Figure 90a). The CD spectra at time zero of the IAPP/LL-37 mixture resulted to have a similar structure to the spectra of LL-37 alone, but there is a clear difference between the spectrum of the mixtures from the sum of the spectra of the two peptides, indicating an interaction between the two. This feature was not observed in the 1/1 mixture of IAPP and scrLL-37, indicating no interaction between the two peptides and no effect on IAPP secondary structure from scrLL-37. By contrast, the IAPP/LL-37 mixture exhibited an increasing random coil content indicating the formation of soluble and unordered hetero-complexes and the suppression of IAPP misfolding into β-sheet rich fibrils (Figure 90b). The spectra of LL-37 alone at time zero exhibited a maximum around 198 nm and two minima, a pronounced one at 227 nm due to an $n \rightarrow \pi^*$ transition and one at 210 nm, indicating mainly an α-helix and/or β-sheet secondary structure. The α-helix formation of LL-37 is known to be concentration-dependent. In a monomeric form, LL-37 is unstructured and it assembles into ordered helical structures in its oligomeric state (79, 80). This behavior is led by the amphipathic nature of this peptide, which tends to fold into helices to avoid contact between the apolar residues and the solution (80). Furthermore, crystal structural studies evidenced that in the presence or absence of detergents LL-37 displays an anti-parallel dimer formed by two α-helices, which arrange in a head-to-tail manner to form tetrameric supramolecular structures (79). Time-dependent spectra of LL-37, show an overall decrease of the signal, probably due to oligomerization, and a transition from an α-helix/β-sheet and β-turn, to an α-helix secondary structure (Figure 90c).

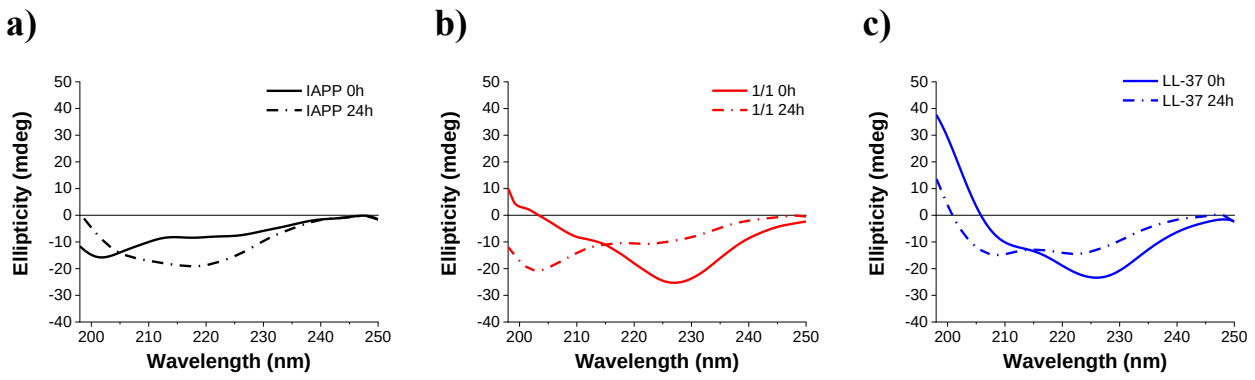

Figure 90. Characterization of the IAPP/LL-37 interaction. Far-UV CD spectra of (a) IAPP (black lines, 5 µM), (b) IAPP/LL-37 mixture (red lines, 1/1, 5 µM each), and (c) LL-37 (blue lines, 5 µM). Continuous lines represent CD spectra at 0 hours and dotted lines represent spectra at 24 hours. Measurements were performed in aqueous buffer 1×b, pH 7.4, containing 1% HFIP.

As CD results suggested the formation of hetero-complexes, to further characterize these species, NuPAGE followed by Western Blot assay were performed. Using glutaraldehyde, the IAPP/LL-37 complexes were cross-linked and then separated by NuPAGE. The complexes were then observed through WB analysis and anti-IAPP and anti-LL-37 antibodies. Anti-IAPP WB showed that IAPP solutions contained low MW oligomers extending from dimers to hexamers, as well as high MW aggregates as visible from the smear band at the top of the gel. When IAPP was mixed with LL-37 in 1/0.1, the pattern of the bands was the same as IAPP, since the concentration of LL-37 was not enough to have an inhibitory effect. The IAPP/LL-37 1/1 mixture exhibited a different pattern: the low molecular weight oligomers present in the incubation of IAPP alone, and to which the cytotoxic effect is attributed to (143-145), were not observed, whereas a novel band at ~15 kDa was found, confirming the presence of an IAPP/LL-37 hetero-complex attributable to hetero-tetramers. Interestingly the hetero-tetramer is present also in the 1/2 and 1/5 (IAPP/LL-37) incubations, correlating with the ThT dye binding results, which confirmed the suppression of the amyloid formation. The band at ~15 kDa of the IAPP/LL-37 equimolar mixture was also found in the WB with anti-LL-37 antibody, confirming the presence of the hetero-complexes. As a control, LL-37 alone was incubated at the indicated concentrations and equally treated. The WB analysis with anti-LL-37 showed the band at 15 kDa as well, attributable to homo-tetramers of LL-37. It has been shown that LL-37 mainly assembles into tetrameric structures and that these oligomers are building blocks for supramolecular structures responsible for the antibacterial effect of this peptide (79, 80, 133). Similarly, IAPP/LL-37 hetero-tetramers are the major hetero-oligomeric species found in the cross-linking studies, suggesting that their presence is crucial for the inhibitory effect of LL-37 on IAPP self-assembly (Figure 91).

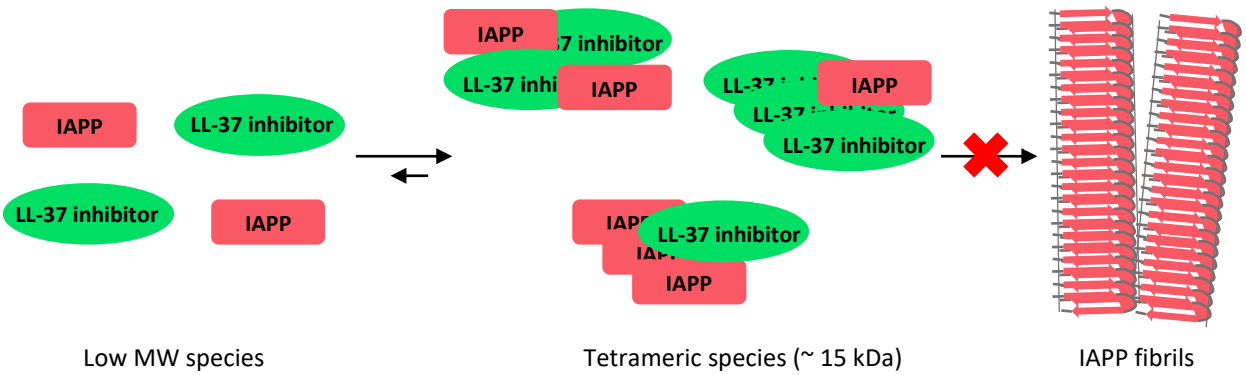

Figure 91. Proposed mechanism of the inhibition of IAPP fibril formation of LL-37 via the formation of hetero-tetramers of IAPP and LL-37.

To further characterize the IAPP/LL-37 hetero-complexes, we asked which was their geometry of interaction and which residues are involved at the interface. We assumed that the two peptides interact in a helical state since LL-37 and a pre-fibrillar IAPP are known to be α-helical (15, 79). A Rosetta docking of a 1/1 IAPP/LL-37 complex showed that residues Phe17, Leu28, Arg29, Leu31, Val32, Pro33 of LL-37 and Ala8, Leu12, and Asn22 of IAPP significantly contribute to stabilizing the interaction. Furthermore, the docking carried out in a 1/2 IAPP/LL-37 stoichiometry suggested that IAPP interacts mainly with one of the two helices and with residues involving the central/C-terminal region (residues from 12 to 32). On the other hand, one of the two LL-37 molecules interacts with its C-terminus as for the 1/1 complex.

Given these results, we questioned which are the regions of LL-37 mediating its interaction with IAPP. To address this question peptide array experiments were carried out. Decamers covering the full sequence of LL-37 shifted by one residue were synthesized. Glass slides probed with N-terminal fluorescently labeled IAPP revealed two binding regions of the LL-37 sequence: LL-37(1-15) and LL-37(18-34) corresponding to an N-terminal and a C-terminal segment respectively.

Furthermore, two "binding cores" within these regions were identified, which are LL-37(6-10) (FRKSK) and LL-37(25-27) (KDF). Interestingly the two binding cores found, in particular the C-terminal one, are included in the regions LL-37(17(18)-29) and LL-37(13-32) which are known to have antiviral, antibacterial, and immunoregulatory roles and have been used as a basis for drug design (54, 76, 130, 146). In particular, these roles were identified in the regions of the peptide which have more pronounced α-helical propensity and hydrophobicity (54, 147).

Subsequently, the regions and residues of the IAPP sequence that play an important role in its interaction with LL-37 were investigated. Within the IAPP sequence, IAPP(8-28) has been shown to be the major surface for both the self-interaction of IAPP and its cross-interaction with Aβ (26). In particular, IAPP(8-18) and IAPP(22-28) were identified as the "hot regions" of both the IAPP/IAPP and IAPP/Aβ interaction interface (26, 52). With the same rational approach, IAPP segments were titrated with different amounts of LL-37 and their binding affinity was obtained. The two IAPP segments, IAPP(1-18) and IAPP(19-37), which extend the whole IAPP sequence, led to a weak/no binding. IAPP(1-18) was found to bind with a $K_d > 1.25$ μM, while no binding until 1.25 μM was found for IAPP(19-37). Next, the core IAPP(8-28) and IAPP(8-28)GI were tested. IAPP(8-28)GI ([(N-Me)G24, (N-Me)I26]–IAPP(8-28)) is a double N-methylated IAPP mimic with high solubility but no inhibitory properties (26, 52) which was applied for as a substitute of the highly amyloidogenic segment IAPP(8-28). The two segments showed binding to LL-37. IAPP(8-28) bound with a $K_d > 1.25$ μM, while IAPP(8-28)GI showed a higher binding affinity. The app. K_d was 372.4 (± 64.3) nM, which is only a 4-fold weaker binding compared to the app. K_d of the binding affinity of LL-37 to Fluos-IAPP (88.1 (± 12.0) nM). The two segments IAPP(8-18) and IAPP(22-28) which dissect IAPP(8-28) into two parts showed no binding affinity to LL-37 until 1.25 μM, leading to the conclusion that their co-presence is required for the IAPP/LL-37 association. IAPP(1-7) also showed no binding affinity to LL-37, indicating that the N-terminus of IAPP is not involved in the IAPP/LL-37 interaction interface (Table 32). In conclusion, studies identified IAPP(1-18), and especially IAPP(8-28) as the binding cores for the IAPP/LL-37 interaction interface. The residues Ala8, Leu12, and Asn22, which are part of IAPP(8-28), were found via Rosetta docking to particularly stabilize the IAPP/LL-37 interaction. Taken together, these results underline the importance of this IAPP region for the interaction with LL-37. Instead, the two segments IAPP(8-18) and IAPP(22-28), which are crucial for the IAPP self-interaction and cross-interaction with Aβ, were found not to be sufficient for the interaction with LL-37.

Table 32. Identification of IAPP regions that bind full-length LL-37 and determination of apparent binding affinities ($K_{d,app}$) by fluorescence titration assays.

Fluos-IAPP segments	**$K_{d,app}$ (±SD) (for LL-37)[a]**
Fluos-IAPP(1-18)	> 1.25 µM
Fluos-IAPP(1-7)	n.b. [b]
Fluos-IAPP(19-37)	n.b. [b]
Fluos-IAPP(8-28)	> 1.25 µM
Fluos-IAPP(8-28)GI	372.4 (± 64.3) nM
Fluos-IAPP(8-18)	n.b. [b]
Fluos-IAPP(22-28)	n.b. [b]

[a] App. K_ds, means (±SD) from 3 binding curves. Determined via titrations of fluorescein-labeled peptides (Fluos-peptides, 5nM) with non-labeled LL-37. [b] n.b., no binding at peptide concentrations ≤ 1.25µM, (aq. buffer 1×b, pH 7.4, containing 1% HFIP).

Next, we asked within the 8-28 region, which are the key residues of the IAPP sequence for the interaction with LL-37. It has been already shown that Phe15, Leu16, Phe23, and Ile26 of the IAPP sequence are mediating the interaction with both IAPP and Aβ40(42). In fact, binding affinity studies proved that the interaction is dramatically affected if all four residues are replaced with alanine (128). Using the same rational approach, fluorescence spectroscopic titrations were carried out in which IAPP alanine mutants were titrated with increasing amounts of LL-37. Fluos-4Ala led to a weak binding affinity to LL-37, as no app. K_d could be determined until 1.25 µM while Fluos-IAPP bound to LL-37 with high affinity (app. K_d 88.1 (± 12.0) nM). This result clearly shows that these four IAPP residues are crucial not only for the self- and cross-interaction with Aβ40(42) but also for the cross-interaction with LL-37. Furthermore, to verify if all the four residues need to be replaced to lose the interaction between IAPP and LL-37, N-terminal carboxyfluorescein double alanine mutants were tested as well. Fluos-A15,23, Fluos-A15,16, and Fluos-A23,26 exhibited a high binding affinity to LL-37 comparable to Fluos-IAPP, leading to the conclusion that all four residues must be replaced to weaken the binding affinity.

Table 33. Identification of key IAPP residues for the binding of full-length LL-37 and determination of apparent binding affinities ($K_{d,app}$) by fluorescence titration assays

Fluos-IAPP alanine mutants	**$K_{d,app}$ (±SD) (for LL-37)[a]**
Fluos-A15,23	110.6 ± 46.1 nM
Fluos-A15,16	129.2 nM [b]
Fluos-A23,26	169.9 ± 58.9 nM
Fluos-4Ala	> 1.25 µM

[a] App. K_ds, means (±SD) from 3 binding curves. Determined via titrations of fluorescein-labeled peptides (Fluos-peptides, 5nM) with non-labeled LL-37 (aq. buffer 1×b, pH 7.4, containing 1% HFIP). [b] Preliminary experiment carried out by Linus Wollenweber (129). App. K_d, representative from 2 binding curves.

To investigate whether the amyloid inhibitory function of LL-37 is in the same segment responsible for its antibacterial/antiviral role, the sequence was dissected into two parts, LL-37(1-14), containing the N-terminus and LL-37(15-37), containing the C-terminus (78, 130). First, the inhibitory function against the aggregation of IAPP into cytotoxic species was tested. As described in 4.1.11, both segments were unable to inhibit the fibrillogenesis and toxicity of IAPP in a 1/1 ratio, confirming that a partial segment was not sufficient to interfere with IAPP aggregation. To evaluate whether the primary structure of LL-37 is sufficient to have an inhibitory effect or whether also the secondary structure of the peptide plays a role, ThT binding and MTT reduction assays were carried out. IAPP was incubated alone and in the co-presence of equimolar amounts of LL-37(1-14) and LL-37(15-37). Experiments revealed no inhibition of IAPP fibrillogenesis and cell-damaging effects already at 24 hours, suggesting that a covalent bond between the two segments of LL-37 is required to have suppression of amyloidogenicity. Moreover, far-UV circular dichroism of the mixture of LL-37(1-14)

and LL-37(15-37) was carried out. Spectra revealed a random coil structure of the mixture of the two peptides with a signal intensity corresponding to the sum of the spectra of the single peptides, suggesting no interaction between the two segments and consequently no change of their secondary structure when mixed in solution. Fluorescence titrations were carried out to evaluate the binding affinity of these segments towards monomeric IAPP. Experiments revealed that the C-terminal segment LL-37(15-37) is responsible for the interaction with IAPP, as the app. K_d value of the binding affinity was comparable to the full-length LL-37 (39.1 (± 2.2) nM and 88.1 (± 12.0) nM respectively), both in the nM range. In contrast, LL-37(1-14) was found to bind around 30 times weaker with an app. K_d in the μM range (2.54 (± 0.5) μM) (Table 34). Results suggest that although the central/C-terminal segment of LL-37 is responsible for the high affinity for IAPP, it is not sufficient to interfere with the aggregation kinetics of IAPP and that the concomitant presence of both N-/C-terminal regions is required for an inhibitory effect.

Table 34. Determination of apparent binding affinities ($K_{d,app}$) of LL-37, LL-37(1-14), and LL-37(15-37) to monomeric IAPP by fluorescence titration assays.

LL-37 segments	**$K_{d,app}$ (±SD) (for Fluos-IAPP)[a]**
LL-37	88.1 (± 12.0) nM
LL-37(1-14)	2.54 (± 0.5) μM
LL-37(15-37)	31.9 (± 2.2) nM

[a] App. K_ds, means (±SD) from 3 binding curves. Determined via titrations of fluorescein-labeled IAPP (Fluos-IAPP, 5nM) with non-labeled LL-37 segments (aq. buffer 1×b, pH 7.4, containing 1% HFIP).

Taken all together, these studies of the IAPP/LL-37 interaction interface suggest that IAPP interacts with LL-37 with the core region localized between amino acids 8 to 28. Within this region Phe15, Leu16, Phe23, and Ile26 were found to be crucial, as the simultaneous lack of all these residues causes a loss of interaction between the two peptides. Regarding LL-37, two major binding cores were found for the interaction with IAPP: LL-37(1-15) and LL-37(18-34). Additional studies led to the conclusion that the central/C-terminal region of LL-37 mediates the high binding affinity with IAPP. Results are summarized in Scheme 3.

Scheme 3. IAPP and LL-37 regions and residues involved in the IAPP/LL-37 interaction interface. The IAPP region (8-28) was identified via fluorescence spectroscopy titrations (red box). Within this region, when residues 15, 16, 23, 26 (red) are mutated the interaction between the two peptides is lost. LL-37(1-15) and LL-37(18-34) were identified as binding cores of the IAPP/LL-37 interaction interface via peptide array (blue boxes). Binding cores are highlighted in blue.

Concentration dependence experiments for LL-37, scrLL-37, and the two segments LL-37(1-14) and LL-37(15-37) were carried out via far UV circular dichroism. LL-37 exhibited an α-helix/β-sheet and β-turn structure, with a maximum at 198 nm and two minima, one at 210 nm and one at 227 nm. LL-37 is known to be an anti-parallel dimer formed by α-helices (79) and its secondary structure is known to be dependent on concentration, anion/cation concentration, and pH (80). In Figure 30a it is shown that LL-37 has no concentration dependence between 2 and 10 μM and a strong decrease of the signal at 20 μM due to the formation of soluble oligomers. It has been shown that at low concentrations (10^{-7} M), LL-37 is mainly disordered and that the amount of helical content increases at higher concentrations. The helix-coil equilibrium is a typical behavior of peptides able to form amphipathic helices, which correlates also with the transition from a monomeric to an oligomeric state, which consists of tetramers and hexamers as major species (79, 80).

Additional studies showed that in physiological salt concentrations, LL-37 forms oligomers containing up to six or seven units and that the interaction is mainly favored by the N-terminus of the peptide, leading the helices to organize in a parallel manner (148, 149). The scrambled sequence of LL-37 is mainly unstructured without any concentration dependence in the current experimental conditions. When the N-terminal and the C-terminal segments, LL-37(1-14) and LL-37(15-37) respectively, were tested no concentration dependence and disordered structures were found. Despite these peptides are random coiled, the comparison between the two shows that LL-37(15-37) has a slightly higher structural content as there is an unpronounced minimum at ~222 nm due to residual α-helical or β-sheet content (Figure 92).

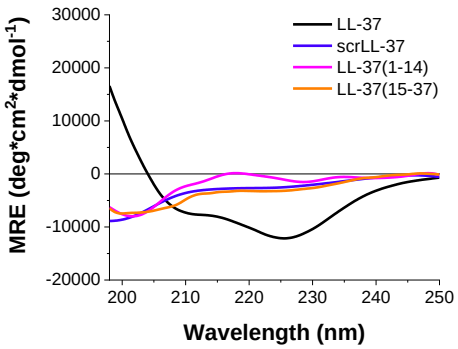

Figure 92. Conformations of LL-37, scrambled LL-37, LL-37(1-14) and LL-37(15-37) determined via far-UV CD spectroscopy. CD spectra were measure at 5 μM concentration (aqueous buffer 1×b, pH 7.4, containing 1% HFIP).

In fact, it is known that in LL-37 the N-terminus is less structured than the rest of the sequence and is responsible for 20-30% of the random coil content found (66). Next, TFE titrations were performed to evaluate the helical propensity of LL-37 and scrLL-37. 2,2,2-trifluoroethanol is known to promote protein unfolding and at high concentration induces α-helical structures in peptides with helical propensities (131). As expected, LL-37 exhibited a high helical propensity and had a transition point around 8% TFE. The scrLL-37 instead, had a transition to helix around 21% TFE indicating that the primary structure of the peptide is fundamental for its secondary structure. Studies conducted by Linus Wollenweber showed that the two segments LL-37(1-14) and LL-37(15-37) have a different helical propensity when titrated with increasing amounts of TFE (129). The N-terminal segment LL-37(1-14) displayed a significantly lower helical propensity than the central/C-terminal segment LL-37(15-37), as the obtained T_M was 20%, compared to 5% of LL-37(15-37) (Figure 93). In good agreement with our studies, CD spectroscopic experiments showed that LL-37 adopts a partial α-helix conformation in structure-inducing environments as TFE. The helical content of this peptide was often found around 70-80%, due to the hydrophobic N-terminus which does not easily fold into an α-helix (66).

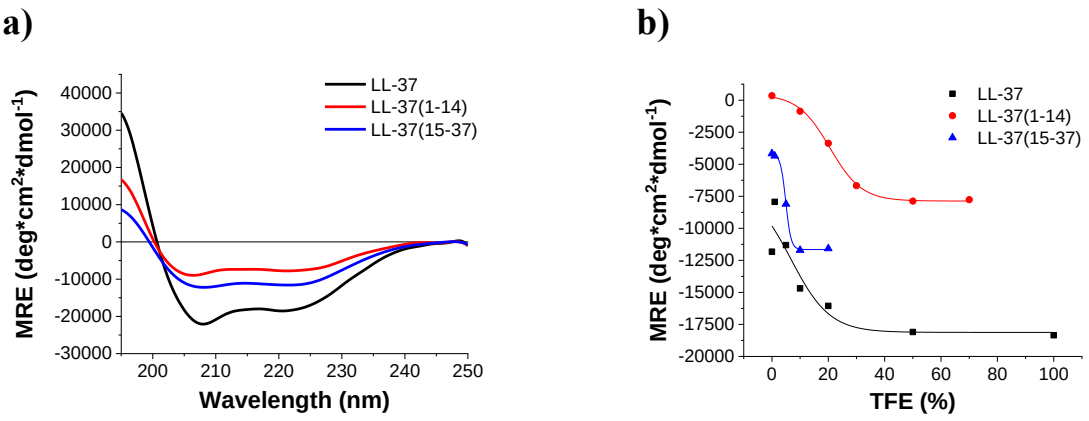

Figure 93. Comparison of the α-helical propensity of LL-37, LL-37(1-14), and LL-37(15-37) obtained via CD spectroscopy. a) CD spectra of LL-37(black), LL-37(1-14) (red), and LL-37(15-37) (blue) at their maximal helical content (100%, 70% and 20% TFE respectively). b) Plot of minima at 222 nm versus the TFE amounts (%) of the CD spectra of the peptides shown in a). Measurements were performed at 5 µM in aqueous buffer 1×b, pH 7.4, containing 1% HFIP and the indicated amounts of TFE. Data of LL-37(1-14) and LL-37(15-37) was obtained by Linus Wollenweber (129).

Next, we asked whether the ability of LL-37 to be an inhibitor of IAPP fibrillogenesis and cytotoxicity is related to its primary structure, to its secondary structure, or both factors. The mixture of LL-37(1-14) and LL-37(15-37) showed no inhibitory effect of IAPP self-assembly into toxic species and, in addition, the mixture of the two still had a random coil structure with no interaction between the two segments (Figure 94).

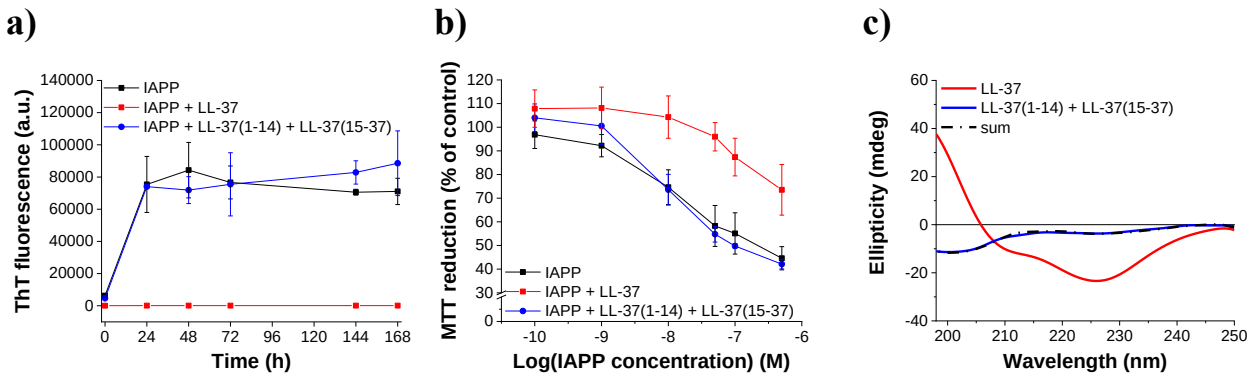

Figure 94. Effects of the primary and secondary structure of LL-37 on IAPP amyloid formation and cytotoxicity. a) Fibrillogenesis of IAPP (16.5 µM) and its mixtures with LL-37(1/1) or LL-37(1-14) and LL-37(15-37) (1/1/1) (means (±SD), 3 assays); b) effects of the mixtures on cell viability: solutions from a) were added to cultured RIN5fm cells (24 hours aged). Cell viability was determined by MTT reduction (means (±SD), 3 assays, n=3 each). c) Far-UV spectra of LL-37 (5 µM) or the mixture of LL-37(1-14) and LL-37(15-37) (1/1, 5 µM each), the mathematical sum of LL-37(1-14) and LL-37(15-37) is shown.

The studies suggest that both the sequence and the secondary structure have remarkable roles for the inhibitory function of LL-37, since both scrLL-37 and the mixture of LL-37(1-14) and LL-37(15-37) were found to be non-inhibitors of IAPP self-association.

Last, 2-photon microscopy was applied to further characterize the IAPP/LL-37 complexes. TAMRA-IAPP was incubated with FAM-LL-37 in 1/1 and 1/5 ratio. The 1/1 mixture was characterized by amorphous aggregates, in which IAPP is clustered by LL-37. Given these results, we hypothesize that, by surrounding IAPP, LL-37 inhibits its elongation into cytotoxic amyloid fibrils, forming the hetero-complexes that were also observed in the cross-linking studies. Additionally, FRET was observed between the two peptides, validating their interaction. Also, in the 1/5 mixture similar structures were found, correlating with the ThT binding assay

results, in which LL-37 could block the fibrillogenesis of IAPP. Additionally, large fibrils that incorporate both peptides were found, as also observed via TEM imaging. This finding supports the hypothesis that these large fibrillar assemblies are not amyloidogenic, as they are unable to bind the ThT dye, but result cytotoxic to RIN5fm cells.

In this first part of my work, LL-37 was identified as a nanomolar inhibitor and binding partner of IAPP. It was found that LL-37 could effectively suppress IAPP self-association in vitro and bind both low MW and fibrillar IAPP species. Results showed that it could interfere with IAPP aggregation kinetics by binding prefibrillar species and sequestering them into soluble and non-toxic hetero-complexes. Additionally, LL-37 binds IAPP fibrils, turning them into species that have no seeding ability for IAPP aggregation. LL-37(6-10) and LL-37(25-27) were identified as the two core regions that mediate the IAPP/LL-37 interaction, but the central/C-terminal region was found to mediate the interaction of LL-37 with IAPP, although this segment was not sufficient to suppress IAPP amyloidosis. On the other hand, IAPP interacts with the region extending from position 8 to position 28. Particularly, the binding affinity was lost when Phe15, Leu16, Phe23, and Ile26 were replaced with alanine residues.

Nowadays, antimicrobial peptides became interesting drug candidates, thanks to their multifunctional nature. In fact, they have an antimicrobial, antiviral, anticancer effect and overcome bacterial resistance (150). Several advantages are correlated to their use in addition to their various functions. Antimicrobial peptides exhibit good solubility, present a structure-activity relationship, and are synthesized quite easily as their length is modest (151, 152). For all these reasons, the FDA has approved some antimicrobial peptides as drugs for the treatment of several Gram-positive and Gram-negative bacterial infections (152). On the other hand, AMPs have been shown to exhibit cytotoxicity, immunogenicity, and hemolytic activity, which can cause severe problems in their long-term application (150, 152). Currently, studies are in progress to solve the downside of their application in the clinics as they appear to be promising drug candidates.

The involvement of LL-37 in T2D is yet to be investigated. Reports show that the level of CAMP expression in T1D patients is significantly reduced, compared to T2D patients, which might suggest that the AMP production may not be related to T2D (153). Furthermore, the correlation between T2D, antimicrobial activity, and levels of vitamin D in the serum was studied. T2D patients have low levels of vitamin D and have a high risk of tuberculosis infection, which may be due to an irregular response of the immune system. Vitamin D, in turn, regulates the expression levels of LL-37. Results show no direct correlation between vitamin D levels in the serum and LL-37 expression, indicating that the connection between T2D and LL-37 might follow a diverse path (154). Overall, the deficiency of LL-37 is related to pancreatic β-cell inflammation and treatments with cathelicidin lead to a reduction of inflammatory response, as well as an improvement of β-cell functions (155). With the support of other findings, we hypothesize that LL-37, produced by pancreatic β-cells or permeated by neutrophils in pancreatic inflammatory processes, might slow down the pathogenesis of T2D by suppressing β-cell damage caused by IAPP aggregation (98, 156, 157) (Scheme 4). Studies on the biological relevance of the IAPP/LL-37 interaction should be carried out, as the LL-37 can be taken as a scaffold for the design of candidate drugs that combine anti-amyloid, antimicrobial and immunoregulatory functionalities (114).

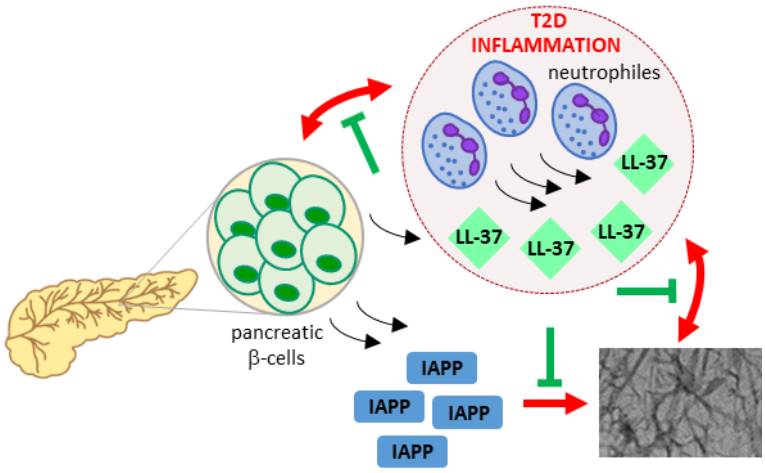

Scheme 4. Proposed inhibitory role of LL-37 in T2D inflammation, β-cell degeneration due to pancreatic amyloid formation. The figure is taken from Armiento et al. (ACIE, 2020) (114).

To date, AMPs are considered to be a promising alternative to combat antibiotic resistance, an increasingly prominent problem for patient care (158, 159). In fact, due to their multifunctional role and different mechanism of action, AMPs are considered less prone than antibiotics to cause resistance (160). Several LL-37 derived segments have been investigated for their antimicrobial role, with the aim to retain the antimicrobial activity of LL-37 and eliminate the unwanted properties (158). To design these sequences, the N-terminus is generally removed, as it is known that it is not important for the antimicrobial activity (161), and the first two residues are responsible for peptide instability (158, 162). On the other hand, the central/ C-terminal region of LL-37 is responsible for the antimicrobial activities of this peptide (93), while the region extending from residue 32 to 37 is not crucial for the interaction with bacterial membranes (158, 162). Based on these findings, several LL-37 segments have been studied for their potent antimicrobial function. LL-31 has been shown to be the most effective peptide against the Gram-negative bacterium *Burkholderia pseudomallei*, the aetiological agent of melioidosis (163). Saporito et al. showed that the 12-mers FK-12, KR-12, and VQ-12^{V26} have potent activity against *Staphylococcus epidermidis*, a pathogen resistant to antibiotic treatment and able to penetrate the skin barrier causing chronic infections (164). Furthermore, KS-30 and KR-20, together with LL-37, have been suggested to be developed as effective therapeutics against *Acinetobacter baumannii*, a Gram-negative nosocomial pathogen, related to various infections (165). Currently, several studies are carried out to improve and understand how LL-37 and its segments could be applied for the treatment of bacterial infections (158).

5.2 Identification of partial LL-37 segments able to inhibit IAPP fibrillogenesis and cytotoxicity

The second aim of my work was the identification of the shortest LL-37 derived segment, which could still efficiently suppress IAPP self-assembly into cell-damaging assemblies. A rational design of LL-37 segments was carried out by systematically shortening the sequence at the N-terminus or the C-terminus. Results obtained by the peptide array (section 4.1.8) were taken as a basis for dissecting the sequence into two parts. Consequently, based on the knowledge that LL-37 contains an α-helical secondary structure extending from residue 2 to 31 and an unordered C-terminus (88), the sequence was systematically shortened at the C-terminus or at the N-terminus (Figure 95), to verify if there was any structure-activity relationship.

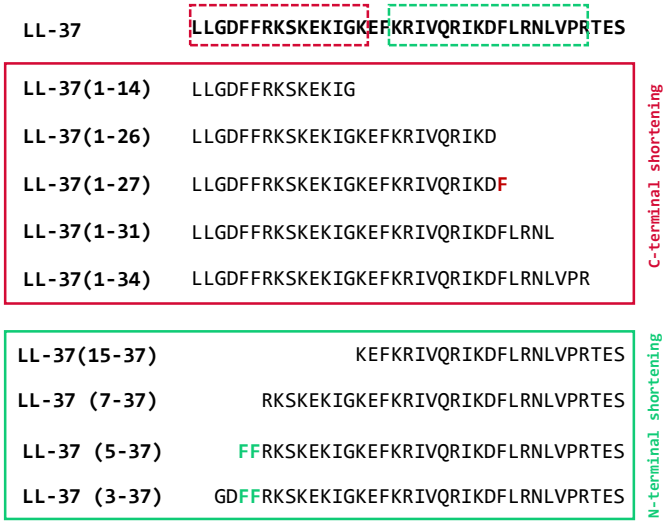

Figure 95. Rational design approach of C- and N-terminal truncated LL-37 segments. Red and green dashed boxes indicate the two regions of LL-37 mediating its interaction with IAPP (section 4.1). Consequently, C-terminal and N-terminal shortening were carried out (red and green boxes respectively) and roles of phenylalanine residues were investigated.

For the synthesis of the LL-37 derived segments, the Fmoc-SPPS strategy was applied. For this purpose, Wang resin was chosen, as LL-37 is found in nature with a carboxy-terminus (66). All the syntheses were successful as the pure peptides of interest could be isolated with high purity via RP-HPLC after one or two purification rounds. For all the sequences containing aspartic acid, the Fmoc-deprotection was carried out with a solution of 20% piperidine in DMF containing 0.1 M of HOBt, to avoid the aspartimide formation during side reactions (105). The strategy was successful since no aspartimide was identified in all syntheses. The synthesis protocols were progressively improved to avoid the formation of acetylated side-products that could be identified via MALDI-TOF. In Table 18, the main side products recurring in the syntheses of the N-terminal truncated segments are reported. In general, for all the syntheses the most challenging couplings were Ile^{20}, Arg^{19}, Lys^{18}, Phe^{17}, Glu^{16}, Gly^{14}, Ile^{13}, Asp^{4}, and Leu^{2}. For these positions, the reaction conditions were modified to have a higher coupling yield. In fact, for difficult couplings the reaction time was increased, HATU was used instead of HBTU as the coupling reagent due to its higher reactivity (166), higher amounts of reactants were applied, and/or couplings were repeated multiple times. However, for the longer peptides, such as LL-37(1-34), LL-37(1-31), LL-37(3-37), the yield of pure product was particularly low (<10 %). We observed that the low yield was due to the formation of the side-products described above, which elute at the same retention time as the target product, but also to possible interchain reactions (167, 168) as the substitution level (SL) of the peptide on the resin was high. A lower SL could be helpful to increase the purification yield of these peptides and could be applied in future syntheses. All cleavages were carried out with a TFA/H_2O mixture and no problems were observed with this procedure. For the purification of the peptide via RP-HPLC, different gradients were tested. In Table 19, the gradients that led to the best purification yield are shown for each peptide.

Circular dichroism studies were carried out to evaluate the secondary structure of the LL-37 derived segments. Regarding the C-terminal truncated sequences, LL-37(1-14), as well as LL-37(1-26) and LL-37(1-27) exhibited no oligomerization propensity and an amount of random coil unfolding. As expected, LL-37(1-14) was majorly disordered and by the elongation of the sequence, the amount of structured α-helix and β-sheet/turn content increased. In fact, in the spectra of LL-37(1-26) and LL-37(1-27), a minimum at 227 nm was visible, which was missing in the spectra of LL-37(1-14). Additionally, the solubility of LL-37(1-14) was higher than the more structured segments, which tend to assemble at 20 μM. As shown in the work of Wang et al. (88), LL-37(1-31) showed majorly an α-helix/β-sheet content compared to the shorter segments, but not as ordered as LL-37. LL-37(1-34) exhibited the highest structural content, with an α-helix/β-sheet content comparable to the native sequence of LL-37 (Figure 96a). It is known that alcohols denature the native state of proteins. HFIP is often used to unfold amyloids like IAPP and Aβ or prions (142, 169) and it is known to induce α-helical state to different proteins like β-lactoglobulin and melittin (170). Additionally, simulations show that in a mixture with water, HFIP clusters around the peptides, excluding water and inducing local interactions that lead to ordered secondary structures (171). To evaluate the effect of HFIP on the secondary structure of LL-37 and its segments, CD spectra were also recorded in aqueous buffer. LL-37, LL-37(1-34), and LL-37(1-31) resulted mainly helical and no pronounced minima at 226 nm were shown compared to the spectra in the presence of HFIP, indicating that the β-sheet/turn signal might be induced by the presence of HFIP. LL-37(1-27), LL-37(1-26), and LL-37(1-14) resulted unordered as expected (Figure 96b).

The N-terminal truncated fragments were examined via circular dichroism as well. The longest segment, LL-37(3-37), exhibited the higher α-helix/β-sheet/turn structural content, comparable to LL-37. In fact, spectra show two minima, one at 208 and one more pronounced at 226 nm and one maximum at 198 nm, which were observed also in the native sequence. The peptide exhibited an oligomerization propensity between 10 and 20 μM, similarly to LL-37. By shortening the sequence, a loss of secondary structure was observed in LL-37(5-37) and, even more, in LL-37(7-37). These two peptides still have a helical content, but the two minima previously mentioned have the same signal intensity, suggesting a loss of β-sheet/turn content. When the N-terminus was dramatically shortened, leading to LL-37(15-37), a total loss of secondary structure and oligomerization propensity was observed (Figure 96c). In absence of HFIP, LL-37(3-37) is mainly helical, while LL-37(5-37) and LL-37(7-37) show a dramatic loss of secondary structure compared to their spectra in presence of HFIP. Last, LL-37(15-37) exhibited mainly a random coil structure (Figure 96d). Results show that HFIP is inducing an α-helix/β-sheet secondary structure to LL-37 and its segments.

These findings clearly support previous studies carried out on the structure of LL-37, which suggest that the structure of LL-37 can be divided into three parts with different features. The N-terminus is apolar, hydrophobic, and unordered; the central region is mainly α-helical, and the short C-terminus is hydrophilic and dynamically mobile (54, 88).

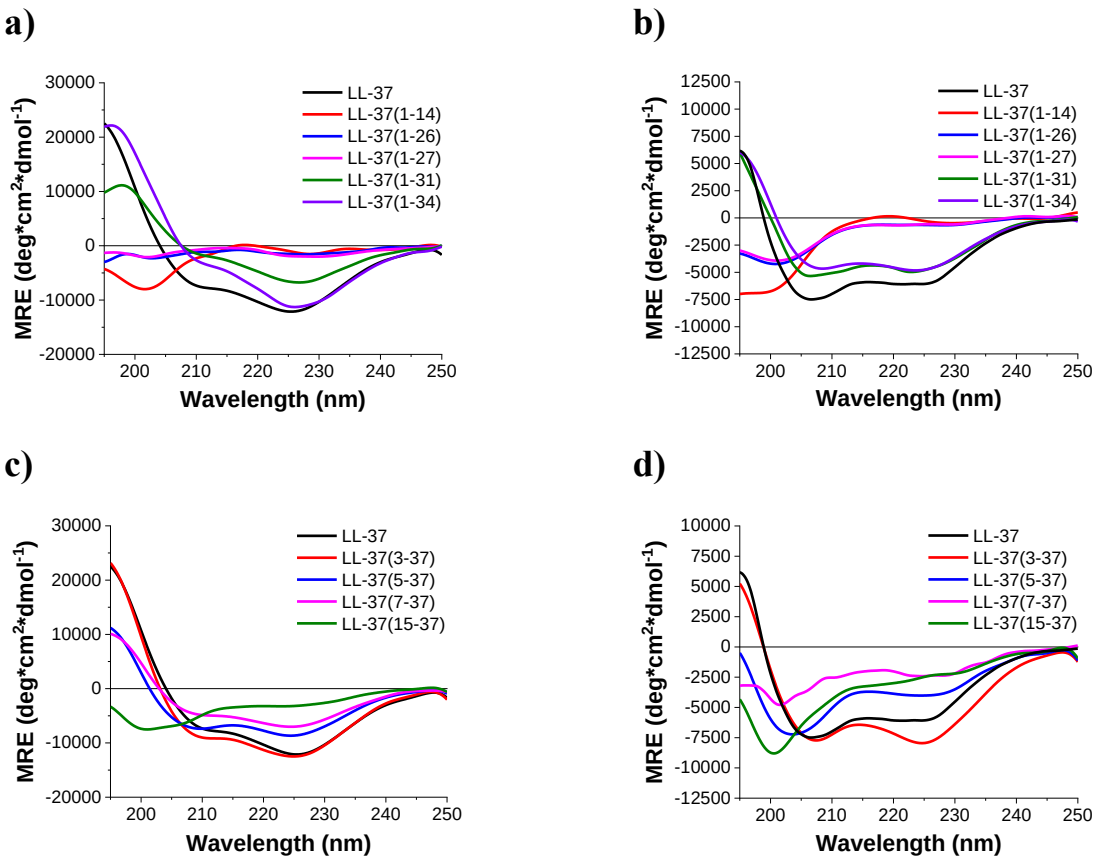

Figure 96. Secondary structure of C- or N-terminal truncated LL-37 segments, assessed by far-UV CD spectroscopy. a) CD spectra of C-terminal truncated segments at 5 µM in aqueous buffer 1×b, pH 7.4, containing 1% HFIP. b) CD spectra of C-terminal truncated segments at 5 µM in aqueous buffer 1×b, pH 7.4. c) CD spectra of N-terminal truncated segments at 5 µM in aqueous buffer 1×b, pH 7.4, containing 1% HFIP. d) CD spectra of C-terminal truncated segments at 5 µM in aqueous buffer 1×b, pH 7.4.

To compare the amount of helical structure of these peptides, values at 222 nm were compared. The signal is comparable for LL-37, LL-37(3-37), and LL-37(1-34), which are also the sequences that are most effective against IAPP aggregation. When the sequences are shortened, the helical content is diminished. LL-37(5-37) has an MRE that is 2/3 and LL-37(7-37) has half of the signal of the full-length peptide. In the case LL-37(15-37), the signal at 222 nm is circa 4-times less than LL-37. Regarding the C-terminal segments, LL-37(1-31) contains half of the helical structure of LL-37. Further shortening of the sequence led to a dramatic loss of helical structure, as LL-37(1-27), LL-37(1-26), and LL-37(1-14) have similar MRE intensities (Figure 97a). Similarly, also the MRE values at 227 nm were compared, as this signal is attributable to a β-sheet/turn structure. LL-37 and LL-37(3-37) have a comparable signal intensity, whereas LL-37(1-34) has a loss of circa 1/4 of the β-sheet/turn content. A similar trend can be identified for the other segments: LL-37(5-37) has an MRE which is 2/3 and LL-37(7-37) has half of the signal of the full-length peptide, as for the MRE at 222 nm. LL-37(1-31) contains circa half of the β-sheet/turn structure of LL-37, while all the shorter segments undergo a loss of structured content (Figure 97b).

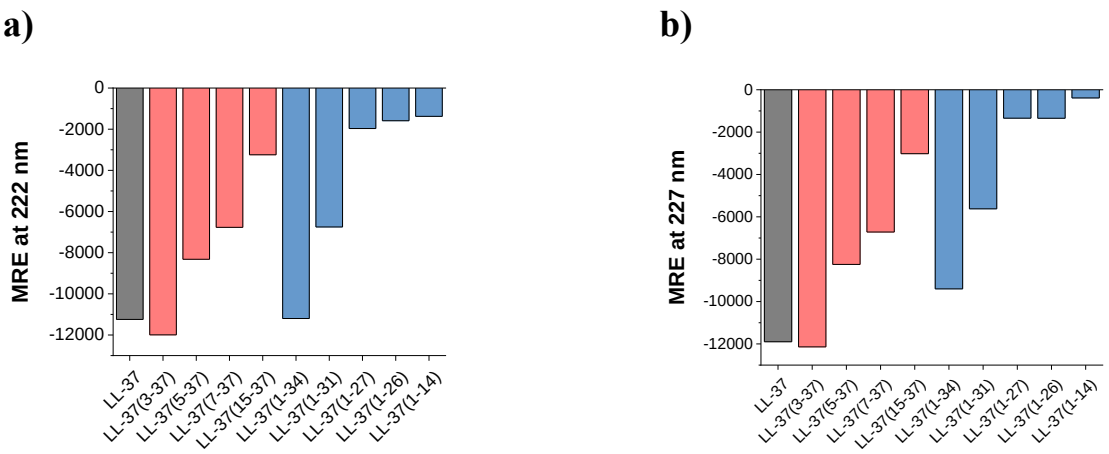

Figure 97. MRE values of LL-37, C-terminal, and N-terminal segments at 222 and 227 nm obtained via CD spectroscopy. a) MRE at 222 nm of LL-37 (grey), LL-37(3-37), LL-37(5-37), LL-37(7-37), and LL-37(15-37) (red), LL-37(1-34), LL-37(1-31), LL-37(1-27), LL-37(1-26), and LL-37(1-14) (blue). b) MRE at 227 nm of LL-37 (grey), LL-37(3-37), LL-37(5-37), LL-37(7-37), and LL-37(15-37) (red), LL-37(1-34), LL-37(1-31), LL-37(1-27), LL-37(1-26), and LL-37(1-14) (blue). MRE values are taken from measurements performed at 5 µM in aqueous buffer 1×b, pH 7.4, containing 1% HFIP.

Finally, LL-37(3-34), shortened at the C- and at the N-terminus, was examined. Despite the peptide was structured and exhibited a clear α-helix/β-sheet, β-turn content, a slight oligomerization propensity was observed around 20 µM, but with no striking effect on the solubility, unlike LL-37(1-34) and LL-37(3-37). Additionally, LL-37(3-34) is more helical than LL-37(1-34) and LL-37(3-37). In fact, LL-37(3-34) presents two minima, one at 208 and one at 226 nm with similar signal intensities. LL-37(1-34) and LL-37(3-37) exhibit the same signals, but the minimum at 226 nm is more pronounced, indicating a higher β-sheet/turn content (Figure 98a). In aqueous buffer, all the peptides are mainly α-helical, but LL-37(3-34) clearly shows a loss of secondary structure, due to lower overall signal intensity and a shift of one of the two minima from 208 nm to 204 nm (Figure 98b). The findings suggest the Leu1 and Leu2 or Thr35, Glu36, and Ser37 confer the β-sheet/β-turn content to the LL-37 segments and are required for the α-helix secondary structure.

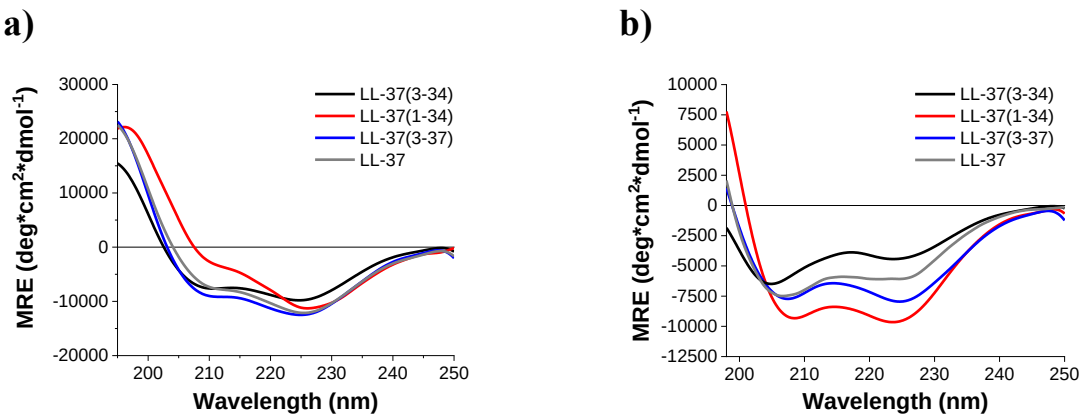

Figure 98. Secondary structure of LL-37(3-34), LL-37(1-34), LL-37(3-37), or LL-37 assessed by far-UV CD spectroscopy. a) Measurements were performed at 5 µM in aqueous buffer 1×b, pH 7.4, containing 1% HFIP. b) Measurements were performed at 5 µM in aqueous buffer 1×b, pH 7.4.

Next, the MRE values at 222 and 227 nm of LL-37(3-34) were compared to the ones of the native sequence and LL-37(3-37) and LL-37(1-34). As shown in Figure 99a the helical structure is slightly diminished when both C- and N-termini are neglected. When the MRE values at 227 nm are compared, LL-37(3-34) has a similar β-sheet/turn structure to LL-37(1-34) (Figure 99b). In general, the shortening of both C- and N-termini results in a weak loss of α-helix and β-sheet/turn content.

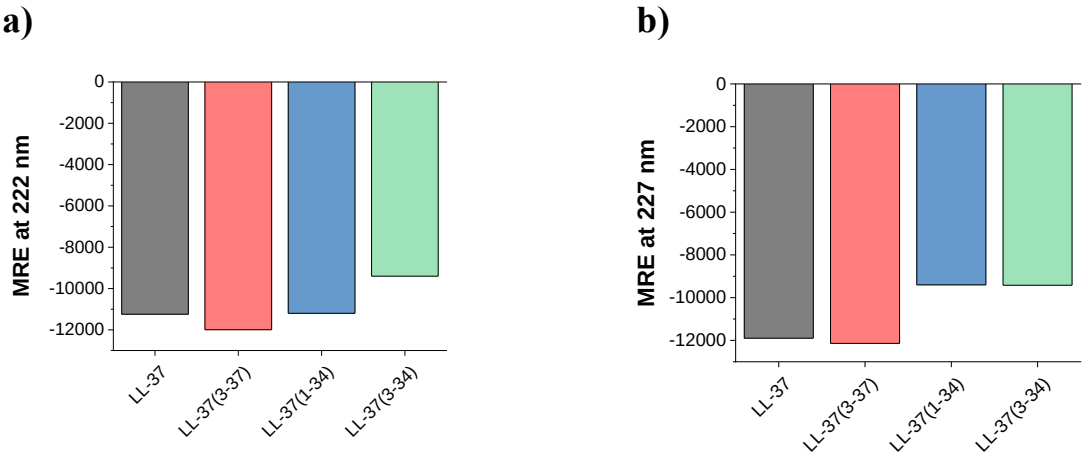

Figure 99. MRE values of LL-37, LL-37(3-37), LL-37(1-34), and LL-37(3-34) at 222 and 227 nm obtained via CD spectroscopy. a) MRE values at 222 nm. b) MRE values at 227 nm. MRE values are taken from measurements performed at 5 μM in aqueous buffer 1×b, pH 7.4, containing 1% HFIP.

The helical propensity of the C- and N-terminal truncated LL-37 segments was investigated via TFE CD spectroscopic titrations. A comparison of the spectra of the C-terminal truncated segments at the maximum amount of helical content clearly shows that LL-37, LL-37(1-34), and LL-37(1-31) have the highest helical content. In fact, the overall signal of LL-37(1-31) and LL-37 at the maxima of their helical content is comparable, in accordance with the finding that LL-37(1-31) contains the residues responsible for the helical character of LL-37 (132). The shorter peptides show lower signals, in accordance with our CD studies (Figure 100a). The shortest segment, LL-37(1-14), which displayed a random coil, had a T_M at 20% TFE (129), which was significantly lower than the native LL-37 , with a T_M at 8%. Similar behavior was observed for LL-37(1-27), a random coil segment that showed a two-state transition with a T_M at 18% TFE. LL-37(1-31), which displayed a β-sheet/turn and α-helix secondary structure, had a T_M at ~16% TFE indicating a higher helical propensity than the unstructured segments. The longest segment LL-37(1-34) showed the highest helical propensity and a T_M at 12%, similar to LL-37 (Figure 100b). Similar studies were carried out for the N-terminal truncated sequences. As expected, the overall signal at the maxima of their helical content is similar for LL-37 and LL-37(3-37), while shorter peptides have significantly less intense CD spectra (Figure 100c). Unexpectedly, LL-37(15-37) revealed the highest helical propensity with a T_M at only 5% TFE (129), although this peptide is unordered in absence of TFE. LL-37(5-37) and LL-37(3-37), which have a α-helical, β-sheet/β-turn structure, exhibited T_M values of 17% and 11% TFE respectively, indicating that longer sequences have a higher helical propensity (Figure 100d).

In general, our results suggest that truncated sequences that exhibit a lower α-helical propensity than LL-37, exhibit also lower inhibitory potency of IAPP aggregation. It has been shown that LL-37 and its derivatives have a linear association between immunoregulatory function and α-helical propensity. A segment of LL-37, IG-19, and four of its scrambled sequences were investigated for this purpose. Among the five peptides, IG-19 showed the highest percentage of α-helix according to the helical predictions, it could suppress the lipopolysaccharides (LPS)-induced pro-inflammatory cytokine and chemokine production, as well as induce the production of cytokine IL-1RA in macrophage-like THP-1 cells, which has an anti-inflammatory effect (147).

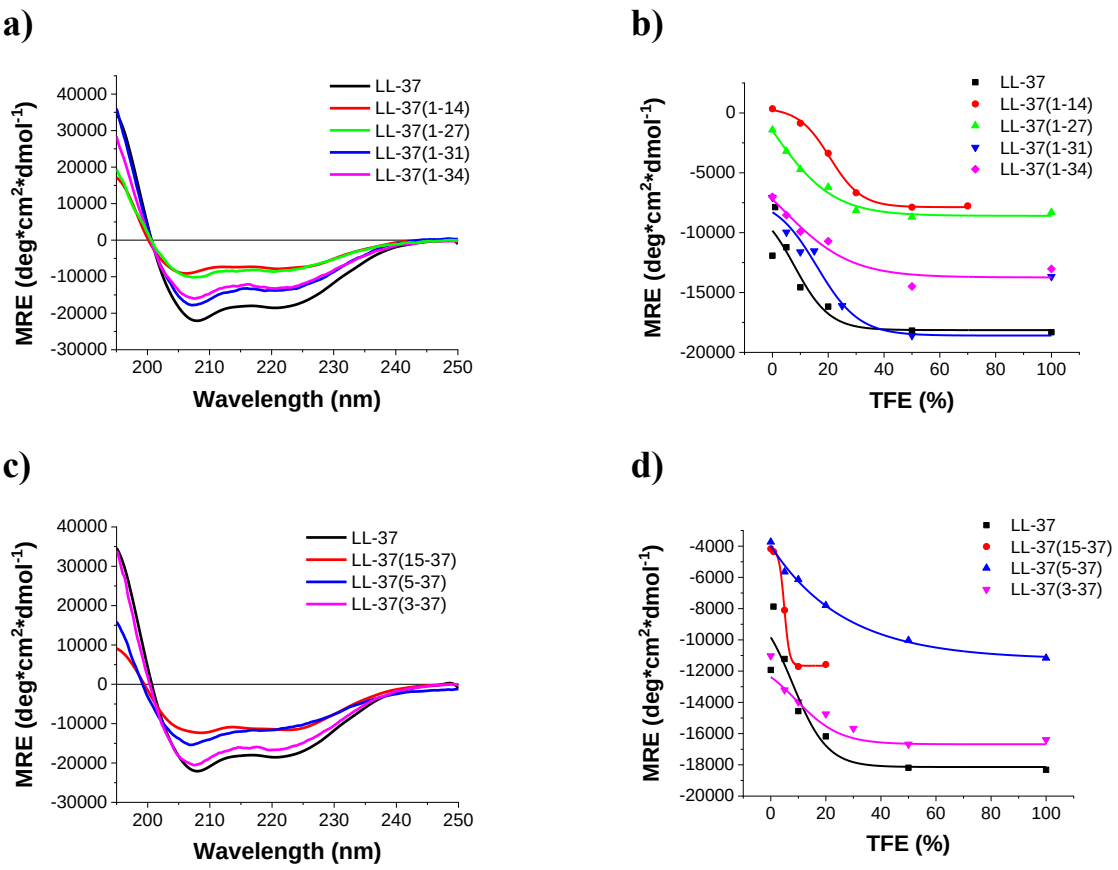

Figure 100. Comparison of the α-helical propensity of LL-37 and LL-37 N- and C-terminal truncated segments obtained via CD spectroscopy. a) CD spectra of LL-37, LL-37(1-14), LL-37(1-27), LL-37(1-31), and LL-37(1-34) at their maximal helical content (100%, 70%, 100%, 100%, and 100% TFE respectively). b) Plot of minima at 222 nm versus the TFE amounts (%) of the CD spectra of the peptides shown in a). c) CD spectra of LL-37, LL-37(15-37), LL-37(5-37), and LL-37(3-37) at their maximal helical content (100%, 20%, 100%, and 100% TFE respectively). d) Plot of minima at 222 nm versus the TFE amounts (%) of the CD spectra of the peptides shown in c). Measurements were performed at 5 µM in aqueous buffer 1×b, pH 7.4, containing 1% HFIP and the indicated amounts of TFE.

The C- and N-terminal truncated peptide, LL-37(3-34) exhibited similar properties to LL-37(1-34) and LL-37(3-37). In fact, this peptide exhibited a high helical content in the presence of 100% TFE (Figure 101) and a T_M at 16% TFE versus the 12%, 11%, and 8% TFE of LL-37(1-34), LL-37(3-37), and LL-37 respectively. In accordance with the CD studies, these results suggest that Leu1 and Leu2 or Thr35, Glu36, and Ser37 are important for the β-sheet/turn content of this segment but do not significantly affect its helical structure.

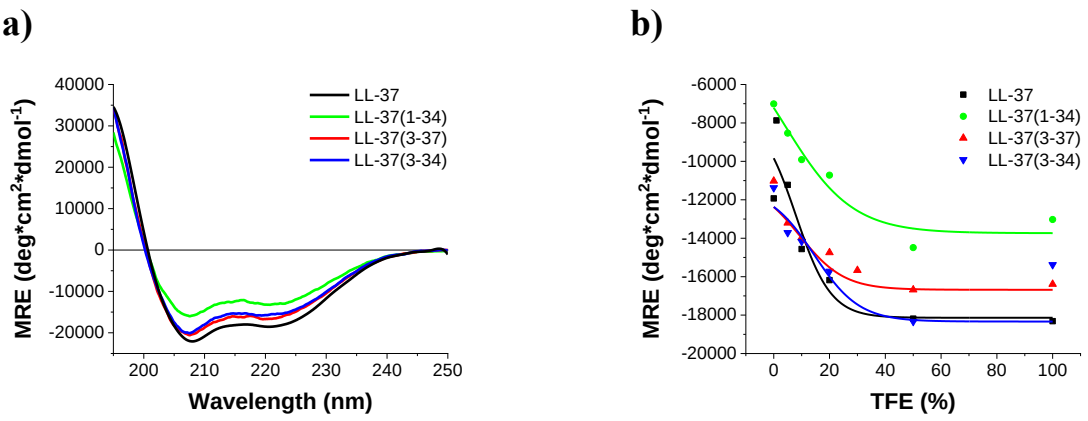

Figure 101. Comparison of the α-helical propensity of LL-37, LL-37(1-34), LL-37(3-37), and LL-37(3-34) obtained via CD spectroscopy. a) CD spectra of LL-37, LL-37(1-34), LL-37(3-37), and LL-37(3-34) at their maximal helical content (100% TFE). b) plot of minima at 222 nm versus the TFE amounts (%) of the CD spectra of the peptides shown in a). Measurements were performed at 5 µM in aqueous buffer 1×b, pH 7.4, containing 1% HFIP and the indicated amounts of TFE.

We next asked, whether the C-terminal/N-terminal truncated LL-37 segments could intervene in the aggregation of IAPP into cytotoxic assemblies and if there was any correlation between structure and amyloid inhibitory properties. The role of the N-terminal part of LL-37 was studied first. As previously shown, LL-37 is able to block IAPP aggregation into cytotoxic β-sheet rich fibrils until 7 days. LL-37(1-34) showed similar properties. Furthermore, its IC_{50} at 24 hours was determined, which resulted to be in the nM range as for LL-37 (23.7 (± 5.9) nM). LL-37(1-31), known to comprise the segment of LL-37 folded in an α-helix (132), showed inhibition of fibrillogenesis and cytotoxicity until 144 hours, but not after 7 days. Additional studies are currently in progress to investigate the role of Val32 and Pro33 for the inhibitory activity of LL-37. Preliminary results show that LL-37(1-33) can still block the IAPP amyloid formation. LL-37(1-32) will be then synthesized to elucidate if Val32 is crucial for the inhibitory potency of LL-37.

The further C-terminal shortening resulted in a loss of any interference with the aggregation kinetics of IAPP. In fact, LL-37(1-27) and LL-37(1-26) exhibited similar results and both peptides had a similar aggregation kinetic as IAPP alone. Additionally, these results suggested that Phe27 does not play a role in the inhibitory properties of LL-37. It is known that residues Phe5, Phe6, and Phe27 are strongly conserved within the cathelicidin family (79). They are also responsible for the interaction of LL-37 amphipathic helices with detergent molecules and micelles, used as a membrane mimic (79, 88). Molecular dynamics simulations show that the phenylalanines throughout the LL-37 sequence play an important role in the insertion of LL-37 in bacterial membrane models (172). Finally, LL-37(1-14), the shortest N-terminal segment synthesized, did not have any effect on IAPP aggregation (Figure 102).

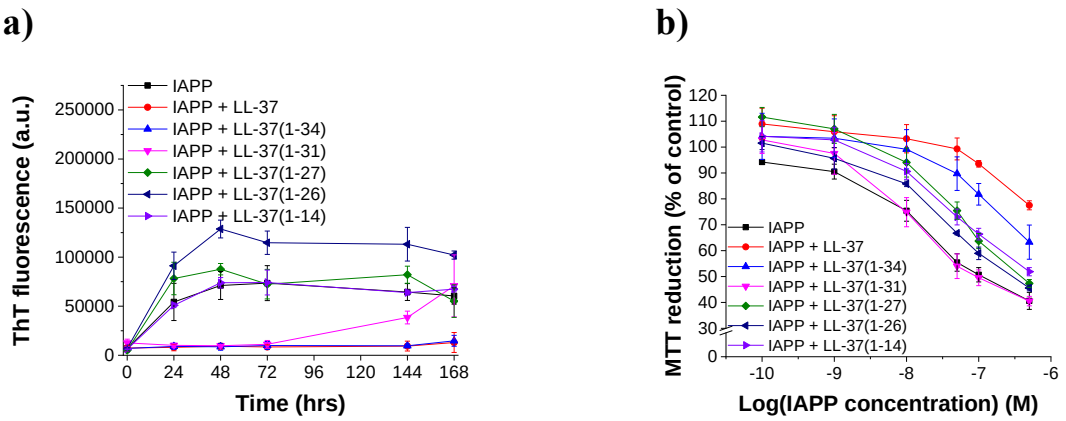

Figure 102. Effects of LL-37 and LL-37 C-terminal truncated segments on IAPP amyloid formation and cytotoxicity. a) Fibrillogenesis of IAPP (16.5 μM) and its mixtures with LL-37 (1/1), LL-37(1-34) (1/1), LL-37(1-31) (1/1), LL-37(1-27) (1/1), LL-37(1-26) (1/1) or LL-37(1-14) (1/1) (means (±SD), 3 assays); b) effects on cell viability: solutions from a) were added to cultured RIN5fm cells (7 days aged). Cell viability was determined by MTT reduction (means (±SD), 3 assays, n=3 each).

The non-inhibitors LL-37(1-27) and LL-37(1-26) could not exhibit any effect on IAPP fibrillogenesis until a 10-fold excess, confirming that their effectiveness is at least 10 times less than LL-37. The partial inhibitor LL-37(1-31) exhibited a full inhibitory effect only when incubated in 10-fold excess to IAPP.

Studies carried out on the antimicrobial activity against a Gram-negative bacterium, *B. pseudomallei*, of a library of LL-37 segments revealed that LL-37(1-31) exhibited a strong antibacterial effect, as LL-37. Shorter C-terminal truncated sequences, as LL-37(1-25), LL-37(1-19), and LL-37(1-13) showed reduced to no bactericidal activity. In this context, no correlation between secondary structure and antimicrobial activity could be identified. In fact, the propensity to adopt an α-helix was similar for LL-37, LL-37(1-31), and LL-37(1-25) which had different bactericidal effects (163). Although the core for the bactericidal activity of LL-37 was found between residues 17 and 29, the C-terminus, particularly the VPRTES segment, plays an important role in the insertion of LL-37 in the bacterial cell walls and the modulation of the oligomerization of the peptide on the membrane (173). In contrast, our studies suggest that the helical conformation of the peptides is related to the anti-amyloid function, as only LL-37(1-34) and LL-37(1-31) exhibited an α-helix and β-sheet/turn structure and inhibited IAPP fibril formation at least partially.

Similarly, the effect of C-terminal segments of LL-37 on IAPP aggregation was studied. The longest segment LL-37(3-37) exhibited an inhibitory effect comparable to the native peptide. Its IC_{50} at 24 hours, equal to 18.9 (± 0.9) nM, confirmed that its inhibitory potency is in the nM range. The shorter segment LL-37(5-37) could interfere with the aggregation of IAPP into cytotoxic assemblies until 72 hours. Its effect at 7 days was only partial, although the cytotoxicity could still be blocked. When residues 5 and 6, both phenylalanine, were neglected the whole inhibitory potency was disrupted. As a matter of fact, LL-37(7-37) could not inhibit the aggregation of IAPP already at 24 hours, suggesting that these two residues play a key role in the inhibitory function of LL-37 towards IAPP. Lastly, LL-37(15-37) showed no inhibitory effect already at 24 hours (Figure 103). Additionally, LL-37(15-37) and LL-37(7-37) exhibited an inhibitory potency that is at last 10 times weaker than the native sequence. In fact, the lag phase of the IAPP aggregation kinetics was only delayed, but no inhibitory effect could be observed until 7 days. LL-37(5-37) could fully inhibit the fibril formation when mixed with IAPP in 10-fold excess. Several LL-37 N-terminal truncated segments have been investigated for their antimicrobial activity. LL-37(7-37) and LL-37(13-37) are active against biofilm formation from *P. aeruginosa*. Both of them formed an α-helix in aqueous buffer, while shorter segments, that did not form helices, were not active against the bacteria in the biofilm (174). Additionally, N-terminal truncated segments, such as LL-37(3-37) (fragment 106) and LL-37(7-37) (fragment 110), were studied regarding their antimicrobial effect. The lack of the hydrophobic N-terminus did not negatively affect the antimicrobial

activity against *E. coli*, *P. earuginosa*, *S. aureus*, and *C. albicans*, but these segments resulted less toxic to human cells than the parent peptide (175). Our studies observed that the α-helix and β-sheet/turn conformation is required for efficiently blocking the aggregation of IAPP into cell-damaging species. Also, when residues Phe5 and Phe6 are neglected from the sequence, the inhibitory effect is drastically reduced, underlining the importance of these two residues.

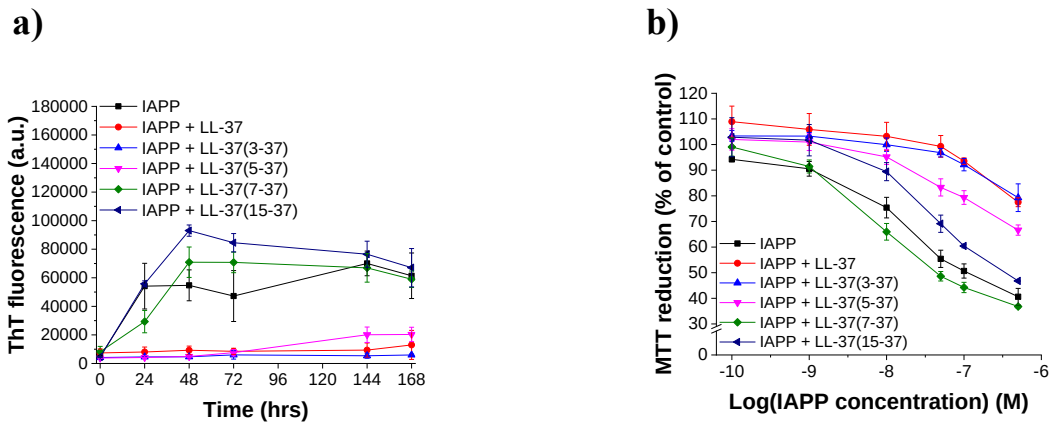

Figure 103. Effects of LL-37 and LL-37 N-terminal truncated segments on IAPP amyloid formation and cytotoxicity. a) Fibrillogenesis of IAPP (16.5 μM) and its mixtures with LL-37 (1/1), LL-37(3-37) (1/1), LL-37(5-37) (1/1), LL-37(7-37) (1/1) or LL-37(15-37) (1/1) (means (±SD), 3 assays); b) effects on cell viability: solutions from a) were added to cultured RIN5fm cells (7 days aged). Cell viability was determined by MTT reduction (means (±SD), 3 assays, n=3 each).

Taken together, results show that LL-37, LL-37(3-37), and LL-37(1-34) have similar inhibitory potency of IAPP fibril formation. Compared to LL-37, LL-37(3-37), and LL-37(1-34) exhibit a similar half-maximal inhibitory concentration (IC_{50}) at 24 hours, as shown in Figure 104.

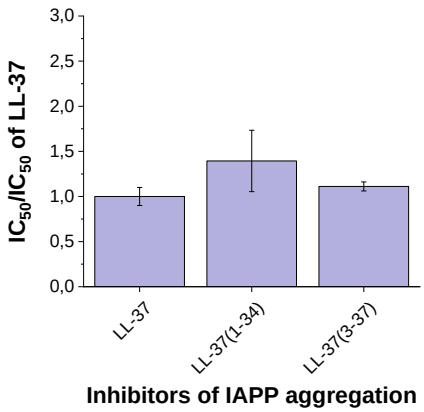

Figure 104. Relative half-maximal inhibitory concentration (IC_{50}) of LL-37 and LL-37 segments required to inhibit IAPP fibril formation.

To conclude, LL-37(5-37) and LL-37(1-31) have an inhibitory potency that is 10-fold weaker than the native sequence, while the shorter segments LL-37(7-37), LL-37(15-37), LL-37(1-27), and LL-37(1-26) have an inhibitory potency which is more than 10-fold weaker than LL-37 (Figure 105).

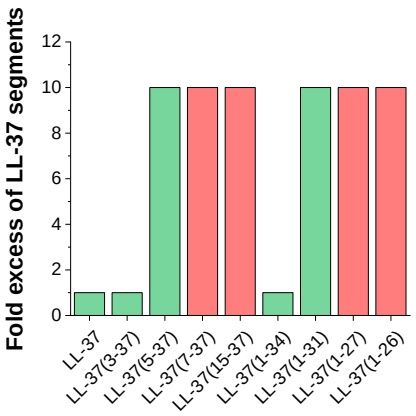

Figure 105. Amounts of LL-37 and LL-37 segments required to inhibit IAPP fibril formation. The bar plot shows the excess of inhibitors tested. Green bars represent inhibitory concentrations; red bars represent no inhibitory effect.

Next, we asked if the LL-37(3-34) could intervene in IAPP aggregation into cell-damaging species. In fact, LL-37(1-34) and LL-37(3-37) are the shortest LL-37 derived peptides that exhibited similar inhibitory potency and structural characteristics as the native peptide. We decided then to neglect both C- and N-terminal amino acids and study the characteristics of this segment. Inhibition studies suggested that LL-37(3-34) can only partially intervene in IAPP amyloid formation. The aggregation was delayed for 72 hours, but after 7 days there was no inhibitory effect on the aggregation of IAPP and on its cytotoxicity (Figure 106a, b). On the other hand, studies show that several LL-37 segments, neglecting both C- and N-termini, have potent antimicrobial and biocidal effects (146, 165, 176). In particular LL-37(15-32) (KE18) and LL-37(18-29) (KR12), which showed a higher amphipathic character compared to LL-37, exhibited also a higher antimicrobial effect, underlining the structure-activity relationship of these peptides (176). In our studies, the amphipathic helix structure is not sufficient to have a full suppression of IAPP amyloidogenesis. Our structural and inhibition studies show that peptides that exhibit only a helical conformation are only partial inhibitors, as LL-37(3-34) (Figure 106c). An α-helix and β-sheet/turn structure correlated with a potent suppression of IAPP fibril formation and cytotoxicity. These studies suggest that the lack of both C- and N-termini affects the inhibitory effect of the peptide.

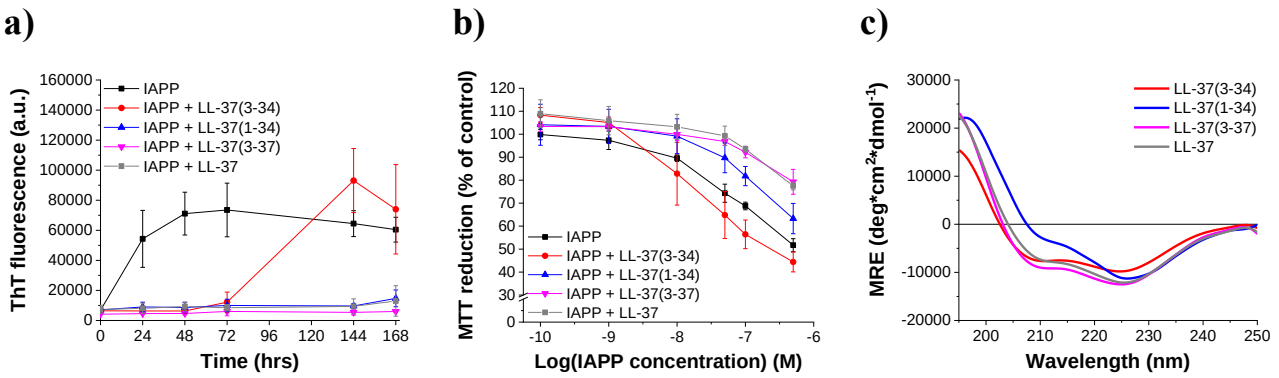

Figure 106. Effects of LL-37 C- and N-terminal truncated segments on IAPP amyloid formation and cytotoxicity. a) Fibrillogenesis of IAPP (16.5 μM) and its mixtures with LL-37(3-34) (1/1), LL-37(1-34) (1/1), LL-37(3-37), or LL-37 (1/1) (means (±SD), 3 assays); b) effects on cell viability: solutions from a) were added to cultured RIN5fm cells (7 days aged). Cell viability was determined by MTT reduction (means (±SD), 3 assays, n=3 each). c) Secondary structure of LL-37(3-34), LL-37(1-34), LL-37(3-37), or LL-37 assessed by far-UV CD spectroscopy. Measurements were performed at 5 μM in aqueous buffer 1×b, pH 7.4, containing 1% HFIP.

Circular dichroism and ThT/MTT assays results suggest that there is a structure-activity relationship (SAR). The structure-activity relationship of LL-37 and its segments has been extensively investigated, with regards

to their antimicrobial activity. In 1998, Johansson and his group observed that the helical, oligomeric conformation of LL-37 is fundamental for its antimicrobial activity. They showed that LL-37 exhibits its strongest antimicrobial activity only when it is folded in a helical manner (80). Furthermore, Wang et al. identified the core of the antimicrobial and anticancer activities in LL-37(13-37). This segment contains a central amphipathic helix, in contrast to the N-terminal segment LL-37(1-12), which is more hydrophobic, contains only a short helix, and is not toxic to either bacteria or cancer cells (161). Later studies reduced the antimicrobial core of LL-37 to KR-12, extending from residue 18 to 29 (132). As previously shown, our studies suggest that an α-helix/β-sheet secondary structure is necessary to have inhibitory activity. The two peptides that can fully inhibit IAPP fibril formation in a comparable way to LL-37, LL-37(1-34) and LL-37(3-37), exhibit α-helix/β-sheet structure, with a maximum at 198 nm and two minima, one at 208 nm and a more intense one at 226 nm. The structure of the peptides that show only a partial inhibitory effect, like LL-37(5-37) and LL-37(1-31), have a partially reduced helicity and the intensity of the two minima at 208 and 226 nm is comparable, indicating also a loss of β-sheet/turn content. In a similar manner, also LL-37(3-34) exhibits partially IAPP aggregation and cell-damaging effect. This peptide also presents mainly an α-helix secondary structure and almost no β-sheet content. In conclusion, we can affirm that there is a structure-activity relationship. The contemporary presence of α-helix and β-sheet/turn content is required for these peptides to be efficient inhibitors of IAPP fibrillogenesis.

Previous studies done via peptide array showed that both regions extending from positions 6 to 10 (FRKSK) and 25 to 27 (KDF) of the LL-37 sequence are binding cores, mediating the IAPP/LL-37 interaction. To further characterize the IAPP/LL-37 interaction interface, the binding affinities to monomeric IAPP were determined. Results showed that the N-terminus of LL-37 is not strongly mediating the interaction with IAPP. In fact, the app. K_d for LL-37(1-14) resulted in a binding affinity around 30 times weaker than for LL-37 (Table 35 and Figure 107). By elongating the sequence to LL-37(1-26), the binding affinity increases, and a nanomolar app. K_d could be obtained which is only ~ 2.5 weaker than the native sequence. The binding affinity increased by 10 times by only adding Phe27 to the sequence, indicating the important role of this residue for the IAPP/LL-37 interaction. Regarding LL-37(1-31) and LL-37(1-34), the binding affinity became stronger and comparable to the native sequence, suggesting that the central part of the sequence is involved in the IAPP/LL-37 interface.

Table 35. Binding of LL-37 and its C-terminal truncated segments to monomeric IAPP and determination of apparent binding affinities ($K_{d,app}$) by fluorescence titration assays.

LL-37 segments	**$K_{d,app}$ (±SD) (for Fluos-IAPP)[a]**
LL-37(1-14)	2.54 (± 0.5) μM
LL-37(1-26)	227.7 (± 2.1) nM
LL-37(1-27)	24.2 (± 4.2) nM
LL-37(1-31)	18.4 (± 6.8) nM
LL-37(1-34)	132.4 (± 3.2) nM
LL-37	88.1 (± 12.0) nM

[a] App. K_ds, means (±SD) from 3 binding curves. Determined via titrations of fluorescein-labeled IAPP (Fluos-IAPP, 5nM) with non-labeled LL-37 segments (aq. buffer 1×b, pH 7.4, containing 1% HFIP).

Interestingly, the C-terminus was found to give a major contribution to the interaction surface. All C-terminal segments, LL-37(3-37), LL-37(5-37), LL-37(7-37), and LL-37(15-37), bound to Fluos-IAPP with comparable strength to LL-37 (Table 36 and Figure 107). These findings are indeed in line with the molecular docking studies. As previously discussed, the molecular docking results suggest that in the IAPP/LL-37 1/1 and 1/2 complexes, the LL-37 regions from 17 to 33 and from 12 to 32 respectively stabilize the interaction between the two peptides.

Table 36. Binding of LL-37 and its N-terminal truncated segments to monomeric IAPP and determination of apparent binding affinities ($K_{d,app}$) by fluorescence titration assays.

LL-37 segments	**$K_{d,app}$ (±SD) (for Fluos-IAPP)[a]**
LL-37(3-37)	101.9 (± 56.0) nM
LL-37(5-37)	56.5 (± 8.8) nM
LL-37(7-37)	58.8 (± 7.5) nM
LL-37(15-37)	31.9 (± 2.2) nM
LL-37	88.1 (± 12.0) nM

[a] App. K_ds, means (±SD) from 3 binding curves. Determined via titrations of fluorescein-labeled IAPP (Fluos-IAPP, 5nM) with non-labeled LL-37 segments (aq. buffer 1×b, pH 7.4, containing 1% HFIP).

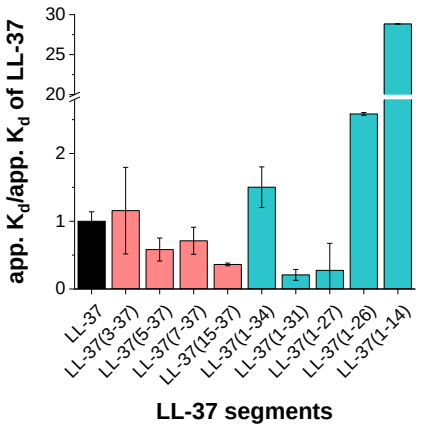

Figure 107. Relative app. K_ds of the interaction of LL-37 and LL-37 segments to monomeric IAPP.

In general, the binding studies suggest that a nanomolar affinity is not sufficient to have an anti-amyloid effect. Several segments which showed strong binding to monomeric IAPP could not intervene in its aggregation and cytotoxicity.

Lastly, cross-linking studies were carried out to have further insights into the mechanistic aspects of the inhibition potencies of the LL-37 segments. It has been previously discussed that LL-37 forms a hetero-complex with IAPP of circa 15 kDa and that this complex occurs only when an inhibitory effect is present. Similarly, we asked if these complexes are formed between IAPP and the shortened LL-37 segments. IAPP solutions contained low MW oligomers extending from dimers to hexamers, as well as high MW aggregates as visible from the smear band at the top of the gel. When IAPP was mixed in 1/1 with the N-terminal segments different results were obtained. The inhibitor LL-37(1-34) and the partial inhibitor LL-37(1-31) exhibited low MW complexes and the hetero-band of 15 kDa, confirming the presence of the hetero-tetramer complex between IAPP and the inhibitors. If IAPP is mixed with non-inhibitors like LL-37(1-27), LL-37(1-26), and LL-37(1-14), which had no effect on the lag phase of IAPP aggregation, this hetero-complex is not present (Figure 67b). Furthermore, the pattern of the bands was the same as the IAPP incubation, confirming that these peptides do not affect its aggregation. The C-terminal segments behave in a similar manner. The hetero-tetramer band was visible for the 1/1 mixtures of IAPP with LL-37(3-37), LL-37(5-37), and LL-37(7-37), but not for the mixture with LL-37(15-37). In fact, it has been shown that LL-37(3-37) and LL-37(5-37) inhibit fully or partially, respectively the aggregation of IAPP. LL-37(7-37) has still a slight effect on IAPP amyloidogenesis at 24 hours, as shown in the ThT assay studies, and this might explain the presence of the hetero-complex. LL-37(15-37) does not have any effect on the misfolding of IAPP and presents a similar pattern to IAPP in the cross-linking studies (Figure 67a). Of note, also the incubations of the LL-37 segments detectable by the anti-LL-37 antibody presented a homo-tetrameric band at 15 kDa. It is known that LL-37 assembles into tetrameric complexes (133), and according to our results also the segments of LL-37 do. In

conclusion, these studies suggest that the presence of an IAPP/inhibitor hetero-tetramer is required to observe at least a partial inhibitory effect of IAPP self-assembly.

In this second part of my work the shortest LL-37 truncated peptides which can inhibit IAPP fibril formation as LL-37 were identified. LL-37(1-34) and LL-37(3-37) inhibit IAPP aggregation of IAPP as the native peptide. Additionally, when both C- and N-termini are neglected, the inhibitory potency is significantly weakened. Studies also suggest a structure-activity relationship. The peptides that could efficiently block IAPP aggregation have an α-helix-/β-sheet, β-turn secondary structure. When the β-sheet content is lost, the inhibitory effect is weaker or completely lost if the peptides are unstructured. Binding studies confirmed what was discussed in the first section: the IAPP/LL-37 interaction is mainly mediated by the central/C-terminal region of LL-37, although its presence is not sufficient to have an inhibitory effect. Finally, studies suggest the IAPP-LL-37 segments tetrameric complexes are the main hetero-oligomeric species and that they may underlie the inhibitory effect of the LL-37 segments. Results of this chapter are summarized in Table 37.

Table 37. Overview of the biophysical characterization and interactions of LL-37 segments with IAPP.

Peptide	Inhibition of IAPP fibril formation	Secondary structure (1xb + 1% HFIP)	IAPP/LL-37 hetero-tetramer (~15 kDa)	Binding affinity to monomeric IAPP
LL-37	✓	α-helix/β-sheet	✓	88.1 (± 12.0) nM
LL-37(3-37)	✓	α-helix/β-sheet	✓	101.9 (± 56.0) nM
LL-37(5-37)	partially ✓	α-helix	✓	51.3 (± 15.0) nM
LL-37(7-37)	✗	partially α-helix	✓	62.7 (± 17.8) nM
LL-37(15-37)	✗	unordered	✗	31.9 (± 2.2) nM
LL-37(1-14)	✗	unordered	✗	2.54 (± 0.5) µM
LL-37(1-26)	✗	unordered	✗	227.7 (± 2.1) nM
LL-37(1-27)	✗	unordered	✗	24.2 (± 4.2) nM
LL-37(1-31)	partially ✓	partially α-helix/ β-sheet	✓	18.4 (± 6.8) nM
LL-37(1-34)	✓	α-helix/β-sheet	✓	132.4 (± 3.2) nM
LL-37(3-34)	partially ✓	α-helix	-	34.7 (± 7.1) nM

Legend: ✓= the peptide is an inhibitor of IAPP amyloid formation; ✗= the peptide cannot block IAPP amyloid formation; - = not determined.

5.3 Identification of FF as key residues for the inhibitory effect of LL-37 on IAPP amyloidogenesis and cytotoxicity

In the third part of this work, we investigated the role of Phe5 and Phe6 on the inhibitory potency of LL-37 on IAPP self-assembly. In section 4.2 the shortening of the LL-37 was carried out, to find the shortest LL-37 sequence that could inhibit the amyloid formation. In these studies, it was clear that when the phenylalanine residues 5 and 6 were neglected from the sequence, the inhibitory potency was completely lost. Considering these results, we further investigated these findings by systematically substituting Phe5 and Phe6 with alanine in LL-37, LL-37(3-37), and LL-37(5-37). The aromatic residues of LL-37 (Phe5, Phe6, Phe17, Phe27) are involved in micelle and membrane binding (88, 130). The aromatic residues are also highly conserved within the cathelicidin family and are also involved in the self-assembly of LL-37. Phe5 and Phe6 play a role in the oligomerization of LL-37, as they stack on each other as a result of an aromatic-aromatic interaction. In fact, a LL-37 derived sequence, in which these residues were replaced, showed a lower oligomerization propensity (130). Further on, structural studies revealed that Phe5, Phe6 and Phe27 form adjacent nest-like structures, that stabilize a fiber-like tetrameric structure (79).

As for the LL-37 segments, also the LL-37 derived alanine mutants were obtained via the Fmoc-SPPS strategy. For most of these peptides, TentaGel R PBH resin was chosen, since the maximum SL obtainable with this resin is 0.2 mmol/g, and from our previous experience we observed that a lower SL could facilitate the difficult couplings and reduce the eventual formation of side-products (167, 168). Also in this case, all syntheses were successful and all pure products could be obtained after one or two rounds of RP-HPLC purification. As all the sequences contained aspartic acid, the Fmoc-cleavage was carried out with 20% piperidine in DMF containing 0.1 M HOBt (105), and no aspartimide formation was observed. The protocol described in section 4.3.1 is a result of years of synthesis and empirical observations on how to improve the yield of the products by reducing the formation of the acetylated side products. The coupling conditions for Ile^{20}, Arg^{19}, Lys^{18}, Phe^{17}, Glu^{16}, Gly^{14}, Ile^{13}, Asp^{4}, and Leu^{2} (Table 18) were further improved using stronger reaction conditions, like applying the reactive HATU as coupling reagent (166), higher amounts of reagents, and/or couplings were repeated multiple times. This approach allowed us to obtain the full-length sequence single and double alanine mutants with high purity, which was not possible with a highly substituted Wang resin. All cleavages were carried out with a TFA/H_2O mixture and no problems were observed with this procedure. For the purification of these peptides via RP-HPLC, different gradients were tested, and the ones that gave the best yield are reported in Table 26.

The effect of these substitutions on the secondary structure of LL-37 was evaluated via circular dichroism. The double alanine mutant, LL-37A5,6 exhibited an oligomerization propensity at 20 μM, just like LL-37. The striking difference was rather observed in the secondary structure. In fact, LL-37A5,6 exhibits less signal, referable to less helical content than LL-37, and its β-sheet/turn content is absent. The two minima at 206 and 222 nm have comparable intensities, suggesting that the peptide is mainly α-helical. The single alanine mutant LL-37A5 oligomerized at a concentration of 10 μM, but its secondary structure is quite similar to LL-37. Also LL-37A6 presents an α-helix/β-sheet secondary structure, suggesting that the single substitution of Phe5 or Phe6 does not have a dramatic effect on the conformation of the peptide (Figure 108a). In absence of HFIP in the assay buffer, LL-37 displays an α-helical structure. In contrast, LL-37A5,6 partially loses its helical content induced by the HFIP, and a partially unordered structure is visible (Figure 108b). These circular dichroism studies suggest the importance of Phe5 and Phe6 for the helical content of LL-37. The secondary structure of the single alanine mutants in aqueous assay buffer was very different. LL-37A5 and LL-37A6 showed similar secondary structures, with a maximum at 198 nm and two minima, one at 208 nm and the more intense one at 224 nm indicating an α-helix and β-sheet/turn content. In these exceptional cases, the effect of HFIP on the secondary structure was not as evident as for all the other peptides studied, since the β-sheet/turn content was not induced by the HFIP (Figure 108b).

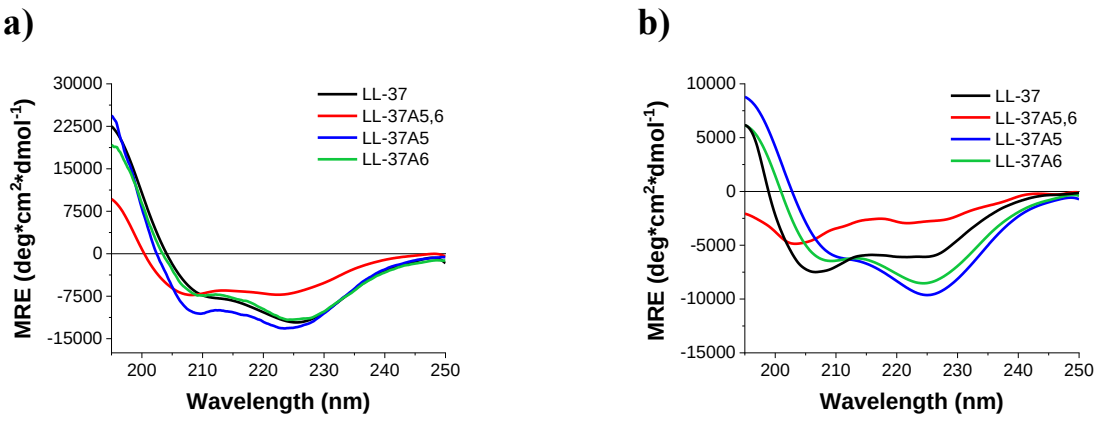

Figure 108. Secondary structure of LL-37, LL-37A5,6, LL-37A5, or LL-37A6 assessed by far-UV CD spectroscopy. a) Secondary structure of LL-37, LL-37A5,6, LL-37A5, or LL-37A6. Measurements were performed at 5 µM in aqueous buffer 1×b, pH 7.4, containing 1% HFIP. b) Secondary structure of LL-37, LL-37A5,6, LL-37A5, or LL-37A6. Measurements were performed at 5 µM in aqueous buffer 1×b, pH 7.4.

With regards to the shorter sequences LL-37(3-37) and LL-37(5-37), only the double alanine mutants were investigated to support the findings for the native peptide. LL-37(3-37) exhibited a significant loss of secondary structure when the two alanine residues were introduced. LL-37(3-37)A5,6, definitely presents less structural content and less β-sheet secondary structure, as the two minima at 208 and 222 nm in the spectra have the same intensity (Figure 109a). LL-37(5-37)A5,6 behaved likely: compared to LL-37(5-37), this peptide clearly presents less structural content, indicated by its reduced signal. Also, for this peptide, the minimum at 204 nm is more pronounced than the one at 224 nm and the signal at 198 nm is significantly reduced compared to LL-37(5-37), which indicates a transition to a partial random coil state (Figure 109b). In general, these studies show that the substitution of the FF motif with alanine residues leads to a general loss of structural content and of β-sheet/turn signal in comparison to LL-37 (Figure 109).

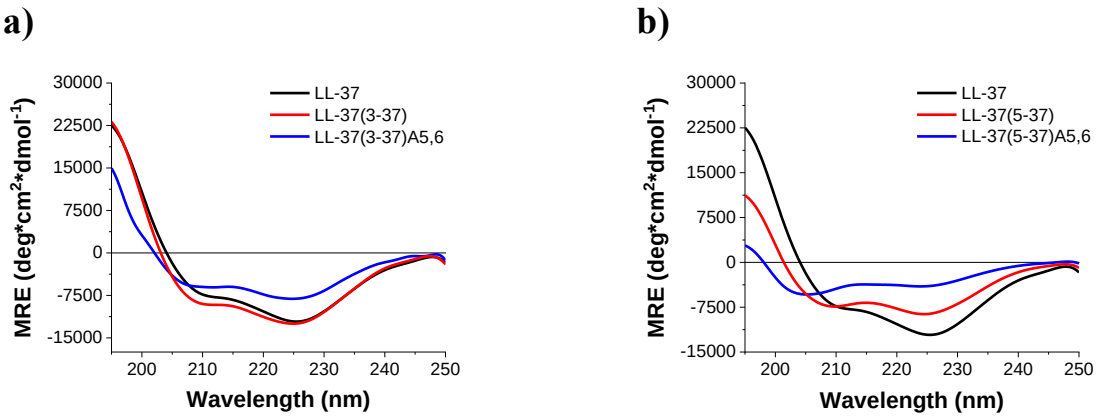

Figure 109. Secondary structure of LL-37, LL-37(3-37), LL-37(3-37)A5,6 or LL-37(5-37), LL-37(5-37)A5,6 assessed by far-UV CD spectroscopy. Measurements were performed at 5 µM in aqueous buffer 1×b, pH 7.4, containing 1% HFIP.

To compare the effect of the alanine substitutions on the secondary structure of LL-37 and its segments, MRE values at 222 nm and 227 nm were plotted, indicative for the α-helix and the β-sheet/turn secondary structures respectively. A similar effect is observed at 222 and 227 nm for all peptides. LL-37A5,6 exhibits a loss of both α-helix and β-sheet/turn structure, as the MRE values are approximately half compared to the native sequence. In contrast, the single alanine mutants LL-37A5 and LL-37A6 have similar secondary structures to LL-37. A similar effect is visible for LL-37(3-37)A5,6 and LL-37(5-37)A5,6: their α-helix and β-sheet/ turn structure is

circa the half of their non-mutated analogs (Figure 110a, b). As previously observed the substitution of Phe5 and Phe6 with alanine causes an overall loss of secondary structure.

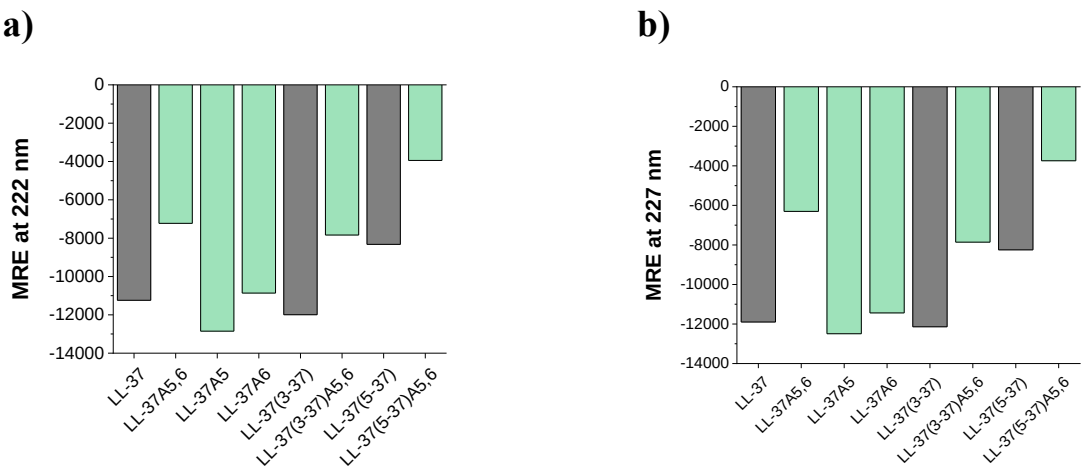

Figure 110. MRE values of LL-37 and LL-37 alanine mutants at 222 and 227 nm obtained via CD spectroscopy. a) MRE at 222 nm of LL-37, LL-37(3-37), and LL-37(5-37) (grey), and LL-37A5,6, LL-37A5, LL-37A6, LL-37(3-37)A5,6, and LL-37(5-37)A5,6 (green). b) MRE at 227 nm of LL-37, LL-37(3-37), and LL-37(5-37) (grey), and LL-37A5,6, LL-37A5, LL-37A6, LL-37(3-37)A5,6, and LL-37(5-37)A5,6 (green). MRE values are taken from measurements performed at 5 μM in 10 mM sodium phosphate buffer, pH 7.4, containing 1% HFIP.

The helical propensity for LL-37A5,6 was investigated via CD spectroscopic titration with increasing amounts of TFE, known to induce a helical conformation (131). As already discussed above, LL-37A5,6 displays an α-helix secondary structure already without the presence of TFE. As shown in Figure 111a, the overall helical content is significantly less for the double alanine mutant as shown from the significantly different signal intensities. In fact, the titration slightly increased the amount of helical content of LL-37A5,6, and the T_M was estimated at 2% TFE versus the 4-times higher T_M at 8% of the native sequence (Figure 111b). Unlike LL-37, LL-37A5,6 does not display a minimum at 227 nm which is attributed to a β-sheet/turn content and this might explain why the amounts of TFE required to have an α-helix structure are higher for LL-37. LL-37A5 and LL-37A6 exhibit an α-helix and β-sheet/turn secondary structure without TFE with a maximum at 198 nm and the two minima at 208 and a more marked one at 226 nm, similar to LL-37. The titration with various amounts of TFE led to the transition of these peptides structures to α-helices with T_M values at 21 and 20% respectively. These results suggest that the single substitution of the Phe5 or Phe6 did not affect the β-sheet/turn content of these peptides, but caused a loss of the helical propensity of LL-37 (T_M: 8% TFE) as the transitions occur for these peptides with 2.5-fold more TFE amount (Figure 111b).

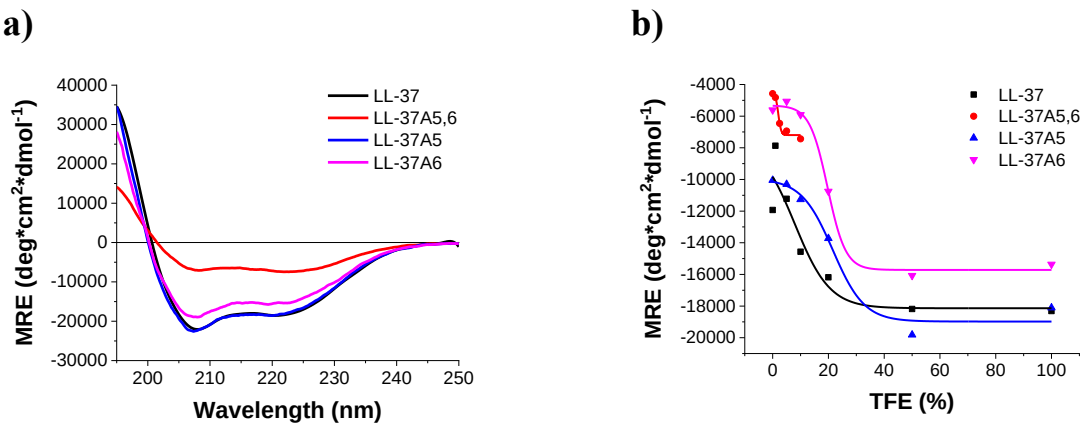

Figure 111. Comparison of the α-helical propensity of LL-37, LL-37A5,6, LL-37A5, or LL-37A6 obtained via CD spectroscopy. a) CD spectra of LL-37, LL-37A5,6, LL-37A5, and LL-37A6 at their maximal helical content (100%, 10%, 100%, and 100% TFE respectively). b) Plot of minima at 222 nm versus the TFE amounts (%) of the CD spectra of the peptides shown in a). Measurements were performed at 5 µM in aqueous buffer 1×b, pH 7.4, containing 1% HFIP and the indicated amounts of TFE.

Next, we asked whether the replacement of FF with alanine would affect the inhibitory potency of the peptides against IAPP fibril formation. In fact, we previously observed a structure-activity relationship, so we expected to see differences for the alanine mutants as their structural content was reduced. Interestingly, our hypothesis was confirmed by the ThT and MTT assay results. LL-37A5,6 in fact could inhibit IAPP amyloid formation for 48 hours and its cytotoxicity only for 24 hours when mixed with IAPP in equimolar amounts. Furthermore, also in 10-fold molar excess, LL-37A5,6 could not inhibit with IAPP aggregation fully, leading to the conclusion that Phe5 and Phe6 are crucial, as the inhibitory potency was weakened at least 10 times by the alanine mutations compared to LL-37 (Figure 112 and Figure 113).

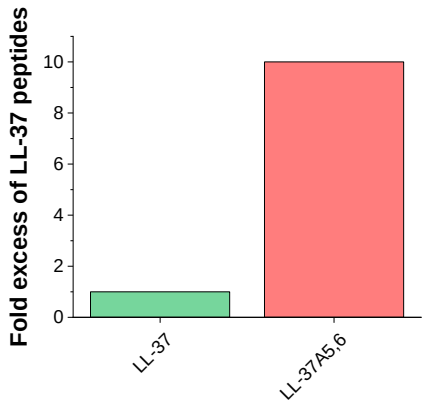

Figure 112. Amounts of LL-37 and LL-37A5,6 required to inhibit IAPP fibril formation. Bar plot shows the excess of inhibitor tested. Green bar represents inhibitory concentrations; red bar represents no inhibitory effect.

We then investigated what is the effect of the single phenylalanine residues, so LL-37A5 and LL-37A6 were tested towards their inhibitory potency. Surprisingly, LL-37A5 and LL-37A6 did not have significant differences from LL-37A5,6. Both peptides had a partial inhibitory effect, only until 72 hours, as LL-37A5,6 (Figure 113). Results show that both phenylalanine residues are important for the inhibitory potency of LL-37, but with no additive effect.

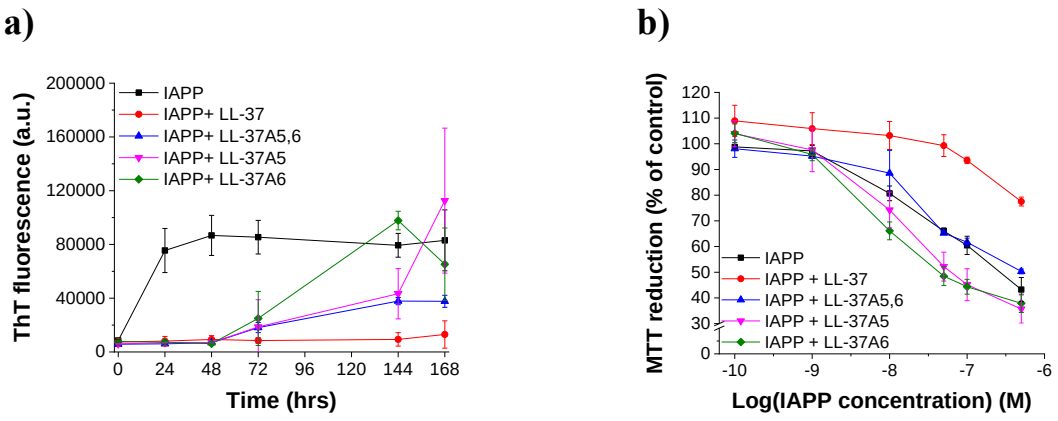

Figure 113. Effects of LL-37, LL-37A5,6, LL-37A5, or LL-37A6 on IAPP amyloid formation and cytotoxicity. a) Fibrillogenesis of IAPP (16.5 µM) and its mixtures with LL-37 (1/1), LL-37A5,6 (1/1), LL-37A5 (1/1) or LL-37A6 (1/1) (means (±SD), 3 assays); b) effects on cell viability: solutions from a) were added to cultured RIN5fm cells (7 days aged). Cell viability was determined by MTT reduction (means (±SD), 3 assays, n=3 each).

A similar effect was observed for LL-37(3-37). This peptide is a potent inhibitor of IAPP fibril formation, but when the alanine mutations were introduced in LL-37(3-37)A5,6, the inhibitory potency was reduced from 168 hours to 24 hours (Figure 114).

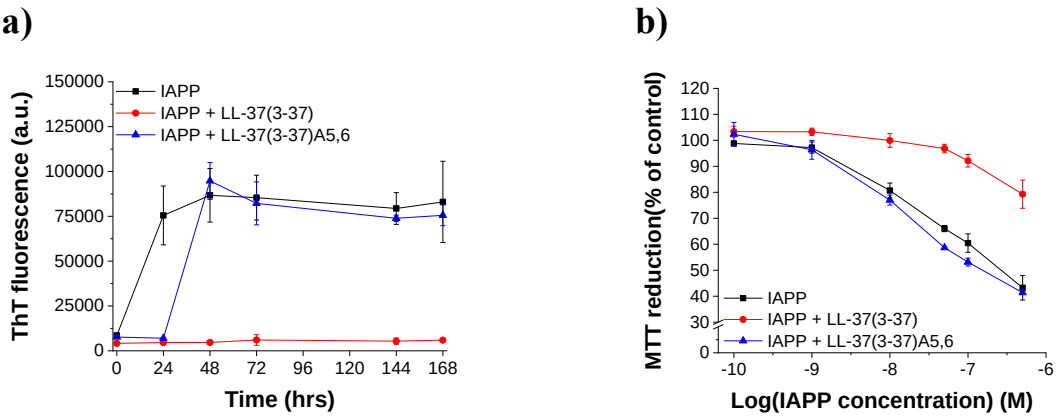

Figure 114. Effects of LL-37(3-37) or LL-37(3-37)A5,6 on IAPP amyloid formation and cytotoxicity. a) Fibrillogenesis of IAPP (16.5 µM) and its mixtures with LL-37(3-37) (1/1), or LL-37(3-37)A5,6 (1/1) (means (±SD), 3 assays); b) effects on cell viability: solutions from a) were added to cultured RIN5fm cells (7 days aged). Cell viability was determined by MTT reduction (means (±SD), 3 assays, n=3 each).

Last, also LL-37(5-37)A5,6 was tested. This peptide could not interfere with IAPP aggregation at all, whereas LL-37(5-37) could at least delay the lag phase of aggregation for 72 hours (Figure 115). These results identified the FF motif of LL-37 as crucial for the interference of LL-37 and its derived peptides with IAPP amyloidogenesis and cytotoxicity.

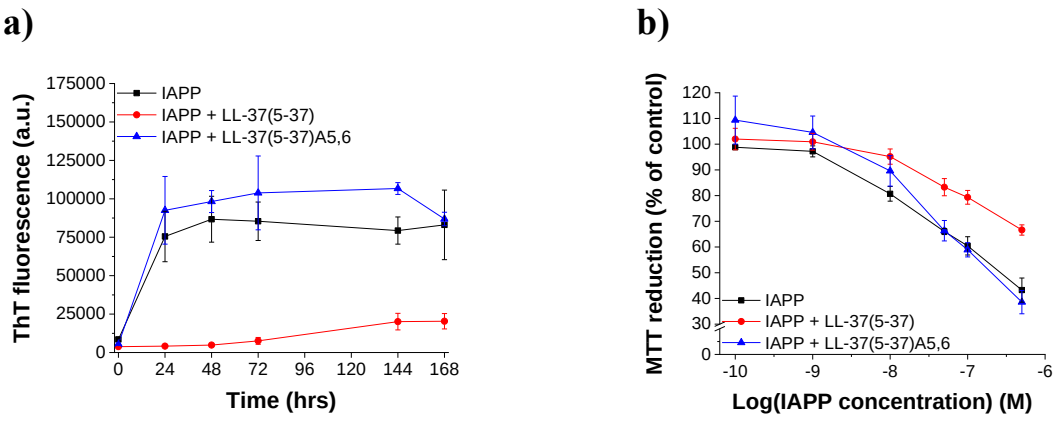

Figure 115. Effects of LL-37(5-37) or LL-37(5-37)A5,6 on IAPP amyloid formation and cytotoxicity. a) Fibrillogenesis of IAPP (16.5 µM) and its mixtures with LL-37(5-37) (1/1), or LL-37(5-37)A5,6 (1/1) (means (±SD), 3 assays); b) effects on cell viability: solutions from a) were added to cultured RIN5fm cells (7 days aged). Cell viability was determined by MTT reduction (means (±SD), 3 assays, n=3 each).

Clearly, our inhibition studies indicate that Phe5 and Phe6 have a crucial role in the ability of LL-37 to interfere with the aggregation of IAPP. Further studies are currently in progress to investigate if also Phe17 and Phe27 are crucial for the inhibition of IAPP self-assembly. Preliminary studies show that Phe17 is not crucial for the inhibitory potency of LL-37, since LL-37A17 effectively blocks IAPP fibril formation. The aromatic residues are known to play an important role in the properties of this peptide. All the phenylalanine residues are responsible for the association of the peptide with anionic lipid micelles (132). This hydrophobic and aromatic surface of the peptide can be also exploited for drug delivery purposes, as they have been also identified to interact with aliphatic chains of GMOs, nanocarriers based on glycerol monooleate used for delivery of AMPs and maximizing their bactericidal activity (177). Furthermore, the introduction of phenylalanine residues increased the antibacterial activity of other AMPs (178, 179). In the case of protonectin, an AMP derived from the wasp *Agelaia pallipes* active against both Gram-positive and Gram-negative bacteria, the introduction of phenylalanine into the sequence increased the selectivity towards Gram-positive bacteria due to different interaction with the bacterial membranes (178). The introduction of phenylalanine zippers in the design of AMPs induced anticancer and apoptotic properties to the peptide FR-15 (179).

The effect of the alanine substitutions of the IAPP/LL-37 binding affinity was verified via fluorescence spectroscopic titrations. LL-37A5,6 exhibited strong binding to monomeric IAPP, leading to an app. K_d of 182.8 (± 20.9) nM which is comparable to the one found for LL-37, which is 88.1 (± 12.0) nM. LL-37(3-37) and LL-37(3-37)A5,6 exhibited high binding affinities for Fluos-IAPP, leading to app. K_ds of 101.9 (± 56.0) nM and 22.9 (± 4.9) nM respectively. Last, LL-37(5-37) and LL-37(5-37)A5,6 also bound to Fluos-IAPP with app. K_d values of 56.5 (± 8.8) nM and 173.5 (± 106.6) nM, respectively (Table 38).

Table 38. Effect of alanine mutation of Phe5 and Phe6 on the binding to monomeric IAPP and determination of apparent binding affinities ($K_{d,app}$) by fluorescence titration assays.

LL-37 segments	**$K_{d,app}$ (±SD) (for Fluos-IAPP)[a]**
LL-37	88.1 (± 12.0) nM
LL-37A5,6	182.8 (± 20.9) nM
LL-37(3-37)	101.9 (± 56.0) nM
LL-37(3-37)A5,6	22.9 (± 4.9) nM
LL-37(5-37)	56.5 (± 8.8) nM
LL-37(5-37)A5,6	173.5 (± 106.6) nM

[a] App. K_ds, means (±SD) from 3 binding curves. Determined via titrations of fluorescein-labeled IAPP (Fluos-IAPP, 5nM) with non-labeled LL-37 alanine mutants (aq. buffer 1×b, pH 7.4, containing 1% HFIP).

Overall, the replacement of both Phe5 and Phe6 residues with alanine did not significantly affect the binding affinity of these peptides to monomeric-IAPP, suggesting that these two aromatic residues have a strong effect on the inhibitory properties but not on the interaction with IAPP. In fact, the app. K_ds of the binding affinity are 2-fold weaker in the case of LL-37A5,6 and LL-37(5-37)A5,6 compared to LL-37 and LL-37(5-37) respectively, but in the case of LL-37(3-37)A5,6 the binding affinity is approximately 2 times better compared to LL-37(3-37), suggesting no particular trend in the binding affinity when Phe5 and Phe6 are replaced with alanine (Figure 116). These results confirm that as long as the central/C-terminal regions of LL-37 are present, the binding affinity to Fluos-IAPP is not affected.

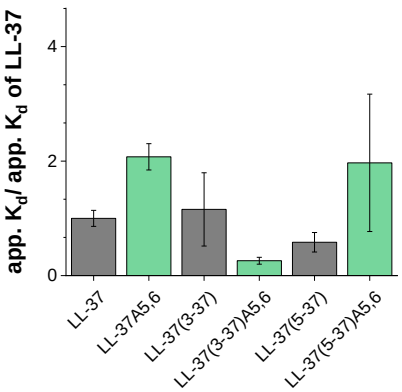

Figure 116. Relative app. K_ds of the binding affinity of LL-37 and LL-37 alanine mutants to monomeric IAPP.

Sancho-Vaello et al. showed that LL-37 forms tetrameric supramolecular assemblies. Phe5, Phe6, together with Phe27, are highly conserved in the cathelicidin family and they form a hydrophobic scaffold, which stabilizes the tetrameric structure (79). Interestingly, the results of my thesis suggest that LL-37 forms hetero-complexes with IAPP, particularly hetero-tetramers. Additionally, Phe15 and Phe23 of IAPP are required for the cross-interaction of IAPP with Aβ42 (128). For the reasons mentioned above, we asked whether Phe5 and Phe6 of LL-37 could interact with Phe15 and Phe23 of IAPP to stabilize the hetero-tetrameric assemblies. Binding affinity studies between Fluos-A15,23 and LL-37 led to the app. K_d value of 132.3 (± 78.5) nM, which is very similar to the app. K_d value of the binding affinity of the two peptides with no alanine mutations (88.1 (± 12.0) nM). Results underline that these four aromatic residues do not contribute significantly to the binding affinity of the IAPP/LL-37 interaction.

To further characterize the effect of the FF motif on the formation of the IAPP/LL-37 hetero-complexes, cross-linking studies were performed. IAPP presented low MW complexes, mostly from dimers to hexamers, as well as high MW aggregates. The mixtures of IAPP with LL-37, LL-37(3-37), and LL-37(5-37) present the band at 15 kDa, attributable to the hetero-tetramers, and no high MW complexes were observed, as already discussed in section 5.2. When IAPP was co-incubated with LL-37A5,6 and LL-37(3-37)A5,6, the hetero-complex at 15 kDa was still observed and the high MW complexes were reduced. This result correlates with the ThT binding assay result, as LL-37A5,6 can inhibit IAPP fibril formation for 72 hours and LL-37(3-37)A5,6 for 24 hours. By contrast, when IAPP is incubated with LL-37(5-37)A5,6, low and high MW complexes are present and no hetero-tetramer was visible, as for the incubation of IAPP alone (Figure 84). In fact, this peptide has no effect on IAPP aggregation already at 24 hours and therefore does not form any hetero-tetramer with it. In general, results confirm that the mechanism of inhibition of IAPP self-assembly involves the formation of a tetrameric structure between IAPP and the inhibitor. Furthermore, the substitution of Phe5 and Phe6 with alanine does not preclude the formation of hetero-complexes as already suggested by the binding affinity studies.

Given these results, we next asked what is the effect of single alanine mutations on the hetero-complex formation. When IAPP was mixed with LL-37A5 or LL-37A6 at time zero, no evident difference with the double alanine mutant LL-37A5,6 was observed. These peptides form low MW complexes with IAPP, as well as the hetero-complex at ~15 kDa, as for LL-37A5,6. In fact, the single alanine mutants show a partial inhibitory effect, therefore a hetero-complex at time zero was expected. We consequently asked if the hetero-complex was still present after 7 days of incubation time, where no inhibition was observed. In this case, the hetero-complex is only clearly visible for the incubation with LL-37, while in the mixtures with LL-37A5,6, LL-37A5, and LL-37A6 the band at 15 kDa was significantly diminished (Figure 85). Results support the hypothesis that the hetero-complex formation underlies the capability of these peptides to inhibit IAPP fibril formation. Last, we asked whether the substitution of Phe5 and Phe6 would affect the inhibition property of LL-37 to block Aβ42 aggregation. In fact, it has been shown that Aβ42 and LL-37 are binding partners and that LL-37 inhibits its amyloid aggregation and cytotoxic effect (99). The studies carried out by the Barron group were inspired by the fact that both Aβ42 and LL-37 have an FF motif conserved within the sequence, which is KLVFF and DFFRK respectively, which are known to contribute to the self-assembly (180) of these two peptides (79, 99). Instead, Santos et al. showed that PMSα3 and LL-37 are also selective binders of α-synuclein toxic species, blocking the aggregation and cell-damaging effects of α-synuclein. The mechanism behind their inhibitory activity is not based on sequence homology, like in the case of Aβ42 (99) and IAPP (114), but on the cationic and amphipathic helical character of these peptides (104). Our studies suggest that when the Phe5 and Phe6 are neglected, the inhibitory potency of LL-37 is reduced. In fact, the Aβ42 fibril formation and cytotoxicity were partially blocked when Aβ42 was incubated with LL-37A5,6. To conclude, the FF motif seems to have an effect on the ability of LL-37 to inhibit the fibril formation of amyloids. Specifically, this effect is more evident in the case of IAPP amyloidogenesis rather than in Aβ42 aggregation. Furthermore, as previously shown using surface plasmon resonance, LL-37 interacts with Aβ40 in its monomeric/low-MW state, leading to an app. K_d value in the µM range (99). We confirmed the presence of this interaction in the experimental conditions used for the binding affinity assays (1xb buffer, pH 7.4, containing 1% HFIP). Fluorescence spectroscopic titrations yielded an app. K_d value above 10 µM for the interaction of LL-37 with Aβ40 monomers and no binding until 5 µM could be determined for the Aβ40 oligomers. Results confirmed that LL-37 binds preferably low-MW oligomers as shown by Barron et al. (99).

The third part of my work underlined the importance of the Phe5 and Phe6 aromatic residues of the LL-37 sequence for the inhibition of IAPP self-assembly. Both neglecting or substituting these two residues affects 1st) the secondary structure of the peptide and, 2nd) the inhibitory potency of the peptides against amyloid formation, although these residues do not significantly participate in the IAPP/LL-37 interaction interface. Results are summarized in Table 39.

Table 39. Overview of the biophysical characterization and interactions of LL-37 Phe5 and Phe6 alanine mutants with IAPP.

Peptide	Inhibition of IAPP fibril formation	Secondary structure	IAPP/LL-37 hetero-tetramer (~15 kDa)	Binding affinity to monomeric IAPP
LL-37	✓	α-helix/β-sheet	✓	88.1 (± 12.0) nM
LL-37A5,6	partially ✓	α-helix	✓	182.8 (± 29.9) nM
LL-37A5	partially ✓	α-helix/β-sheet	✓	-
LL-37A6	partially ✓	α-helix/β-sheet	✓	-
LL-37(3-37)	✓	α-helix/β-sheet	✓	101.9 (± 56.0) nM
LL-37(3-37)A5,6	✗	α-helix	✗	22.9 (± 4.9) nM
LL-37(5-37)	partially ✓	α-helix	✓	56.5 (± 8.8) nM
LL-37(5-37)A5,6	✗	partially unordered	✗	173.5 (± 106.6) nM

Legend: ✓= the peptide is an inhibitor of IAPP amyloid formation; ✗= the peptide cannot block IAPP amyloid formation; - = not determined.

6 Conclusions

Protein misfolding is linked to the pathogenesis of many neurodegenerative diseases and the formation of amyloid fibrils. In particular, the aggregation of islet amyloid polypeptide (IAPP) is linked to pancreatic inflammation and β-cell degeneration in type 2 diabetes (T2D) patients. Due to the devastating effects of amyloidosis, there are many studies nowadays that aim to interfere with amyloid fibril formation, and several designed peptides were proven to successfully delay amyloid self-assembly in vitro (23). In this work, the effect of the only human cathelicidin known, LL-37, on IAPP fibril formation and cytotoxicity was investigated. LL-37 is a 37-amino acid long peptide known for its antimicrobial, antiviral, and immunoregulatory role, and proven to interfere with the aggregation of amyloid beta (Aβ), an amyloidogenic peptide involved in the pathogenesis of Alzheimer's disease (AD).

Results of the first part of this work suggested that LL-37 binds IAPP with nanomolar affinity. In fact, LL-37, which shares high sequence similarity with IAPP (42%), interacts with it in its monomeric and fibrillar states. Furthermore, in vitro studies showed that LL-37 was found to block IAPP aggregation into cytotoxic species in an equimolar ratio, by the formation of soluble and non-toxic amorphous aggregates containing both peptides. Furthermore, LL-37 was found to efficiently bind IAPP fibrils, converting them into species with no seeding ability. Cross-linking studies showed the formation of a hetero-tetramer between IAPP and LL-37 only in the presence of inhibitory concentration of LL-37 giving an insight into the mechanism of inhibition of this peptide. Using a peptide array, LL-37(6-10) and LL-37(25-27) were identified as the binding cores of the interaction with IAPP. In addition, the whole sequence was dissected into two parts, LL-37(1-14) and LL-37(15-37), each containing one binding core. Via fluorescence spectroscopic titrations, it was shown that the central/C-terminal region contained in LL-37(15-37) is mediating the interaction of LL-37 with IAPP and that the N-terminus is only weakly contributing to the affinity of the IAPP/LL-37 interaction. Of note, these results were supported by molecular docking findings that identified the region extending from residue 17 to 27 as the core of the interaction with IAPP. In addition, titrations via fluorescence spectroscopy suggested that IAPP(8-28) binds to LL-37 with high affinity. The next question was which is the shortest LL-37 segment that retains the inhibitory potency of LL-37. To address it, the LL-37 was rationally shortened at its C- and/or N-terminus and the synthesized segments were tested in vitro to evaluate their inhibitory potencies. The C-terminal shortened segments were LL-37(1-34), LL-37(1-31), LL-37(1-27), LL-37(1-26), and LL-37(1-14). Out of these, only LL-37(1-34) retained the inhibitory potency of LL-37 for the inhibition of IAPP fibril formation. LL-37(1-31) was only able to delay the fibril formation, while all other segments had no effect, also at 10-fold molar excess to IAPP. The N-terminal truncation led to LL-37(3-37), LL-37(5-37), LL-37(7-37), and LL-37(15-37). Out of these segments, LL-37(3-37) was the only segment able to inhibit IAPP fibril formation at 1/1 as LL-37. LL-37(5-37) only partially interfered with the aggregation of IAPP into cell-damaging species, while all other segments had an inhibitory potency that was more than 10-times weaker than LL-37. When both N- and C-terminus were neglected, leading to LL-37(3-34) the inhibitory potency of LL-37 of the aggregation of IAPP into fibrils was partially lost. Circular dichroism studies on the secondary structure of these peptides and their oligomerization evidenced a structure-activity relationship. In fact, all IAPP inhibitors, like LL-37, LL-37(1-34), and LL-37(3-37) displayed a specific CD spectrum, indicative of α-helix and/or β-sheet/turn structural contents. Of note, the lack of this specific CD "signature" in all the other segments correlated with a partial and/or no inhibitory ability. Further studies on the binding affinity of the partial LL-37 segments, confirmed the findings of the first part of this work: the central/C-terminus of LL-37 mediates its binding with IAPP and the nanomolar binding affinity of shorter LL-37 segments to IAPP is not sufficient to have an inhibitory effect on its amyloid formation. In the third part of this work, the role of two residues Phe5 and Phe6 of the LL-37 sequence was investigated. Interestingly, when the LL-37 sequence was shortened it was evidenced that the inhibitory potency of LL-37 was completely lost when these two residues were neglected. To confirm these findings, double and single alanine mutants were synthesized. LL-37A5,6 could only partially inhibit the aggregation of IAPP into cytotoxic species also in 10-fold excess. Furthermore, the single Ala mutants, LL-37A5 and LL-37A6 showed similar inhibitory potency to LL-37A5,6, confirming

that both residues are important for the inhibitory effect of LL-37. A similar effect was observed also for shorter segments: LL-37(3-37)A5,6 and LL-37(5-37)A5,6 showed reduced or no inhibitory capability, compared to their non-mutated sequences. Circular dichroism studies showed a loss of α-helix and/or β-sheet/turn structure when both alanine residues were introduced to replace the FF motif. This correlated with the loss of inhibitory function. Although these two residues were found to be crucial for the inhibitory activity of LL-37 against the aggregation of IAPP into amyloidogenic species, their presence is not important for the high binding affinity. Of note, it was also shown that LL-37A5,6 has a weaker inhibitory effect than LL-37 on Aβ42 aggregation into cytotoxic species, with Phe5 and Phe6 being important for the inhibitory potency of LL-37 on Aβ42 aggregation as well. To conclude, LL-37 was identified as a potent inhibitor of IAPP fibril formation into cell damaging species. The biological role of this interaction should be further investigated as LL-37 or partial segments could be candidates for interfering with the β-cell inflammatory process.

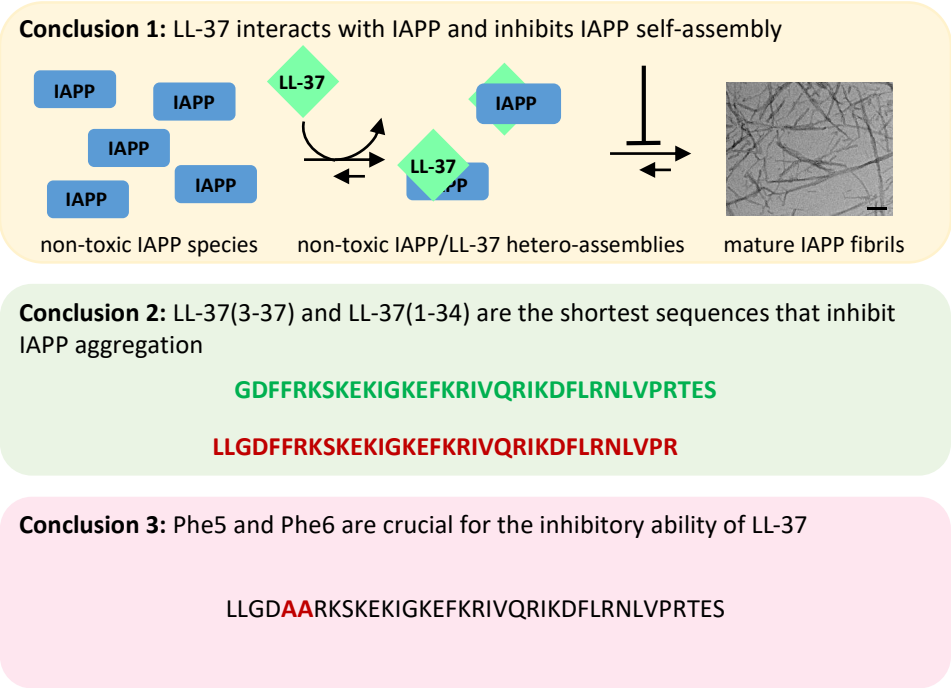

Scheme 5. Schematic representation of the results of this work. In the first part, LL-37 was identified as an inhibitor of IAPP amyloid formation. The second part of this work identified LL-37(3-37) and LL-37(1-34) as the shortest segments that retain inhibitory potency. In the third part, the role of Phe5 and Phe6 on the structure, function, and inhibitory properties of LL-37 was investigated.

7 Appendix

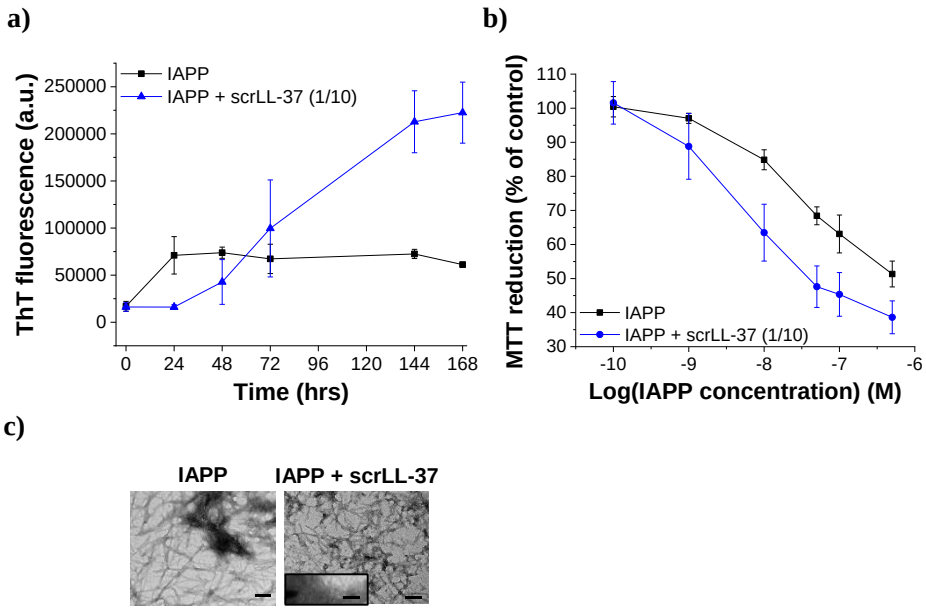

Appendix Figure A 1. Effects of scrLL-37 on IAPP amyloid formation and cell-damaging effects. a) Fibrillogenesis of IAPP (16.5 µM) and its mixtures with scrambled LL-37 (1/10) (means (±SD), 3 assays). b) Effects on cell viability: solutions from a) were added to cultured RIN5fm cells (7 days aged). Cell viability was determined by MTT reduction (means (±SD), 3 assays, n=3 each). c) TEM images of solutions of a) (7 days aged) as indicated (bars, 100 nm). The figure is taken from Armiento et al. (ACIE, 2020) (114).

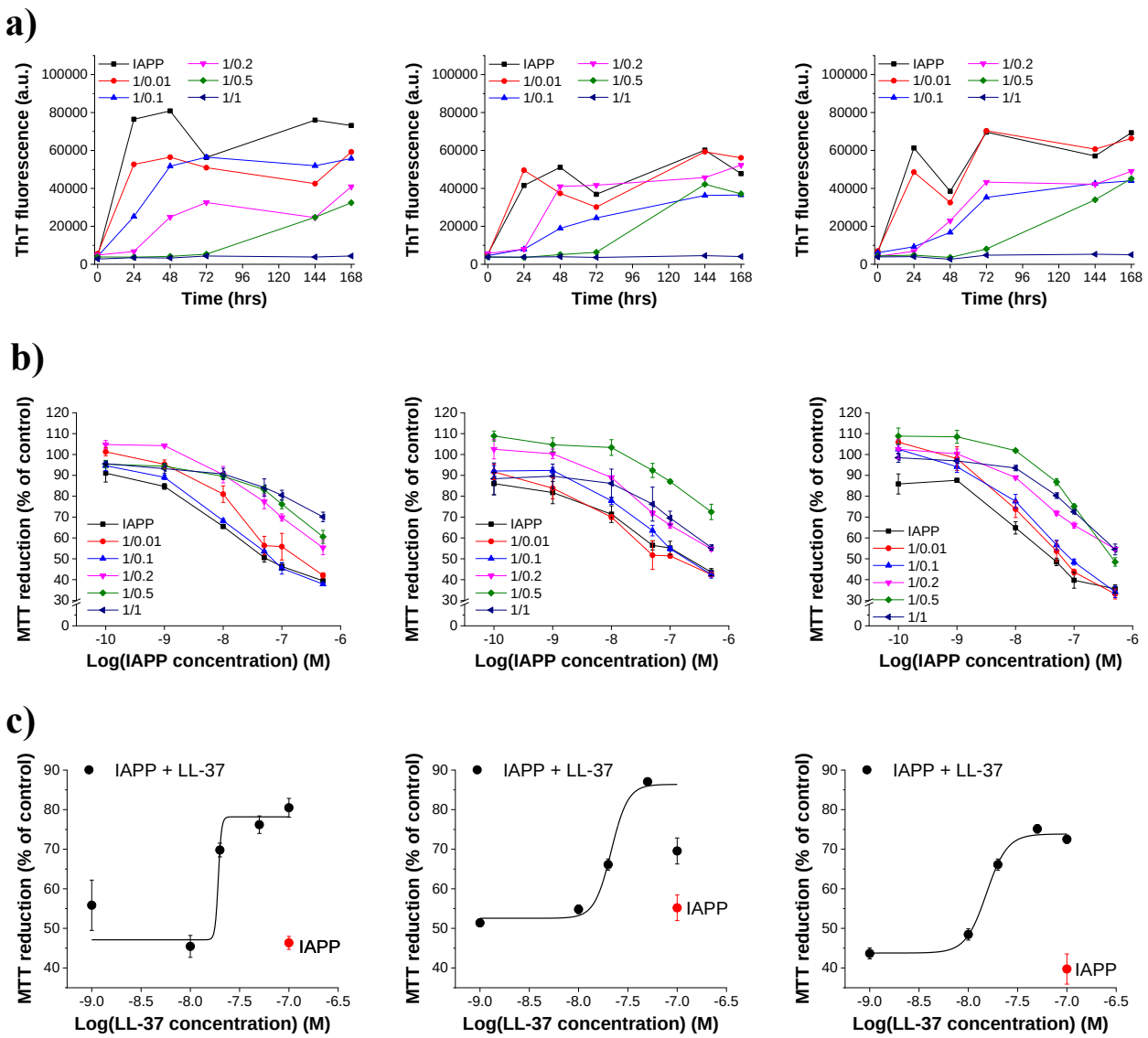

Appendix Figure A 2. Dose-dependence of the inhibitory effect of LL-37 on IAPP fibrillogenesis and cytotoxicity. a) Fibrillogenesis of IAPP (16.5 µM) alone or with different molar ratios of LL-37 as indicated (1 assay each); effects on cell viability: solutions from a) were added to cultured RIN5fm cells (24 hours aged). c) IC_{50} of the inhibitory effect of LL-37 on cytotoxic effects of IAPP determined by titration of IAPP (100 nM) with LL-37 (1 assay each, n=3).

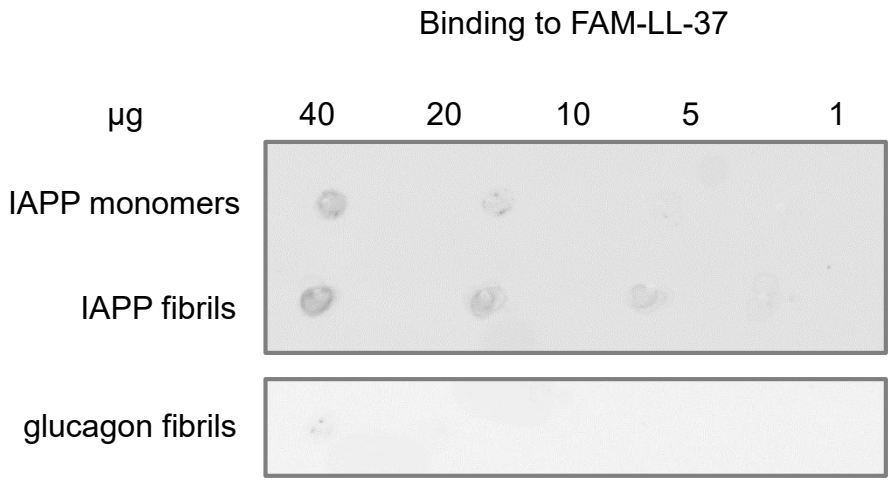

Appendix Figure A 3. Intrinsic fluorescence of IAPP monomers, IAPP fibrils, and glucagon fibrils. IAPP monomers, fIAPP, and glucagon fibrils were spotted onto a nitrocellulose membrane and probed with ThT buffer (50 mM sodium phosphate buffer, containing 100 mM NaCl) containing 1% HFIP. Representative membrane is reported (n=3).

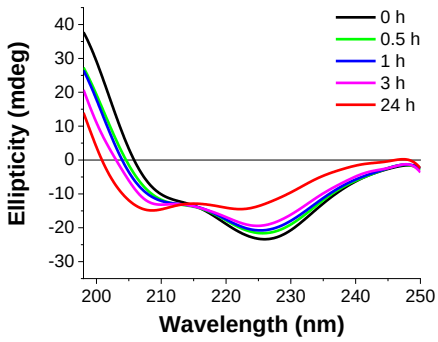

Appendix Figure A 4. Characterization of the IAPP/LL-37 interaction. Far-UV CD spectra of LL-37 (5 µM). Measurements were performed in aqueous buffer 1×b, pH 7.4, containing 1% HFIP.

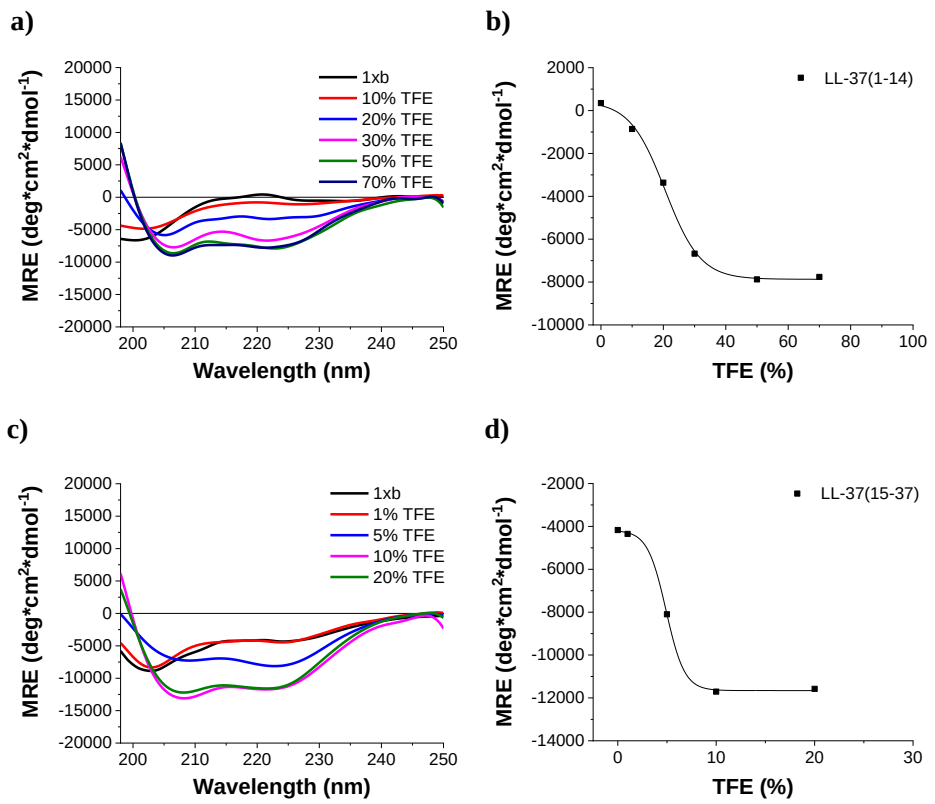

Appendix Figure A 5. Effects of TFE on the conformation in aqueous solution of a) LL-37(1-14), c) LL-37(15-37) assessed by far-UV CD spectroscopy. Experiments were performed at peptide concentrations of 5 µM aqueous buffer 1×b, pH 7.4, containing 1% HFIP with the indicated amounts of TFE. b), d) plots of minima at 222 nm versus the TFE amounts (%) of the CD spectra of the peptides shown in a) and c) respectively. Linus Wollenweber's data (129).

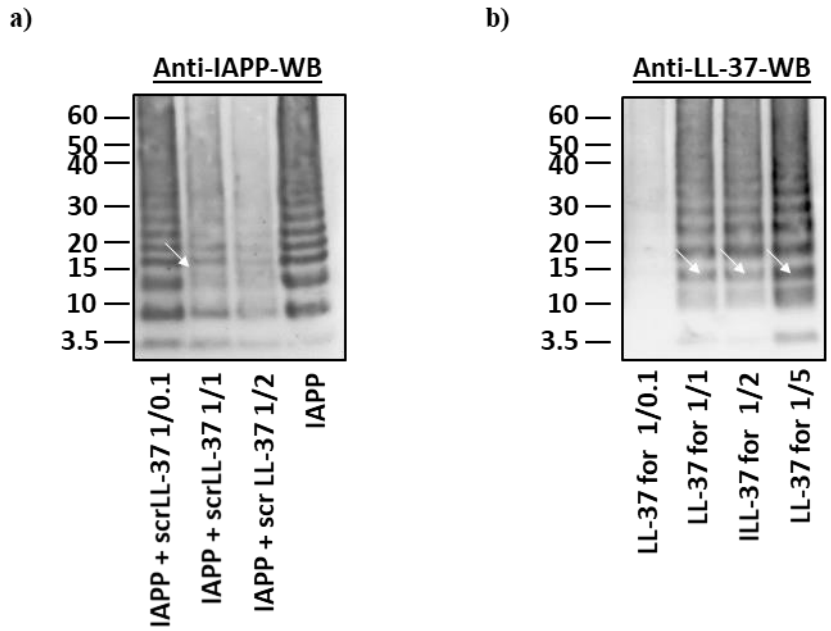

Appendix Figure A6. Characterization of the scrLL-37-IAPP hetero-assemblies via cross-linking (pH 7.4). a) NuPAGE and WB with IAPP (30 µM) and its mixtures with scrLL-37 (1/0.1, 1/1, and 1/2) is shown. Representative gel is reported (n>5). b) Characterization of LL-37 homo-oligomers (including homotetramers at ~15 kDa) via cross-linking (pH7.4). NuPAGE and WB with LL-37 (3, 30, 60, and 150 µM) is shown. Representative gel is reported (n=3). The figure is taken from Armiento et al. (ACIE, 2020) (114).

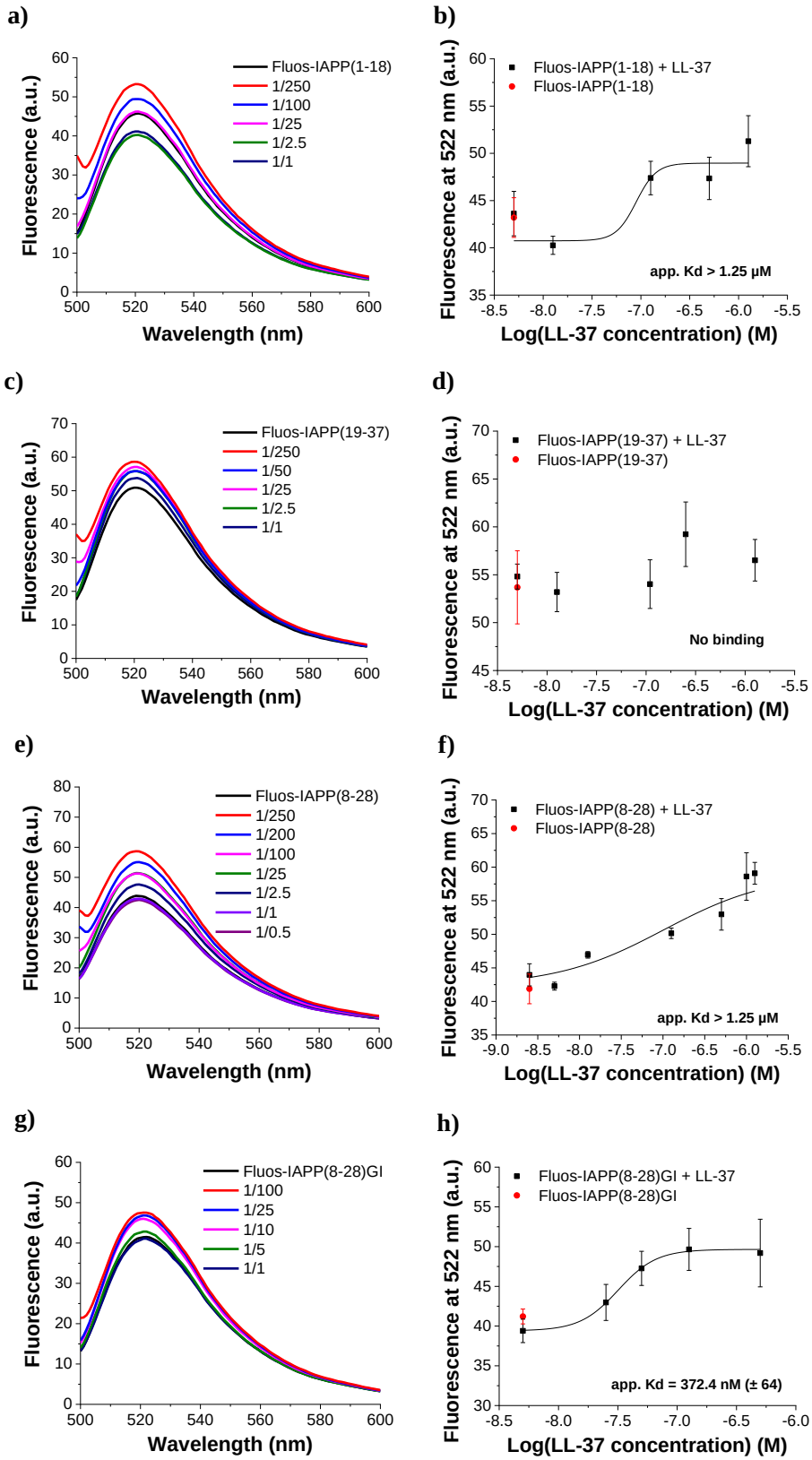

Appendix Figure A 7. Determination of app. K_ds of interactions of oligomeric LL-37 species with IAPP segments by fluorescence spectroscopy. Panels a), c), e), g) show fluorescence spectra of Fluos-IAPP segments (5nM) alone and their mixtures with various amounts of LL-37; the molar ratios of Fluos-IAPP segments/LL-37 are as indicated. Panels b), d), f), h) show the binding curves of Fluos-IAPP(1-18) (b), Fluos-IAPP(19-37) (d), Fluos-IAPP(8-28) (f), Fluos-IAPP(8-28)GI (h) with LL-37; app. K_ds are means (±SD) from 3 binding curves. Measurements were performed in aqueous buffer 1×b, pH 7.4, containing 1% HFIP.

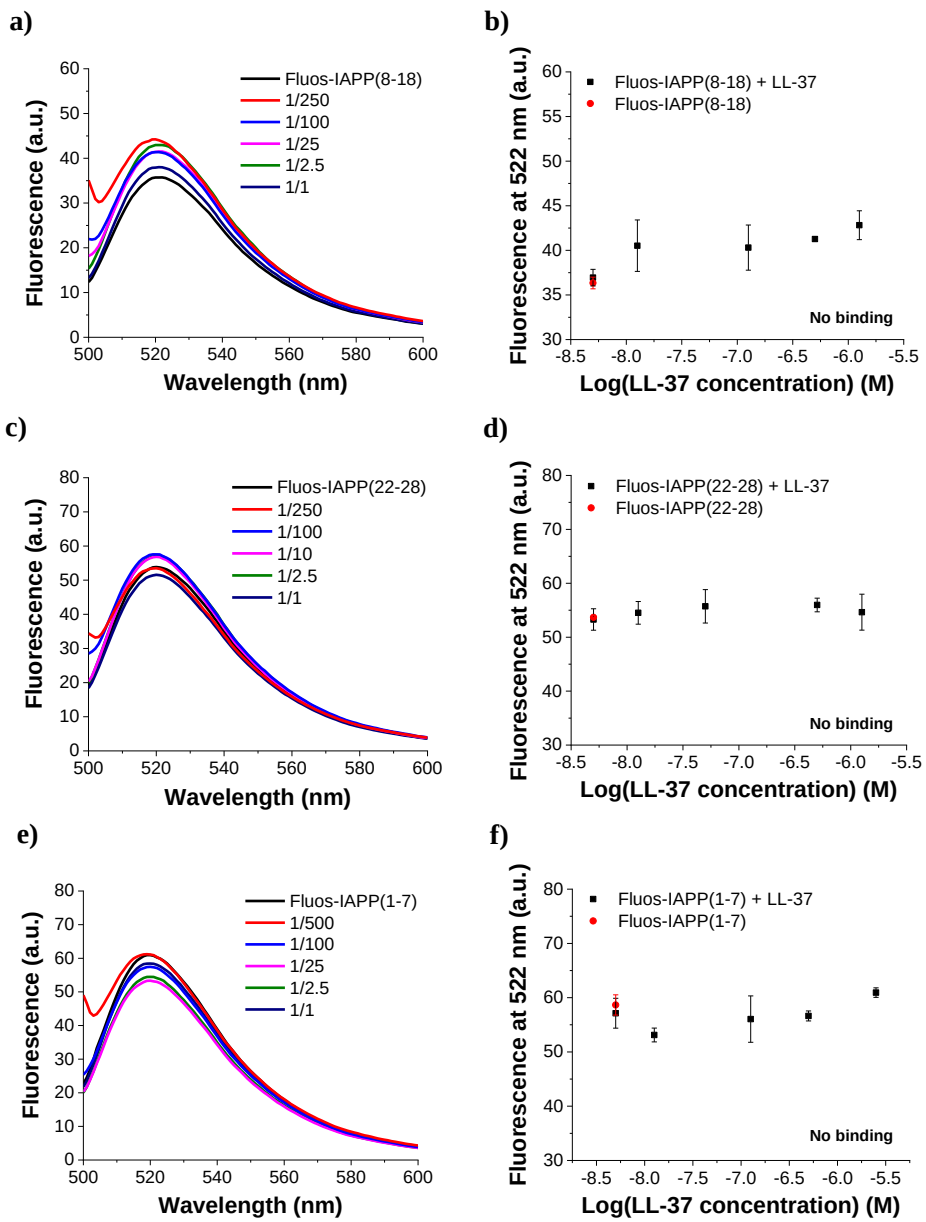

Appendix Figure A 8. Determination of app. K_ds of interactions of oligomeric LL-37 species with IAPP segments by fluorescence spectroscopy. Panels a), c), e) show fluorescence spectra of Fluos-IAPP segments (5nM) alone and their mixtures with various amounts of LL-37; the molar ratios of Fluos-IAPP segments/LL-37 are as indicated. Panels b), d), f) show the binding curves of Fluos-IAPP(8-18) (b), Fluos-IAPP(22-28) (d), Fluos-IAPP(1-7) (f) with LL-37; app. K_ds are means (±SD) from 3 binding curves. Measurements were performed in aqueous buffer 1×b, pH 7.4, containing 1% HFIP.

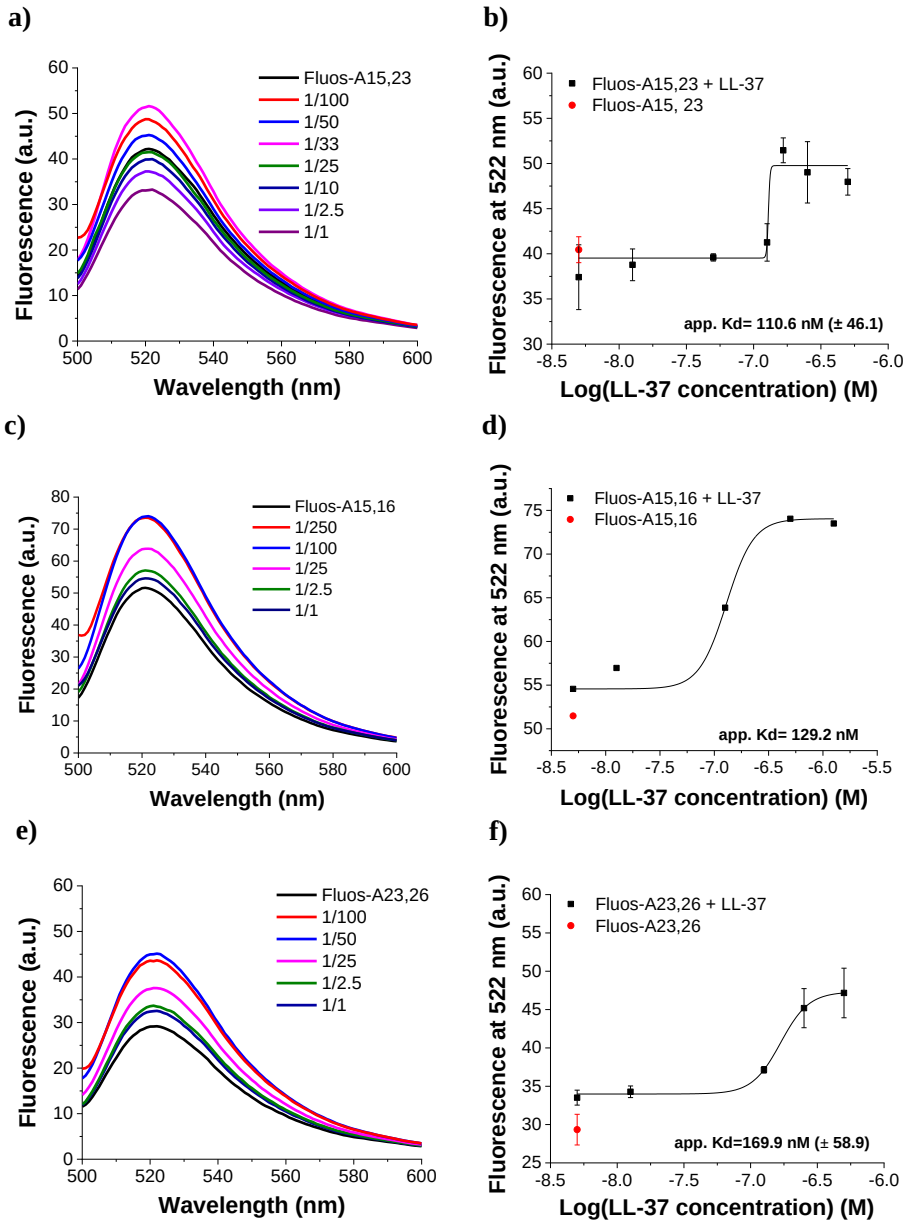

Appendix Figure A 9. Determination of app. K_ds of interactions of oligomeric LL-37 species with IAPP alanine mutants by fluorescence spectroscopy. Panels a), c), e) show fluorescence spectra of Fluos-IAPP alanine mutants (5nM) alone and their mixtures with various amounts of LL-37; the molar ratios of Fluos-IAPP alanine mutants/LL-37 are as indicated. Panels b), d), f) show the binding curves of Fluos-A15,23 (b), Fluos-A15,16 (d), Fluos-A23,26 (f) with LL-37; app. K_ds in (b) and (f) are means (±SD) from 3 binding curves. For curve (d) a representative experiment is reported (n=2)). (Linus Wollenweber's data (129)). Measurements were performed in aqueous buffer 1×b, pH 7.4, containing 1% HFIP.

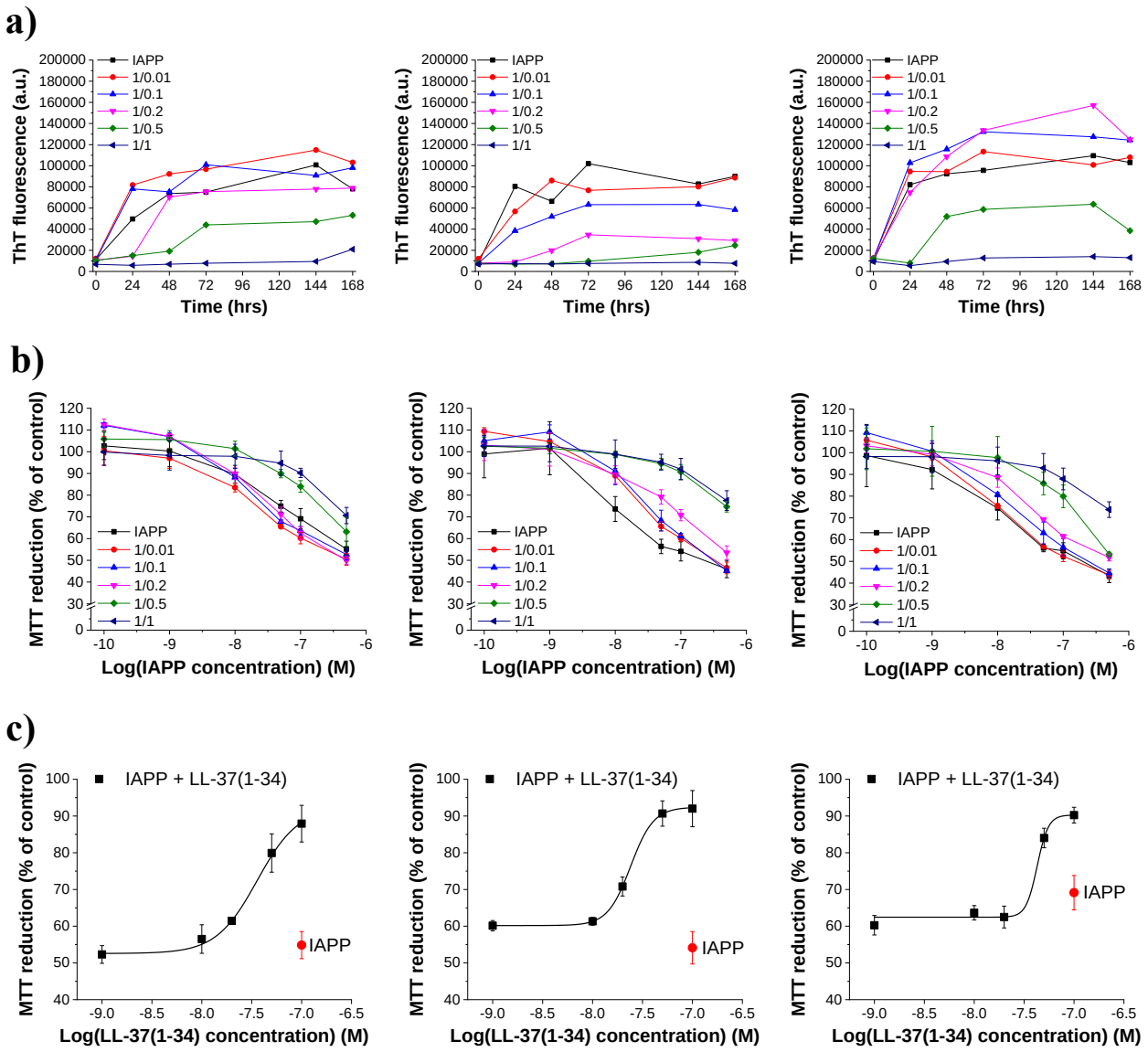

Appendix Figure A 10. Dose-dependence of the inhibitory effect of LL-37(1-34) on IAPP fibrillogenesis and cytotoxicity. a) Fibrillogenesis of IAPP (16.5 µM) alone or with different molar ratios of LL-37(1-34) as indicated (1 assay each); effects on cell viability: solutions from a) were added to cultured RIN5fm cells (24 hours aged). c) IC_{50} of the inhibitory effect of LL-37(1-34) on cytotoxic effects of IAPP determined by titration of IAPP (100 nM) with LL-37(1-34) (1 assay each, n=3).

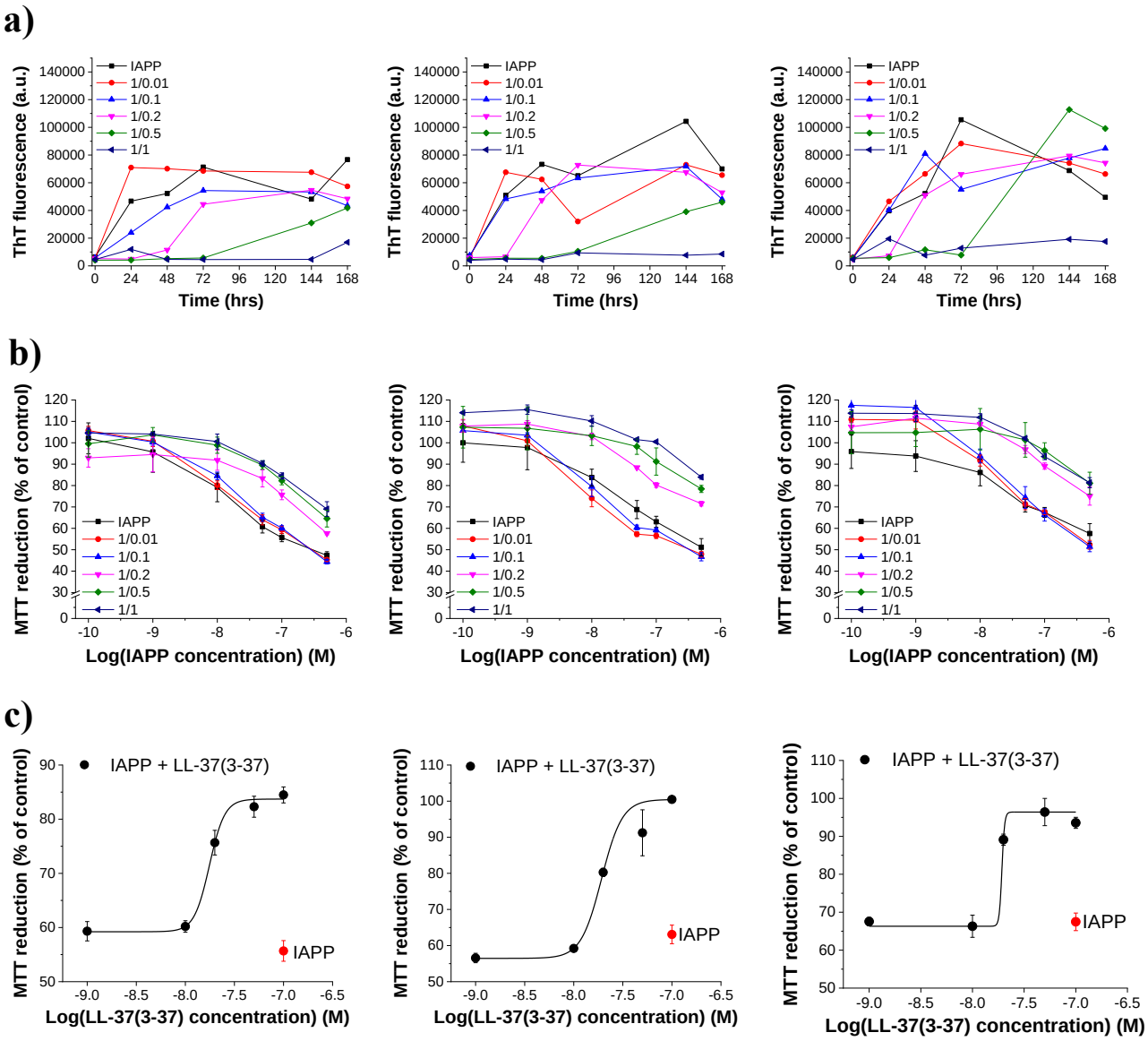

Appendix Figure A 11. Dose-dependence of the inhibitory effect of LL-37(3-37) on IAPP fibrillogenesis and cytotoxicity. a) Fibrillogenesis of IAPP (16.5 µM) alone or with different molar ratios of LL-37(3-37) as indicated (1 assay); effects on cell viability: solutions from a) were added to cultured RIN5fm cells (24 hours aged). c) IC_{50} of the inhibitory effect of LL-37(3-37) on cytotoxic effects of IAPP determined by titration of IAPP (100 nM) with LL-37(3-37) (1 assay, n=3).

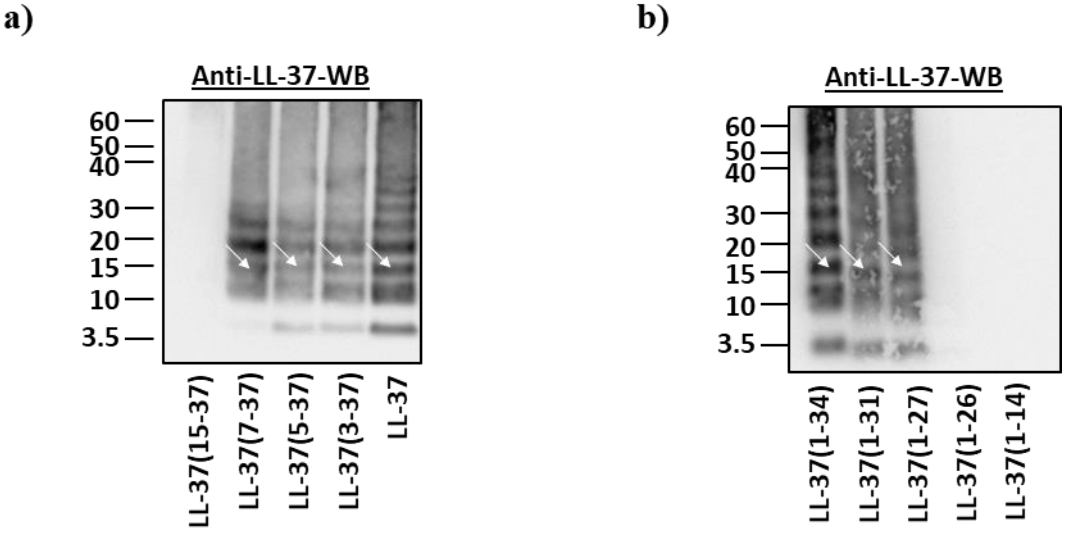

Appendix Figure A 12. Characterization of LL-37 segments homo-oligomers via cross-linking (pH 7.4). a) NuPAGE and WB with LL-37(15-37), LL-37(7-37), LL-37(5-37), and LL-37(3-37) (30 μM) are shown. Representative gel is reported (n=2). b) NuPAGE and WB with LL-37(1-34), LL-37(1-31), LL-37(1-27), LL-37(1-26), and LL-37(1-14) (30 μM) is shown. Representative gel is reported (n=2).

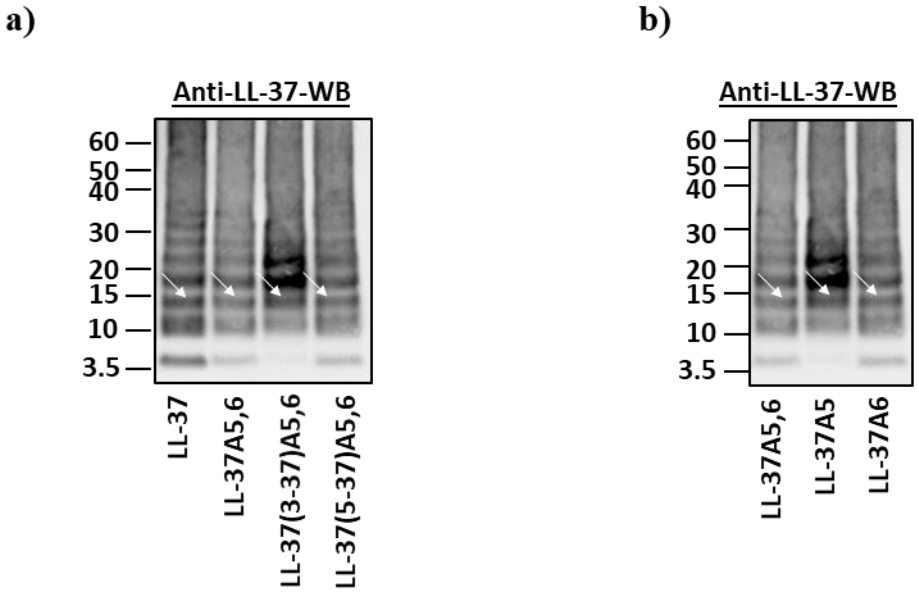

Appendix Figure A 13. Characterization of LL-37 alanine mutants homo-oligomers via cross-linking (pH 7.4). a) NuPAGE and WB with LL-37, LL-37A5,6, LL-37(3-37)A5,6,and LL-37(5-37)A5,6 (30 μM) are shown. Representative gel is reported (n=3). b) NuPAGE and WB with LL-37A5,6, LL-37A6, and LL-37A5 (30 μM) is shown. Representative gel is reported (n=3).

List of tables

List of figures

List of appendix figures

List of schemes

8 References

1. F. Chiti, C. M. Dobson, Protein Misfolding, Amyloid Formation, and Human Disease: A Summary of Progress Over the Last Decade. *Annu Rev Biochem* **86**, 27-68 (2017).
2. J. D. Sipe, A. S. Cohen, Review: history of the amyloid fibril. *J Struct Biol* **130**, 88-98 (2000).
3. F. Chiti, C. M. Dobson, Protein misfolding, functional amyloid, and human disease. *Annu Rev Biochem* **75**, 333-366 (2006).
4. D. S. Eisenberg, M. R. Sawaya, Structural Studies of Amyloid Proteins at the Molecular Level. *Annu Rev Biochem* **86**, 69-95 (2017).
5. R. Riek, D. S. Eisenberg, The activities of amyloids from a structural perspective. *Nature* **539**, 227-235 (2016).
6. H. Bennhold, Eine specifische Amyloidfärbung mit Kongorot. *Műnchen. Med. Wochenschrift* **44**, 1537-1538 (1922).
7. M. R. Nilsson, Techniques to study amyloid fibril formation in vitro. *Methods* **34**, 151-160 (2004).
8. K. P. Nilsson, Small organic probes as amyloid specific ligands--past and recent molecular scaffolds. *FEBS Lett* **583**, 2593-2599 (2009).
9. M. Tornquist *et al.*, Secondary nucleation in amyloid formation. *Chem Commun (Camb)* **54**, 8667-8684 (2018).
10. A. Mukherjee, C. Soto, Prion-Like Protein Aggregates and Type 2 Diabetes. *Cold Spring Harbor Perspectives in Medicine* **7** (2017).
11. P. Westermark, A. Andersson, G. T. Westermark, Islet amyloid polypeptide, islet amyloid, and diabetes mellitus. *Physiol Rev* **91**, 795-826 (2011).
12. A. Abedini, A. M. Schmidt, Mechanisms of islet amyloidosis toxicity in type 2 diabetes. *FEBS Lett* **587**, 1119-1127 (2013).
13. R. Akter *et al.*, Islet Amyloid Polypeptide: Structure, Function, and Pathophysiology. *J Diabetes Res* **2016**, 2798269 (2016).
14. L. Marzban *et al.*, Role of beta-cell prohormone convertase (PC)1/3 in processing of pro-islet amyloid polypeptide. *Diabetes* **53**, 141-148 (2004).
15. J. J. Wiltzius, S. A. Sievers, M. R. Sawaya, D. Eisenberg, Atomic structures of IAPP (amylin) fusions suggest a mechanism for fibrillation and the role of insulin in the process. *Protein Sci* **18**, 1521-1530 (2009).
16. J. J. Wiltzius *et al.*, Atomic structure of the cross-beta spine of islet amyloid polypeptide (amylin). *Protein Sci* **17**, 1467-1474 (2008).
17. J. A. Williamson, A. D. Miranker, Direct detection of transient alpha-helical states in islet amyloid polypeptide. *Protein Sci* **16**, 110-117 (2007).
18. O. Sumner Makin, L. C. Serpell, Structural characterisation of islet amyloid polypeptide fibrils. *J Mol Biol* **335**, 1279-1288 (2004).
19. C. Roder *et al.*, Cryo-EM structure of islet amyloid polypeptide fibrils reveals similarities with amyloid-beta fibrils. *Nat Struct Mol Biol* **27**, 660-667 (2020).
20. R. Gallardo *et al.*, Author Correction: Fibril structures of diabetes-related amylin variants reveal a basis for surface-templated assembly. *Nat Struct Mol Biol* **27**, 1094 (2020).
21. Q. Cao, D. R. Boyer, M. R. Sawaya, P. Ge, D. S. Eisenberg, Cryo-EM structure and inhibitor design of human IAPP (amylin) fibrils. *Nat Struct Mol Biol* **27**, 653-659 (2020).
22. A. Kapurniotu, Enlightening amyloid fibrils linked to type 2 diabetes and cross-interactions with Abeta. *Nat Struct Mol Biol* **27**, 1006-1008 (2020).
23. V. Armiento, A. Spanopoulou, A. Kapurniotu, Peptide-Based Molecular Strategies To Interfere with Protein Misfolding, Aggregation, and Cell Degeneration. *Angew Chem Int Ed Engl* **59**, 3372-3384 (2020).

24. A. Kapurniotu, A. Schmauder, K. Tenidis, Structure-based design and study of non-amyloidogenic, double N-methylated IAPP amyloid core sequences as inhibitors of IAPP amyloid formation and cytotoxicity. *J Mol Biol* **315**, 339-350 (2002).
25. L. M. Yan, M. Tatarek-Nossol, A. Velkova, A. Kazantzis, A. Kapurniotu, Design of a mimic of nonamyloidogenic and bioactive human islet amyloid polypeptide (IAPP) as nanomolar affinity inhibitor of IAPP cytotoxic fibrillogenesis. *Proc Natl Acad Sci U S A* **103**, 2046-2051 (2006).
26. E. Andreetto *et al.*, A Hot-Segment-Based Approach for the Design of Cross-Amyloid Interaction Surface Mimics as Inhibitors of Amyloid Self-Assembly. *Angew Chem Int Ed Engl* **54**, 13095-13100 (2015).
27. P. Sormanni, F. A. Aprile, M. Vendruscolo, Rational design of antibodies targeting specific epitopes within intrinsically disordered proteins. *Proc Natl Acad Sci U S A* **112**, 9902-9907 (2015).
28. P. Krotee *et al.*, Common fibrillar spines of amyloid-beta and human islet amyloid polypeptide revealed by microelectron diffraction and structure-based inhibitors. *J Biol Chem* **293**, 2888-2902 (2018).
29. A. Frydman-Marom, R. Shaltiel-Karyo, S. Moshe, E. Gazit, The generic amyloid formation inhibition effect of a designed small aromatic beta-breaking peptide. *Amyloid* **18**, 119-127 (2011).
30. K. N. Huggins *et al.*, Designed hairpin peptides interfere with amyloidogenesis pathways: fibril formation and cytotoxicity inhibition, interception of the preamyloid state. *Biochemistry* **50**, 8202-8212 (2011).
31. C. A. Lane, J. Hardy, J. M. Schott, Alzheimer's disease. *Eur J Neurol* **25**, 59-70 (2018).
32. A. Alzheimer, Über eine eigenartige Erkrankung der Hirnrinde. *Allgemeine Zeitschrift fur Psychiatrie und Psychisch-gerichtliche Medizin.* **64**, 146-148 (1907).
33. R. J. Bateman *et al.*, Autosomal-dominant Alzheimer's disease: a review and proposal for the prevention of Alzheimer's disease. *Alzheimers Res Ther* **3**, 1 (2011).
34. P. B. Verghese, J. M. Castellano, D. M. Holtzman, Apolipoprotein E in Alzheimer's disease and other neurological disorders. *The Lancet Neurology* **10**, 241-252 (2011).
35. J. A. Schneider, Z. Arvanitakis, S. E. Leurgans, D. A. Bennett, The neuropathology of probable Alzheimer disease and mild cognitive impairment. *Ann Neurol* **66**, 200-208 (2009).
36. A. Serrano-Pozo, M. P. Frosch, E. Masliah, B. T. Hyman, Neuropathological alterations in Alzheimer disease. *Cold Spring Harb Perspect Med* **1**, a006189 (2011).
37. R. Tarawneh, D. M. Holtzman, The clinical problem of symptomatic Alzheimer disease and mild cognitive impairment. *Cold Spring Harb Perspect Med* **2**, a006148 (2012).
38. F. Kamenetz *et al.*, APP processing and synaptic function. *Neuron* **37**, 925-937 (2003).
39. H. S. Nhan, K. Chiang, E. H. Koo, The multifaceted nature of amyloid precursor protein and its proteolytic fragments: friends and foes. *Acta Neuropathol* **129**, 1-19 (2015).
40. R. G. Canter, J. Penney, L. H. Tsai, The road to restoring neural circuits for the treatment of Alzheimer's disease. *Nature* **539**, 187-196 (2016).
41. A. T. Petkova, W. M. Yau, R. Tycko, Experimental constraints on quaternary structure in Alzheimer's beta-amyloid fibrils. *Biochemistry* **45**, 498-512 (2006).
42. A. T. Petkova *et al.*, A structural model for Alzheimer's beta -amyloid fibrils based on experimental constraints from solid state NMR. *Proc Natl Acad Sci U S A* **99**, 16742-16747 (2002).
43. M. A. Walti *et al.*, Atomic-resolution structure of a disease-relevant Abeta(1-42) amyloid fibril. *Proc Natl Acad Sci U S A* **113**, E4976-4984 (2016).
44. L. Gremer *et al.*, Fibril structure of amyloid-beta(1-42) by cryo-electron microscopy. *Science* **358**, 116-119 (2017).
45. P. Bharadwaj *et al.*, The Link between Type 2 Diabetes and Neurodegeneration: Roles for Amyloid-beta, Amylin, and Tau Proteins. *J Alzheimers Dis* **59**, 421-432 (2017).

46. K. Akter *et al.*, Diabetes mellitus and Alzheimer's disease: shared pathology and treatment? *Br J Clin Pharmacol* **71**, 365-376 (2011).
47. J. Miklossy *et al.*, Beta amyloid and hyperphosphorylated tau deposits in the pancreas in type 2 diabetes. *Neurobiol Aging* **31**, 1503-1515 (2010).
48. K. Jackson *et al.*, Amylin deposition in the brain: A second amyloid in Alzheimer disease? *Ann Neurol* **74**, 517-526 (2013).
49. G. S. Watson *et al.*, Insulin increases CSF Abeta42 levels in normal older adults. *Neurology* **60**, 1899-1903 (2003).
50. B. O'Nuallain, A. D. Williams, P. Westermark, R. Wetzel, Seeding specificity in amyloid growth induced by heterologous fibrils. *J Biol Chem* **279**, 17490-17499 (2004).
51. L. M. Yan, A. Velkova, M. Tatarek-Nossol, E. Andreetto, A. Kapurniotu, IAPP mimic blocks Abeta cytotoxic self-assembly: cross-suppression of amyloid toxicity of Abeta and IAPP suggests a molecular link between Alzheimer's disease and type II diabetes. *Angew Chem Int Ed Engl* **46**, 1246-1252 (2007).
52. E. Andreetto *et al.*, Identification of hot regions of the Abeta-IAPP interaction interface as high-affinity binding sites in both cross- and self-association. *Angew Chem Int Ed Engl* **49**, 3081-3085 (2010).
53. M. E. Oskarsson *et al.*, In vivo seeding and cross-seeding of localized amyloidosis: a molecular link between type 2 diabetes and Alzheimer disease. *Am J Pathol* **185**, 834-846 (2015).
54. M. F. Burton, P. G. Steel, The chemistry and biology of LL-37. *Nat Prod Rep* **26**, 1572-1584 (2009).
55. A. Fleming, On a Remarkable Bacteriolytic Element found in Tissues and Secretions. *Proc. R. Soc. Lond. B.* **93**, 306-317 (1922).
56. T. Nakatsuji, R. L. Gallo, Antimicrobial peptides: old molecules with new ideas. *J Invest Dermatol* **132**, 887-895 (2012).
57. R. J. Dubos, Studies on a Bactericidal Agent Extracted from a Soil Bacillus : I. Preparation of the Agent. Its Activity in Vitro. *J Exp Med* **70**, 1-10 (1939).
58. R. J. Dubos, Studies on a Bactericidal Agent Extracted from a Soil Bacillus : Ii. Protective Effect of the Bactericidal Agent against Experimental Pneumococcus Infections in Mice. *J Exp Med* **70**, 11-17 (1939).
59. R. J. Dubos, R. D. Hotchkiss, The Production of Bactericidal Substances by Aerobic Sporulating Bacilli. *J Exp Med* **73**, 629-640 (1941).
60. B. M. G. Gause G. F, Gramicidin S and its use in the Treatment of Infected Wounds. *Nature* **154**, 703 (1944).
61. Y. Shai, Mechanism of the binding, insertion and destabilization of phospholipid bilayer membranes by alpha-helical antimicrobial and cell non-selective membrane-lytic peptides. *Biochim Biophys Acta* **1462**, 55-70 (1999).
62. K. Matsuzaki, Why and how are peptide-lipid interactions utilized for self-defense? Magainins and tachyplesins as archetypes. *Biochim Biophys Acta* **1462**, 1-10 (1999).
63. L. Yang, T. M. Weiss, R. I. Lehrer, H. W. Huang, Crystallization of antimicrobial pores in membranes: magainin and protegrin. *Biophys J* **79**, 2002-2009 (2000).
64. Y. Lai, R. L. Gallo, AMPed up immunity: how antimicrobial peptides have multiple roles in immune defense. *Trends Immunol* **30**, 131-141 (2009).
65. M. Zasloff, Antimicrobial peptides of multicellular organisms. *Nature* **415**, 389-395 (2002).
66. U. H. Durr, U. S. Sudheendra, A. Ramamoorthy, LL-37, the only human member of the cathelicidin family of antimicrobial peptides. *Biochim Biophys Acta* **1758**, 1408-1425 (2006).
67. M. L. Mangoni, Host-defense peptides: from biology to therapeutic strategies. *Cell Mol Life Sci* **68**, 2157-2159 (2011).
68. Y. Lai, R. L. Gallo, Toll-like receptors in skin infections and inflammatory diseases. *Infect Disord Drug Targets* **8**, 144-155 (2008).

69. K. De Smet, R. Contreras, Human antimicrobial peptides: defensins, cathelicidins and histatins. *Biotechnol Lett* **27**, 1337-1347 (2005).
70. R. I. Lehrer, Primate defensins. *Nat Rev Microbiol* **2**, 727-738 (2004).
71. R. Gennaro, M. Zanetti, Structural features and biological activities of the cathelicidin-derived antimicrobial peptides. *Biopolymers* **55**, 31-49 (2000).
72. R. M. van Harten, E. van Woudenbergh, A. van Dijk, H. P. Haagsman, Cathelicidins: Immunomodulatory Antimicrobials. *Vaccines (Basel)* **6** (2018).
73. R. Bals, J. M. Wilson, Cathelicidins--a family of multifunctional antimicrobial peptides. *Cell Mol Life Sci* **60**, 711-720 (2003).
74. M. Zanetti, The role of cathelicidins in the innate host defenses of mammals. *Curr Issues Mol Biol* **7**, 179-196 (2005).
75. J. B. Cowland, A. H. Johnsen, N. Borregaard, hCAP-18, a cathelin/pro-bactenecin-like protein of human neutrophil specific granules. *FEBS Lett* **368**, 173-176 (1995).
76. D. Xhindoli *et al.*, The human cathelicidin LL-37--A pore-forming antibacterial peptide and host-cell modulator. *Biochim Biophys Acta* **1858**, 546-566 (2016).
77. A. F. Gombart, N. Borregaard, H. P. Koeffler, Human cathelicidin antimicrobial peptide (CAMP) gene is a direct target of the vitamin D receptor and is strongly up-regulated in myeloid cells by 1,25-dihydroxyvitamin D3. *FASEB J* **19**, 1067-1077 (2005).
78. F. Porcelli *et al.*, NMR structure of the cathelicidin-derived human antimicrobial peptide LL-37 in dodecylphosphocholine micelles. *Biochemistry* **47**, 5565-5572 (2008).
79. E. Sancho-Vaello *et al.*, Structural remodeling and oligomerization of human cathelicidin on membranes suggest fibril-like structures as active species. *Sci Rep* **7**, 15371 (2017).
80. J. Johansson, G. H. Gudmundsson, M. E. Rottenberg, K. D. Berndt, B. Agerberth, Conformation-dependent antibacterial activity of the naturally occurring human peptide LL-37. *J Biol Chem* **273**, 3718-3724 (1998).
81. L. Steinstraesser *et al.*, Host defense peptides in wound healing. *Mol Med* **14**, 528-537 (2008).
82. N. Mookherjee *et al.*, Systems biology evaluation of immune responses induced by human host defence peptide LL-37 in mononuclear cells. *Mol Biosyst* **5**, 483-496 (2009).
83. E. Gazit, A. Boman, H. G. Boman, Y. Shai, Interaction of the mammalian antibacterial peptide cecropin P1 with phospholipid vesicles. *Biochemistry* **34**, 11479-11488 (1995).
84. D. Vandamme, B. Landuyt, W. Luyten, L. Schoofs, A comprehensive summary of LL-37, the factotum human cathelicidin peptide. *Cell Immunol* **280**, 22-35 (2012).
85. Z. Oren, J. C. Lerman, G. H. Gudmundsson, B. Agerberth, Y. Shai, Structure and organization of the human antimicrobial peptide LL-37 in phospholipid membranes: relevance to the molecular basis for its non-cell-selective activity. *Biochem J* **341 (Pt 3)**, 501-513 (1999).
86. A. L. den Hertog *et al.*, Candidacidal effects of two antimicrobial peptides: histatin 5 causes small membrane defects, but LL-37 causes massive disruption of the cell membrane. *Biochem J* **388**, 689-695 (2005).
87. P. Bergman, L. Walter-Jallow, K. Broliden, B. Agerberth, J. Soderlund, The antimicrobial peptide LL-37 inhibits HIV-1 replication. *Curr HIV Res* **5**, 410-415 (2007).
88. G. Wang, K. M. Watson, R. W. Buckheit, Jr., Anti-human immunodeficiency virus type 1 activities of antimicrobial peptides derived from human and bovine cathelicidins. *Antimicrob Agents Chemother* **52**, 3438-3440 (2008).
89. P. G. Barlow *et al.*, Antiviral activity and increased host defense against influenza infection elicited by the human cathelicidin LL-37. *PLoS One* **6**, e25333 (2011).
90. E. Piktel *et al.*, The Role of Cathelicidin LL-37 in Cancer Development. *Arch Immunol Ther Exp (Warsz)* **64**, 33-46 (2016).

91. S. B. Coffelt *et al.*, The pro-inflammatory peptide LL-37 promotes ovarian tumor progression through recruitment of multipotent mesenchymal stromal cells. *Proc Natl Acad Sci U S A* **106**, 3806-3811 (2009).
92. W. K. Wu *et al.*, The host defense peptide LL-37 activates the tumor-suppressing bone morphogenetic protein signaling via inhibition of proteasome in gastric cancer cells. *J Cell Physiol* **223**, 178-186 (2010).
93. K. Bandurska, A. Berdowska, R. Barczynska-Felusiak, P. Krupa, Unique features of human cathelicidin LL-37. *Biofactors* **41**, 289-300 (2015).
94. S. Realegeno, R. L. Modlin, Shedding light on the vitamin D-tuberculosis-HIV connection. *Proc Natl Acad Sci U S A* **108**, 18861-18862 (2011).
95. S. Morizane *et al.*, Cathelicidin antimicrobial peptide LL-37 in psoriasis enables keratinocyte reactivity against TLR9 ligands. *J Invest Dermatol* **132**, 135-143 (2012).
96. P. Y. Ong *et al.*, Endogenous antimicrobial peptides and skin infections in atopic dermatitis. *N Engl J Med* **347**, 1151-1160 (2002).
97. L. D. Pound *et al.*, Cathelicidin Antimicrobial Peptide: A Novel Regulator of Islet Function, Islet Regeneration, and Selected Gut Bacteria. *Diabetes* **64**, 4135-4147 (2015).
98. J. Sun *et al.*, Pancreatic beta-Cells Limit Autoimmune Diabetes via an Immunoregulatory Antimicrobial Peptide Expressed under the Influence of the Gut Microbiota. *Immunity* **43**, 304-317 (2015).
99. E. De Lorenzi *et al.*, Evidence that the Human Innate Immune Peptide LL-37 may be a Binding Partner of Amyloid-beta and Inhibitor of Fibril Assembly. *J Alzheimers Dis* **59**, 1213-1226 (2017).
100. Y. X. Guo *et al.*, 1,25-Dihydroxyvitamin D3 regulates expression of LRP1 and RAGE in vitro and in vivo, enhancing Abeta1-40 brain-to-blood efflux and peripheral uptake transport. *Neuroscience* **322**, 28-38 (2016).
101. A. Cederlund *et al.*, Label-free quantitative mass spectrometry reveals novel pathways involved in LL-37 expression. *J Innate Immun* **6**, 365-376 (2014).
102. Y. Liu *et al.*, The membrane-active amphibian peptide caerin 1.8 inhibits fibril formation of amyloid beta1-42. *Peptides* **73**, 1-6 (2015).
103. H. Wong, J. H. Bowie, J. A. Carver, The solution structure and activity of caerin 1.1, an antimicrobial peptide from the Australian green tree frog, Litoria splendida. *Eur J Biochem* **247**, 545-557 (1997).
104. J. Santos *et al.*, alpha-Helical peptidic scaffolds to target alpha-synuclein toxic species with nanomolar affinity. *Nat Commun* **12**, 3752 (2021).
105. J. Martinez, M. Bodanszky, Side reactions in peptide synthesis. IX. Suppression of the formation of aminosuccinyl peptides with additives. *Int J Pept Protein Res* **12**, 277-283 (1978).
106. T. Vojkovsky, Detection of secondary amines on solid phase. *Pept Res* **8**, 236-237 (1995).
107. E. Kaiser, R. L. Colescott, C. D. Bossinger, P. I. Cook, Color test for detection of free terminal amino groups in the solid-phase synthesis of peptides. *Anal Biochem* **34**, 595-598 (1970).
108. M. W. Friedmann, L. D., Stoichiometry of Formation of Ruhermann's Purple in the Ninhydrin Reaction. *Bioorganic Chemistry* **3**, 267-280 (1974).
109. M. Friedman, Applications of the ninhydrin reaction for analysis of amino acids, peptides, and proteins to agricultural and biomedical sciences. *J Agric Food Chem* **52**, 385-406 (2004).
110. D. M. Walsh *et al.*, A facile method for expression and purification of the Alzheimer's disease-associated amyloid beta-peptide. *FEBS J* **276**, 1266-1281 (2009).
111. A. Jan, D. M. Hartley, H. A. Lashuel, Preparation and characterization of toxic Abeta aggregates for structural and functional studies in Alzheimer's disease research. *Nat Protoc* **5**, 1186-1209 (2010).
112. E. Andreetto, L. M. Yan, A. Caporale, A. Kapurniotu, Dissecting the role of single regions of an IAPP mimic and IAPP in inhibition of Abeta40 amyloid formation and cytotoxicity. *Chembiochem* **12**, 1313-1322 (2011).

113. P. K. K. Smith, R. I.; Hermanson, G. T.; Mallia, A. K.; Gartner, F. H.; Fronzano, M. D.; Fujimoto, E. K.; Goeke, N. M.; Olson, B. J.; Klenk, D. C., Measurement of Protein Using Bicinchoninic Acid. *Analytical Biochemistry* **150**, 76-85 (1985).
114. V. Armiento *et al.*, The Human Host-Defense Peptide Cathelicidin LL-37 is a Nanomolar Inhibitor of Amyloid Self-Assembly of Islet Amyloid Polypeptide (IAPP). *Angew Chem Int Ed Engl* **59**, 12837-12841 (2020).
115. K. Tenidis *et al.*, Identification of a penta- and hexapeptide of islet amyloid polypeptide (IAPP) with amyloidogenic and cytotoxic properties. *J Mol Biol* **295**, 1055-1071 (2000).
116. M. Tatarek-Nossol *et al.*, Inhibition of hIAPP amyloid-fibril formation and apoptotic cell death by a designed hIAPP amyloid- core-containing hexapeptide. *Chem Biol* **12**, 797-809 (2005).
117. B. Dursina *et al.*, Interaction of yeast Rab geranylgeranyl transferase with its protein and lipid substrates. *Biochemistry* **41**, 6805-6816 (2002).
118. R. Kayed *et al.*, Conformational transitions of islet amyloid polypeptide (IAPP) in amyloid formation in vitro. *J Mol Biol* **287**, 781-796 (1999).
119. M. Lacy *et al.*, Identification of an Arg-Leu-Arg tripeptide that contributes to the binding interface between the cytokine MIF and the chemokine receptor CXCR4. *Sci Rep* **8**, 5171 (2018).
120. C. Katz *et al.*, Studying protein-protein interactions using peptide arrays. *Chem Soc Rev* **40**, 2131-2145 (2011).
121. R. P. Nanga, J. R. Brender, S. Vivekanandan, A. Ramamoorthy, Structure and membrane orientation of IAPP in its natively amidated form at physiological pH in a membrane environment. *Biochim Biophys Acta* **1808**, 2337-2342 (2011).
122. H. Park *et al.*, Simultaneous Optimization of Biomolecular Energy Functions on Features from Small Molecules and Macromolecules. *J Chem Theory Comput* **12**, 6201-6212 (2016).
123. J. J. Gray *et al.*, Protein-protein docking with simultaneous optimization of rigid-body displacement and side-chain conformations. *J Mol Biol* **331**, 281-299 (2003).
124. N. A. Marze, S. S. Roy Burman, W. Sheffler, J. J. Gray, Efficient flexible backbone protein-protein docking for challenging targets. *Bioinformatics* **34**, 3461-3469 (2018).
125. M. W. Huang X., A time-efficient, linear-space local similarity algorithm. *Advances in Applied Mathematics* **12**, 337-357 (1991).
126. L. L. Del Mercato *et al.*, Charge transport and intrinsic fluorescence in amyloid-like fibrils. *Proc Natl Acad Sci U S A* **104**, 18019-18024 (2007).
127. F. T. Chan *et al.*, Protein amyloids develop an intrinsic fluorescence signature during aggregation. *Analyst* **138**, 2156-2162 (2013).
128. M. Bakou *et al.*, Key aromatic/hydrophobic amino acids controlling a cross-amyloid peptide interaction versus amyloid self-assembly. *J Biol Chem* **292**, 14587-14602 (2017).
129. L. Wollenweber, Synthesis and studies of peptides from the interaction interface of the human cathelicidin LL-37 with islet amyloid polypeptide. *Unpublished bachelor's thesis, Technische Universität München* (2020).
130. G. Wang, B. Mishra, R. F. Epand, R. M. Epand, High-quality 3D structures shine light on antibacterial, anti-biofilm and antiviral activities of human cathelicidin LL-37 and its fragments. *Biochim Biophys Acta* **1838**, 2160-2172 (2014).
131. K. Yamaguchi, H. Naiki, Y. Goto, Mechanism by which the amyloid-like fibrils of a beta 2-microglobulin fragment are induced by fluorine-substituted alcohols. *J Mol Biol* **363**, 279-288 (2006).
132. G. Wang, Structures of human host defense cathelicidin LL-37 and its smallest antimicrobial peptide KR-12 in lipid micelles. *J Biol Chem* **283**, 32637-32643 (2008).
133. E. Sancho-Vaello *et al.*, The structure of the antimicrobial human cathelicidin LL-37 shows oligomerization and channel formation in the presence of membrane mimics. *Sci Rep* **10**, 17356 (2020).

134. J. R. Brender *et al.*, Biphasic effects of insulin on islet amyloid polypeptide membrane disruption. *Biophys J* **100**, 685-692 (2011).
135. L. Tomasinsig *et al.*, The human cathelicidin LL-37 modulates the activities of the P2X7 receptor in a structure-dependent manner. *J Biol Chem* **283**, 30471-30481 (2008).
136. X. Chen *et al.*, Human antimicrobial peptide LL-37 modulates proinflammatory responses induced by cytokine milieus and double-stranded RNA in human keratinocytes. *Biochem Biophys Res Commun* **433**, 532-537 (2013).
137. M. Shahmiri *et al.*, Membrane Core-Specific Antimicrobial Action of Cathelicidin LL-37 Peptide Switches Between Pore and Nanofibre Formation. *Sci Rep* **6**, 38184 (2016).
138. R. Sood, Y. Domanov, M. Pietiainen, V. P. Kontinen, P. K. Kinnunen, Binding of LL-37 to model biomembranes: insight into target vs host cell recognition. *Biochim Biophys Acta* **1778**, 983-996 (2008).
139. K. Zeth, E. Sancho-Vaello, The Human Antimicrobial Peptides Dermcidin and LL-37 Show Novel Distinct Pathways in Membrane Interactions. *Front Chem* **5**, 86 (2017).
140. Y. Engelberg, M. Landau, The Human LL-37(17-29) antimicrobial peptide reveals a functional supramolecular structure. *Nat Commun* **11**, 3894 (2020).
141. C. B. Andersen, D. Otzen, G. Christiansen, C. Rischel, Glucagon amyloid-like fibril morphology is selected via morphology-dependent growth inhibition. *Biochemistry* **46**, 7314-7324 (2007).
142. N. Hirota, K. Mizuno, Y. Goto, Group additive contributions to the alcohol-induced alpha-helix formation of melittin: implication for the mechanism of the alcohol effects on proteins. *J Mol Biol* **275**, 365-378 (1998).
143. J. J. Meier *et al.*, Inhibition of human IAPP fibril formation does not prevent beta-cell death: evidence for distinct actions of oligomers and fibrils of human IAPP. *Am J Physiol Endocrinol Metab* **291**, E1317-1324 (2006).
144. C. G. Glabe, R. Kayed, Common structure and toxic function of amyloid oligomers implies a common mechanism of pathogenesis. *Neurology* **66**, S74-78 (2006).
145. A. Abedini *et al.*, Time-resolved studies define the nature of toxic IAPP intermediates, providing insight for anti-amyloidosis therapeutics. *Elife* **5** (2016).
146. G. Wang *et al.*, Design of Antimicrobial Peptides: Progress Made with Human Cathelicidin LL-37. *Adv Exp Med Biol* **1117**, 215-240 (2019).
147. M. Hemshekhar, S. Faiyaz, K. G. Choi, O. V. Krokhin, N. Mookherjee, Immunomodulatory Functions of the Human Cathelicidin LL-37 (aa 13-31)-Derived Peptides are Associated with Predicted alpha-Helical Propensity and Hydrophobic Index. *Biomolecules* **9** (2019).
148. D. Xhindoli, S. Pacor, F. Guida, N. Antcheva, A. Tossi, Native oligomerization determines the mode of action and biological activities of human cathelicidin LL-37. *Biochem J* **457**, 263-275 (2014).
149. D. Xhindoli *et al.*, New aspects of the structure and mode of action of the human cathelicidin LL-37 revealed by the intrinsic probe p-cyanophenylalanine. *Biochem J* **465**, 443-457 (2015).
150. H. Moravej *et al.*, Antimicrobial Peptides: Features, Action, and Their Resistance Mechanisms in Bacteria. *Microb Drug Resist* **24**, 747-767 (2018).
151. A. Izadpanah, R. L. Gallo, Antimicrobial peptides. *J Am Acad Dermatol* **52**, 381-390; quiz 391-382 (2005).
152. J. Lei *et al.*, The antimicrobial peptides and their potential clinical applications. *Am J Transl Res* **11**, 3919-3931 (2019).
153. H. Brauner *et al.*, Markers of innate immune activity in patients with type 1 and type 2 diabetes mellitus and the effect of the anti-oxidant coenzyme Q10 on inflammatory activity. *Clin Exp Immunol* **177**, 478-482 (2014).

154. M. T. Herrera, Y. Gonzalez, F. Hernandez-Sanchez, G. Fabian-San Miguel, M. Torres, Low serum vitamin D levels in type 2 diabetes patients are associated with decreased mycobacterial activity. *BMC Infect Dis* **17**, 610 (2017).
155. C. Cristelo, A. Machado, B. Sarmento, F. M. Gama, The roles of vitamin D and cathelicidin in type 1 diabetes susceptibility. *Endocr Connect* **10**, R1-R12 (2021).
156. S. Morikawa *et al.*, IAPP/amylin deposition, which is correlated with expressions of ASC and IL-1beta in beta-cells of Langerhans' islets, directly initiates NLRP3 inflammasome activation. *Int J Immunopathol Pharmacol* **32**, 2058738418788749 (2018).
157. S. L. Masters *et al.*, Activation of the NLRP3 inflammasome by islet amyloid polypeptide provides a mechanism for enhanced IL-1beta in type 2 diabetes. *Nat Immunol* **11**, 897-904 (2010).
158. K. E. Ridyard, J. Overhage, The Potential of Human Peptide LL-37 as an Antimicrobial and Anti-Biofilm Agent. *Antibiotics (Basel)* **10** (2021).
159. E. F. Haney, S. K. Straus, R. E. W. Hancock, Reassessing the Host Defense Peptide Landscape. *Front Chem* **7**, 43 (2019).
160. H. S. Joo, C. I. Fu, M. Otto, Bacterial strategies of resistance to antimicrobial peptides. *Philos Trans R Soc Lond B Biol Sci* **371** (2016).
161. X. Li, Y. Li, H. Han, D. W. Miller, G. Wang, Solution structures of human LL-37 fragments and NMR-based identification of a minimal membrane-targeting antimicrobial and anticancer region. *J Am Chem Soc* **128**, 5776-5785 (2006).
162. M. Wanmakok, S. Orrapin, A. Intorasoot, S. Intorasoot, Expression in Escherichia coli of novel recombinant hybrid antimicrobial peptide AL32-P113 with enhanced antimicrobial activity in vitro. *Gene* **671**, 1-9 (2018).
163. S. Kanthawong *et al.*, Antimicrobial and antibiofilm activity of LL-37 and its truncated variants against Burkholderia pseudomallei. *Int J Antimicrob Agents* **39**, 39-44 (2012).
164. P. Saporito, M. Vang Mouritzen, A. Lobner-Olesen, H. Jenssen, LL-37 fragments have antimicrobial activity against Staphylococcus epidermidis biofilms and wound healing potential in HaCaT cell line. *J Pept Sci* **24**, e3080 (2018).
165. X. Feng, K. Sambanthamoorthy, T. Palys, C. Paranavitana, The human antimicrobial peptide LL-37 and its fragments possess both antimicrobial and antibiofilm activities against multidrug-resistant Acinetobacter baumannii. *Peptides* **49**, 131-137 (2013).
166. F. Albericio, A. El-Faham, Choosing the Right Coupling Reagent for Peptides: A Twenty-Five-Year Journey. *Org. Process Res. Dev.* **22**, 760-772 (2018).
167. V. K. Sarin, S. B. H. Kent, A. R. Mitchell, R. B. Merrifield, A General Approach to the Quantitation of Synthetic Efficiency in Solid-Phase Peptide Synthesis as a Function of Chain Length. *J. Am. Chem. Soc.* **106**, 7845-7850 (1984).
168. J. P. Tam, Y. Lu, Coupling Difficulty Associated with Interchain Clustering and Phase Transition in Solid Phase Peptide Synthesis. *J. Am. Chem. Soc.* **117**, 12058–12063 (1995).
169. C. J. Barrow, A. Yasuda, P. T. Kenny, M. G. Zagorski, Solution conformations and aggregational properties of synthetic amyloid beta-peptides of Alzheimer's disease. Analysis of circular dichroism spectra. *J Mol Biol* **225**, 1075-1093 (1992).
170. N. Hirota, K. Mizuno, Y. Goto, Cooperative alpha-helix formation of beta-lactoglobulin and melittin induced by hexafluoroisopropanol. *Protein Sci* **6**, 416-421 (1997).
171. D. Roccatano, M. Fioroni, M. Zacharias, G. Colombo, Effect of hexafluoroisopropanol alcohol on the structure of melittin: a molecular dynamics simulation study. *Protein Sci* **14**, 2582-2589 (2005).
172. S. Jahangiri, M. Jafari, M. Arjomand, F. Mehrnejad, Molecular insights into the interactions of GF-17 with the gram-negative and gram-positive bacterial lipid bilayers. *J Cell Biochem* **119**, 9205-9216 (2018).

173. A. de Miguel Catalina *et al.*, The C-Terminal VPRTES Tail of LL-37 Influences the Mode of Attachment to a Lipid Bilayer and Antimicrobial Activity. *Biochemistry* **58**, 2447-2462 (2019).
174. C. Nagant *et al.*, Identification of peptides derived from the human antimicrobial peptide LL-37 active against biofilms formed by Pseudomonas aeruginosa using a library of truncated fragments. *Antimicrob Agents Chemother* **56**, 5698-5708 (2012).
175. C. D. Ciornei, T. Sigurdardottir, A. Schmidtchen, M. Bodelsson, Antimicrobial and chemoattractant activity, lipopolysaccharide neutralization, cytotoxicity, and inhibition by serum of analogs of human cathelicidin LL-37. *Antimicrob Agents Chemother* **49**, 2845-2850 (2005).
176. Y. Luo *et al.*, The Naturally Occurring Host Defense Peptide, LL-37, and Its Truncated Mimetics KE-18 and KR-12 Have Selected Biocidal and Antibiofilm Activities Against Candida albicans, Staphylococcus aureus, and Escherichia coli In vitro. *Front Microbiol* **8**, 544 (2017).
177. M. Z. R. Innocenti Malini, M. Gontsarikb, K. Maniura-Weberb, R. M. Rossi, F. Spanoa and S. Salentinig, Self-assembly of glycerol monooleate with the antimicrobial peptide LL-37: a molecular dynamics study. *RSC Adv.* **10**, 8291-8302 (2020).
178. J. Peng *et al.*, The introduction of L-phenylalanine into antimicrobial peptide protonectin enhances the selective antibacterial activity of its derivative phe-Prt against Gram-positive bacteria. *Amino Acids* **53**, 23-32 (2021).
179. A. K. Tripathi *et al.*, Selective phenylalanine to proline substitution for improved antimicrobial and anticancer activities of peptides designed on phenylalanine heptad repeat. *Acta Biomater* **57**, 170-186 (2017).
180. L. O. Tjernberg *et al.*, Arrest of beta-amyloid fibril formation by a pentapeptide ligand. *J Biol Chem* **271**, 8545-8548 (1996).

Contribution by students to data reported in this thesis

- Linus Wollenweber carried out circular dichroism studies, fluorescence spectroscopic titrations, and inhibition studies via ThT binding assay during his Bachelor thesis work. L. Wollenweber, Synthesis and studies of peptides from the interaction interface of the human cathelicidin LL-37 with islet amyloid polypeptide. *Unpublished bachelor's thesis, Technische Universität München* (2020).

- Sophie von Schönberg carried out the synthesis of LL-37(1-14) and LL-37(3-37) during her research internship, which was co-supervised by me.

- Stefanie Grümbel carried out the synthesis of LL-37(1-26), LL-37(3-37), LL-37(5-37), LL-37(3-37)A5,6, and LL-37(5-37)A5,6 during her research internship, which was co-supervised by me.

- Vincenz Buschinger carried out the synthesis of LL-37(1-10), LL-37(20-31), and LL-37(3-37) during his research internship, which was co-supervised by me.

Publications and scientific presentations

- V. Armiento, K. Hille, D. Naltsas, J. S. Lin, A. E. Barron, A. Kapurniotu, The Human Host-Defense Peptide Cathelicidin LL-37 is a Nanomolar Inhibitor of Amyloid Self-Assembly of Islet Amyloid Polypeptide (IAPP). *Angew Chem Int Ed Engl* **59**, 12837-12841 (2020).

- V. Armiento, A. Spanopoulou, A. Kapurniotu, Peptide-Based Molecular Strategies To Interfere with Protein Misfolding, Aggregation, and Cell Degeneration. *Angew Chem Int Ed Engl* **59**, 3372-3384 (2020).

- Poster presentation at the 4th Ulm Meeting "Biophysics of Amyloid Formation", Ulm Germany, Feb. 2020. Title: "Identification of a novel IAPP amyloid suppressing interaction: The human cathelicidin LL-37 is a nanomolar inhibitor of amyloid self-assembly of IAPP".

Acknowledgments

A heartfelt thank you to all the people who made it possible for me to get this far and complete this thesis work. First, I would like to thank my supervisor Prof. Dr. Aphrodite Kapurniotu, who was always ready to give me the right directions at every stage of the realization of my scientific work. Thanks to you, I have increased my knowledge and skills as a scientist and developed a stronger personality.

I thank Prof. Dr. Jürgen Bernhagen for the cooperation and the scientific advice over these years, and his collaborators Dr. Omar El Bounkari for the help with the 2-PM experiments, and Christine Krammer for the help with the peptide arrays. Thank you, Dr. Carsten Peters and Prof. Dr. Sevil Weinkauf for your support with TEM microscopy, and Dr. Pamina Katzman for your advice, for performing measurements, and analyzing the data of AUC experiments. Thank you Dr. Andrea Di Luca for performing the docking studies.

A special thank you goes to all my colleagues of the Kapurniotu research group for standing by me during this intense period and rejoicing, along with me, in our achievements. In particular, I thank Kathleen Hille for her great contributions to my work, from the synthesis to the MALDI, for her innumerable advice to solve daily lab challenges, and for our cheerful moments together. I express my gratitude to Denise Naltsas for the development of the peptide arrays. Thank you for your sensitive nature, and your unlimited patience. Thank you for listening to my outpourings, thank you for all the light-hearted moments. I would also like to thank Beatrice Dalla Volta for being so effervescent and for her contagious laugh. Together, we had many “Italian moments” that made me feel back home. Thank you, Simon Hornung, or “technical support Hornung”, for your IT and emotional support. Thank you for the valuable and passionate scientific discussions and for always being there in the moments of need. I would also like to thank Christos Kontos for his wise, Greek, philosophical advice and the funny moments together, as well as for the ESI measurements. Thank you Karin Tas for your experimental advice and the ESI samples analysis and Hendrik Wunderlich for your vivid interest in my scientific work. You all made it very easy to work in such a great and entertaining lab environment.

I am grateful for meeting you, Sofia. Thank you for sharing with me laughter, interests, long discussions, and delightful moments that I will always remember.

Un ringraziamento speciale va a Giacomo e Leila. Grazie per le bellissime cene passate insieme, piene di discorsi divertenti e impegnati. Grazie per essere stati presenti in tutti questi anni e per aver condiviso momenti importanti delle nostre vite.

Ringrazio di cuore i miei amici di una vita. Grazie a Cristina, per essere la mia compagna di viaggio in tutti questi anni e per aver dimostrato che la nostra amicizia è più forte di qualsiasi distanza. Ringrazio Gaia, e Daniele per essere stati sempre presenti e per avermi sempre accolta con un sorriso ad ogni mio ritorno. Grazie per aver ascoltato i miei sfoghi, grazie per tutti i momenti di spensieratezza.

Non posso non menzionare la mia famiglia, in particolare mia madre Sabrina e mia sorella Clarice che da sempre mi sostengono nella realizzazione dei miei progetti. Non finirò mai di ringraziarvi per avermi permesso di arrivare fin qui.

Infine vorrei ringraziare Andrea per avermi reso una persona migliore. Grazie per tutto il tempo che mi hai dedicato. Grazie perché ci sei sempre stato in questo affascinante percorso chiamato vita.

Ad meliora et maiora semper!